CORA Cork Open Research Archive
Cartlann Taighde Oscailte Chorcaí

Title	Next generation technologies for 100 Gb/s PON systems
Authors	Dalla Santa, Marco
Publication date	2019
Original Citation	Dalla Santa, M. 2019. Next generation technologies for 100 Gb/s PON systems. PhD Thesis, University College Cork.
Type of publication	Doctoral thesis
Rights	© 2019, Marco Dalla Santa. - http://creativecommons.org/licenses/by-nc-nd/3.0/
Download date	2026-10-31 03:28:14
Item downloaded from	https://hdl.handle.net/10468/7985



UCC
University College Cork, Ireland
Coláiste na hOllscoile Corcaigh

National University of Ireland, Cork



UCC
Coláiste na hOllscoile Corcaigh, Éire
University College Cork, Ireland

Next Generation Technologies for 100 Gb/s PON Systems

Thesis presented by
Marco Dalla Santa

for the degree of
Doctor of Philosophy

Photonic Systems Group, Tyndall National Institute
Department of Electrical and Electronic Engineering
University College Cork

Research Supervisor: Paul Townsend
Research Co-Supervisor: Giuseppe Talli
Research Advisor: Cleitus Antony
Head of Department: Liam Marnane

March 2019

Table of Contents

1 Introduction **1**

1.1 Context and motivation 1

1.2 Thesis overview 6

2 Next Generation Passive Optical Networks **11**

2.1 Optical access networks 12

2.1.1 PON evolution roadmap 16

2.2 Performance metrics 18

2.2.1 Bit error rate 19

2.2.2 Eye diagram 21

2.3 PON impairments 23

2.3.1 Optoelectronics impairments 23

2.3.2 Fibre impairments 30

2.3.3 Optical amplification 41

2.4 Route to 100G PON 46

2.4.1 Enhanced bit-rate 46

2.4.2 Chromatic dispersion tolerance 48

2.4.3 Power budget 48

2.5 Summary 49

3 Advanced Modulation Formats in Passive Optical Networks **51**

3.1 DMT modulation for XG-PON enhanced rate 52

3.1.1 Discrete multi-tone modulation 52

3.1.2 Demonstration of G-PON devices bit-rate enhancement 59

3.2 25G PAM4 and EDB modulation for NG-PON2 bit-rates 65

3.2.1 Multilevel amplitude modulation 66

3.2.2 Thermal noise limit 70
3.2.3 Bandwidth requirements 73
3.2.4 Chromatic dispersion tolerance 76
3.3 Linear burst-mode receiver 83
3.3.1 Linear burst-mode receiver design 83
3.3.2 Experimental setup 87
3.3.3 Receiver settling time 89
3.3.4 Receiver dynamic range 91
3.4 PAM4 hierarchical modulation 93
3.4.1 Hierarchical modulation with interleaved ONUs detection scheme 94
3.4.2 Experimental demonstration of power budget extension 99
3.5 Summary 106

4 Chromatic Dispersion Management in Passive Optical Networks 109
4.1 Adaptive burst-mode linear equaliser for upstream traffic 111
4.1.1 FFE and DFE filters 112
4.1.2 Filter parameters optimisation 116
4.1.3 Impairment compensation 130
4.1.4 25G burst-mode upstream system demonstration 135
4.2 Chirp controlled directly modulated laser transmitters . . 141
4.2.1 Chirp in directly modulated lasers 142
4.2.2 Narrow optical filtering technique 151
4.2.3 CML transmission performance 153
4.3 Summary 162

5 Optical Amplification Strategies for Burst-Mode Systems 165
5.1 Raman amplifiers for PON upstream traffic 166
5.1.1 Raman based optical amplification 166
5.1.2 G-PON reach extender 170
5.1.3 XG-PON reach extender 177
5.1.4 100G-PON reach extender 185
5.2 Burst-mode gain controlled SOAs 196

5.2.1 Semiconductor optical amplifiers 197
5.2.2 SOA and multilevel modulation formats 203
5.2.3 Gain controlled pre-amplified receiver demonstration 211
5.3 Summary 224

6 Conclusions **227**
6.1 Contributions overview 227
6.2 Future work 232

List of Publications **235**

List of Acronyms **238**

List of Figures **242**

Bibliography **251**

Statement of Originality

This is to certify that the work I am submitting is my own and has not been submitted for another degree, either at University College Cork or elsewhere. All external references and sources are clearly acknowledged and identified within the contents. I have read and understood the regulations of University College Cork concerning plagiarism.

The best climber is the one
who's having the most fun.

Alex Lowe

Acknowledgements

A doctorate is one of the longest lasting and most committing projects in many people's lives. It requires a combination of determination, luck, perseverance, and hard work to get to the finish line, and an invaluable ally on this adventure is represented by the people you share it with. For me this was a journey inside a journey, starting a PhD in a new and unknown place was a challenge, with its highs and lows, failures and successes, great experiences and shared moments. Looking back now I see great memories, the beauty of getting to know the world through its people, friendships that will last for life, and much more. To all of you who have been a part of my life in Cork, small or big, a huge thank you for what you gave and meant to me.

I would like to thank, in particular, my supervisor for giving me the opportunity of joining the Photonic Systems Group, where I lived the academic world with great freedom and support. I want to thank everyone in the group for their help and everyone who contributes in making Tyndall a memorable place to work in. I also want to thank all the friends from my years in Italy with whom I keep in touch, despite the distance. Every time we meet it feels like the previous time was just the day before, and this is a very special thing.

Finally and mostly I want to thank who really got me to this point, which is my family. Thank you, Mum and Dad, for having always supported me without pushing, for having always believed in me without demanding, for having taught me the sense of responsibility and respect by being the first and brightest example. You always gave me everything I could have desired for, but didn't forget to teach me the value of simplicity. For all of this I will be eternally grateful to you. Thank you my brother, for all the time we spent together and for being my first friend and greatest companion of games and explorations back in the days.

Abstract

The worldwide explosion of Internet traffic demand is driving the research for innovative solutions in many aspects of the telecommunication world. In access systems, passive optical networks (PONs) are becoming the preferred solution towards which most providers are migrating thanks to the unrivalled bandwidth they can offer. PON systems with a capacity of 100 Gb/s are envisioned as the solution to the dramatic increase in bandwidth and will be essential to support the future fixed and mobile broadband services. However, many challenging aspects have to be addressed in order to overcome the limitations imposed by the physical layer while meeting the economical requirements for mass deployment. In this thesis a comprehensive approach is taken in order to address the most compelling problems and investigate a series of solutions to the current capacity limitations of PONs.

Advanced modulation formats are used to achieve bit-rate enhancement from 10 Gb/s to 25 Gb/s re-using the same optoelectronic devices in order to provide a 2.5x increase in transmission speed without resorting to a newer, more expensive generation of higher speed devices. The management of chromatic dispersion is also addressed in order to extend the reach of the networks beyond the standard 20 km using either electronic or optical based compensation strategies. Transmission of 25 Gb/s traffic over fibre lengths of 40 and 50 km is demonstrated confirming the suitability of the proposed technologies for extended reach networks which could greatly reduce the number of existing nodes and hence the capital and operational costs of PONs. Optical amplification strategies are also discussed as a means to improve the physical reach of the networks, both in terms of distance and number of customers. Raman amplifiers and semiconductor optical amplifiers are investigated in order to extend the reach of a PON upstream channel. The results demonstrate a reach of up to 50 km which is more than double the typical fibre length of 20 km adopted in deployed systems today. A number of customers, up to 512, was also demonstrated in a 20 km network, increased from the typical 32 or 64 users of most commercial networks.

1 Introduction

In the last 20 years an exceptional growth in bandwidth demand to access the Internet has occurred and this trend is expected to continue, if not increase, over the coming years. This growth is due to the wider proliferation of Internet access across the globe, driven by services with increasing popularity like cloud storage and computing, video streaming, Internet television and the rapid diffusion of mobile devices, just to name a few. The global Internet traffic has been steadily increasing over the last decades and is predicted to grow at a compound annual growth rate (CAGR) of 24 % in the period 2016-2021 [1]. Currently the transmission speed bottleneck of the Internet is the access network, which covers the last span of the communication between customers and the closest Central Office node. This access network nowadays still largely relies on copper based communication but the digital subscriber line (DSL) technologies are reaching their capacity limit and cannot support the foreseen traffic growth. Optical fibre communication, on the other hand, can offer a much greater bandwidth and provide a channel with higher capacity. In the next generation of systems the optical transmission will be brought closer to the end customers in order to exploit the superior performance of the fibre and provide a solution to the increasing bandwidth demand.

1.1 Context and motivation

The Internet is enabled by a physical network infrastructure capable of transferring data across the globe. This complex structure can be divided into three hierarchical levels which are called the core network, the metro network and the access network (Fig. 1.1). The difference is in their geographic coverage and data traffic capacity. The core network is the backbone of the Internet and is made of links spanning up

to several thousands of kilometres, connecting together large cities and metropolitan areas inside a country or connecting different countries and even continents. Core network links make use of the most refined technologies available to ensure the best performance. The metro network connects the main distribution nodes to the closest core node and has ranges of typically 40 to a few hundreds of km, 300-400 km, generally covering large cities or metropolitan areas. Fibre optics is a well-established technology for core and metro networks because it offers unrivalled bandwidth compared to other transmission mediums and the high installation and operational costs are justified by the large amount of end customers availing of these network links. Access networks cover the last span, from the metro node to the customer premises, providing Internet connection to the end users. Access hence needs a capillary structure in order to provide appropriate geographic coverage, and at the same time suffers from stricter cost restrictions due to the limited number of customers availing of the network. Also the cost distribution is peculiar in access networks where the equipment at the user side tends to be more cost critical than the one in the Central Office because it is dedicated for a single customer and not shared among the network users. The global increase of Internet traffic will affect all the network layers, however while core and metro networks are already entirely relying on optical fibres, access networks will have to go through an extensive upgrade of the physical

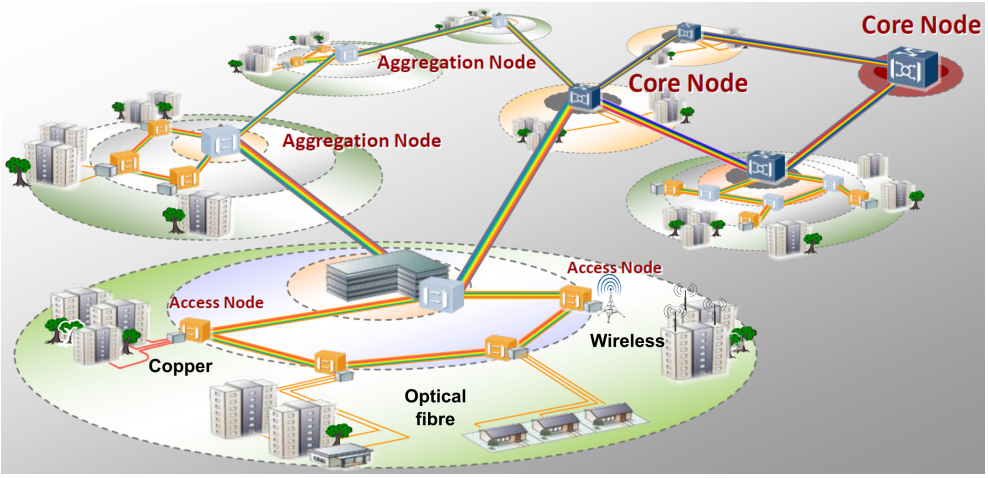


Figure 1.1: Structure of the Internet physical network layers. Adapted from [2].

layer which is still largely based on copper. Identifying the right compromise between performance and cost will be essential to encourage the diffusion of optical technologies in the cost-constrained segment of access networks.

The International Telecommunication Union (ITU) latest 2017 statistic report reveals that 3578 million people use the Internet. Worldwide, 53.6 % of households have access to the Internet through either wired or wireless technology, a percentage that increase to 84.4 % when considering developed countries [3]. The global number of fixed-broadband subscriptions has increased by 9 % annually in the last five years, from 2012 to 2017, and 330 million new fixed-broadband subscriptions have been added. As of 2017 there are 998 million active fixed broadband subscriptions [3]. DSL is still the dominant fixed-broadband technology worldwide with 4.7 connections for every 100 inhabitants but is followed closely by fibre to the home (FTTH) and fibre to the building (FTTB), which account for 4.5 subscriptions per 100 inhabitants. The share of fibre in total fixed-broadband subscriptions is highest in Asia and Pacific countries and the Commonwealth of Independent States. An interesting trend is that developing countries and least developed countries are now deploying fibre infrastructure directly, leapfrogging cable and DSL technology which have been instead re-used extensively in Europe in an attempt to avoid or delay big capital investments needed to deploy new fibre infrastructure. In the latest report from the Organisation for Economic Co-operation and Development (OECD) the percentage of broadband connections backed by optical fibre was 23.3 % among the adhering countries, with peaks of above 70 % in countries as Korea and Japan (Fig. 1.2) [4]. According to the same report, OECD countries have experienced an average 14.6 % increase in fibre subscription during 2017, with Ireland measuring a striking 420 % [4].

The trend is clearly visible looking at how the distribution of access broadband technologies in Sweden has evolved between 2013 and 2017 (Fig. 1.4) [5]. Fibre based Internet access has increased from 18 % to 51 % in the space of four years, absorbing customer segments from all the alternative technologies which reported a decrease in the number of subscriptions.

PONs are the preferred system deployed for optical access because

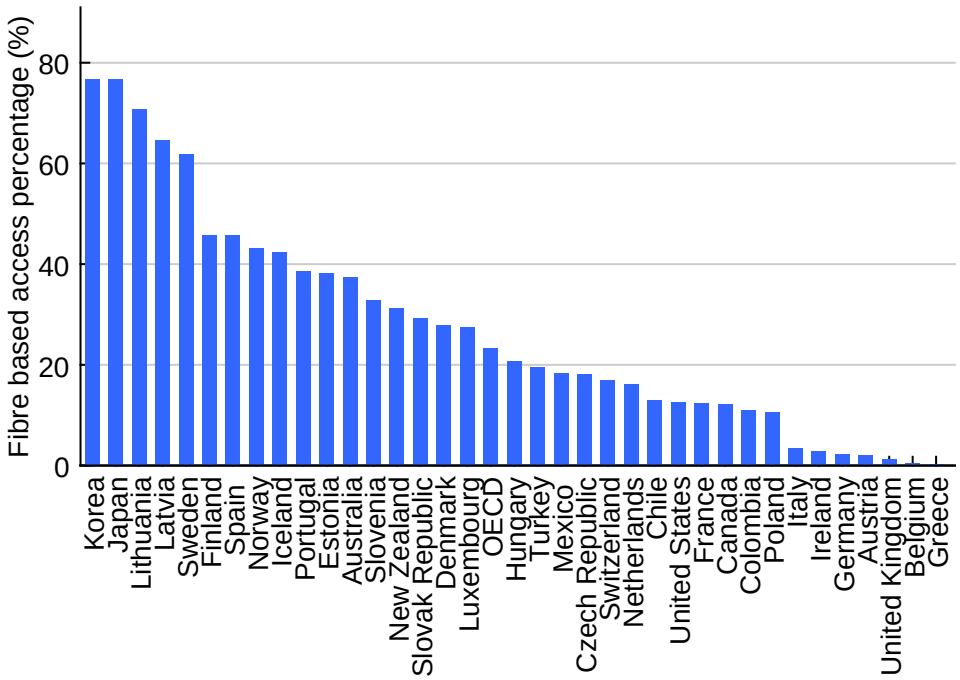


Figure 1.2: Percentage of fibre based fixed-broadband in OECD countries, December 2017.

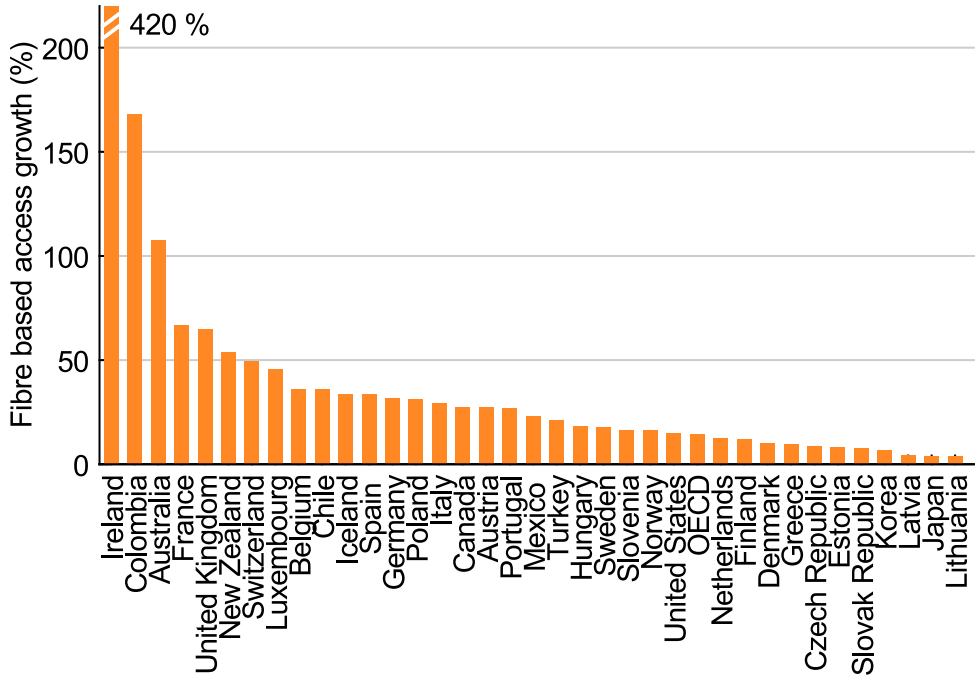


Figure 1.3: Fibre based fixed-broadband growth from December 2016 to December 2017 in OECD countries.

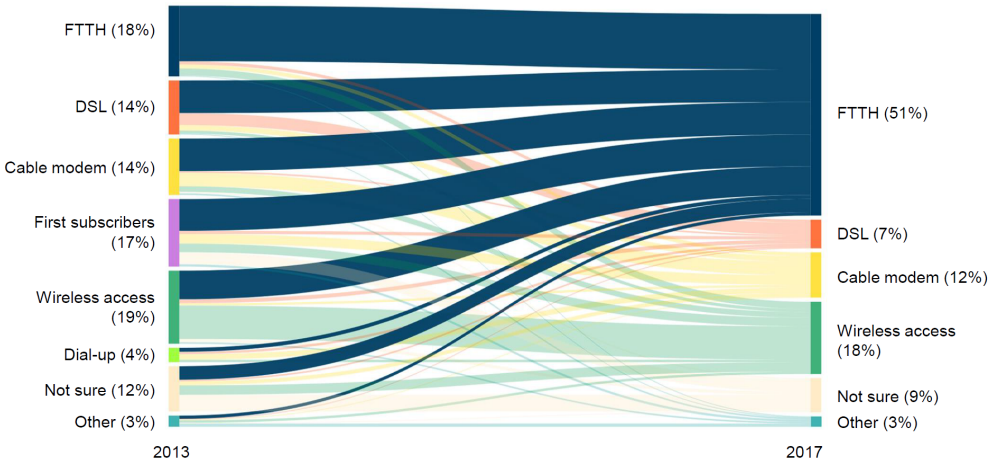


Figure 1.4: Access medium distribution between 2013 and 2017 in Sweden [5].

they are a cost-effective point-to-multipoint solution that provides connection from the metro node to a multitude of users allowing for partial sharing of resources. Compared to other optical access solutions PONs minimise the amount fibre and active components in the network allowing for great reduction in the overall deployment and operational costs. Point-to-point networks or active optical networks offer higher performance to the customers but in many application their cost is prohibitive for adoption. A recent report from Zion Market Research reveals that the global Gigabit-capable passive optical network (G-PON) equipment market is expected to reach a value of USD 25.82 billion by 2024, from USD 5.50 billion in 2017, growing at a CAGR of around 24.72% between 2018 and 2024 [6]. The predicted growth in fibre access connections is not only due to the residential fixed broadband demand but also to the upcoming 5G mobile communication standard which will need a capillary high performance underlying transport network [7–9].

In order to effectively tackle the rise in bandwidth demand, PONs not only have to increase the number of installed systems but also their capacity. Currently the majority of deployed networks are G-PON systems with asymmetric speed of 2.5 Gb/s in downstream and 1.25 Gb/s upstream [10], and the most recent standards that can be adopted offer either a 10 Gb/s symmetric transmission speed over a single wavelength (XGS-PON), or up to 40 Gb/s with wavelength multiplexing (next-generation passive optical network 2 (NG-PON 2)). In order to

respond to the increasing pressure of delivering higher speed broadband service, PONs with speed per wavelength above 10 Gb/s are currently under standardisation by both the Institute of Electrical and Electronics Engineers (IEEE) and the ITU with their 100G Ethernet passive optical network (100G-EPON) and high-speed passive optical network (HS-PON) respectively [11, 12]. Several technological challenges need to be addressed to meet the physical requirements of these next generation of networks. Improved bit-rate is desired, along with enhancement of the physical reach and number of customers, all of which requires a new family of technologies to be investigated and implemented.

1.2 Thesis overview

In this thesis a comprehensive approach is taken towards the development of a 100 G PON based on wavelength multiplexing of four 25 Gb/s channels. Figure 1.5 shows a simple schematic of a PON highlighting the main impairments encountered in the implementation of higher performance networks. The 100 G PONs will be based on multiple channels with a bit-rate of 25 Gb/s. However, in order to improve the modulation speed beyond 10 Gb/s, a new family of higher bandwidth opto-electronic components is needed. The high cost of these devices might be an obstacle for their adoption in access networks in the near future. On the other hand, 10 G components are readily available for high volume production at an affordable price and can rely on a well established fabrication process. More advanced modulation formats can be used to

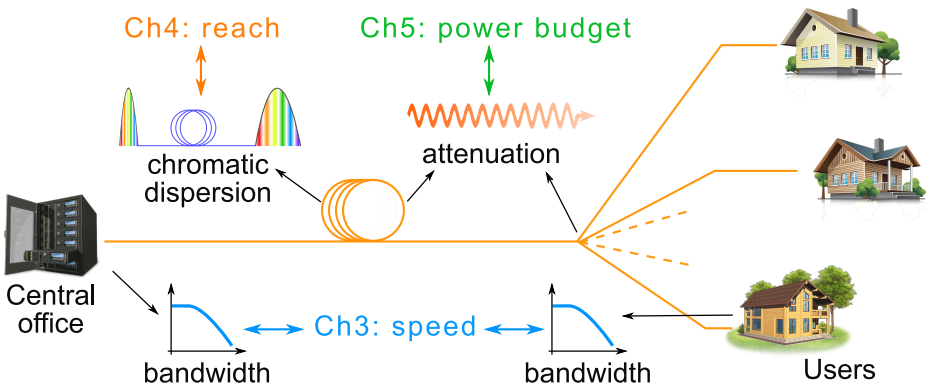


Figure 1.5: Major impairments in PON systems addressed in this thesis.

exploit more efficiently the available bandwidth and hence are seen as promising solutions to enhance the bit-rate of the current generation of optoelectronic devices in a cost-effective way. When the data transmission speed is increased, chromatic dispersion (CD) affects more heavily the signal quality due to the higher symbol-rate and/or higher constellation complexity. Hence, CD becomes a more serious impairment than it is in legacy PONs and compensation strategies must be considered to avoid irrecoverable signal distortions. Various compensation schemes can be implemented, either optically or electronically and both at the transmitter or the receiver to increase the transmission reach. The use of higher speed data transmission also means that the minimum optical power required at the receiver is higher. This, along with the insertion losses of the additional components necessary to operate a multiple wavelength network, means that optical amplification might be necessary in next-generation networks in order to meet the power budget specification of legacy systems. Different technologies and system architectures can be adopted for both downstream and upstream amplification researching the most cost-effective solution.

Outline of the thesis

The thesis presents a set of contributions towards the realisation of 100 Gb/s optical access networks addressing the most challenging technological aspects. In Chapter 2, optical access networks, PONs in particular, are introduced and the roadmap and challenges towards the realisation of next-generation networks are discussed.

Chapter 3 addresses the issue of bandwidth limitation in PON transceivers and introduces the use of more spectrally efficient modulation formats to achieve higher bit-rate in a cost-effective way, opening the possibility of re-using the previous generation of optoelectronic devices. Three different intensity-modulation/direct-detection (IMDD) modulation formats are analysed to address their potential to enable 25 Gb/s single channel traffic: discrete multitone (DMT), 4-level pulse-amplitude modulation (PAM4) and electrical duo-binary (EDB). PAM4 and EDB are investigated in detail and their advantages over non-return to zero (NRZ) in terms of bandwidth requirements and chromatic disper-

sion tolerance are shown. For the more challenging burst-mode upstream direction a novel linear burst-mode receiver (BM-Rx) is characterised using advanced modulation formats which require a linear channel. PAM4 is also demonstrated in a downstream application where it provides extension of the network power budget exploiting the distribution network asymmetry without bit-rate reduction and/or optical amplification.

In Chapter 4 the limitations due to CD are addressed with two different approaches. The first solution investigated targets the upstream direction and makes use of electronic linear filtering at the Central Office to implement a burst-mode electronic dispersion compensation (EDC). The second approach is intended for downstream traffic and adopts narrow optical filtering to implement a chirp managed laser (CML) transmitter to reduce the effect of chirp during transmission over fibre. Both solutions propose the use of a single device placed at the network Central Office, either the upstream receiver or the downstream transmitter, to provide cost-effective solutions attractive for access networks.

Chapter 5 describes optical amplification solutions, necessary to improve the power budget of the network, focusing specifically on the upstream direction where burst-mode traffic compatibility must be ensured. Raman based amplification is investigated in a configuration that preserves the passive network structure, providing optical gain to the upstream transmission using high-power semiconductor laser pumps at the Central Office. Semiconductor optical amplifiers (SOAs) are proposed for the realisation of a pre-amplified upstream receiver which performs optical power equalisation of the incoming bursty traffic and makes use of a simple AC coupled photoreceiver.

Figures 1.6 and 1.7 present an overview of the thesis contribution in the context of the upcoming 100 G PON systems. In figure 1.6 the topics presented in each Chapter are presented in the context of their impact on PONs, where the aim is to increase the bit-rate and reach in both length and number of users. More complex modulation formats are investigated for both upstream and downstream purpose while other solutions are tailored to a specific traffic direction. In particular, EDC and optical amplification are proposed for the upstream traffic while CMLs and hierarchical modulation aim to improve the downstream performance.

Figure 1.7 shows the transceiver blocks impacted by the various solu-

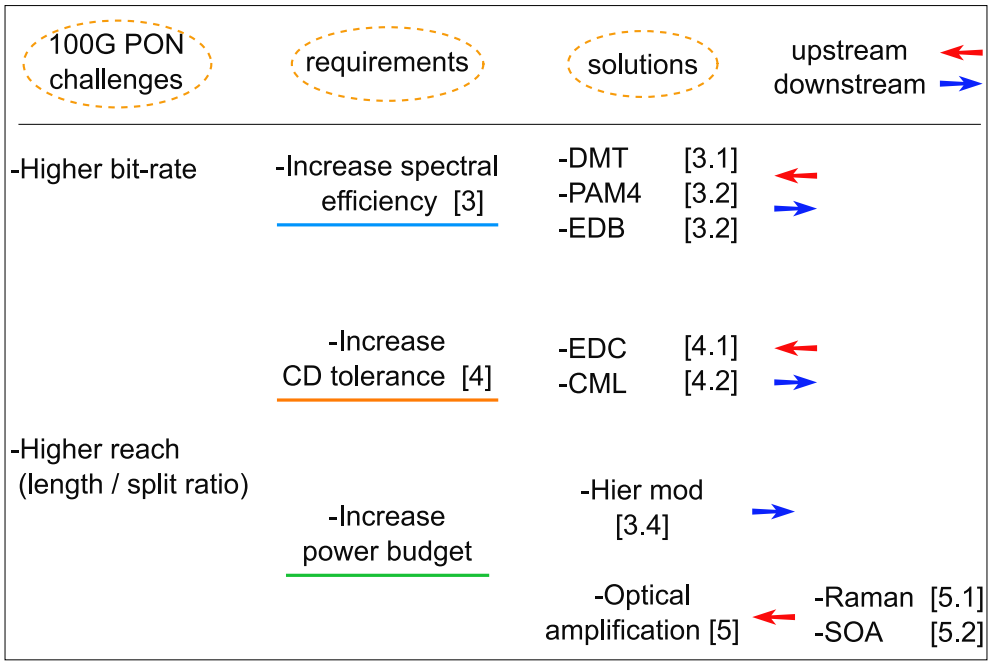


Figure 1.6: Overview of contributions presented in the thesis with relevant Sections in brackets.

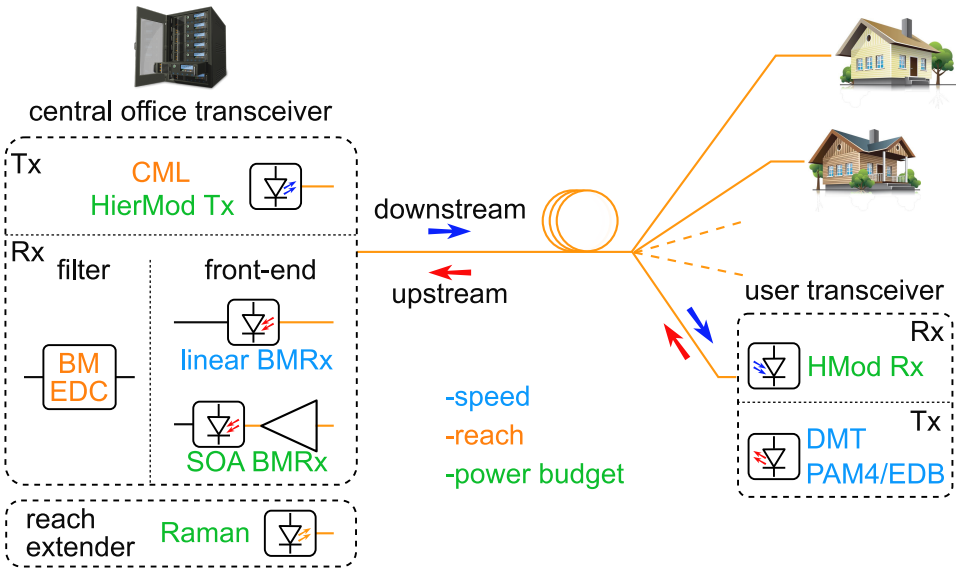


Figure 1.7: Areas of investigation in PONs addressed in this thesis.

tions proposed. The majority of the contributions focus on the Central Office transceiver since more complex technologies can be employed in this location as the cost is shared among all the network users. This transceiver could host the more expensive CML downstream transmitter and upstream burst-mode receiver, either electrically or optically implemented. To mitigate the effect of CD burst-mode EDC filtering can also be added in the same receiver. The Central Office is also the site of the Raman amplifier reach extender used for power budget extension.

2 Next Generation Passive Optical Networks

Optical access networks are a strong candidate among the technologies supporting broadband services, competing with other solutions such as copper (either twisted pair or coaxial) and wireless. The competition is mostly driven by the search for the best compromise between a cost affordable solution and its bandwidth. While copper is still largely employed, mostly because of legacy systems already in place which have been constantly modernised, it is clear that optical fibre is the only technology which will be able to support the predicted growth in bandwidth demand worldwide. This is confirmed by the observed migration towards fibre based broadband at the expense of DSL and by the high volume deployment of optical systems in developing countries instead of copper based solutions.

In this Chapter, an overview of optical access systems is given in Section 2.1 where PONs, which are the dominant technology in this segment, are presented along with a brief historical evolution of PON standards. Section 2.2 introduces the main metrics used throughout the thesis to evaluate the performance of optical communication links. The fundamental aspects of bit error rate (BER) and eye diagram are presented. In Section 2.3, the common impairments of optical communication systems are reported and in particular the ones which are more relevant to PONs. Finally, Section 2.4 presents and introduces the 100 G PON system currently under standardisation where research efforts are concentrated. The targets and main challenges in the realisation of this next generation network are discussed.

2.1 Optical access networks

Since the development of practical optical fibre communication systems, the widespread introduction of optical based broadband access has been predicted. The original vision was to replace the copper telephone lines with fibre, but that has not happened rapidly. Instead, a wide variety of architectures with deeper fibre penetration was developed where the fibre network was taken closer to the end customer, including PON-based fibre to the premises. When FTTH development began in the 1990s, both fibre and the optoelectronic components needed to operate the network were costly. This directed the majority of the work towards PON where fibre and devices are shared, and that decision is responsible for the vast majority of FTTH today being based on PON systems. PONs intrinsically have the advantage of reducing the number of transceiver at the Central Office, compared to point-to-point alternatives, which results in lower footprint and power consumption. It is interesting to note that the original motivation of sharing expensive fibre and optics is not true any more, with PON optical transceivers now available for less than $ 10 each and optical fibre having a cost similar to copper twisted pairs. What still holds is the high installation and operation cost of an extensive access network and this has been the continuing reason for the dominance of PON technologies, since they minimise the required network infrastructure and require minimal maintenance compared to copper technologies [13]. Another advantage is the intrinsic traffic aggregation that is obtained with the adoption of PONs. This simplifies the aggregation layer switch, generally Ethernet, that is located in the exchange node. As port count is always limited, with a current generation PON the number of ports of the switch matrix can be reduced, for example, by a factor of 32 or 64. The installation of this fibre infrastructure is the major cost, reaching up to 80 % of the total cost for FTTH, so it is highly desirable to reuse the infrastructure through several PON generations and possibly for more than just a single service, for example combining residential and business subscribers or mobile cell sites [14]. Since not all users are simultaneously active in a PON, the network capacity can be redistributed between the users via dynamic bandwidth allocation in order to make a more efficient usage of the available bandwidth. Statistical multiplexing

is intrinsic in PONs and thanks to this, in order to offer the same quality of service, a point-to-point network would require a higher aggregated capacity.

Access networks are now becoming optical everywhere around the globe, substituting the declining copper lines, all the way from the Central Office up to the home/building or radio antenna. FTTH increases the user bandwidth to hundreds of Mbit/s bidirectionally and does it at a similar cost to copper access since the external plant is highly simplified by deploying common PONs, powering and maintenance are avoided and it can even make local offices redundant. It is also possible to realise intermediate network solutions, where the optical fibre is not reaching the customer house but its premises. These are generally referred to as fibre to the x (FTTx) and comprise fibre to the node (FTTN), fibre to the cabinet (FTTC), FTTB and FTTH, which offer an increasing penetration of fibre. The variety of fibre based solutions offers a degree of flexibility in selecting the best trade-off between cost and performance when a network is designed in a specific area.

Several topologies of optical access networks are possible, in particular point-to-point networks, active optical switched networks and PONs (Figure 2.1). In point-to-point networks, the packet switching is performed at the Central Office and every customer is provided with an exclusively dedicated optical link. While this has the advantage of being able to deliver a high bandwidth service, it is expensive to deploy and operate because there is no resource sharing and the link costs have to be covered by a single customer. Similar solutions have been adopted for business customers with high bandwidth requirements and higher economic budget available. In active optical networks, the packet switching is relocated from the Central Office to a remote active node closer to the customer premises. This allows for partial sharing of the fibre but at the same time it introduces the need for a remote electrically powered hardened cabinet. The introduction of a remote switching node reduces the size of the Central Office switch, typically reducing the number of its ports by between one and two orders of magnitude. In PONs the active node is replaced with a passive optical splitter which does not require power supply and the management of packet-based traffic is performed at the Central Office. This provides a lean physical structure and max-

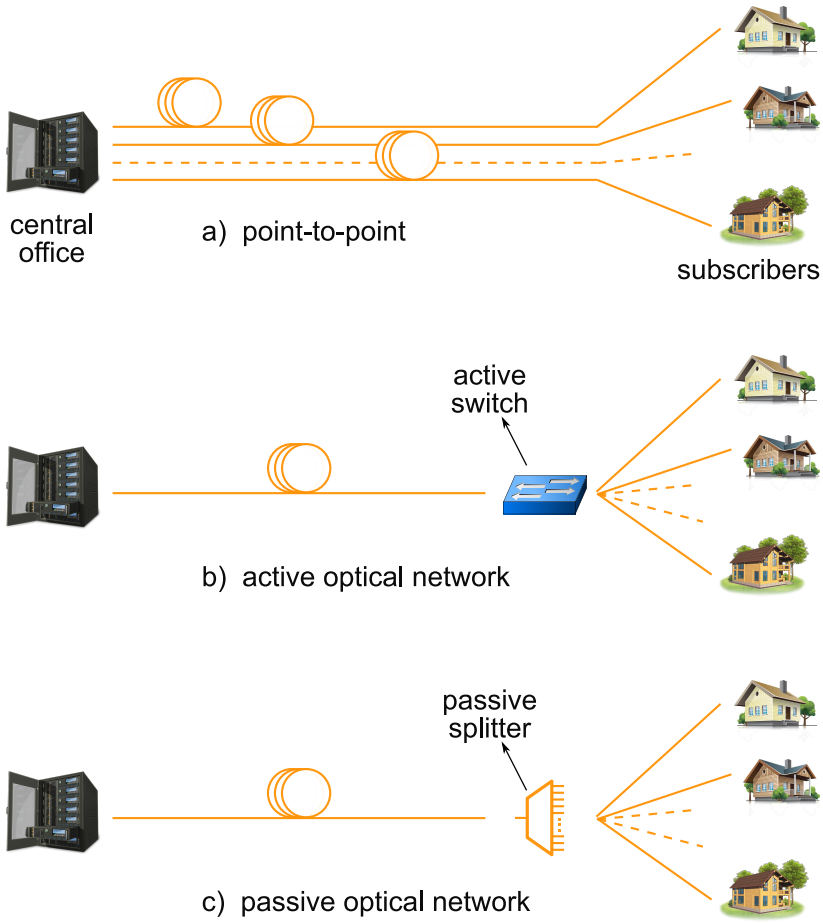


Figure 2.1: Optical access networks architectures.

imises the sharing of optical fibre and devices. All of these networks have had some successful commercial deployment, however, PONs are the preferred solution thanks to their cost-effectiveness which is derived from the efficient resource sharing [15].

PONs are point-to-multipoint networks with a tree architecture where a single Central Office, also called the optical line terminal (OLT), is connected to a node of the metro network on one side, and to multiple end customers on the other side (Figure 2.2). The PON structure offers a capillary access to the Internet network enabling end users to communicate with the metro and core links. A PON typically consists of an OLT and several optical network units (ONUs). In the simplest topology, an optical trunk line (OTL) is the single span of fibre shared among all the ONUs, at the end of which a passive optical splitter is located. The splitter distributes identical copies of the downstream signal to all the

ONUs and merges the upstream signals travelling from the users towards the OLT. Single mode fibres (SMFs) are used in the network to ensure a single-mode propagation regime and support higher physical reach than would be possible with multi-mode fibres. While a double fibre configuration is possible, downstream and upstream generally coexist on the same fibre using coarse wavelength division multiplexing (CWDM), with the two signals well spaced in frequency so that inexpensive filters can be used to separate them. A time division multiple access (TDMA) protocol is adopted to provide access to the medium to the users, with time-slots exclusively dedicated to each ONU both for the downstream and upstream. While this is not of great difficulty for the downstream, it poses more challenges in the upstream direction. In the downstream direction the entirety of the transmission is detected by every ONU, as would happen in a broadcast scenario, and proper addressing and encoding ensure that the intended payload is received and decoded by the correct ONU only.

On the other hand, in the upstream the ONUs need to be synchronised to ensure multiple transmissions are not happening during the same time slot. Each ONU must ensure that its transmitter is switched on during a limited time only and is in an off-state during the time dedicated to other users' transmissions. This type of traffic, where bursts are alternated on the same channel, is called burst-mode and requires specifically designed devices. Due to the asymmetric nature of the network and varia-

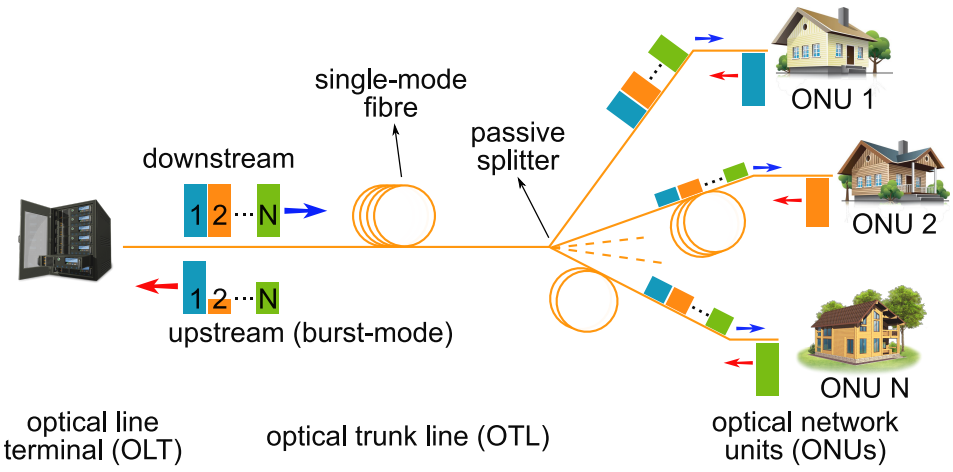


Figure 2.2: Passive optical network structure.

tion in the transmitted optical powers, the optical bursts generated from different ONUs reach the OLT receiver with a different optical power, where the difference between the most and the least energetic bursts is called the differential optical path loss. This introduces a dynamic range (DR) in the traffic, which is determined by the combination of different path losses along the network and different launched powers among the ONUs, and its maximum value is typically limited to 20 dB in PON standards. This comes from the maximum difference of 15 dB in the optical distribution network (ODN) losses and the variation in the ONU transmitter power, limited to a maximum of 5 dB. A special optoelectronic receiver, called BM-Rx, is needed at the OLT to properly decode the signal without information loss. This receiver has to adjust to different power levels as well as synchronise the phase on a burst-by-burst basis in a short period of time in order to avoid large overhead transmission, which would degrade the overall net bit-rate of the network. In order to simplify their design BM-Rxs are usually equipped with electrical limiting amplifiers, however the adoption of newer transmission technologies is driving the necessity for a linear optical-electrical interface. A novel linear burst-mode transimpedace amplifier (BM-TIA), which is a critical building block of a BM-Rx, is presented in Section 3.3 of this work and demonstrated to support an enhanced bit-rate in the upstream.

2.1.1 PON evolution roadmap

With the fibre reaching the user premises, and the bandwidth demands exponentially increasing beyond 100 Mb/s per user and much more for 4G and 5G mobile front-hauling, telecommunication operators require an unconstrained upgrade path towards a next generation of PON systems. Operators will benefit from the huge potential bandwidth of the installed fibre as only a small portion of the fibre bandwidth itself is exploited, with the limiting factor typically being the transceivers. Different upgrade strategies are being proposed by industry, standard bodies and research institutions, but the architecture is always based on a point-to-multipoint tree topology, sharing the maximum length of feeder fibre and OLT ports. For several generations of PONs, it has been a key requirement from network operators that these systems could coexist on the same fibre

infrastructure as the previous ones. As well as facilitating the wholesale reuse of the deployed fibre infrastructure, this also enables a smooth evolution of individual subscribers from one system to the next, without forced migration of all subscribers.

PON technology has gone through the standardisation of several systems from two standardisation bodies, the ITU and the IEEE. The ITU started the development of its first standard, A-PON, in 1995 which was a 155 Mb/s symmetric bi-directional transmission system. The following B-PON, G-PON and 10-Gigabit-capable passive optical network (XG-PON) were mainly driven by the progress in the underlying opto-electronics and kept a similar physical layer with progressively enhanced rates [16, 17]. Each system represented a four-fold speed increase but all of these essentially used the same TDMA system, with wavelength division multiplexing (WDM) for co-existence of upstream and downstream traffic over a single fibre splitter-based PON [13]. The latest of these single channel systems is XG-PON which has a downstream capacity of 10 Gb/s over a single channel, and 2.5 Gb/s in upstream. The IEEE variants were Ethernet passive optical network (EPON) and 10G EPON which had significant deployment in Japan and South Korea, while ITU standards have been more common in North America and Europe. Unlike the copper access systems, the upgrade of PON does not require changes to the optical fibre network infrastructure: all of the systems

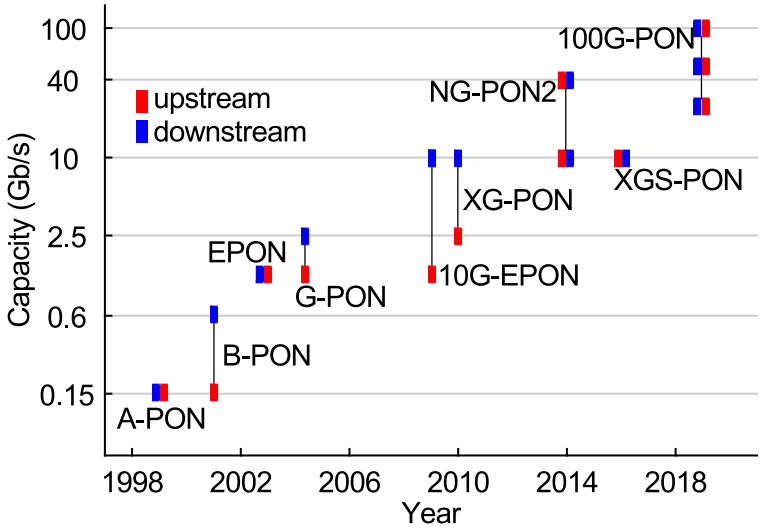


Figure 2.3: Evolution of PON standards capacities in 20 years.

have the same reach and power budget, and the bandwidth of the fibre is far wider than any other access system could use. This is important to justify the business case for fibre deployment, since it is so expensive and, therefore, must be amortised over as long a period as possible. In all likelihood, the PONs being deployed today will still be in use decades from now. This has also motivated the coexistence capability of all these systems: it is possible to operate three generations of PON system on a single system [13].

The first system to be developed beyond 10 Gb/s operation was the NG-PON 2 standard. The ITU NG-PON 2 was a big evolutionary jump from the previous systems in that it introduced multi wavelength operation in order to reach total bandwidths of 40 Gb/s [18]. This was the first standard with 4 to 8 WDM channels which uses time and wavelength division multiplexing (TWDM) channels at 2.5 to 10 Gb/s and also allows the possibility of point-to-point WDM dedicated channels. This considerably increased device complexity and raised channel crosstalk issues, as the system must keep the ONU transmissions separated in wavelength as well as time. This requires the ONU laser to be very spectrally pure and well controlled, with minimal energy in other channels, and the ONUs need to be tunable to select the desired channel. The NG-PON 2 has been an ambitious step and the development of the necessary optoelectronics did not follow quickly at an affordable cost. Research on enabling devices is still ongoing and cost reduction will happen, but it will take time. This caused an impasse, as operators have gigabit rate PONs that they would like to upgrade and are not willing to wait. This helped to motivate the latest ITU PON standard, XGS-PON, which is a symmetrical version of XG-PON with 10 Gb/s upstream and downstream [19]. This standard provides a solution to increase the bit-rate to a symmetric 10 Gb/s without the complexity of WDM operation and can respond to the operators' need for increased bandwidth while waiting for WDM optoelectronics to be available at a commercial scale.

2.2 Performance metrics

The quality of a transmission link is ultimately described by its accuracy in delivering a message, hence the number of errors that are introduced in

the original data sequence during modulation, propagation and reception of the lightwave signal is of primary concern.

2.2.1 Bit error rate

The bit error rate (BER) is used to quantify the probability of having errors in the signal and is defined as the ratio between the number of bits erroneously detected and total number of transmitted bits:

$$BER = \frac{n_{errors}}{n_{bits}} \tag{2.1}$$

In a simple binary system, with modulated symbols being 0 and 1, the BER is expressed as

$$BER = p_0 P(1|0) + p_1 P(0|1) = \frac{1}{2}[P(0|1) + P(1|0)] \tag{2.2}$$

which is the weighted sum of the probabilities for a transmitted 0 to be detected as 1, and for a 1 being detected as 0. In a binary transmission of a random or pseudo-random data pattern, $p_0 = p_1 = \frac{1}{2}$.

The BER of a signal depends on its statistical properties which are determined by noise and distortions. In a thermal noise limited scenario the noise can be described by Gaussian statistics with zero mean and variance σ^2, with normal distribution expressed as

$$f(x|mean, variance) = f(x|\mu, \sigma^2) = \frac{1}{\sigma\sqrt{2\pi}} e^{-\frac{(x-\mu)^2}{2\sigma^2}}. \tag{2.3}$$

It is useful to introduce the error function and complementary error function as follows:

$$erf(x) = \frac{2}{\sqrt{\pi}} \int_0^x e^{-t^2} dt \qquad , \qquad erfc(x) = 1 - erf(x) = \frac{2}{\sqrt{\pi}} \int_x^\infty e^{-t^2} dt \tag{2.4}$$

For a binary constellation signal affected by additive-white-Gaussian-noise (AWGN), in which I_0 and I_1 are the average photo-current for symbols 0 and 1 respectively, σ_0, σ_1 their respective noise variances, and the symbol decision threshold is set at a current I_{th} (Figure 2.4), the following expressions are obtained [20, 21]:

$$P(0|1) = \frac{1}{\sigma_1\sqrt{2\pi}} \int_{-\infty}^{I_{th}} e^{-\frac{(I-I_1)^2}{2\sigma_1^2}} dI = \frac{1}{2} erfc\left(\frac{I_1 - I_{th}}{\sqrt{2}\sigma_1}\right) \tag{2.5}$$

$$P(1|0) = \frac{1}{\sigma_0\sqrt{2\pi}} \int_{I_{th}}^{+\infty} e^{-\frac{(I-I_0)^2}{2\sigma_0^2}} dI = \frac{1}{2} erfc\left(\frac{I_{th} - I_0}{\sqrt{2}\sigma_0}\right) \tag{2.6}$$

$$BER = \frac{1}{4}\left[erfc\left(\frac{I_1 - I_{th}}{\sqrt{2}\sigma_1}\right) + erfc\left(\frac{I_{th} - I_0}{\sqrt{2}\sigma_0}\right)\right] \tag{2.7}$$

The decision current threshold I_{th} is optimal when:

$$\frac{(I_{th} - I_0)^2}{2\sigma_0^2} = \frac{(I_1 - I_{th})^2}{2\sigma_1^2} + \log\left(\frac{\sigma_1}{\sigma_0}\right). \tag{2.8}$$

In AWGN conditions at the receiver, the same noise variance is observed for both symbols, $\sigma_1 = \sigma_0$, and, hence, the last term of Equation 2.8 is null. This is because thermal noise is independent of the average photocurrent and, hence, affects in equal measure both symbols. The value of I_{th} that minimises the BER is obtained from:

$$\frac{(I_{th} - I_0)}{\sigma_0} = \frac{(I_1 - I_{th})}{\sigma_1}. \tag{2.9}$$

Introducing the quality factor Q as:

$$Q = \frac{I_1 - I_0}{\sigma_1 + \sigma_0} \tag{2.10}$$

the signal BER is then determined by the Q parameter:

$$BER = \frac{1}{2} erfc\left(\frac{Q}{\sqrt{2}}\right) \tag{2.11}$$

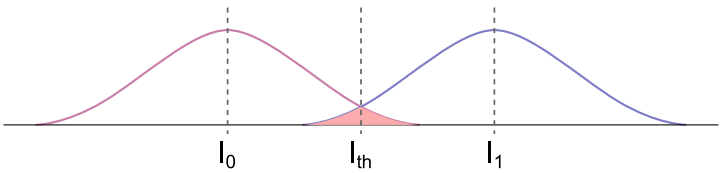


Figure 2.4: Gaussian distribution of binary symbols and decision regions.

A similar equation can be obtained for higher order amplitude modulation constellations with M equidistant symbols, such as PAM4 for $M = 4$. Under the AWGN assumption, for an average photo-current I_{avg} and with equal noise distribution σ_N for every modulated symbol, the symbol error rate (SER) results in [22, 23]:

$$SER = \frac{M-1}{M} erfc\left(\frac{I_{avg}}{\sqrt{2}\sigma_N(M-1)}\right) = \frac{M-1}{M} erfc\left(\frac{SNR}{\sqrt{2}(M-1)}\right). \tag{2.12}$$

When Gray coding is used,

$$BER \simeq \frac{1}{log_2 M} SER \tag{2.13}$$

is also valid as it is assumed that nearly all errors arise between neighbouring regions in which the encoded words only differ by one bit.

2.2.2 Eye diagram

The eye diagram is a visually intuitive instrument which provides an insight into the quality of the signal and the impairments of the transmission link [23]. An eye diagram is so called because of its resemblance to a human eye, for a binary modulation, and is obtained by superimposing multiple traces of the same signal. As a general example of how to generate an eye diagram, a long pseudo random binary sequence (PRBS) sequence, a_k, is transmitted over a channel at a frequency $R = \frac{1}{T}$. Portions of the received sequence taken at intervals $[t_1, t_1 + T), [t_1 + T, t_1 + 2T), [t_1 + 2T, t_1 + 3T), ...$ are mapped on the same interval of length T (Figure 2.5). Because of the way this is constructed, every trace of the diagram carries the information of its previous symbols in the profile of its rising or falling edge. The use of a high order PRBS sequence in particular is important to ensure that inter-symbol interference (ISI) contributions are captured in the eye diagram.

Looking at Figure 2.6 the height a of the eye diagram is an indicator of the noise immunity of the system which depends on the spacing between two symbols' average photo-currents and the noise distribution affecting them. The width b indicates the immunity with respect to phase deviations from the optimum sampling point. The histograms on the side

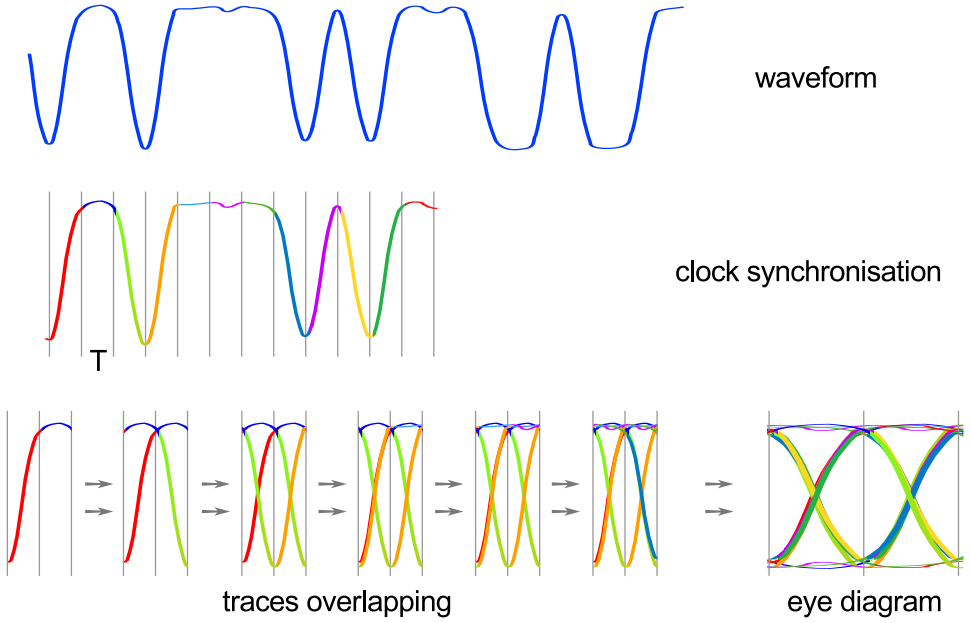


Figure 2.5: Generation of an eye diagram through superposition of delayed copies of a waveform.

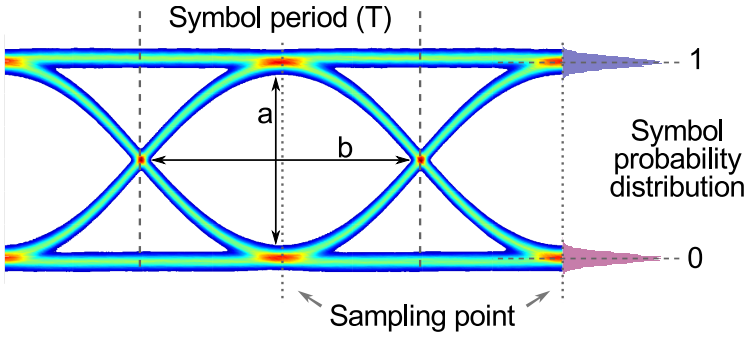


Figure 2.6: Binary eye diagram with constellation symbol distributions at the sampling point.

show the distribution of the received constellation symbols measured at the optimum sampling point.

Figure 2.7 shows eye diagrams, along with the corresponding symbols probability distribution at the sampling point, for various common impairments of optical communication links. It is easy to distinguish how the symbol's Gaussian distribution in the first example suggests the presence of thermal noise while the multiple traces obtained for bandwidth limitations and chromatic dispersion are a clear sign of ISI. In the case of electrical bandwidth limitations the eye diagram is symmetric as the slow

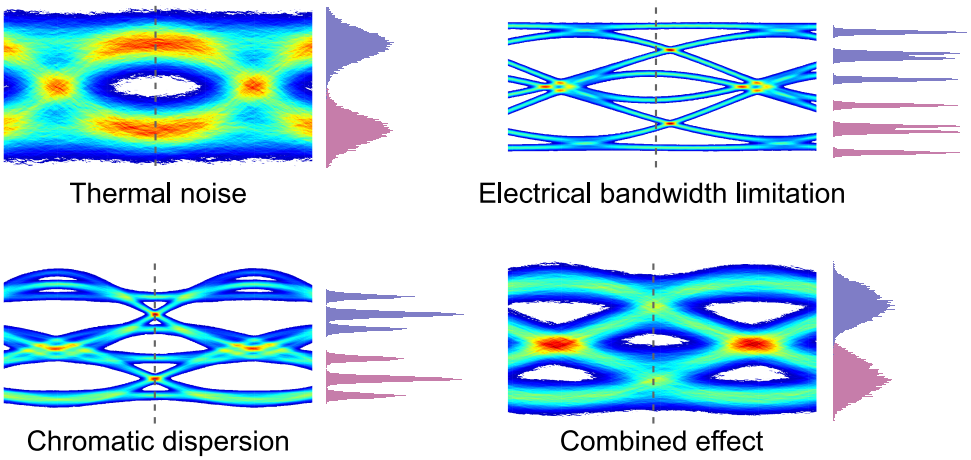


Figure 2.7: Effect of various optical link impairments on a binary eye diagram.

pulse response affects similarly the rising and falling edge of the signal. For distortions caused by chromatic dispersion instead, the eye diagram is asymmetric and more features appear on the high power symbols.

2.3 PON impairments

The required increase of bit-rate and reach of PONs poses new challenges on the physical layer design in order to meet the desired performance in a cost-effective way. Performance limitations in optical communication systems are due to both optoelectronic components and the optical fibre through which the signal propagates. In this Section the aspects most relevant to PONs are introduced and discussed while factors that have a significant impact on higher capacity systems are omitted.

2.3.1 Optoelectronics impairments

Optoelectronic devices are employed in the transceivers to achieve optical modulation, by means of either direct modulation or external modulation, and optical to electrical signal conversion at the receiver. Modulators and photodetectors determine the maximum symbol-rate that the system can achieve because of their finite bandwidth. Photodiodes introduce noise when the incident optical signal is converted into an electrical signal and this behaviour is governed by different noise mechanisms.

Optoelectronics bandwidth

The limited bandwidth of the frequency-response of the optoelectronic devices at the transmitter and receiver limits the Baud-rate of the data signal that can be supported without introduction of a high amount of ISI and the consequent degradation in performance. The bandwidth critical components in a PON are generally the electronic driver circuitry and modulator at the transmitter, the photodiode and the transimpedance amplifier (TIA) at the receiver.

Message symbols are transmitted in a sequence at a rate called the Baud-rate of the transmission, where one Baud equals one symbol per second. If the channel bandwidth is limited, as if a low-pass filter is applied, symbol pulses are spread out in time, or dispersed. A minimum interval between pulses must be ensured to avoid ISI between successive pulses. The maximum symbol rate supported in a transmission link is therefore limited by the channel bandwidth. From the Nyquist criterion, symbols may be communicated without ISI at a modulation rate of $R = \frac{1}{T}$, where T is the symbol period, provided that the channel has a bandwidth equal to at least $\frac{1}{2T}$ [23]. Optimised filter shapes can be used to ensure transmission of pulses at the Nyquist rate without ISI, however their implementation can be costly for access systems. In a practical NRZ system, the optimum receiver bandwidth required to limit the degradation introduced by ISI is $\frac{2}{3}$ of the Baud-rate, or equal to the Baud-rate for systems operating away from a thermal noise limited regime [24–26].

In optical transceivers, bandwidth limitations arise from the modulation bandwidth of the transmitter and the frequency response of the receiver. High bandwidth directly modulated lasers (DMLs) or electro-absorption modulators (EAMs) for the transmitter, and positive-intrinsic-negatives (PINs) or avalanche photodiodes (APDs) for the receiver, are more expensive, more power hungry and ensuring sufficient yield requires the development of robust fabrication processes. Also, the electronic driver and TIA circuits need to be designed with sufficient bandwidth in order to work at the desired bit-rate. Hence, the increase of signal Baud-rate might not be achievable due to the lack of availability of affordable optoelectronics and this drives the research into more spectrally compact modulation formats where more bits per symbol are

encoded. The use of multi-level modulation formats beyond binary signalling is a possible solution because at the same Baud-rate, and hence required bandwidth, these can enhance the information content of the transmission system.

Photo-receiver noise

An optoelectronic receiver detects the incoming optical signal and converts it into the electrical domain for further processing and data recovery. In optical communications such a receiver uses a photodiode to convert the incident light into a photo-current. In photodiodes the current generated is proportional to the power of the incident electromagnetic radiation, rather than its amplitude, and they are hence called square-law detectors. The linear relation between photo-current, i_P, and incident optical power, $P_{OPT_{in}}$, is expressed as:

$$i_P(t) = RP_{OPT_{in}}(t) \tag{2.14}$$

where the parameter R $[A/W]$ is called responsivity and indicates the efficiency of the light conversion process in the diode. A photodiode has both an optical and an electrical bandwidth. The former is determined by the dependence of R on the wavelength and determines the optical frequency interval in which the receiver can operate with sufficient efficiency. This is determined by the characteristics of the semiconductor material employed for the fabrication of the diode, which has a range of wavelengths where stimulated absorption occurs for a significant portion of the incident light. The electrical bandwidth is the frequency up to which the diode can generate an electrical signal proportional to the time-varying optical input power. This is described by the 3 dB cut-off of the frequency response and determines the maximum Baud-rate supported by the receiver without introducing ISI.

The most common type of semiconductor detector is the PIN photodiode in which an intrinsic region, with very light or no doping, is inserted in between a p-n junction. The name PIN photodiodes derives from the alternation of positive, intrinsic and negative doped layers in the semiconductor structure. The intrinsic region is generally wide so that the absorption of the incoming photons has greater probability of tak-

ing place in the intrinsic region rather than in the p-doped or n-doped regions. Because of the very low density of free carriers in the intrinsic region and its high resistivity, the applied bias drops almost entirely across the i-region. The high electric field across the intrinsic region ensures that the electron-hole pairs generated in the intrinsic region are separated and drift rapidly to the n- and p- contact [20, 27, 28]. The electrical bandwidth of a PIN photodiode depends on the time needed by the electron and holes to travel from the stimulated absorption region to the electrical contacts and, hence, is ultimately limited by the transit time across the i-region. The second important factor in determining the receiver bandwidth is the time constant of the electrical circuit used to process the diode photo-current, in particular its RC constant. In high-speed applications it is hence desirable for the photodiode to have small capacitance.

When the photodiode noise is taken in account the output current can be expressed as

$$i_P = RP_{OPT_{in}} + i_d + i_\nu \tag{2.15}$$

where the first of the noise terms is the dark current i_d, which is the current generated in the photodiode without any input optical power. Dark current originates from thermally generated electron hole pairs and is generally negligible in communication photodiodes compared to other noise sources. The term i_ν is the noise generated by the detector which, in a PIN photodiode, is the sum of thermal noise and shot noise.

Thermal noise

Thermal noise is generated in all resistive materials and is dependent on the temperature and electrical bandwidth of the measuring system. In a resistive material at a finite temperature the electrons are in constant random motion, colliding with each other and with atoms of the material. As each electron carries a charge, its motion produces a short impulse of current. The average value of the currents generated in this process is zero, which means there is no overall charge transport, however the large amount of electrons and collisions causes a measurable alternating component with a statistical power distribution which sums to the detected signal [29]. The thermal noise could be reduced by cooling the system or changing the resistor value, although the latter has repercussions on

the achievable bandwidth. In a photo-receiver, the load resistor adds this fluctuating current, known as thermal noise, to the photo-current generated by the diode. The variance of the thermal noise is

$$\sigma_{th}^2 = \frac{4k_B T}{R_L} B_e \tag{2.16}$$

where k_B is the Boltzmann constant, T the material absolute temperature in [K], R_L the value of the load resistor and B_e is the receiver electrical bandwidth. Taking into account only the thermal noise, the signal to noise ratio (SNR) of the detected signal can be expressed as

$$SNR = \frac{i_P^2}{\sigma_{th}^2} = \frac{(RP_{OPT})^2 R_L}{4k_B T B_e} \ . \tag{2.17}$$

When the detector operates in this thermal-noise limited regime, the SNR is proportional to the square of the incoming optical power, because the thermal noise is only dependent on the receiver temperature and bandwidth. The thermal noise in a real system is mostly determined by the characteristics of the TIA used, after the photodiode, for amplification of the photo-current.

Shot noise

Shot noise in electronic circuits consists of random fluctuations of the electric current due to the discrete nature of charged particles. It originates from the fact that an electron is generated by each incident photon, but the process happens at random times following a Poisson distribution. The random generation time of electrons in response to a constant optical signal creates a current fluctuation, called shot noise, whose variance is

$$\sigma_{sh}^2 = 2qi_P B_e \tag{2.18}$$

where q is the electronic charge $q = 1.602 \cdot 10^{-19}\ C$. Considering only the contribution of shot noise, the SNR at the detector can be expressed as

$$SNR = \frac{i_P^2}{\sigma_{sh}^2} = \frac{RP_{Opt}}{2qB_e} \ . \tag{2.19}$$

For a shot limited system the SNR varies linearly with the incident optical power, differently from the thermal noise, because the amount of shot noise generated is itself proportional to the signal photo-current.

The total noise current, ignoring the dark current, is obtained by adding the thermal and shot noise contributions and its variance is given by

$$\sigma_N^2 = \sigma_{th}^2 + \sigma_{sh}^2 = \frac{4k_BT}{R_L}B_e + 2qi_PB_e \tag{2.20}$$

from which the SNR of the signal results in

$$SNR = \frac{i_P^2}{\sigma_{sh}^2} = \frac{RP_{Opt}}{4k_BTB_e + 2qB_e} \ . \tag{2.21}$$

It can be observed that in order to obtain $\sigma_{sh}^2 > \sigma_{th}^2$ the optical input power must satisfy

$$P_{in} > \frac{2k_BT}{qRR_L} \tag{2.22}$$

and assuming room temperature conditions of $T = 300$ K, and $R = 50\ \Omega$ impedance matching, this results in a discriminant $P_{in} \simeq 1$ mW. In non amplified optical communication systems it is hence common for a receiver to be operated in the thermal noise limited regime.

Sensitivity

The noise equivalent power (NEP) of a PIN photodiode is by definition the optical input power which produces an additional output power identical to the noise power, for a certain electrical bandwidth, B_e. In this condition the SNR is equal to 1. The NEP is expressed in $\mathrm{pW}\sqrt{\mathrm{Hz}}$ and the minimum detectable power for a given receiver electrical bandwidth, B_e, is

$$P_{floor} = NEP\sqrt{B_e} \ . \tag{2.23}$$

In a thermal noise limited scenario where $\sigma_0 = \sigma_1$ and assuming negligible current associated to the constellation symbol 0 ($I_0 = 0$), the quality factor Q introduced in equation 2.10 is equal to:

$$Q = \frac{I_1}{2\sigma_0} = \frac{\sqrt{SNR}}{2} \ . \tag{2.24}$$

Using Equation 2.11, a BER estimation can then be obtained for a given NEP and B_e as a function of the received optical power, which determines the signal SNR. Assuming 50% duty cycle of the binary modulation the optical power of a modulated 1, P_{sig_1}, is twice the average incident power

P_{sig} into the photodiode. The SNR is equal to

$$SNR = \frac{P_{sig_1}}{P_{floor}} = \frac{2P_{sig}}{P_{floor}} \ . \tag{2.25}$$

The condition $I_0 = 0$, used to derive the approximate Equation 2.24, is based on the assumption that the signal has a high extinction ratio (ER). In PONs, where the ER can be lower than 5 dB, a more rigorous analysis is needed in order to take in account the not negligible power of modulated zeros.

The curve in Figure 2.8 shows the theoretical derivation of the BER as a function of the received optical power when only the effect of thermal noise is taken into consideration. For the calculations, a receiver bandwidth of 8 GHz and NEP of 25 pW$\sqrt{\text{Hz}}$ were used. The received optical power that corresponds to a specific BER, for example 10^{-3} which is a common reference value for pre-forward error correction (FEC) application, is called sensitivity and is a metric used to compare the performance of a system. The presence of additional sources of impairments in the system, for example bandwidth restrictions or CD, has the effect of requiring more optical power at the receiver side to obtain the same BER, and hence worsen the sensitivity.

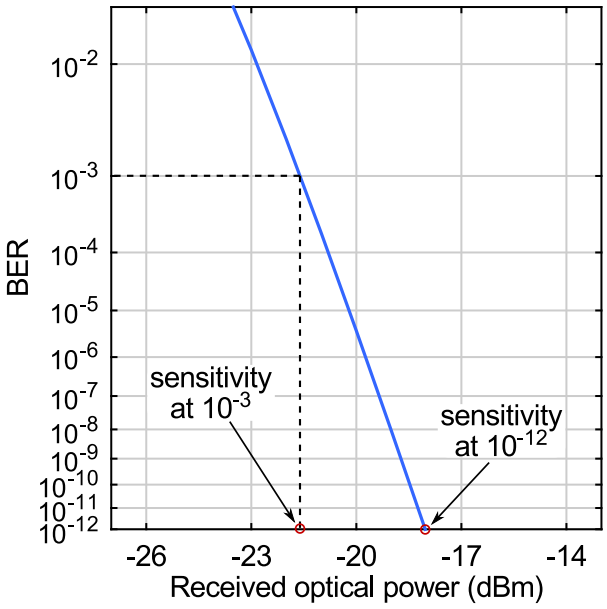


Figure 2.8: BER of a thermal noise limited 10 Gb/s NRZ OOK transmission.

2.3.2 Fibre impairments

A lightwave signal travelling through a fibre is subjected to many effects limiting the performance of an optical communication system, especially as the bit-rates or fibre distances are increased. An optical pulse propagating along a fibre is affected by both dispersive and nonlinear effects which change the shape and spectrum of the original pulse. The linear effects, which are the most relevant to PONs, are explained in more detail in this Section and a brief introduction is given to the fibre nonlinear phenomena.

Fibre attenuation

When an optical beam propagates through an optical fibre its power is reduced due to various sources of attenuation affecting the travelling electromagnetic radiation. The amplitude, $A(L)$, of a signal propagating along a fibre at the length L can be expressed as

$$A(L) = A(0)e^{-L\frac{\alpha}{2}} \tag{2.26}$$

where $A(0)$ is the electrical field at the input, for a fibre length equal to zero, and α is the attenuation coefficient. The signal optical power, $|A(L)|^2$, decreases exponentially along the fibre, as expressed by $e^{-L\alpha}$. Because of the exponential dependence, α is generally expressed in dB per length unit, and its relation to the linear attenuation coefficient is:

$$\alpha_{dB} = -\frac{10}{L} log\left[\frac{P(L)}{P(0)}\right] \simeq 4.343\ \alpha\ . \tag{2.27}$$

The fibre attenuation has both intrinsic causes, due to intrinsic properties of the silica glass, and extrinsic factors caused by material impurities and manufacturing processes.

The intrinsic attenuation is due to material absorption and Raleigh scattering [20]. Intrinsic material absorption losses are due to the electronic and vibrational resonances associated with the specific molecules. In the case of silica, electronic resonances occur in the ultraviolet region, for wavelengths shorter than 0.4 μm, where the energy of the radiation is sufficient to move electrons of the silica molecules from the valence to

the conduction band, with consequent radiation absorption. This phenomenon is negligible in the infrared region, where vibrational resonances occur instead for wavelengths above 1.6 μm. The interaction between the atomic structure and the electromagnetic field increases the vibrational energy of the former and provokes attenuation of the latter. Intrinsic material absorption for silica is lower than 0.1 dB/km in the wavelength region between 0.8 μm and 1.6 μm.

Rayleigh scattering is a loss mechanism that arises from localised microscopic fluctuations in the material density. This inhomogeneous density is caused by the random movement of silica molecules in the molten state which are then frozen in place when the glass is cooled during fabrication. The resultant microscopic density variations cause fluctuations of the refractive index at a scale smaller than the optical wavelength of the light propagating through the fibre. In such a material the light scattering takes place in the form of Rayleigh scattering. When light is scattered by particles which are very small compared to the wavelength, the ratio of the amplitude of the vibrations of the scattered and incident light varies inversely as the square of the wavelength. Hence the intensity of the light scales as the inverse fourth power, or $\alpha_R \propto \frac{1}{\lambda^4}$.

Extrinsic absorption is caused by the presence of impurities in the silica fibre introduced during the manufacturing process. The main source of extrinsic absorption is due to the presence of water vapour in the form of hydroxide ion, OH^-. The ion vibrational states cause absorption peaks at wavelengths of 0.95 μm, 1.24 μm and 1.38 μm when residual water vapour is present in silica fibre. At 1.38 μm the OH^- absorption is 48 $dB/km \cdot ppmw$ (parts per million weight), hence the need for modern manufacturing to reduce the OH^- ion concentration below 10^{-8} to lower the 1.38 μm absorption peak below 1 dB/km. Figure 2.9 shows the attenuation profile of different silica fibres in the range of wavelengths commonly employed for telecommunications and the communication windows that are commonly used, corresponding to the low absorption region of the wavelength spectrum. It can be appreciated from the graph how the fabrication process has been improved over the years to suppress the attenuation peak caused by the presence of the hydroxide ion.

Attenuation can also be induced by curvatures in the optical guide and these can be distinguished as macro-bending losses and micro-

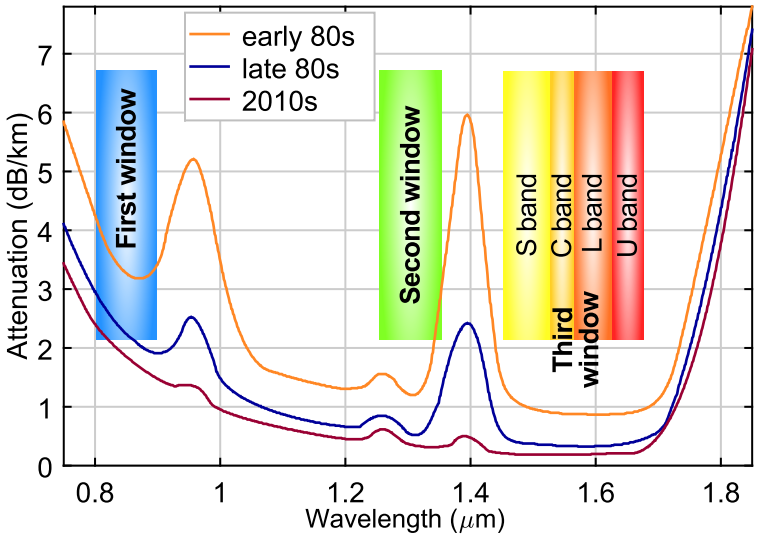


Figure 2.9: SMF attenuation profile for different generations of fibre and transmission windows used for optical communication [30].

bending losses [31]. The first occur when the fibre is bent and, as a result, the propagating mode hits the core cladding interface at an angle that does not ensure total internal reflection and generates leakage into the cladding. The macro-bending losses are proportional to the bending radius and also depend on the radiation wavelength. To avoid them care must be taken during the cabling installation phase to avoid sharp bending of the fibre. Micro-bending losses, on the other hand, are caused by small, random curvatures in the fibre which are induced during manufacturing and cabling. Micro-bending losses also transfer power from the guided modes to irradiated modes in the cladding and their magnitude increases with wavelength.

Attenuation in an optical communication system decreases the optical power reaching the receiver, thereby lowering its SNR and limiting the reach of a transmission within which the receiver sensitivity is met. In state-of-the-art fibre manufacturing attenuation coefficients below 0.2 dB/km can be achieved, in the 1.5 μm region.

Dispersion

In an optical communication system dispersion is the dependence of the group velocity on the signal wavelength, or on the propagation mode. Dispersion generally causes broadening in time of a light pulse as it

propagates along the fibre. However, with engineering of the transmitted signal, chromatic dispersion can also lead to pulse compression. The spreading out of the pulse causes ISI which introduces distortions and limits the data-rate and maximum length of the optical link. Various dispersive phenomena take place in optical fibre systems.

Modal dispersion

Multimode optical fibres have a core diameter ranging between 50 μm and 80 μm, which, at optical communication frequencies, allows the propagation of multiple modes. When in a lightwave signal travelling through a multimode fibre several propagation modes are excited, each of these modes travels at a different speed through a fibre span. The broadening of a light pulse due to different propagation speed of the modes is known as multi-path dispersion, or modal dispersion. In a multimode fibre different rays travel along paths of different lengths. As a result, these rays are dispersed in time at the end of the fibre, even if they travelled at the same speed within the silica fibre. Because different modes are associated with different light paths, the mode following the shortest overall path near the centre of the core arrives at the end of the fibre before the mode following the longer outer path. In a multimode fibre an optical pulse may comprise a significant number of modes and, hence, the potential for pulse broadening and signal degradation due to modal dispersion is considerable. A short pulse would broaden significantly as a result of different path lengths.

A multimode transmission system has to be designed in order to avoid temporal overlap of components from different propagation modes, and this heavily limits the achievable Baud-rate and/or reach. Due to the low cost and ease of connection, multimode fibres are still the choice for short reach applications where the limited length of the transmission link keeps the overall modal dispersion low. The natural way of eliminating modal dispersion is to use SMFs where the pulse propagation is limited to a single mode regime thanks to the smaller core diameter. All the analysis and experiments presented in this thesis are performed using SMFs, which are the only type of fibre employed in PONs, hence modal dispersion is not taken into account.

Chromatic dispersion

In SMF, the dimension of the core ensures that only a fundamental mode is propagating along the fibre, thereby eliminating the possible impact of modal dispersion in the channel. This provides a great advantage over multi-mode fibres, where dispersion of the propagation modes is generally the major impairment that limits the transmission distance. However, even for single mode propagation, CD causes time broadening of a transmitted pulse. CD is caused by the frequency dependence of the fibre refractive index, which means the various spectral components of a signal propagate with a different group velocity. This dispersion causes the transmitted pulses to spread in time by an amount determined by the length of fibre used. If the symbols broaden beyond their symbol period, invading the neighbouring symbols period, ISI is introduced (Figure 2.10). It is also possible, however, with the use of chirped laser at the transmitter, to achieve compression of the optical pulse propagating through a dispersive fibre.

A specific spectral component with a frequency ω propagates along the fibre with a group velocity v_g defined as

$$v_g = \left(\frac{d\beta}{d\omega}\right)^{-1} \tag{2.28}$$

where β is the propagation constant which uniquely determines a mode describing how its phase varies along the propagation direction. The frequency dependence of the group velocity causes pulse broadening because the various spectral components of the pulse do not arrive simultaneously at the fibre output, dispersing during propagation. The parameter β_2, called group velocity dispersion, determines how much an optical pulse

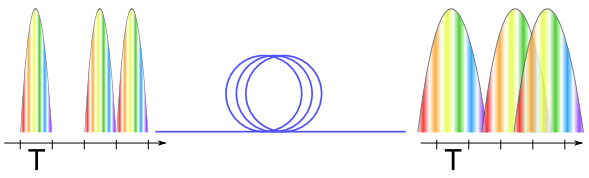


Figure 2.10: Inter-symbol interference caused by pulse spreading over dispersive fibre.

broadens during fibre propagation and is defined as

$$\beta_2 = \frac{d^2\beta}{d\omega^2} \tag{2.29}$$

which is expressed in $[ps^2/km]$. In fibre communication systems it is more common to define CD as a function of wavelength instead of frequency ($\omega = \frac{2\pi c}{\lambda}$) by introducing the parameter D:

$$D = \frac{d\beta_1}{d\lambda} = \frac{d}{d\omega}\left(\frac{1}{v_g}\right)\frac{d\omega}{d\lambda} = -\frac{2\pi c}{\lambda^2}\beta_2 \tag{2.30}$$

whose unit is $[ps/(nm\ km)]$. CD can be positive or negative, using either the parameter D or β_2. Rewriting β_2 as:

$$\beta_2 = \frac{d^2\beta}{d\omega^2} = \frac{d\beta_1}{d\omega} = \frac{d}{d\omega}\left(\frac{1}{v_g}\right) = -\frac{1}{v_g^2}\frac{dv_g}{d\omega} \tag{2.31}$$

offers a more physical interpretation of CD, observing that v_g is the group velocity. For CD to be non zero it means that v_g is dependent on the frequency and, hence, the spectral components of the signal travel with different velocities. In particular, for $\beta_2 > 0$, or $D < 0$, high frequencies have a lower propagation speed than the lower frequencies and this regime is called normal dispersion. For $D > 0$, higher frequencies have a higher group velocity and this is the common case of anomalous dispersion observed in SMF for signals above the zero dispersion wavelength, around 1.3 μm. CD is one of the most serious impairments for transmission around 1.55 μm in SMFs when the Baud-rate is increased because the same amount of pulse broadening causes heavier ISI when the symbol period is reduced. The induced ISI places a limit on the maximum distance a signal can reach without being regenerated or without using dispersion compensation techniques. CD effect is particularly evident when the transmitted signal is chirped, as it is common when employing cost-effective transmitters such as DMLs and EAMs.

The total CD is the sum of three different contributions: material dispersion, waveguide dispersion and profile dispersion. Material dispersion is caused by the dependence of the silica refractive index on the wavelength of the propagating signal. Material dispersion occurs also in a homogeneous medium and, for silica, it is positive for wavelengths above

1.27 μm and negative otherwise. Waveguide dispersion is caused by the guiding properties of the fibre which change with the signal frequency. When the frequency nears the fibre cut-off frequency the propagating mode tends to irradiate in the cladding. On the other hand, for increasing signal frequencies the mode is confined in the core. This means the structure of the propagating mode, and consequentially its propagation constant, is dependent on the signal frequency. In the telecommunication windows region, waveguide dispersion is always negative for SMF but the index profile can be engineered to create fibre with shifted zero-dispersion. Profile dispersion is again caused by the frequency dependence of the refractive index. The refractive index varies differently for core and cladding because of their different doping. As a result, signals at different frequencies experience a different index-profile between core and cladding. This dispersion is, however, negligible in SMF when compared to the two described above.

The CD effect does not disappear completely when operating at the zero dispersion wavelength as the pulse still broadens due to higher order dispersive effects. It can be intuitively noted that D cannot be null for all the frequencies of the pulse spectrum. The higher-order dispersive effects are dependent on the dispersion slope S [20]

$$S = \frac{dD}{d\lambda} \tag{2.32}$$

also called the differential dispersion parameter. This also plays an important role in WDM systems where different channels experience a different amount of CD and simultaneous compensation for all channels becomes more difficult. Higher-order dispersion effects did not play a relevant role in this thesis and hence are not discussed further.

Polarisation mode dispersion (PMD)

A single mode fibre, despite the name, is not truly single mode because it can support propagation of two degenerate modes polarised in orthogonal directions. In ideal optical fibres, these two modes have identical propagation properties and are indistinguishable. In reality, however, fibre birefringence, which is the difference in refractive index experienced by light in different polarisation modes, causes the two polarisation modes to become slightly non-degenerate. The two polarisation states, propa-

gating in the x- and y-directions respectively, are called principal states of polarisation and they are characterised by different mode propagation constants. Birefringence is caused by minute waveguide asymmetries either due to intrinsic perturbations, for example manufacturing imperfections that cause non-circular geometry of the core, or extrinsic perturbations such as pressure, vibrations, bending and temperature variations. In conventional single-mode fibres, birefringence is not constant along the fibre but changes randomly, both in magnitude and direction, because of variations in the core shape (elliptical rather than circular) and the anisotropic stress acting on the core. PMD is a source of pulse broadening caused by fibre birefringence. If the input pulse excites both polarization components it becomes broader as the two components disperse along the fibre because of their different group velocities. In other words, the PMD resulting from fibre birefringence leads to fast and slow modes of propagation and, consequently, to dispersion.

The extent of pulse broadening can be estimated from the time delay occurring between the two polarisation components of the optical pulse for a given length L. However, in real optical fibres, the birefringence changes randomly along the fibre and these changes tend to average the propagation time for the principal states of polarisation. PMD can hence be characterised by a root mean square value obtained by averaging the random perturbations which is proportional to $\sqrt{L}$. Because of the $\sqrt{L}$ dependence, PMD induced pulse broadening is relatively weak compared to the broadening caused by CD.

PMD can become a limiting factor at higher Baud-rates, for example 40 GBd or higher, or in systems designed to operate near the zero-dispersion wavelength of the fibre over long distances. All the experimental results presented in this thesis were carried out at either bit-rates or transmission distances not high enough to allow PMD to become a limiting factor in comparison to other impairments such as CD.

Nonlinear effects

Nonlinear effects are phenomena dependent on the intensity of the electromagnetic field under consideration. In optical fibres nonlinear responses of the silica become significant for intense electromagnetic radi-

ations and are due to changes of the refractive index with the optical intensity or inelastic scattering phenomena.

Stimulated Brillouin scattering (SBS)

SBS causes a loss of power of the incident wave which is governed by an intensity dependent attenuation constant. The intensity of the scattered light grows exponentially with the power of the optical signal. The scattering of an incident photon interacting with the dielectric medium results in the emission of a photon with lower energy, while the energy difference is released in the form of a phonon. SBS is a narrow band effect with a typical bandwidth of 50 MHz compared to signals operating in the terahertz range. The physical process underpinning SBS is the tendency of materials to compress in the presence of an electric field. As a result, an oscillating electric field generates an acoustic wave at a certain frequency which modulates the refractive index of the fibre. The resulting periodic variation behaves similarly to a Bragg grating causing back-reflections of the incident beam. The virtual grating moves with a certain acoustic velocity that depends on the material of the medium, and in silica fibres it causes a shift of approximately 11 GHz at 1.55 μm between the original and reflected signals. Because of its mechanism the scattering only takes place in the backward direction. A common method to suppress SBS is to inject a lightwave signal with a large optical bandwidth. This broadens the Brillouin gain spectrum and, accordingly, reduces the peak gain, hence the scattering becomes significant only at higher signal powers. In PONs, where it is common to employ DML transmitters, which have a broad demission spectrum, SBS is usually not relevant.

Stimulated Raman scattering (SRS)

SRS is also an inelastic scattering but is caused by the interaction between the vibrational states of the atoms in the medium and the incident optical signal. A portion of the photons propagating through the fibre excites the atoms to higher energy vibrational states. This results in the emission of a lower energy photon whereas the remaining energy is absorbed by the silica glass molecules' excited vibrational state. The SRS effect occurs in both co- and counter-propagating directions in optical fibre. The vibrational energy of the silica determines the bandwidth and optical shift of the Raman effect which extends over a much larger

frequency range of more than 20 THz, with two peaks at 13 THz and 15 THz [20]. SRS effects are generally negligible in single wavelength PON systems which operate at relatively low power. However, when multiple PON systems are co-existing on the same optical fibre, Raman effects can cause modulation crosstalk between the signals and power depletion of the signals at shorter wavelengths. Some mitigation techniques have been taken in consideration for similar scenarios in the NG-PON 2 standard, where there are consideration on Raman crosstalk between G-PON and ngpon2 downstream [18]. SRS is treated in more detail in Section 5.1 of this thesis, where it is exploited as the mechanism underpinning Raman optical amplifiers.

Kerr nonlinearities

The refractive index of silica is generally assumed to be power independent in the description of optical fibre communication systems. In reality, at high intensities the refractive index of the material increases with intensity, which means the phase delay gets larger when the optical intensity increases. High power densities are not uncommon in optical fibre communication systems due to the small area of the optical fibre core where modes are confined, even if the absolute powers are in the range of tens of milliwatts. The variation of the refractive index of the medium with the optical power is known as the Kerr effect and is responsible for different effects, depending on the type of input signal.

Self-phase modulation (SPM) is a nonlinear phase modulation of a beam that is caused by its own intensity. This happens because, due to the intensity dependent variations in the refractive index, optical power oscillations in the signal are converted into phase fluctuations. In this way an optical pulse acquires a temporally varying instantaneous frequency, known as chirp. The chirp induced by SPM affects the pulse shape and often leads to additional pulse broadening during fibre propagation. SPM is, generally, not relevant in PONs because the launched power is limited, but it would need to be taken in account if considering DMLs, or optically pre-amplified transmitters, capable of emitting in excess of +10 dBm.

Cross-phase modulation (XPM) is another nonlinear impairment caused by the Kerr effect which occurs when multiple optical channels are propagating simultaneously along the same fibre. In such conditions the

nonlinear phase variation of a specific channel does not solely depend on its own power (SPM) but also on the power of the other optical channels. XPM becomes particularly significant in WDM systems where the total phase shift depends on the powers in all channels and varies from bit to bit, depending on the bit pattern of the neighbouring channels. For this reason XPM can potentially impose greater limitations than SPM in WDM systems since a significant number of channels can contribute to generate the phase fluctuations. The phase shift induced by XPM can occur only when two pulses overlap in time, however pulses in different wavelength channels travel at different velocities. The difference in velocity depends on the channel spacing and, hence, neighbouring channels have a greater impact than widely separated channels. This makes it difficult to estimate the impact of XPM and so a numerical approach is generally used to investigate its effect. In WDM PON systems, NG-PON 2 in particular, where the channels are closely spaced at 100 GHz, XPM could be significant if using high-power transmitters.

Another consequence of the Kerr effect relevant to WDM systems is four-wave mixing (FWM). When two or more signals at different wavelengths propagate along a fibre FWM can lead to the generation of new frequency components. The signals create an oscillation of the total intensity with a frequency which is due to beating of the channels and modulates the refractive index of the fibre. This beating creates additional signals at new frequencies which are a combination of sums and differences of the channels frequencies, and this comes at the expenses of the power of the original signals. FWM requires the channels to be phase-matched and, hence, it often occurs near the zero dispersion wavelength of a fibre. In the IEEE 100G-EPON, where the O-band transmission window was selected, a channel spacing of 800 GHz was chosen in order to mitigate phase matching of the signals. However, FWM could be significant for signals across the zero dispersion wavelength of the fibre and operation outside of the zero dispersion window was recommended.

The nonlinear effects caused by the Kerr effect have negligible or no impact in the experiments conducted in this thesis and, hence, are not discussed further. However, their investigation could be of significant interest for next-generation PON systems.

2.3.3 Optical amplification

Optical amplifiers are a fundamental element in optical communication systems as they offer a solution to greatly increase the span of a fibre link without the need for costly optical-electro-optical regeneration of the signal. Optical amplification compensates for the fibre attenuation directly in the optical domain increasing the intensity of the optical signal and, remarkably, does so irrespective of the specific modulation format or symbol-rate adopted. This means that a link with optical amplification can be upgraded without replacement of the amplifiers, unlike a system with in-line signal regeneration.

An optical amplifier is generally formed by an active medium, which provides gain to the incoming electromagnetic radiation, and a pump source, either optical or electrical. The amplifier can be thought of as a two-level energy system where the pump provides energy to move carriers to an excited energy state from where they are then transferred to the incident signal, at the ground energy state, increasing its optical intensity. Various solutions are available to achieve optical amplification, the most important of which are erbium doped fibre amplifiers (EDFAs), SOAs and Raman amplifiers. Each one of them has advantages and disadvantages compared to the others and could fit better for particular applications, depending on the target costs, performance and physical footprint. Further details on SOAs and Raman amplifiers are provided in the respective Sections of Chapter 5 of this work, where they have been employed to extend the reach of PONs.

Gain saturation

Gain saturation is a phenomenon that originates from the dependence of the amplifier gain, G, on the input power of the signal being amplified, $P_{S,in}$. When this becomes comparable to the amplifier saturation power, P_S, the gain is reduced and, hence, the amplification factor decreases with an increase in the input signal power. The amplifier gain is defined as the ratio between the output and input power of the signal

$$G = \frac{P_{out}}{P_{S,in}} \ . \tag{2.33}$$

The power of the signal propagating through the amplification medium can be expressed as

$$P(z) = P_{S,in}e^{gz} \tag{2.34}$$

where g is the material gain and from which the following holds

$$\frac{dP(z)}{dz} = gP(z) \ . \tag{2.35}$$

The material gain, g, can be expressed as a function of P_S and the small signal gain g_0 [20]

$$g = \frac{g_0}{1 + \frac{P}{P_S}} \tag{2.36}$$

and hence

$$\frac{dP(z)}{dz} = \frac{g_0 P(z)}{1 + \frac{P}{P_S}} \ . \tag{2.37}$$

By integrating this equation over the amplifier length the following relation for the large-signal amplifier gain is obtained:

$$G = G_0 e^{\left(-\frac{G-1}{G}\frac{P_{out}}{P_S}\right)} \ . \tag{2.38}$$

The equation shows that the amplification factor G decreases from its unsaturated value G_0 when P_{out} becomes comparable to P_s. A useful metric commonly used is the output saturation power, which is defined as the output power for which the amplifier gain is reduced by a factor of 2, or 3 dB, from its unsaturated value G_0.

Raman amplifiers, which are addressed in Section 5.1 of this thesis, are generally not affected by significant saturation in power regimes typical of PONs due to the high pump powers used and negligible pump depletion.

On the other hand, SOAs, employed in Section 5.2, suffer from carrier depletion induced saturation. When working in the saturation regime the SOA behaviour becomes nonlinear causing a number of effects to occur including SPM, XPM, FWM, cross-gain modulation, and self-gain modulation. The latter is the only effect of interest in this thesis and is discussed in Section 5.2. When an SOA amplifies a high intensity modulated signal, self-gain modulation can lead to a serious waveform

distortion commonly referred to as patterning. Under these conditions, an SOA behaves as a nonlinear element due to carrier depletion induced saturation. Equations 2.37 and 2.38 offer a simplified description of an SOA and are not sufficient to investigate its non-linear effects. More comprehensive models have to be adopted in order to take in account those phenomena.

Optical noise

Optical amplifiers unavoidably add amplified spontaneous emission (ASE) noise to the signal they amplify. ASE is generated in the optical range where the active medium used can provide gain and, hence, is generally much broader than the signal bandwidth. While the out-of-band ASE, which is the noise in a wavelength region different from the signal one, can be suppressed with appropriate optical filtering, the ASE in the signal bandwidth cannot be separated from the signal. This is the noise added by optical amplifiers to their output signal, which causes degradation of the optical signal to noise ratio. The power spectral density of the ASE, S_{ASE} [W/Hz], can be expressed as [20, 27]

$$S_{ASE} = n_{sp}(G-1)h\nu \tag{2.39}$$

where n_{sp} is a dimensionless parameter larger or equal to unity called the spontaneous-emission factor, G is the amplifier gain, h is Planck's constant and ν is the signal optical frequency. For an ideal amplifier, $n_{sp} = 1$ but, in practical applications, it is generally higher [32]. The ASE power depends on the optical bandwidth B_o where it is measured and, assuming a flat spectrum for S_{ASE}, is related to it by

$$P_{ASE} = 2S_{ASE}B_o \tag{2.40}$$

where the factor of 2 is due to the fact that the spectral density is expressed per mode and, in a SMF, there are two polarisation modes.

The OSNR of an optical signal is by definition the ratio between the signal power and the ASE optical noise power. Using Equation 2.40 the

OSNR can be expressed as

$$OSNR_{out} = \frac{P_{S,out}}{P_{ASE}} = \frac{P_{S,out}}{2S_{ASE}B_o} = \frac{GP_{S,in}}{2n_{sp}(G-1)h\nu_S B_o} \tag{2.41}$$

with $P_{S,in}$ and $P_{S,out} = GP_{S,in}$ the signal input and output power of the amplifier, respectively. To quantify the amplifier impact on the signal OSNR the noise figure (NF) parameter is used, defined as the ratio between the input signal OSNR and the output signal OSNR:

$$NF = \frac{OSNR_{in}}{OSNR_{out}} \tag{2.42}$$

If the signal input is assumed to be only affected by quantum noise fluctuations and using $OSNR_{out}$ as obtained above, the NF results as [33]

$$NF = \left(\frac{P_{S,in}}{h\nu_S B_o}\right)\left(\frac{GP_{S,in}}{2n_{sp}(G-1)h\nu_S B_o}\right)^{-1} = 2n_{sp}\left(\frac{G-1}{G}\right) \tag{2.43}$$

Assuming $G \gg 1$, the above expression gives $NF \approx 2n_{sp}$ which, in an ideal scenario where $n_{sp} = 1$, results in $NF = 2 \approx 3\ dB$, which is the theoretical performance limit. This means in practice that an optical amplifier degrades the OSNR by at least 3 dB.

ASE beat noise

An optical amplifier can be used in front of a photo-receiver to amplify the optical signal incident on it. By increasing the intensity of the optical signal the thermal noise of the photodiode becomes negligible and the performance of the receiver is improved. Optical amplification degrades the signal OSNR because of the incoherent ASE generated in the process. When a signal with limited OSNR is detected by a photodiode this generates currents due to the signal and ASE components beating. The photo-current is proportional to

$$i_P(t) \propto |E_S(t) + E_{ASE}(t)|^2 = |E_S(t)|^2 + 2Re[E_S(t) \cdot E^*_{ASE}(t)] + |E_{ASE}(t)|^2 \tag{2.44}$$

where E_S and E_{ASE} are the electromagnetic field components of the signal and the ASE, respectively. In Equation 2.44 E_{ASE} includes only the ASE components co-polarised with the signal which are contributing

to the noise, because the orthogonally polarised component cannot beat with the signal [20, 27]. The first term of the right side part of the equation is proportional to the signal power and has a non zero average. The second term, with zero average, generates noise due to the beating of signal and ASE. The third term generates both shot noise from the ASE and noise due to the beating of the ASE spectral components. The three noise components due to ASE have the following variances for signal-ASE beating, ASE shot noise, and ASE-ASE beating noise respectively [32]:

$$\sigma^2_{S-ASE} = \frac{4B_e}{B_o}(RP_S)(RP_{ASE}) \tag{2.45}$$

$$\sigma^2_{ASE,sh} = 2qB_e(RP_{ASE}) \tag{2.46}$$

$$\sigma^2_{ASE-ASE} = \frac{B_e}{B_o^2}(2B_o - B_e)(RP_{ASE})^2 \tag{2.47}$$

where B_e is the electrical bandwidth of the receiver and B_o is the optical bandwidth of the optical filter used between the amplifier and photodiode. It is assumed that $B_e \leq \frac{B_o}{2}$. Expressing P_{ASE} as [20, 27, 32]

$$P_{ASE} = (G \cdot NF - 1)h\nu_S B_o \approx G \cdot NFh\nu_S B_o = GP_{ASE,in} \tag{2.48}$$

with $P_{ASE,in}$ the equivalent input power of the ASE into the amplifier, and similarly $P_S = GP_{S,in}$, the above equations can be reformulated as

$$\sigma^2_{S-ASE} \approx 4B_e(h\nu_S)(RG)^2 P_{S,in}NF \tag{2.49}$$

$$\sigma^2_{ASE,sh} \approx 2qB_eB_o(h\nu_S)(RG)NF \tag{2.50}$$

$$\sigma^2_{ASE-ASE} \approx B_e(2B_o - B_e)(h\nu_S)^2(RG)^2NF^2 \tag{2.51}$$

In conditions where $G \gg 1$ and $P_{S,in}$ is significantly higher than $P_{ASE,in}$, the signal-ASE beat noise, σ^2_{S-ASE}, is the dominant contribution. However, if proper optical filtering is not performed after the amplifier and the value of B_o increases, $\sigma^2_{ASE-ASE}$ can become the principal source of impairment [20, 32].

2.4 Route to 100G PON

In order to respond to the increase in bandwidth demand higher capacity PONs beyond NG-PON 2 are being studied and standardised. Currently the IEEE is in the process of standardising transmission at 25 Gb/s per wavelength that could be used to create a single-channel 25G PON, or even a multichannel 50G or 100G PON system [11]. Wavelength multiplexing 4 channels with a bit-rate of 25 Gb/s has been identified as the cost-effective approach to achieve an aggregated 100 Gb/s PON system.

2.4.1 Enhanced bit-rate

The optoelectronic components to realise an NRZ single-wavelength 25 Gb/s channels require high bandwidth and their cost represents a limit to their adoption [34]. It is hence desirable to use 10 G devices which are cheaper and readily available for high volume production even for the enhanced bit-rates of 25 Gb/s. NRZ transmission at 25 Gb/s can be achieved using 10 G optoelectronic components but that is possible only using intense digital signal processing (DSP) in the transceiver to compensate for the lack of bandwidth as shown in many recent works [35–42]. Other approaches improve the transmitter frequency response, making use of additional optical components which increase the complexity and cost of the network [43, 44].

An alternative solution to achieve 25 Gb/s data modulation with 10 G devices is to use more advanced modulation formats to avail of their higher spectral efficiency. While a minimum amount of DSP is needed for the conversion of a data stream from binary to a higher modulation order, they can achieve 25 Gb/s without pre- or post-compensation techniques, either optical or DSP based. The most promising modulation formats are PAM4 and EDB which have constellations of limited complexity but offer a two-fold improvement in spectral efficiency [34, 42, 45–55].

More DSP hungry modulation formats can also be employed such as DMT which can achieve a higher spectral efficiency than PAM4 and EDB [50, 56–62]. However, the implementation of a 25 Gb/s channel DMT requires more complex DSP than PAM4 or EDB, hence, high speed analog to digital converters (ADCs) and digital to analog con-

verters (DACs) are required in the transceiver, and also needs a linear channel. While this is a limit for 25 Gb/s channels, the advantage of DMT is that it is possible to scale the bit-rate on the same physical network without significant increase of the computation complexity of the DSP, reaching 40 or 50 Gb/s with 10 G devices. The same bit-rates can be achieved with PAM4 or EDB but only by adopting intense DSP for pre- and post-compensation and adding ADCs and DACs in order to have a linear electro-optical and optical-electrical interface [62–70]. Hence, for single channel rates higher than 25 Gb/s using 10 G optics, the likelihood of adoption will be determined by the cost, power consumption and availability of ADCs and DACs not only for DMT but also for PAM4 and EDB as the DSP requirements are similar. For such applications DMT could then offer the advantage of lower electronic Baud-rates as well as higher flexibility and software reconfigurability at a similar cost. This means that, if the cost of optoelectronic devices will remain an obstacle to the increase of single-lane bit-rate, DMT could play an important role in the implementation of 40 and 50 Gb/s channels. In Section 3.1 of this work a DMT modulation scheme is demonstrated to enable 10 Gb/s transmission employing a 1 GHz bandwidth limited transmitter thanks to the improved spectral efficiency.

For the upstream transmission the availability of a linear BM-Rx is a key requirement in order to support the adoption of multi-level modulation formats and/or electronic compensation techniques which need a linear copy of the received optical waveform. Linear BM-Rxs have been demonstrated operating with NRZ modulation at 10 Gb/s [71–74] but similar devices are not available yet as commercial products. For higher rates of 25 Gb/s, binary [75] and multi-level BM-Rxs [76, 77] have been reported but, do not provide a linear optical-electrical signal conversion.

In this thesis simple multi-level modulation formats, PAM4 and EDB, are analysed for the realisation of 100 G (25 Gb/s $\times$ 4λ) PON systems based on 10 G optoelectronic devices. A linear 10 G BM-Rx is also demonstrated with the use of PAM4 in order to reach a bit-rate of 25 Gb/s and support electronic equalisation thanks to the receiver linearity [54]. The IEEE 100G-EPON standardisation body recently decided to use 25 Gb/s NRZ transmitters, with either binary or duobinary detection to allow for 10 G receivers to be used [78]. The choice of using

a transmission window in the O-band could leverage the high volume data-centre devices, helping with the cost reduction of high bandwidth components.

2.4.2 Chromatic dispersion tolerance

The main challenges encountered in increasing the transmission bit-rate beyond 10 Gb/s are the decreased CD tolerance and, consequently, reduced fibre reach, as well as the reduction in optical power budget due to the higher minimum received optical power required. Chromatic dispersion can be addressed with optical or electronic post-compensation at the receiver, as well as with pre-compensation techniques at the transmitter. Optical post-compensation, which makes use of dispersion compensating fibre (DCF) or fibre Bragg gratings (FBGs), is effective but requires bulky components and also has to be dimensioned to every specific link to perform at its best, making it unsuitable for burst-mode networks with an asymmetric physical structure. Electronic compensation, on the other hand, can provide reduced footprint, high flexibility and can leverage the progress in complementary metal-oxide-semiconductor (CMOS) based DSP technology with potential advantages both in terms of costs and scalability. In this thesis both an electronic post-compensation and an optical pre-compensation technique are proposed to extend the reach of a 25 Gb/s single channel transmission. The electronic post-compensation is tailored to burst-mode application, while the optical solution is designed for downstream transmitters which could have additional complexity while still preserving a small form factor. In the upcoming 100G-PON standard, the O-band was identified as the preferred transmission window to avoid complications due to CD [78]. This eliminates the need for dispersion compensation at 25 Gb/s, but problems may arise due to FWM.

2.4.3 Power budget

The use of higher bit-rate transmission results in a higher optical power needed at the receiver to correctly decode the information sent because of the decreased SNR, or higher SNR requirements. In addition the wavelength selective components, which are necessary to operate a wavelength

multiplexed network, cause additional insertion losses. Hence, to meet the power budget requirements of the legacy PON systems, it becomes necessary to introduce optical amplification [78]. In the downstream direction a transmitter booster amplifier could be used to increase the fibre launched power, thus employing a single downstream amplifier and avoiding the adoption of multiple, costly, pre-amplified receivers in the ONUs. For the same reason, in the upstream, a pre-amplified solution is preferable because it can share the cost of a single amplifier among all the users, instead of providing every ONU with a high-power optically boosted transmitter. The challenge for the upstream pre-amplifier is the compatibility with the incoming burst-mode traffic which could lead to envelope transients or saturation of the amplifier if not properly designed. Optical amplification strategies are investigated in this thesis for the upstream traffic to enhance the power budget when the single channel bit-rate is increased to 25 Gb/s. Burst-mode capable solutions are designed, making use of either Raman amplification or SOAs.

2.5 Summary

This Chapter reviews the recent trends in optical access networks highlighting the currently ongoing shift towards optical fibre based networks mostly based on the cost efficient PON architecture. The major impairments and challenges encountered in the standardisation of higher capacity optical access networks are discussed.

Section 2.1 describes the architecture of PON systems and provides a brief history of the relevant standardisation activity. The structure of a PON is based on a tree topology point to multi-point architecture where a single Central Office provides connection between a core/metro node to the end customers. Fibre networks based on PON technology are gradually replacing copper cables in access networks thanks to their superior performance and comparable costs. In the past decades the evolution of PON systems was mostly driven by technological advances in the supporting optoelectronic devices, which enabled enhanced bit-rates over a similar network topology. Recently, because of the challenges of developing affordable optics for operation beyond 10 Gb/s, WDM systems have been, or are in the process of being standardised.

In Section 2.2 the BER and the eye diagram, important metrics commonly used to measure the quality of a transmission link, are described. Both are used extensively in the presentation of experimental results throughout this thesis.

Section 2.3 describes the major impairments of optical communication systems, in particular focusing on PONs. The bit-rate increase is limited by the reduced bandwidth of available optoelectronic devices such as DMLs, externally modulated transmitters (EMLs) and photoreceivers. The photoreceiver also adds noise to the signal, in the form of thermal-noise or shot-noise, depending on the operating regime. The propagation of a signal through an optical fibre causes both attenuation, which has to be accounted for in the power budget, and CD which limits the maximum reach of a communication system because of the resultant ISI. Optical amplification can be used to extend the network reach but causes degradation of the OSNR due to the amplifier spontaneous emission noise, which is unavoidably added to the signal. When an optically pre-amplified receiver is used additional sources of noise have to be accounted for, the dominant of which is generally the signal-ASE beating noise.

Section 2.4 discusses the ongoing activities towards the definition of 100 Gb/s optical access systems. The 100 Gb/s PON system currently under study will be enabled by wavelength multiplexing of 4 channels providing a 25 Gb/s bit-rate each. The challenges in the realisation of these higher bit-rate PONs are due to the bandwidth limitation of the optoelectronic devices and more advanced modulation formats can be adopted as a solution. The network reach is limited by CD impairments which are more severe at higher Baud-rates and for more complex modulation formats. The power budget restrictions also come from the higher required optical power at the receiver and the additional insertion losses of wavelength selective components which are necessary for multi wavelength networks.

3 Advanced Modulation Formats in Passive Optical Networks

In the vast majority of deployed PON systems, the optical modulation format of choice is on-off keying (OOK) NRZ due to its inherent simplicity which allows the usage of simple electronic interfaces in the transceivers, such as a two level electrical driver at the transmitter and a single threshold detector at the receiver. However, as seen in Chapter 2, in recent years the price of higher performance optoelectronic components has become prohibitive for the cost-constrained scenario of the access market while DSP, that is based on the well-established CMOS technology, is becoming more affordable. Hence, a notable research effort has gone into the improvement of data-rates so that they can still be supported by the current generation of commercial optoelectronic devices when combined with DSP [34, 45–47, 62]. In a simple NRZ modulated system, linearity is not a strict requirement hence the specification of the devices can be relaxed. This Chapter discusses the basics of higher order modulation formats and their potential application in PON systems, addresses the consequent need for component linearity to support these more advanced modulation formats and proposes a solution to mitigate the effects of the power budget reduction due to the increased SNR requirements.

Initially, Section 3.1 reports on experimental results of DMT modulation, a multi-carrier technique that offers the advantages of encoding multiple bits per symbol, using complex constellations with in-phase and quadrature components, but at the same time suitable for IMDD transmission links. DMT is demonstrated as an option to extend the bit-rate of 1 GHz G-PON components up to 10.4 Gb/s, suitable for XG-PON systems.

In Section 3.2, other modulation formats are addressed, in particular

PAM4 which is a multi-level amplitude modulation technique and partial response signalling or EDB. These modulation formats have higher spectral efficiency than NRZ and also have the advantage over DMT of simpler implementation regarding the electrical components. Even though PAM4 and EDB have higher bandwidth occupancy than DMT, in this work they are demonstrated as a viable and cost-effective way to reach 25 Gb/s with the 10 G generation of optical devices.

The focus of Section 3.3 is then shifted towards the required devices with preliminary results obtained with a new linear BM-TIA prototype developed in the Photonic Systems Group of Tyndall National Institute. Such a receiver is necessary to enable the use of the above mentioned more advanced modulation formats in the burst-mode upstream channel, as linearity must be preserved in the electrical domain for the implementation of DSP functionalities.

Finally Section 3.4 presents an interleaved PAM4 decoding scheme coupled with hierarchical modulation functionalities that avails of the network asymmetry to improve the available power budget for PONs downstream transmissions.

Section 3.5 then briefly summarises and discusses the results obtained and presented throughout the Chapter.

3.1 DMT modulation for XG-PON enhanced rate

In this Section, DMT modulation is investigated as a way to increase the bit-rate of previous generation PON devices to meet the newer targets of the standards exploiting its higher spectral efficiency. Specifically, this Section shows how a G-PON compatible DML transmitter was used in conjunction with DMT to achieve XG-PON compatible transmission rates of 10 Gb/s whilst, on the other hand, the traditional NRZ would necessarily require a newer generation of higher speed optoelectronic devices.

3.1.1 Discrete multi-tone modulation

DMT is a multi-carrier modulation technique that uses the discrete Fourier transform (DFT) to divide the channel into several sine-shaped

orthogonal sub-channels, in a similar fashion to orthogonal frequency division multiplexing (OFDM). DMT effectively is an implementation of OFDM and can be considered a naming convention generally used for application in an IMDD scenario and over a channel with a slowly varying response. With this definition in mind, while OFDM found large usage in wireless communication, DMT has been adopted as a standard for various digital subscriber line (xDSL) systems running over twister-pair copper cable, but both can also be used in optical transmission systems [79]. DMT is an attractive solution for IMDD optical systems as it offers many of the advantages of OFDM while not requiring coherent detection and, for this reason, it is a topic of investigation for PON applications [80]. Real-time operation of DMT transceivers based on field-programmable gate arrays (FPGAs) has been reported [81] as well as field trials of DMT based PON systems [82].

Fundamentals

In DMT, a data sequence of complex-valued symbols is shaped in multi-carrier orthogonal frequency channels. Unlike WDM, the power in the resulting signal is redistributed among long period, narrowband sub-carriers which are orthogonal and, hence, can be partially overlapped to improve the spectral efficiency while not introducing inter-carrier interference. The DFT is used to convert the original sequence of complex numbers $(d_0, d_1, ..., d_{n-1})$ into a new sequence of complex numbers $(S = \{S_0, S_1, ..., S_{n-1}\})$ with specific characteristics [83]. The orthogonality derives from the choice of the DFT as a harmonic series to map the input symbols into orthogonal sine-shaped sub-carriers. The mathematical formulation of the DFT is the following

$$S_m = \sum_{n=0}^{N-1} d_n e^{-j2\pi \frac{nm}{N}} = \sum_{n=0}^{N-1} d_n e^{-j2\pi f_n t_m} \tag{3.1}$$

with $m = 0, 1, ..., N-1$ and having defined $f_n = \frac{n}{N\Delta t}$ and $t_m = m\Delta t$ where Δt is the symbol period of the sequence S transmission. This transformation modulates the data symbols in the different $N_C = N$ total sub-carriers, the quantity of which is determined by the size N of the DFT. All sub-carriers are sine shaped and their periods are multiples

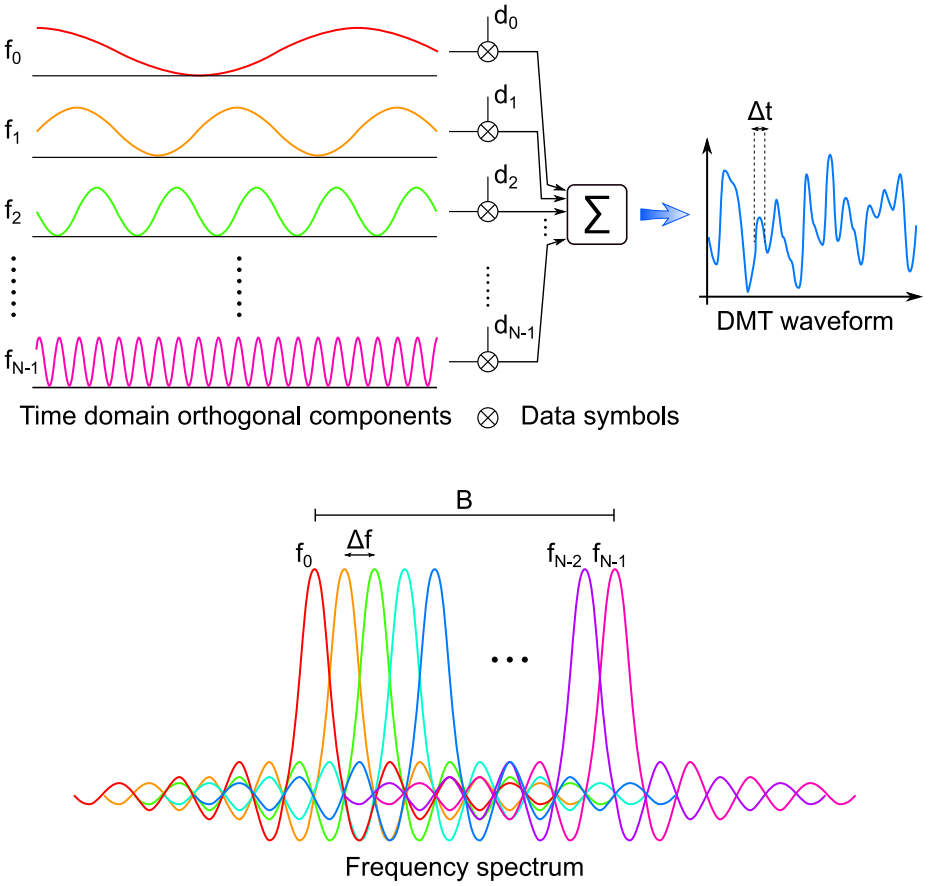


Figure 3.1: DMT generation scheme and frequency distribution of the resultant signal.

of the fundamental. In DMT, contrary to OFDM, a real-valued signal is desired for transmission and this is achieved by making the input of the DFT a signal with Hermitian symmetry, mirroring it with its complex conjugate.

The integral of the product of two sub-carriers over a symbol period is:

$$\frac{1}{T}\int_0^T \left(e^{j2\pi k_1 \frac{t}{T}}\right) * \left(e^{j2\pi k_2 \frac{t}{T}}\right) dt = \frac{1}{T}\int_0^T e^{j2\pi(k_2-k_1)\frac{t}{T}} dt = \begin{cases} 0 & \text{if } k_1 \neq k_2 \\ 1 & \text{if } k_1 = k_2 \end{cases} \tag{3.2}$$

which explains their orthogonality, the integral being null when the sub-carrier indices are different. For a transmission at a baud-rate of R_S the frequency separation between sub-carriers is $\Delta f = \frac{1}{N_C \Delta t} = \frac{R_S}{N_C} = \frac{1}{T}$, where $T = \frac{N_C}{R_S}$ is the DMT symbol period. The signal bandwidth is thus

$B = N_C \Delta f = R_S$ and its baseband real-valued bandwidth occupation is $B_s = \frac{R_S}{2}$.

An interesting aspect of DMT is that, while the required bandwidth only depends on the sample-rate, its spectral profile can be flexibly shaped to optimally adapt to the frequency response of the transmission system (Figure 3.2). Redistributing the transmitted power unequally among the sub-carriers, it is possible to compensate for the frequency response of the system, for example allocating higher power in the sub-carriers subjected to higher attenuation. By measuring the SNR of each sub-carrier at the receiver, and accordingly adjusting its launched power at the transmitter, it is possible to achieve a flat SNR profile after the signal propagation and reception. It is also possible to reduce the modulation orders among sub-carriers or even not allocate data altogether in some of them in the eventuality that their SNR at the receiver is seriously compromised (for example due to frequency notches) [82]. The net bit-rate, R_b, of a DMT transmission like the one described, where the same quadrature amplitude modulation (QAM) constellation of order M

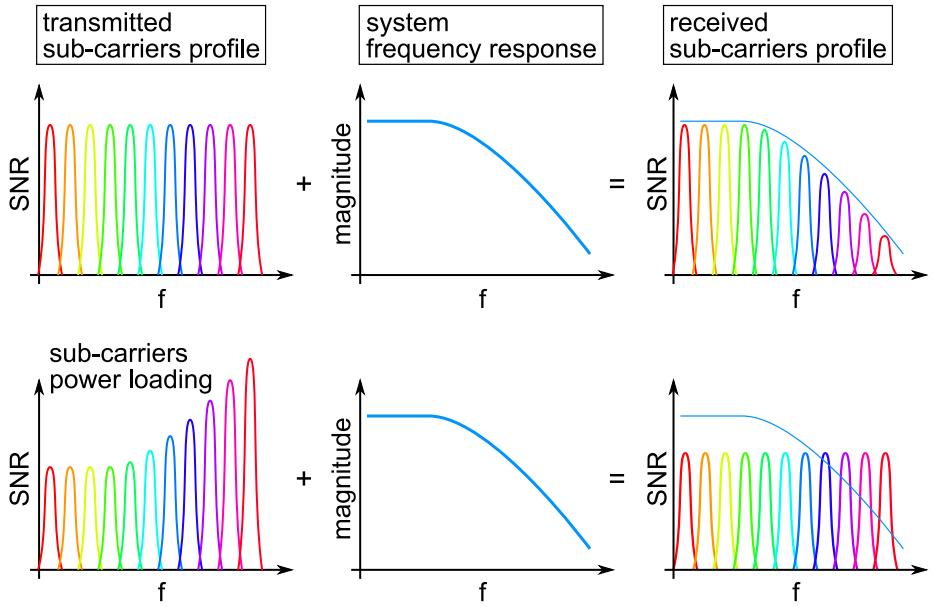


Figure 3.2: DMT sub-carriers SNR profile without and with power loading adjustment at the transmitter.

is used in all sub-carriers, is calculated as:

$$R_b = R_S \frac{N_D}{N_C} \frac{N_C}{N_C + N_p} log_2 M = R_S \frac{N_D}{N_C + N_p} log_2 M \tag{3.3}$$

where N_D are the data-carrying sub-carriers among the N_C total and N_p is the size of the cyclic prefix (CP), explained in the following paragraph. In a DMT system if all the available sub-carriers are loaded with data it results that $N_D = \frac{N_C}{2} - 1$, where the factor 2 in the denominator comes from the added redundancy of introducing the Hermitian symmetry. The expression clearly states how the bit-rate can be increased by employing a higher symbol-rate or by using a more spectrally efficient constellation, for example a higher order QAM. On the other hand, increasing the size of the CP for higher dispersion tolerance, or not encoding data in some of the sub-carriers if the frequency response of the channel presents heavy attenuation notches, diminishes the total bit-rate. From Equation 3.3, it can be observed that a minimum QAM order of 16 is needed for DMT to achieve a spectral efficiency comparable with PAM4 or EDB, which are treated in Section 3.2.

Implementation

A DMT transceiver requires substantial DSP to realise the necessary blocks of the diagrams in Figures 3.3, 3.4. At the transmitter a binary stream of data is firstly mapped into a complex constellation, such as phase-shift keying (PSK) or QAM, of arbitrary size to increase the spectral efficiency of the signal, as more bits per symbol are encoded. The stream of data is then sent through a serial-to-parallel (S/P) converter that formats the symbols in the word size needed for the inverse discrete Fourier transform (IDFT). Before the IDFT block every signal word is mirrored and a new word of doubled size is created attaching its own complex-conjugate to the initial word. By doing so the overall signal is transformed into an Hermitian signal before being processed by the IDFT block and this ensures that its output is a real-valued signal, hence suitable for IMDD systems. The IDFT size determines the number of sub-carriers in the system. After the IDFT a guardband period is added to the DMT words to reduce inter-carrier interference in dispersive systems. This guard period is padded with a CP, which means the

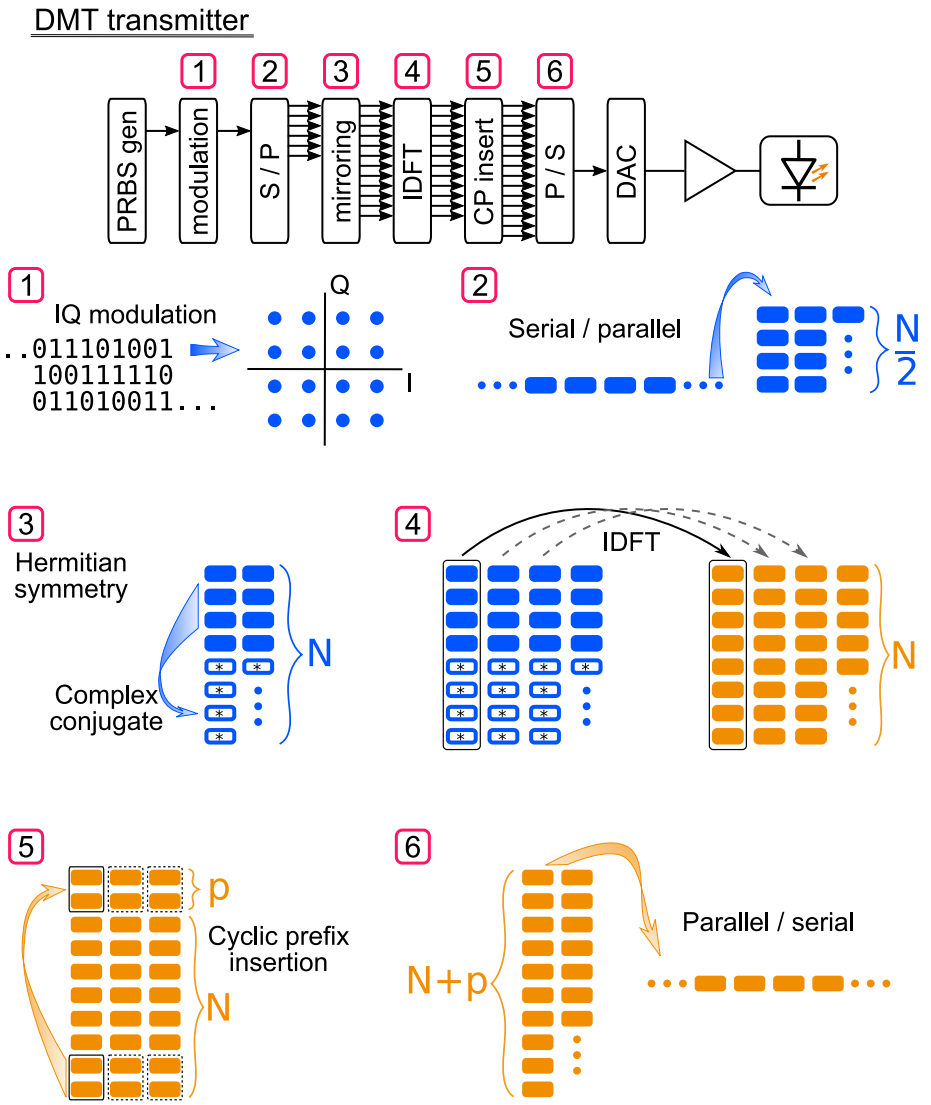


Figure 3.3: DMT transmitter block diagram.

sequence of symbols at the end extremity of the word is attached at its beginning. The CP makes the DMT word cyclical to increase synchronisation tolerance and its size can be increased to improve CD tolerance in optical fibre systems. The DMT words are then serialised again to be transmitted over the channel. The receiver performs the above steps in inverse order to decode the incoming waveform. This is firstly synchronised and arranged again into words of the required size by a S/P. The CP is removed from the words and these are input to the DFT block, whose output is parsed to remove the complex conjugate half of the word and retain only the portion carrying data. A parallel-to-serial (P/S) is

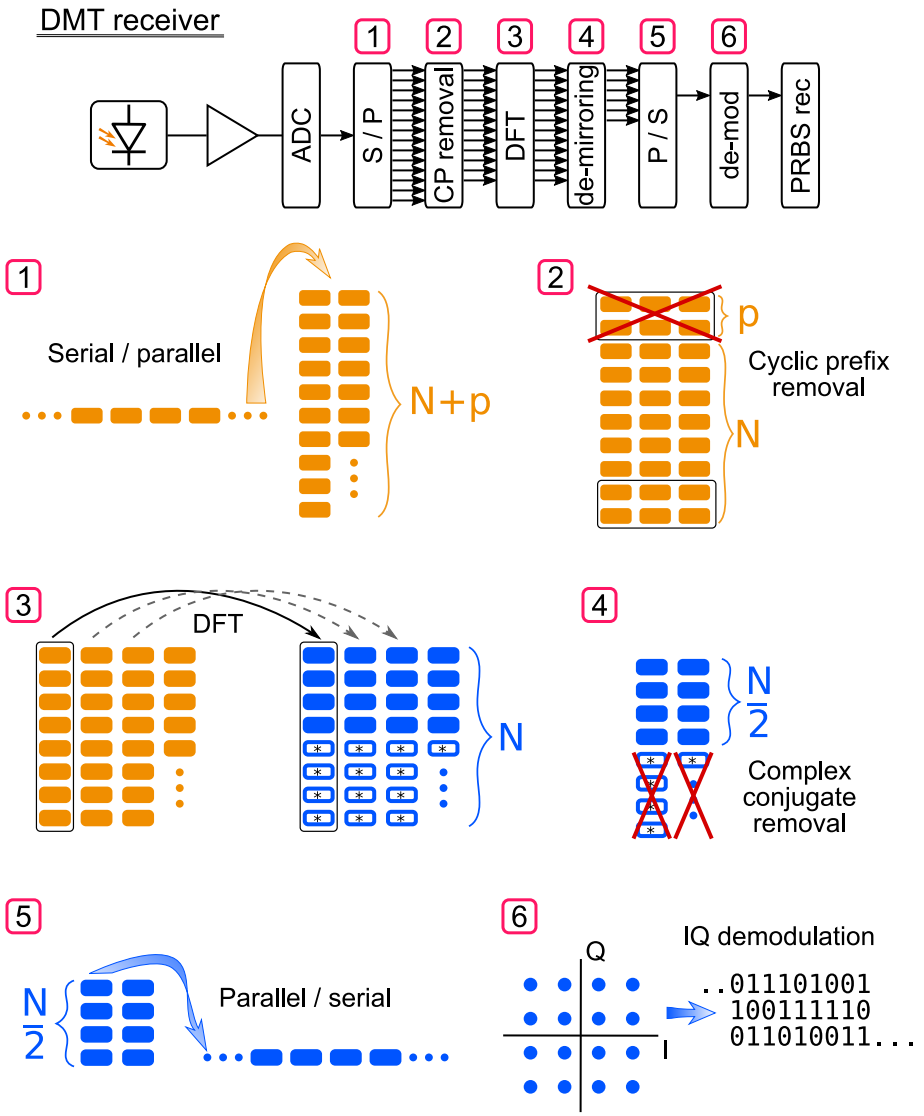


Figure 3.4: DMT receiver block diagram.

then used before de-modulation, according to the constellation used by the transmitter, and the binary data stream is retrieved.

In the DMT experiments conducted as part of this work (Figure 3.5) the transmitter had a power loading feature, similar to that illustrated in Figure 3.2. Before performing the IDFT the relative power of the symbols that are going to be assigned to the various sub-carriers was adjusted in accordance with the attenuation profile of the system. Hence, every sub-carrier at the receiver had similar SNR and BER values and the overall system performance was optimised.

3.1.2 Demonstration of G-PON devices bit-rate enhancement

DMT modulation was used to experimentally demonstrate data-rates higher than 10 Gb/s with a 1 GHz G-PON transmitter. As part of the European FP7 project Quaternian (QUAntum dot Technologies for Extended Reach Nodes In Access Networks) [84] novel DMLs were developed exploiting quantum dot (QD) technology. The aim was to develop high-speed devices with high spectral purity as discrete-mode transmitter lasers for high-speed digital and analogue modulation. The developed lasers achieved high power output and high spectral purity, but did not have sufficient modulation bandwidth or temperature stability performance. Limitations due to the QD material used for laser fabrication lead to a high relaxation oscillation damping which reduced the modulation bandwidth. The DML had a 3 dB bandwidth of 1 GHz which could only support up to 2.5 Gb/s NRZ modulation before incurring bandwidth restrictions. However, it was possible to implement an XG-PON compatible 10 Gb/s transmitter by adopting DMT. The results were achieved thanks to the high spectral efficiency of the modulation format and proved its potential as a candidate for bit-rate increase in existing systems, without requiring the replacement of the optoelectronic devices. A large bandwidth optoelectronic receiver was used in the experiment because a G-PON receiver was not available.

Experimental setup

The experimental setup in Figure 3.5 was assembled in order to validate the performance of DMT to increase the data-rate of bandwidth limited transmitters. A variable sample-rate arbitrary waveform generator (AWG) with 10 bit vertical resolution was used to directly modulate the DMT waveform onto a laser whose bias was fixed at 68 mA. The AWG had a maximum sample rate of 12 GS/s and values of 10 GS/s and 12 GS/s were used in the experiment, with an upsampling factor of 2 or 3 samples per symbol, depending on the Baud-rate investigated. The DML used as transmitter had a 3 dB bandwidth of 1 GHz (Figure 3.6), compatible with a G-PON upstream operating at 1.25 Gb/s or 2.5 Gb/s NRZ modulation. The central emission wavelength was 1306 nm at the operating temperature of 25 °C. A variable optical attenuator (VOA)

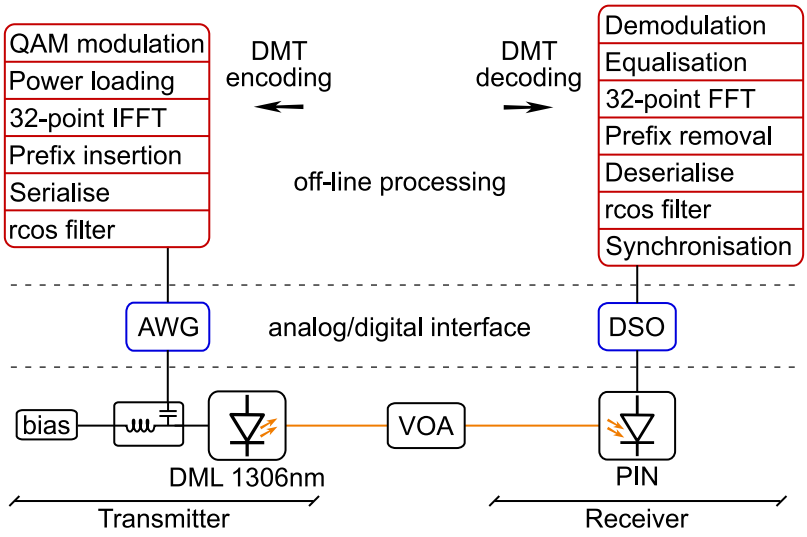


Figure 3.5: Experimental setup for DMT performance characterisation.

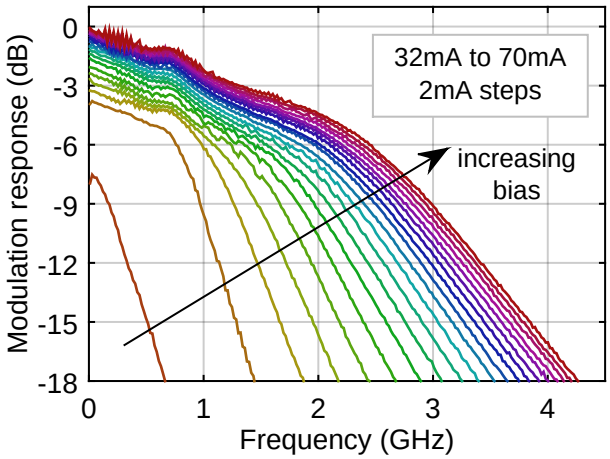


Figure 3.6: Measured bandwidth of DML transmitter under increasing bias.

was placed in front of a linear 10 GHz PIN receiver that converted the optical signal into an electrical waveform captured by a 12.5 GHz digital storage oscilloscope (DSO) sampling the signal at 25 GS/s. The oscilloscope output was processed off-line to evaluated the link BER over the acquisition and analysis of a million bits.

The DMT signal encoding and decoding was implemented off-line using a numerical computing environment where all the necessary functions described above were realised. Fast Fourier transform (FFT) and inverse fast Fourier transform (IFFT) were used as efficient algorithms to numer-

ically compute the DFT and its inverse. Power loading at the transmitter was performed in front of the IFFT block to redistribute power among the sub-carriers and compensate for the frequency roll-off of the system, so that every sub-carrier had similar SNR and BER values at the receiver. The FFT size was 32 and 15 of the sub-carriers were loaded with data encoded in QAM constellations of different order. A CP of 4 was added to the DMT symbols, adding a 12.5 % redundancy. Figure 3.7 shows the frequency response of the transmission system along with the SNR of the sub-carriers measured at the receiver when their transmitted power had a flat frequency profile, that is to say when no power redistribution was performed. The power loading profile used to compensate for the bandwidth limitation is also shown, with a shape mirroring that of the SNR. The SNR profile shows that most of the system bandwidth restriction within 3 GHz is solely due to the DML, as expected due to the higher bandwidth of the other components used. The DMT waveform was filtered with a raised cosine filter with 0.2 roll-off factor to optimise the bandwidth occupancy. At the receiver a one-tap equaliser was used after the FFT block to estimate and compensate for the channel frequency response. The computer generated DMT waveform was loaded into the AWG at the transmitter and the traces captured by the DSO at the receiver were analysed off-line for decoding and performance evaluation.

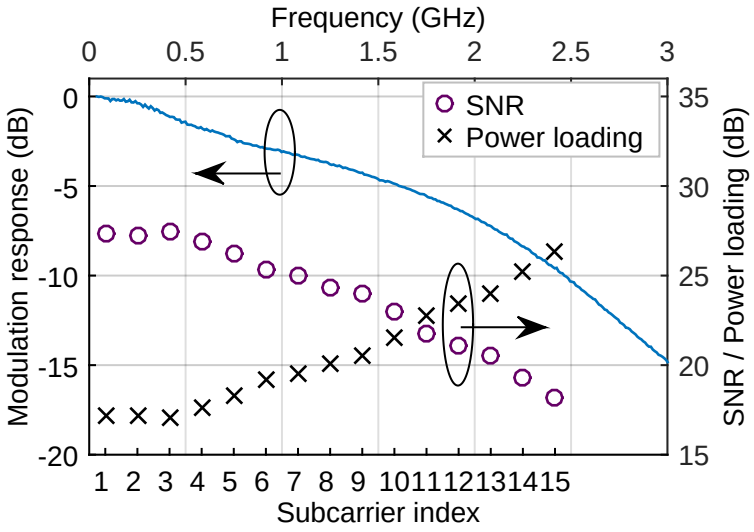


Figure 3.7: System frequency response and power loading profile for data-carrying sub-carriers, with a 5 GBd DMT modulation.

Experimental results

Different combinations of baud-rate and QAM constellation order were investigated and their optical back-to-back (B2B) sensitivity for a 10^{-3} BER was measured (Figure 3.9). Signals were transmitted at baud-rates of 3.3, 4 and 5 GBd and QAM constellation orders were varied from 2 to 128, with their resulting net bit-rates reported in Table 3.1. The power loading profile was optimised for every DMT setting to redistribute the sub-carriers power according to the system conditions and obtain optimum BER performance, as in the example case shown in Figure 3.7. The 10^{-3} BER sensitivity of an NRZ modulated signal for increasing data-rates is also shown in Figure 3.9 for comparison. The NRZ system used a simple single-threshold receiver for symbol detection, with no pre- or post-equalisation of the signal. NRZ has the best sensitivity for bit-rates lower than 3 Gb/s but clearly the DML cannot support rates higher than 5 Gb/s due to the bandwidth restriction induced ISI. On the other hand, DMT can support enhanced bit-rates, achieving values of up to 10.4 Gb/s with a 5 GBd transmission whose spectral occupancy was only 2.5 GHz. The lower baud-rates performed better for net bit-rates lower than 7 Gb/s having the advantage of a lower bandwidth occupation and, hence, suffering less from the attenuation due to the DML modulation response. However, for data-rates in the order of 10 Gb/s, the 5 GBd transmission had the best sensitivity because the high order of the QAM constellations needed for the other cases, namely 128 QAM for 3.3 GBd and 64 QAM for 4 GBd, required higher

bit-rate (Gb/s)			
	baud-rate (GBd)		
QAM order	3.33 GBd	4 GBd	5 GBd
2 QAM	1.39	1.67	2.08
4 QAM	2.78	3.33	4.16
8 QAM	4.17	5.0	6.25
16 QAM	5.55	6.67	8.33
32 QAM	6.94	8.33	10.42
64 QAM	8.33	10.0	/
128 QAM	9.72	/	/

Table 3.1: Net bit-rates (Gb/s) for baud-rate and QAM combinations.

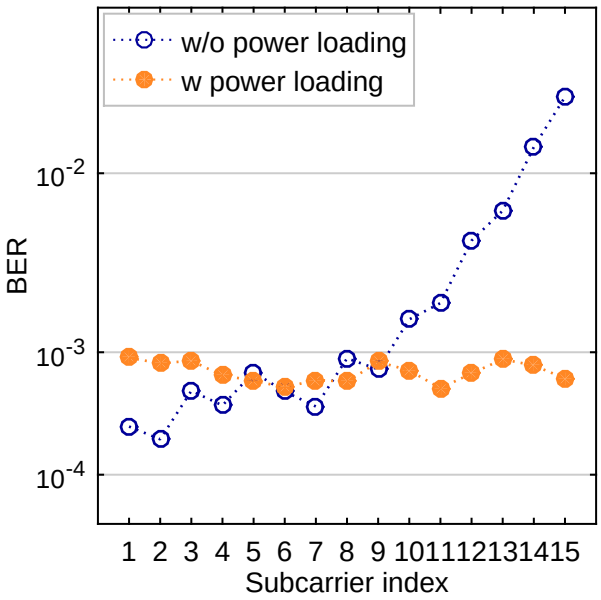


Figure 3.8: BER measured for data sub-carriers with and without power re-distribution.

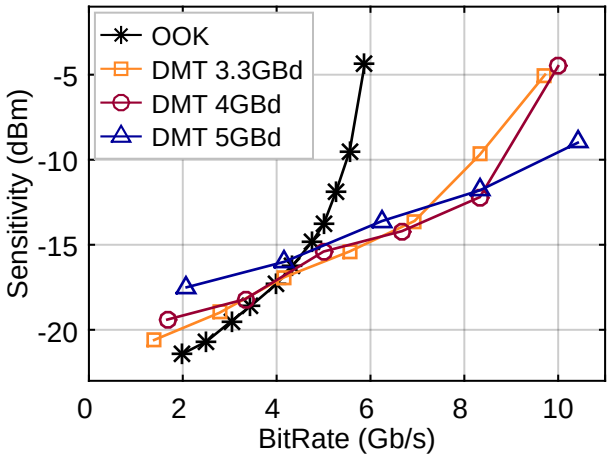


Figure 3.9: Experimental sensitivities in optical B2B for DMT signals at various Baud-rates and NRZ-OOK.

SNR than the 32 QAM used for the 5 GBd experiment (Table 3.1). Despite the restricted DML 1 GHz modulation bandwidth, the 2.5 GHz bandwidth DMT signal was supported thanks to the spectral shaping obtained by performing power re-distribution among sub-carriers. For this last 5 GBd DMT configuration in particular, more comprehensive measurements of its application in a PON scenario are covered in Section

5.1 of this thesis, where optical amplification is added in the link to support higher distances and split-ratio networks.

DMT in future passive optical networks

DMT has been successfully demonstrated to be a viable way to increase device bit-rate thanks to its spectral efficiency, allowing XG-PON compatible 10 G bit-rates with the use of G-PON transmitters, opening the possibility of re-using cheaper devices in the next generation of PONs and, hence, reducing the required investment for the development of new optoelectronic devices. The work that was carried out and presented in this Chapter successfully showed the capabilities of DMT in enabling XG-PON rates with a bandwidth impaired transmitter. The experimental results enabled the target modulation speed and were instrumental for the successful conclusion of the FP7 project Quaternian. This comes, however, at the cost of implementing complex DSP functionalities for the realisation of a DMT transceiver as well as the need for high-speed high-resolution ADC and DAC at the front-end. These aspects cause a consequent increase in price and power consumption of the transceivers. On the performance side, the required receiver sensitivity is also higher than for other multi-level modulation formats, treated elsewhere in this thesis, and this represents a limit for the adoption in PONs due to the required increase in the power budget.

Aiming for the realisation of 25 Gb/s single-lane bit-rates with 10 G devices, the guidelines obtained from the experimental work presented are still valid. Single λ data-rates of 25 Gb/s or higher, with 10 G electro-optical components, can be achieved with DMT [50, 56–61, 85] and the practical adoption limits are due to DSP complexity and reduced sensitivity. In addition, the higher Baud-rate would need to rely more heavily on high-speed ADCs and DACs for the linear electro-optical interfaces, which are expensive and power hungry for adoption in a PON transceiver [86]. Looking at the recent research and standardisation trends [34, 45, 46, 78], DMT does not appear likely to be adopted yet because of its complexity and the need for optical amplification to meet the link budget requirements. Simpler multi-level modulation formats are, hence, investigated in the following Chapter 4, PAM4 and EDB, to

increase the bit-rate aiming at the 100 G (25 Gb/s $\times$ 4λ) PON applications.

Nevertheless, DMT could become an interesting option for even higher line-rates of 40 or 50 Gb/s where the amount of DSP required by simpler modulation formats. such as PAM4, could be comparable to DMT requirements [62–66, 70]. The electronic requirements of a DMT transceiver for higher rates are very similar to the 25 Gb/s ones. On the other hand, scaling the bit-rate of simpler modulation such as PAM4, while using 10 G devices, requires more intense DSP for the implementation of pre-compensation, post-equalisers and decoding algorithms. High resolution electronic front ends will also be needed to support the linearity requirements of digital pre- and post-compensation filtering, ultimately being limited by the availability of ADCs and DACs, as for DMT. If the cost of 25 G optics will remain one of the main obstacles to the realisation of high speed transceivers and 10 G devices will be considered for data-rates around 50 Gb/s, the availability of cost-effective ADCs and DACs will play a key role in defining the future of modulation formats in optical access networks and the flexibility advantages of DMT could make it a favourite over EDB and PAM4.

3.2 25G PAM4 and EDB modulation for NG-PON2 bit-rates

PAM4 and EDB are among the simplest multilevel modulation formats in terms of pre- and post-processing requirements, lower than, for example, DMT, but still providing a two-fold improvement in bandwidth efficiency when compared to OOK NRZ. Thanks to the limited complexity of the supporting electronic components, these are more likely to be adopted in 100 G PON systems as the underlying technology is cheaper and less disruptive, compared to DMT, but still enables enhanced bit-rates of 25 Gb/s using the current commercial generation of 10 G devices. PAM4 and EDB can provide higher speed with minimum intervention in the transceiver design because the optoelectronic components employed would not need replacement. The adoption of appropriate electrical drivers at the transmitter and electrical front-end for

the receiver, along with an interface to the legacy binary system, could increase the single line-rate to 25 Gb/s.

3.2.1 Multilevel amplitude modulation

In most optical communication systems, OOK NRZ has been the reference choice for decades due to the inherent simplicity of the electrical components. However, while still considering the IMDD scenario which is desirable for cost-effective applications like PONs, more spectrally efficient modulation formats are available when multiple amplitude levels are used.

On-off keying non-return to zero

OOK is a binary amplitude modulation format where one bit per symbol is transmitted encoded in a minimum or maximum amplitude state. NRZ means in the case of consecutive high amplitude symbols the signal is not dropped to zero but kept at a high value, relaxing the bandwidth requirements because less level transitions are needed in a symbol period. The corresponding eye diagram is shown in Figure 3.10. NRZ directly employs a binary stream for transmission without encoding and at the receiver a simple comparator is sufficient to detect the amplitude status and decode the information bit. Linearity of the devices is not a concern in NRZ because only two amplitude levels are used and limiting radio frequency (RF) amplifiers or modulators with nonlinear transfer function can be employed. The main drawback of NRZ is the low spectral efficiency due to the single bit of information carried by every symbol. This means the required bandwidth is similar to the Baud-rate, with an optimised value of the 3 dB bandwidth of the system usually equal to approximately 0.75 times the symbol-rate.

Electrical duobinary

EDB is a partial-response signalling technique where controlled ISI is introduced in the signal by letting one pulse spread into the neighbouring ones. By allowing this ISI the pulse duration is longer and, hence, the frequency spectrum becomes narrower. The reduced spectrum is responsible for increased spectral efficiency and improved tolerance to channel

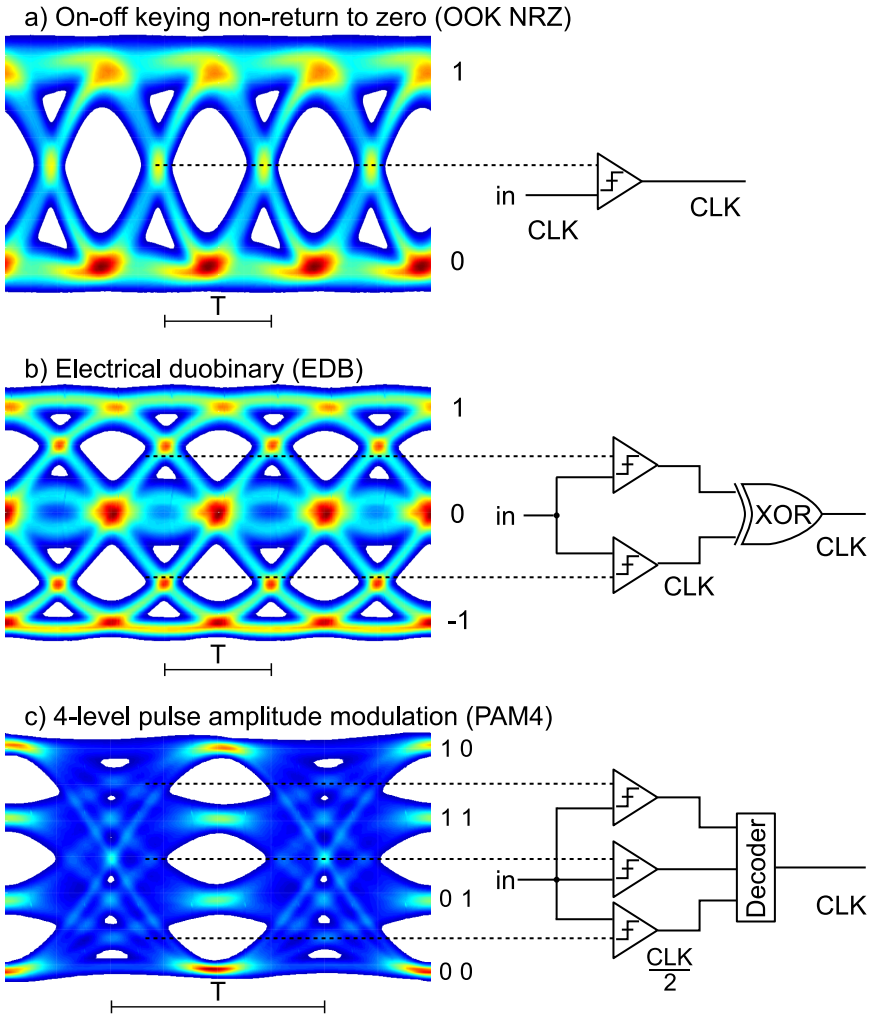


Figure 3.10: Eye diagrams measured in optical B2B and detection schemes for the three modulation formats: a) OOK NRZ, b) EDB and c) PAM4.

distortion. The duobinary encoding is done by summing the signal with a delayed copy of the same and can be achieved either with a delay-and-add filter or with a low-pass electrical filter with a bandwidth of about $\frac{1}{4}$ of the symbol-rate. The resulting duobinary signal c_k after filtering is

$$c_k = a_k + a_{k-1} \tag{3.4}$$

When the input signal a_k is binary, that is $a_k \in \{0, 1\}$, the output is a three-level signal but it is also possible to use, for example, a PAM4 signal for which the resulting duobinary would have 7 amplitude levels. The receiver needs a feedback circuit to remove the ISI introduced with

filtering and recover the original binary stream,

$$\hat{a}_k = c_k - \hat{a}_{k-1} \tag{3.5}$$

however this implementation, with feedback in the decoder, introduces the risk of unbounded error propagation at the receiver as a single error will propagate through the decoding process. Generally a pre-coding is performed at the transmitter to avoid error propagation due to the feedback in the decoder. In this case, the pre-coded signal b_k is encoded from a binary a_k as follows

$$b_k = (a_k - b_{k-1}) \; mod \; 2 \tag{3.6}$$

and, hence, the duobinary signal after filtering is

$$c_k = b_k + b_{k-1} \tag{3.7}$$

and, to recover the estimated sequence $\hat{a_k}$ at the receiver, a modulo operation is sufficient

$$\begin{aligned} \hat{a}_k &= c_k \; mod \; 2 = (b_k + b_{k-1}) \; mod \; 2 = \\ &= ((a_k - b_{k-1}) \; mod \; 2 + b_{k-1}) \; mod \; 2 = \\ &= ((a_k \; mod \; 2) - (b_{k-1} \; mod \; 2) + b_{k-1}) \; mod \; 2 = a_k. \end{aligned} \tag{3.8}$$

For the practical implementation of a NRZ EDB receiver, a two-threshold interface is needed and the original signal is recovered with a logical XOR of the comparator's outputs (Figure 3.10).

For the three levels EDB, assuming the notation $a_k \in \{0, 1\}$ and

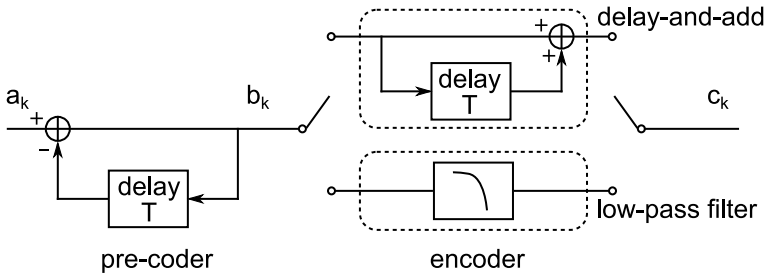


Figure 3.11: Block diagram of a duobinary transmitter with pre-coder and duobinary encoder.

$c_k \in \{-1, 0, 1\}$, it can be observed that, at the receiver, symbols -1 and 1 of c_k correspond to $a_k = 1$ and, for $c_k = 0$, $a_k = 0$. This explains the unequal distribution of the symbols probability in c_k with $P_{-1} = P_1 = \frac{1}{4}$ and $P_0 = \frac{1}{2}$. The output of the duobinary encoder c_k is a correlated signal and, hence, not all possible sequences of three values can occur. For example, a 1 cannot be followed by a -1 and vice-versa, and combinations $\{-1, 0, -1\}$ and $\{1, 0, 1\}$ cannot appear in c_k. This has a significant impact on the dispersion tolerance, as will be evident in the remainder of this Section.

When EDB is implemented on a system with legacy lower bandwidth components, it is possible to avail of the system overall bandwidth to perform duobinary filtering instead of at the transmitter only. In this case, the transmitter bandwidth does not have to be strictly a quarter of the Baud-rate and the combined low-pass filtering effect of the system is exploited instead. This configuration is of interest for a practical implementation because the bandwidth of transmitter components can vary largely and does not necessarily equal the ideal one for duobinary encoding. It is, hence, important to assess the performance and requirements of this realisation to understand whether the transmitter design can be more tolerant in terms of bandwidth and does not require a specific electrical filter. Experimentally, this was implemented using the same transmitter configuration as for the 25 Gb/s NRZ, to generate a binary optical signal, and a 10 G receiver. This approach will be addressed in this work as non-return to zero with duobinary detection (NRZ-EDB) to distinguish it from the duobinary system with a bandwidth limited transmitter.

4-level pulse amplitude modulation

PAM4 is a modulation format that uses 4 different amplitude levels to represent an alphabet of 4 symbols, for example $\{0, 1, 2, 3\}$. A single PAM4 symbol can hence carry two bits of information (Figure 3.10), doubling its spectral efficiency. A PAM4 signal can be obtained combining bit-by-bit two binary streams, called most significant bit (MSB) and least significant bit (LSB), using a constellation map like the one in Table 3.2. Gray coding is commonly used in PAM4 to minimise the BER

PAM4 symbol	MSB	LSB
0	0	0
1	0	1
2	1	1
3	1	0

Table 3.2: Gray mapping of a PAM4 constellation.

in a way such that words encoded in neighbouring symbols only differ by 1-bit and, hence, the approximation $BER \simeq \frac{SER}{2}$ is valid. Thanks to the double spectral efficiency, the Baud-rate of PAM4 is half that required by NRZ to achieve the same bit-rate. This means the required electronic components are working at half speed, making them more affordable and reducing power consumption. The double symbol period is also responsible for higher tolerance to ISI introduced by chromatic dispersion. On the other hand, linearity requirements are more stringent to ensure the equal spacing of the amplitude levels is maintained through transmission.

3.2.2 Thermal noise limit

The different spectral content of the modulation formats is reflected in their amplitude profile, with the more spectral efficient formats having more complex constellations. This causes them to be more sensitive to SNR degradation as more bits are encoded in a single symbol and their detection requires higher signal quality. In an optical thermal noise limited scenario, this means that the minimum required optical power at the receiver end is higher for PAM4 and EDB than NRZ, when the same Baud-rate is used. The comparison was done here for the same effective bandwidth of the components employed in the setup which corresponds to both different bit-rates and Baud-rates. In particular, in order to avoid ISI, the NRZ and PAM4 were used at a Baud-rate of 12.5 GBd, which corresponds to bit-rates of 12.5 Gb/s and 25 Gb/s respectively. On the other hand EDB, which is a partial response modulation and introduces controlled ISI, was tested at 25 GBd, hence 25 Gb/s. With the simple optical B2B setup of Figure 3.12 the BER of the modulation formats was measured as a function of the received optical power. A laser emitting at 1550.116 nm (193.5 THz) was externally modulated with an EAM. The modulator was driven by a DAC capable of generating both

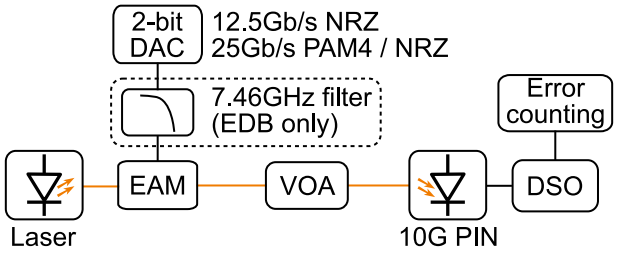


Figure 3.12: Experimental setup for BER measurement of different modulation formats in a 10 G network.

a 12.5 GBd NRZ and PAM4 signal, and a 25 GBd NRZ signal for EDB implementation. The EAM was a device developed for 10 Gb/s systems but its measured 3 dB bandwidth was 21 GHz and, hence, was sufficient to generate a 25 Gb/s NRZ optically modulated signal. An electrical low-pass filter with a 7.46 GHz cut-off frequency was placed in front of the EAM to emulate a bandwidth limited 10 G transmitter. A VOA was placed after the modulator to attenuate the optical power entering the receiver, which was a 10 G PIN photodiode equipped with a linear TIA. The 3 dB bandwidth of the photoreceiver was 10 GHz and its output was captured with a 12.5 GHz, 50 GS/s DSO to be processed off-line. Synchronisation of the pattern and error counting were implemented off-line using a numerical computation software for all the modulation formats analysed. The two variants of EDB discussed earlier were realised by changing the bandwidth of the transmitter. In one case, this was limited with the 7.46 GHz electrical low-pass Bessel filter before the EAM. This filter, having a bandwidth of approximately a quarter of the bit-rate, acted as a duo-binary encoder generating the partial response 3-level signal. The optical signal hence also had three distinct amplitude levels. In the second case, the transmitter bandwidth was not limited and so the signal generated by the EAM was a two level optical NRZ signal. The use of the 10 GHz photoreceiver and DSO successively converted it to a three level waveform which was detected as duo-binary. This approach was called NRZ-EDB in line with the terminology discussed earlier in Section 3.2.1.

The BER as a function of the received optical power is shown in Figure 3.13. The 12.5 Gb/s NRZ, having the simplest constellation, showed the best performance in terms of sensitivity. However, it is worth remem-

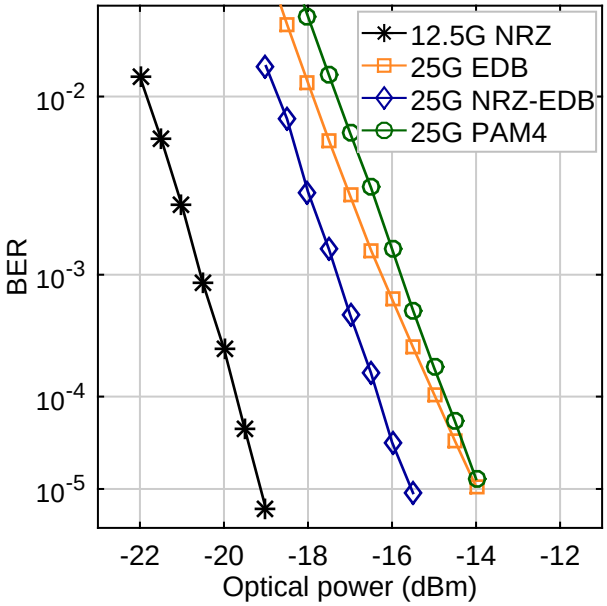


Figure 3.13: Error rate probability of different modulation formats using 10 G class optoelectronic components.

bering that its bit-rate was halved compared to the other modulation formats, which operated at 25 Gb/s. Its sensitivity at a 10^{-3} BER was -20.6 dBm. The two 25 Gb/s EDB approaches showed different BER curves, depending on the transmitter bandwidth, with the EDB transmitter showing a 1 dB penalty compared to the NRZ with duo-binary detection. This is due to the use of 10 G components in the whole network, which further limited the signal bandwidth at the receiver side, thereby introducing additional ISI. The measured sensitivities were -16.3 dBm and -17.3 dBm for EDB and NRZ-EDB, respectively. It is reasonable to expect that intermediate values of transmitter bandwidth would lie in between the two curves measured, hence for any bandwidth transmitter within the interval from 7.46 GHz to 21 GHz, a maximum variation of 1 dB is expected. This is an important guideline result because the bandwidth of 10 G devices can vary significantly and this indicates that precise filtering is not needed to optimise the EDB performance and NRZ-EDB could actually provide a better sensitivity.

PAM4 showed the highest required optical power because of its four amplitude levels, with a sensitivity of -15.8 dBm. A sensitivity difference of 4.8 dB is expected at the same Baud-rate, 12.5 GBd in this case, between NRZ and PAM4 in an AWGN limited scenario and the observed

performance matched with the analytical prediction [22]. PAM4 and EDB had close performance under AWGN conditions with a sensitivity difference of 0.5 dB.

3.2.3 Bandwidth requirements

The bandwidth requirements were evaluated for NRZ, EDB and PAM4, in particular focusing on the receiver side. The bit-rate was fixed at 25 Gb/s in order to provide a fair comparison among the candidate modulation formats for a wavelength multiplexed, 25 Gb/s $\times$ 4λ, 100 G PON and, hence, omitting the 12.5 Gb/s NRZ case. The experimental setup in Figure 3.14 was used to capture optical B2B waveforms. A tunable distributed feedback (DFB) was emitting a signal at 1550.116 nm entering an EAM with a power of +12 dBm. The 3 dB bandwidth of the EAM was 21 GHz, which was sufficient to generate a clean signal for the most bandwidth demanding NRZ (eye diagram of the output shown in Figure 3.10). The modulator was driven by a 2-bit DAC providing a 25 Gb/s, 2, 3 or 4 level signal for NRZ, EDB and PAM4, respectively. An electrical low-pass filter, with a 3 dB cut-off frequency of 7.46 GHz, was used after the DAC to convert the 25 GBd NRZ signal to an EDB one. In all cases, a PRBS 15 bit pattern was used as data content, in the case of PAM4 obtained by summing bit-by-bit two PRBS sequences one of which was delayed by half the length of the pattern. A VOA was used in front of the receiver, which was a linear 50 GHz PIN photodiode. Its output was captured by a 36 GHz DSO and processed off-line for low-pass filtering and error counting. The receiver bandwidth limitation was emulated using off-line processing on the captured waveform, applying a 4th order Bessel filter of the desired bandwidth. The frequency spectra of the electrical

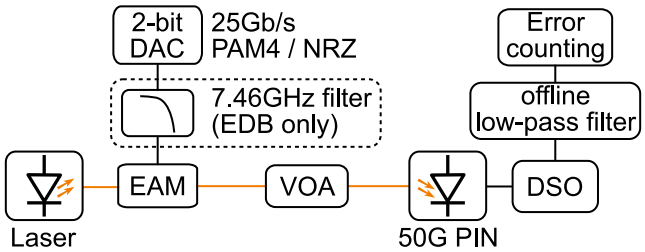


Figure 3.14: Experimental setup for receiver bandwidth requirements measurements.

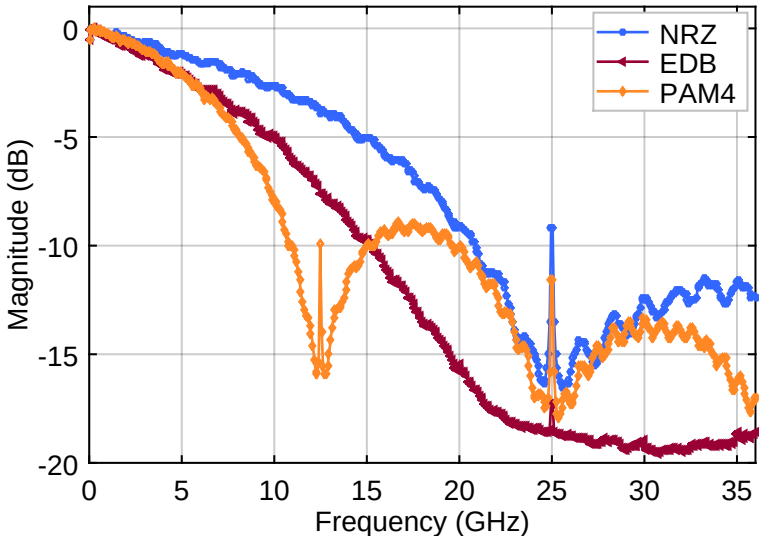


Figure 3.15: Spectra of the three modulation formats at 25 Gb/s at the output of the 2-bit DAC.

signal driving the EAM are shown in Figure 3.15, captured directly at the output of the DAC with a 36 GHz DSO. Clearly, the main lobe of the PAM4 signal is half that of the NRZ one due to the Baud-rate difference. The EDB signal was obtained here with electrical filtering and so its spectral content reflects the frequency response of the specific low-pass filter used and could be different if obtained with a delay-and-add filter. The 3-dB corner of the frequency responses was 10.7 GHz, 7 GHz and 6.2 GHz for NRZ, EDB and PAM4, respectively, and the 6 dB corner frequency increased to 16.3 GHz, 10.9 GHz and 8.9 GHz, respectively. The curves show how both EDB and PAM4 have potential to employ the previous generation of 10 G optoelectronic components while faster devices are needed to support NRZ. The same transmitter signal was used for both NRZ and NRZ with duobinary detection.

Figure 3.16 shows the sensitivity for a 10^{-3} BER as a function of the receiver bandwidth. The best sensitivity for the NRZ was measured for a receiver 3-dB bandwidth of 14.5 GHz. Below this value the BER increased due to the ISI introduced by bandwidth restriction. On the other hand, higher bandwidths worsen the BER because more thermal noise is captured from the receiver in the high-frequency components of the spectrum which only offer marginal contribution to the signal content. Similar behaviour was observed for EDB and PAM4 but their optimal receiver

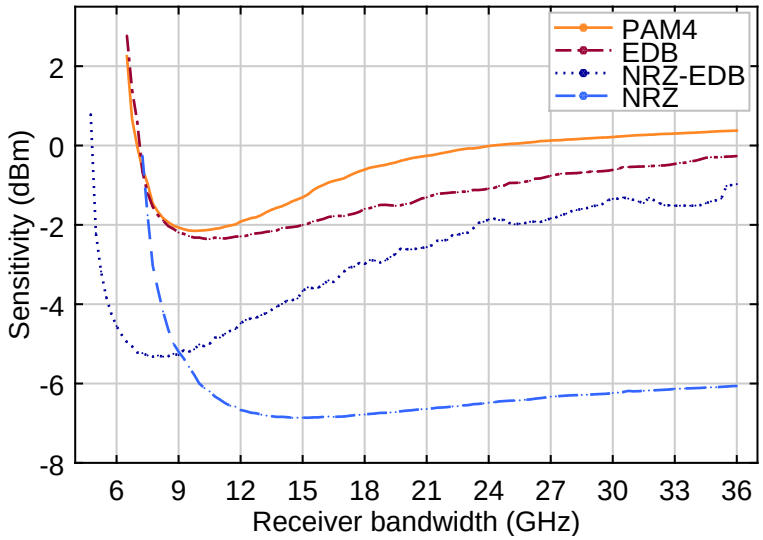


Figure 3.16: Sensitivities of the four modulation formats as a function of the 3 dB bandwidth of the receiver.

3 dB bandwidths were 10.5 GHz and 9.75 GHz, respectively. Also, the sensitivity penalty observed at higher bandwidths was more pronounced because the multi-level modulation formats are more affected by SNR degradation of the signal. For the NRZ-EDB case, limiting the receiver bandwidth proved to be necessary to provide duobinary conversion. A sensitivity penalty of 4 dB was encountered between the optimum receiver bandwidth of 7.75 GHz and the full 36 GHz bandwidth case. The results show how EDB and PAM4 could effectively employ 10 G transmitters and receivers to achieve a 25 Gb/s line rate while NRZ needs devices designed with a higher bandwidth. A higher penalty for EDB and PAM4, compared to NRZ, was observed when comparing these measurements to the previous ones. This is attributed to the high-bandwidth PIN photodiode that was not equipped with a TIA and, due to the high power of the optical input, was operating in a shot-noise dominated regime. This has a different impact on multi-level modulation formats compared to the thermal noise regime of the 10 G PIN with TIA. Nevertheless, the measurements clearly show the impact of the receiver bandwidth on the sensitivity. Also, the absolute values of the sensitivities measured in this experiment were not suitable for PON transceivers because a high bandwidth photodiode was employed without TIA. The choice was made in order to use a receiver with a high bandwidth (50 GHz) and high linearity

thereby eliminating other experimental variables that could influence the results. Similar measurements were repeated for a 10 GHz PIN photodiode receiver with linear TIA implementing additional low-pass filtering via off-line DSP (Figure 3.17). The receiver was, in this case, working in a thermal noise limited regime with negligible contribution from the shot noise and the sensitivities compared closely with the ones obtained in Figure 3.13. The advantage of having additional bandwidth at the transmitter in the NRZ-EDB case is evident when the other components of the network are causing additional bandwidth limitation. While the NRZ-EDB offers its best sensitivity with an off-line low-pass filter as low as 8 GHz, the EDB system improves constantly with the higher available receiver bandwidth. Also, the NRZ-EDB sensitivity is nearly 2 dB better than the EDB one. Transmitter bandwidths between the 7.46 GHz of the filter and the full EAM bandwidth of 21 GHz are expected to offer intermediate performance, offering a wide range of flexibility with the variations expected from practical 10 G components.

3.2.4 Chromatic dispersion tolerance

Chromatic dispersion tolerance was measured for the above modulation formats using a tuneable dispersion compensation module (TDCM) to add flexible amounts of dispersion to the signal. The experimental

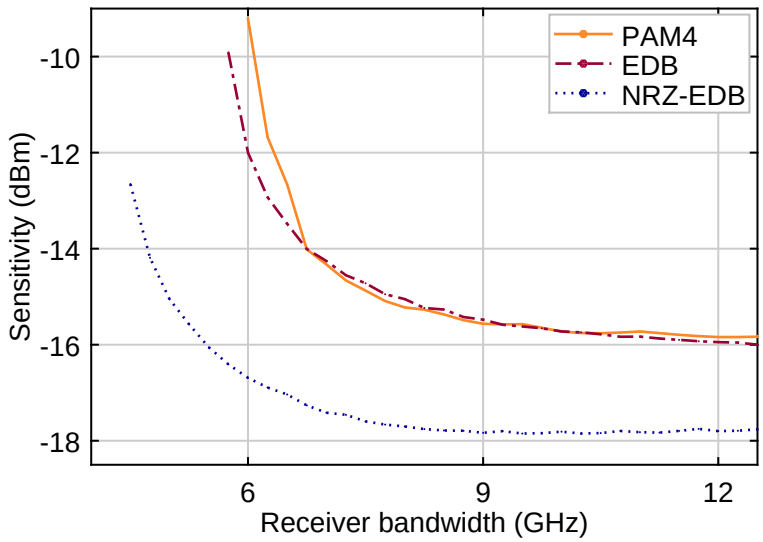


Figure 3.17: Sensitivities of the three modulation formats as a function of the 3 dB bandwidth of the receiver for a 10 G system.

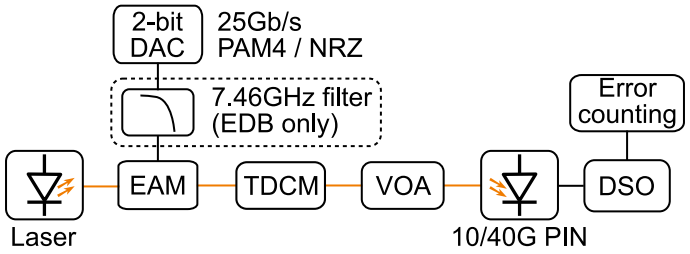


Figure 3.18: Experimental setup for chromatic dispersion measurements.

setup in Figure 3.18 was used, where the transmitter implementation was the same as described above for the bandwidth measurement setup. A TDCM was placed after the modulator and tuned to the same frequency channel as the transmitter to control the amount of dispersion in the signal. A VOA was used in front of the receiver which consisted of a 40 GHz PIN with TIA for NRZ and a 10 GHz PIN with linear TIA for EDB, NRZ-EDB and PAM4. The photoreceiver output was captured by a DSO and processed off-line for error counting.

Dispersion was added in 50 ps/nm steps to the signal and the receiver sensitivity was measured. A range of EAM bias was used to show how bias change can be used as a way of pre-distorting the signal to improve the dispersion tolerance. Changing the bias point affected the chirp but also the linearity of the signal as the transfer function of the EAM was not linear. Also, the ER of the optical signal changed with the bias point because the amplitude of the electrical signal driving the modulator was not varied. The ERs for the highest bias value of -1.68 V were 6.0 dB, 5.5 dB and 6.1 dB for NRZ, EDB and PAM4, respectively, and increased up to a maximum of 7.1 dB, 6.8 dB and 7.4 dB, respectively, for the lowest bias setting.

Figure 3.19 shows the sensitivity of a NRZ 25 Gb/s signal with increasing dispersion and different EAM biases. In B2B the sensitivity was affected minimally by the change in bias because the linearity is not a main concern for a binary modulation format. With the increase of CD the use of a lower bias clearly improved the tolerance of the system and up to 350 ps/nm of CD was supported with a sensitivity of -6.8 dBm. The high Baud-rate of the NRZ transmission is the main reason behind the limit to its dispersion tolerance when ISI becomes more pronounced. The results in this analysis indicate that uncompensated transmission of

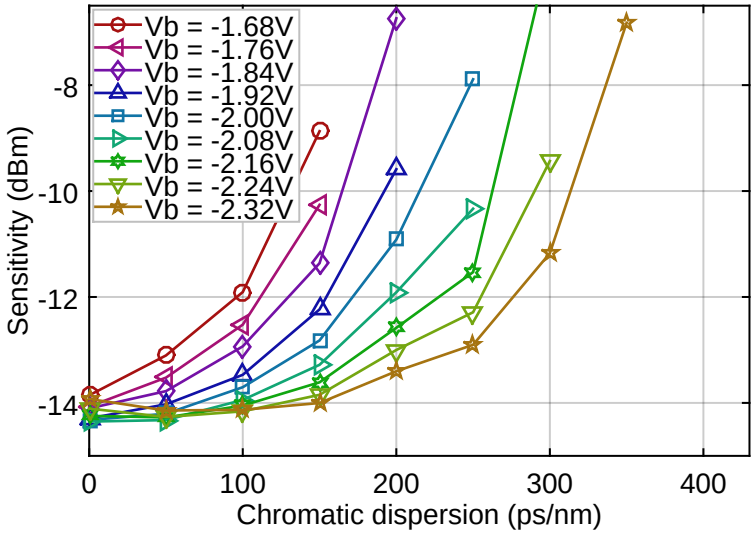


Figure 3.19: Sensitivity of a 25 Gb/s NRZ signal for various EAM bias.

a 25 Gb/s NRZ can be achieved for a maximum CD equivalent to 20 km of SMF in C-band. The sensitivity curves in Figure 3.20 were measured for the EDB system. The EDB signal, despite having the same 25 GBd Baud-rate as the NRZ, showed improved tolerance to dispersion. The lowest bias could offer a sensitivity of -11.9 dBm at a 10^{-3} BER with 700 ps/nm of CD, twice the amount supported by NRZ. This is due to the reduced spectral content of the modulated signal and also to the filtering process at the transmitter that, as discussed earlier, eliminates

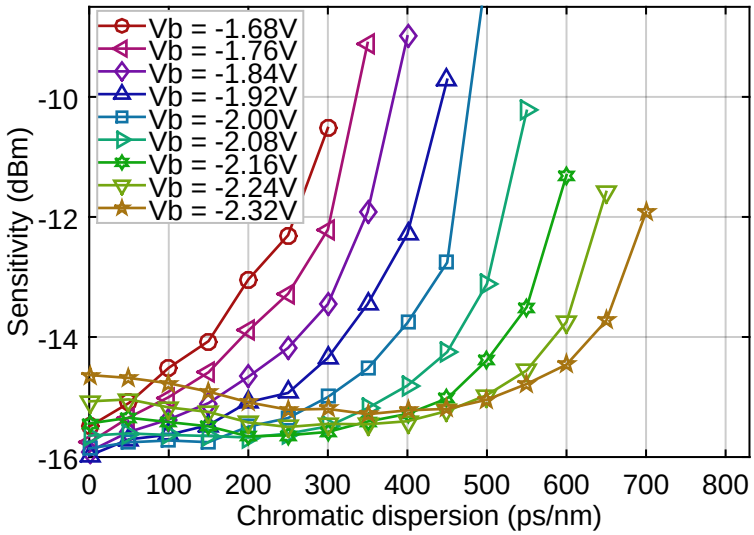


Figure 3.20: Sensitivity of a 25 Gb/s EDB signal for various EAM bias.

certain symbol sequences that are the most affected by dispersion. In B2B a 1.4 dB penalty was measured with respect to the best case when using the lowest bias of −2.32 V because of the linearity degradation introduced.

The NRZ-EDB case was also investigated using the full bandwidth NRZ transmitter with the 10 G receiver. The results in Figure 3.19 show the sensitivity under increasing amounts of CD and for various EAM biases. Similar to the EDB case, lowering the bias improved performance for higher amounts of CD and a −2.32 V EAM bias allowed for transmission with a 700 ps/nm accumulated dispersion. However, NRZ-EDB also showed better overall performance across the entire range of measurements with all the settings being able to support up to 500 ps/nm dispersion. Also, the B2B penalty due to bias induced distortion of the signal was lower because the EAM was driven by a two level signal, instead of three, as in the EDB system. The B2B sensitivity of −17 dBm was 1 dB better than the EDB, as expected from the thermal noise characterisation, and the system could deliver a −13.8 dBm sensitivity with 700 ps/nm of CD, 1.9 dB better than EDB. This shows that a transmitter with higher bandwidth than a quarter-rate EDB filter provides an advantage not only in terms of sensitivity but also CD tolerance. Hence, among the 10 G class devices available, a higher bandwidth transmitter

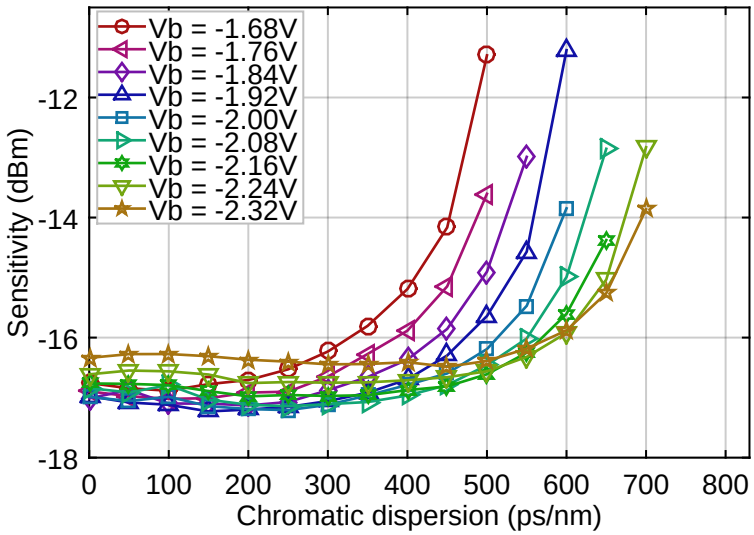


Figure 3.21: Sensitivity of a 25 Gb/s NRZ signal with EDB detection for various EAM bias.

is preferable, provided that the receiver filtering is adequate, either because a 10 GHz photodiode is used or electrical filtering is performed.

PAM4, whose sensitivities are reported in Figure 3.22, showed the highest resilience to CD among all modulation formats. It allowed for up to 800 ps/nm of uncompensated dispersion in the system, accounting for more than 45 km of SMF, showing a sensitivity of −11.6 dBm with the EAM biased at −2.24 V. This is due to the lower Baud-rate that translates to twice the symbol period, 80 ns compared to the 40 ns of NRZ, making it more tolerant to ISI caused by the same amount of CD. In B2B, PAM4 was the most affected by the EAM bias condition due to the unequal level spacing of the four signal levels caused by loss of linearity. When lower bias values were used the best sensitivity was achieved for intermediate values of dispersion, instead of B2B, due to the initial distortion. For the lowest bias, a penalty of 3.0 dB was measured compared to the best case. However, this setting could support 800 ps/nm of dispersion with only a 0.7 dB penalty with respect to its B2B performance.

Figure 3.23 summarises the CD tolerance of the four modulation formats, evaluated in their best case scenario. NRZ is the most impaired of the four, while PAM4 offers the longest reach, thanks to the reduced Baud-rate. For the analysis results related to CD tolerance, the B2B sen-

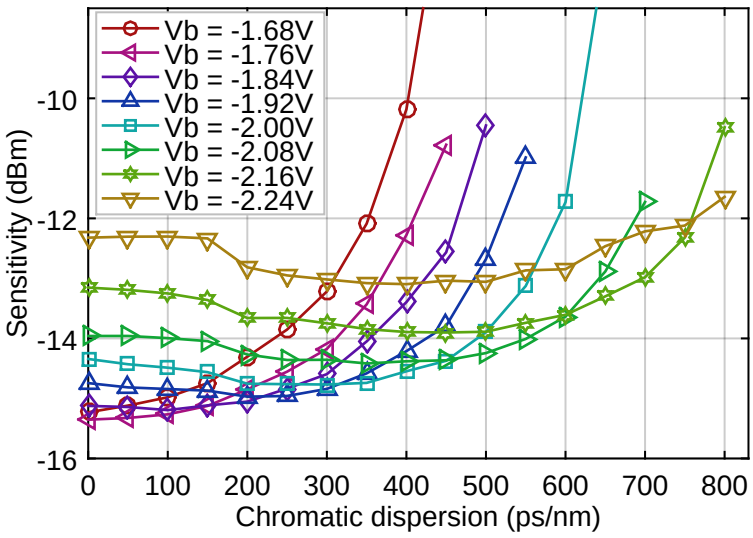


Figure 3.22: Sensitivity of a 25 Gb/s PAM4 signal for various EAM bias.

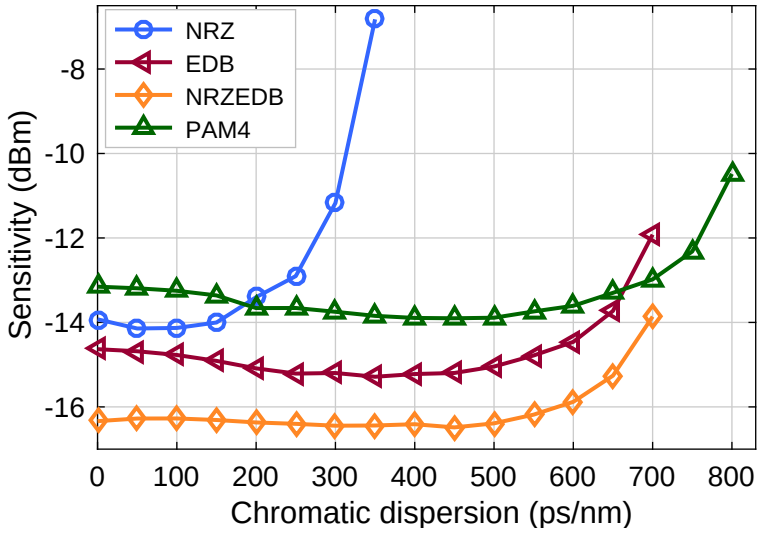


Figure 3.23: Sensitivity of NRZ, EDB, NRZ-EDB and PAM4 modulation under increasing chromatic dispersion.

sitivity obtained for the 25 Gb/s NRZ is worse than the EDB but this is due to the different PIN receivers used, rather than being an intrinsic property of the modulation formats. The 10 G PIN had a responsivity of 0.8 A/W at 1550 nm and a 400 V/W conversion gain from the TIA compared to the 0.5 A/W responsivity and 150 V/W conversion gain of the 40 G photo-receiver. If a photodiode with the same parameters was used for the BER measurements, NRZ would show the best sensitivity, as in the case of Figure 3.16, where the same PIN photodiode was employed.

The analysis presented showed advantages and drawbacks of the most promising candidate modulation formats for 25 Gb/s line rate in PONs. NRZ remains attractive because it offers the simplest implementation for the electronic circuitry in the transceivers. Using similar receivers, NRZ also has a better sensitivity due to the higher level separation in the binary signal (Figure 3.16). However, the speed of the electronic and optical components has to scale-up with the bit-rate, with consequent increase in the device cost and power consumption of the electronics. Also, the high Baud-rate of the signal makes it the most affected by CD, heavily limiting the fibre reach in uncompensated systems.

EDB is obtained through filtering of an NRZ waveform and the speed required for the electronics is equal to the NRZ case, with the addition of a pre-coder at the transmitter and a more complex two threshold

receiver. Also, linearity of the devices is necessary to preserve level spacing through transmission. However, at the cost of this more complex implementation, EDB offers a tolerance to CD which can double the uncompensated fibre reach compared to NRZ. The transceivers only need to be equipped with modulators and photo-receivers whose bandwidth is compatible with the previous generation of devices designed for 10 G NRZ systems. It was shown that, in a full 10 G system, a transmitter bandwidth in excess of the ideal quarter-rate low-pass filter needed for duobinary filtering actually provides better overall performance because the other bandwidth-limited elements of the network contribute to the EDB filtering. These components generate instead additional undesired ISI if an EDB transmitter with a precise quarter-rate bandwidth is used, lowering the system performance.

Lastly, PAM4 has both advantages mentioned for EDB, with an even more pronounced CD tolerance, and, in addition, the operational speed of the entire electronic circuitry of the system is half the bit-rate. This comes at the cost of a more complex circuitry that needs a 2-bit DAC at the transmitter and a three-threshold receiver. The sensitivity of EDB and PAM4 using the same devices was comparable and so one does not offer a clear advantage over the other in terms of link power-budget. Table 3.3 offers a summary of advantages and disadvantages of the investigated modulation formats in addressing architectural aspects relevant to PON systems.

modulation format	sensitivity	complexity	required bandwidth	dispersion tolerance
NRZ	√√√	√√√	√	√
NRZ-EDB	√√	√√	√√	√√
EDB	√	√√	√√√	√√
PAM4	√	√	√√√	√√√

Table 3.3: Comparison between modulation formats.

3.3 Linear burst-mode receiver

Multilevel modulation formats have the advantage of higher spectral efficiency, as emerged from the experimental demonstrations reported in the previous Sections, but the change from a binary to an M-ary constellation requires all components in the system to be linear in order to preserve unaltered symbol spacing. In PONs all the passive optical components employed are linear, or can generally be considered such at the typical operating power regimes. Hence, the system design needs to focus on optoelectronic components at the transmitter and receiver ends, and on optical amplifiers, if employed. The OLT receiver, which needs burst-mode functionality, is usually the most challenging component in terms of linearity and it is addressed in the following Section. The architectural design of a new linear BM-Rx is firstly presented and discussed and the operation of a prototype BM-TIA, the first building block, is then tested and characterised in a PON scenario.

3.3.1 Linear burst-mode receiver design

The early and current generations of commercial BM-Rxs for PONs generally use a limiting post-amplifier (PA) stage, hence they are not linear. G-PON or XG-PON systems, where the upstream is a 1.25 Gb/s or 2.5 Gb/s NRZ signal, respectively, do not employ electrical equalisation at the receiver and only perform slicing of the incoming binary signal, where the limiting amplifier stage does not represent a limit to performance. However, with the increase in bit-rate and fibre length, tapped delay-line electrical equalisers and more advanced modulation formats are being considered as viable solutions in future PONs, which introduce the need to preserve linearity during the conversion from optical to electrical domain. A linear BM-Rx hence becomes a key device to enable the use of advanced modulations and DSP techniques in PON upstream channels. The desired output of a BM-Rx is an AC coupled signal with no DC level and equal signal amplitude for every burst, irrespective of their input optical power. As the photodiode output current is a DC signal proportional to the incident optical power, the electrical part of the receiver has to perform two key operations: align the DC components of

the bursts and equalise their amplitude.

Generally, in the architecture of a BM-Rx, the BM-TIA provides partial burst amplitude compensation, featuring a variable-gain amplifier, while the PA performs the residual amplitude equalisation. A first approach is to have an AC coupled interface between TIA and PA with large coupling capacitors, as shown schematically in Figure 3.24a). Such an interface is preferred for its simplicity but, for burst-mode traffic, it introduces a trade-off involving envelope transients over the AC-coupled interface between the TIA and PA, due to the high-pass filtering effect. For example, the use of a 100 nF capacitor in the AC interface of a 50 Ω system, to suppress DC level decay during long consecutive identical digits (CID) runs, would create transients on the order of microseconds,

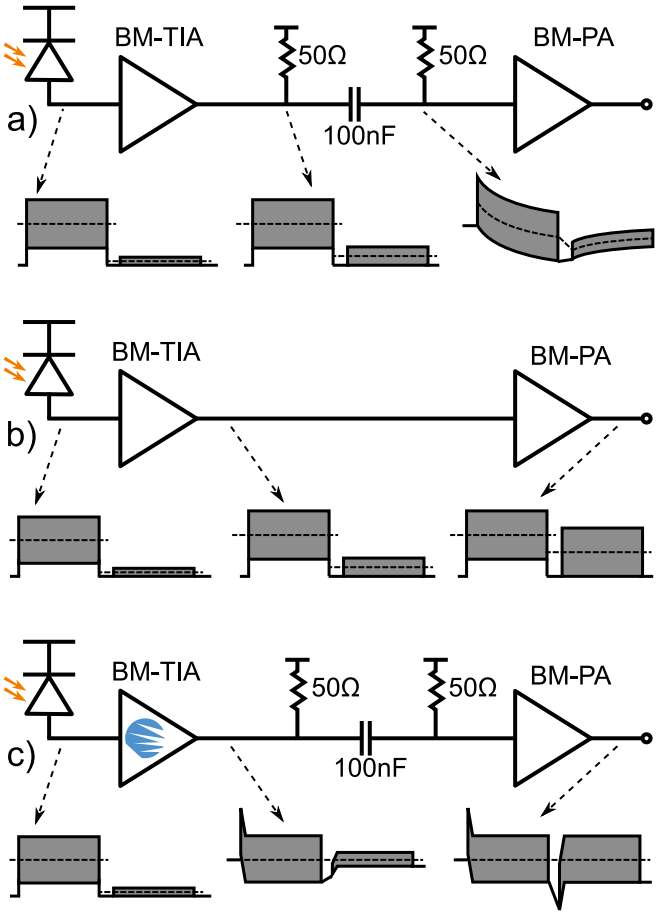


Figure 3.24: Comparison of coupling schemes for BM-TIA and BM PA: a) AC-coupled interface, b) DC-coupled interface, c) AC-coupled interface with novel TIA design.

which are unacceptable for burst-mode operation. The transients can be avoided with the use of a DC coupled interface, as in Figure 3.24b). However, unless the TIA and PA are integrated on the same chip, a DC-coupled interface is generally undesired as it is more difficult to realise, especially if the TIA and PA are developed with different technologies.

The idea behind the newly developed linear BM-Rx is that transients through an AC coupled interface can be avoided if, at the TIA output, the baselines of successive bursts are aligned to the same level, irrespective of the burst amplitude, as in diagram c) of Figure 3.24. This design allows the use of large AC-coupling capacitors between a burst-mode TIA and a burst-mode PA, thus avoiding baseline wander during long strings of CIDs while maintaining a short guard-time between bursts and a short preamble at the start of each burst. Such an AC-coupled interface is preferred over a DC-coupled one as the latter requires specifically co-optimised chipsets while the former can enable easier integration of chip parts from different developers or vendors.

The linear BM-Rx analysed in this Section was developed by the micro-electronic design team in the Tyndall National Institute Photonic Systems Group. The prototype BM-TIA was the first step in the realisation of a complete BM-Rx. The variable-gain PA was not developed in this chip but is not expected to pose important architectural challenges, being a more common device. In addition, the BM-TIA characterised offers an AC coupled interface and, hence, any commercial PA could be employed with minimum compatibility issues. Figure 3.25 shows a schematic diagram of the BM-TIA blocks. The photodetector current is amplified by the TIA A_1. A feedback loop, closed using the operational amplifier OA_1, restores the baseline of successive bursts by adjusting a bias voltage (V_{OC}) inside A_1, such that its averaged output equals the reference level V_{ref}. The output of V_{ref} and A_1 are provided to the differential buffer A_2, which also drives 50 Ω termination resistors, to perform single-ended to differential conversion. This approach of shifting the single-ended output of A_1, with respect to a reference, avoids the dummy TIA conventionally used for single-ended to differential conversion, saving power and chip area. The bandwidth of the feedback loop formed by the amplifier OA_1 can be adjusted by programming on-chip capacitance settings, to make the TIA convergence time faster or slower.

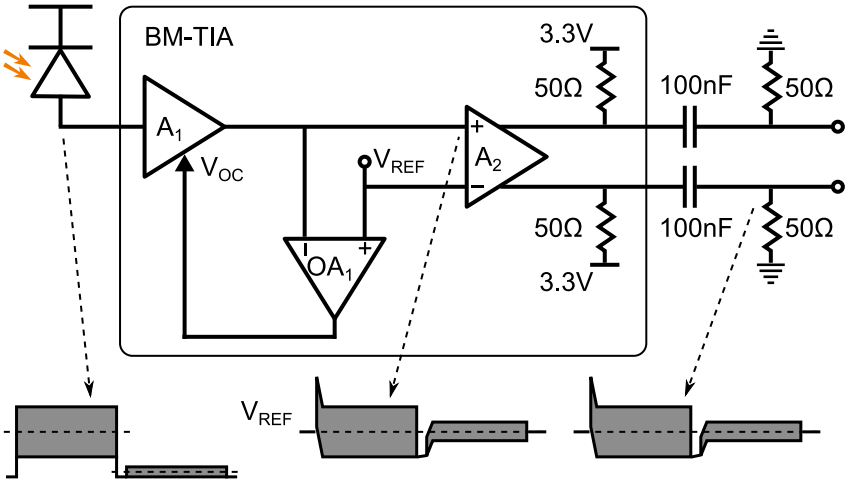


Figure 3.25: Block diagram of developed BM-TIA.

This bandwidth introduces the trade-off among settling time between successive bursts and baseline wander during long CID sequences, which is a key parameter of the receiver. Optimising this trade-off at this stage in the receiver allows for the use of large coupling capacitors between the successive building blocks of the receiver. The strategy used for baseline restoration in this design does not need an external reset signal between bursts, unlike other BM-Rxs, avoiding the necessity of peak detection circuitry in the receiver. It is also to be noted that no specific symbol pattern is needed in the preamble for the gain setting of the receiver, easing the requirements and procedure in the system design.

The device tested was fabricated using 130 nm SiGe BiCMOS technology for the BM-Rx electrical chip, whose area was 1.4x1.3 mm^2. The chip was enclosed in a standard 14-pin butterfly package with differential GPO RF output and equipped with a linear PIN photodiode with a responsivity of 0.5 $\frac{A}{W}$. The photodiode was wire bonded to the electrical chip but the package did not have an aligned optical fibre interface. Hence, the device was mounted on a probe station and a cleaved SMF was vertically aligned on top of the photodiode substrate to perform the measurements. The measured analog bandwidth of the packaged receiver was 12 GHz (Figure 3.26). An external micro-controller was used to set the bandwidth of the BM-TIA restoration feedback loop, setting the capacitance value of an equivalent RC circuit by managing the connections from a capacitor bank.

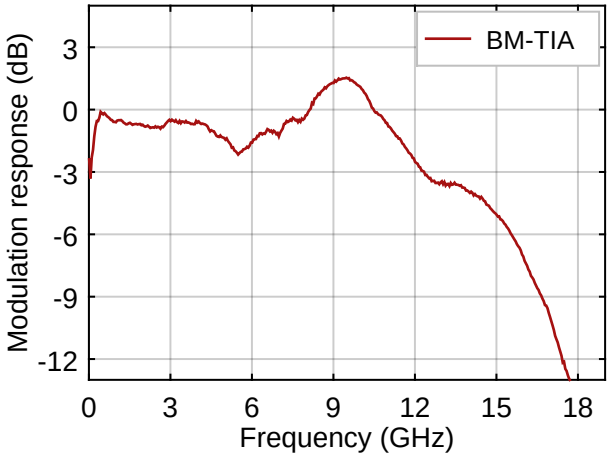


Figure 3.26: Measured bandwidth of BM-TIA.

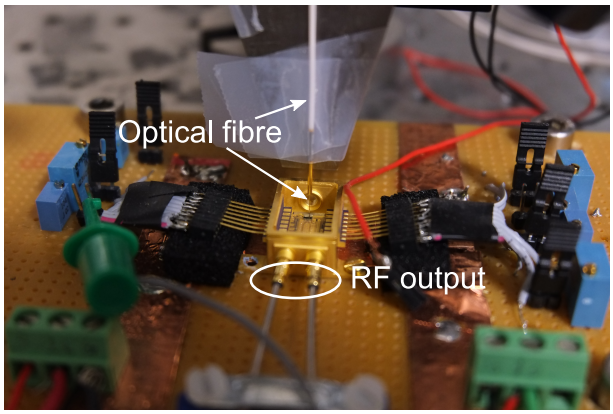


Figure 3.27: Packaged BM-TIA on optical probe station.

3.3.2 Experimental setup

The experimental setup in Figure 3.28 was built to characterise the BM-TIA. Two tuneable lasers were set with their wavelengths on two C-band ITU-T channels, a gain-controlled SOA after each laser was used for carving of the signal, suppressing the emission during the off-state between their transmission bursts. In this setup, two ONUs were implemented and the TDMA protocol was emulated by synchronising the two SOAs's "on" and "off" states. An arrayed waveguide grating (AWG) was used to merge the two optical signals, as it had lower insertion losses than a power coupler and also could suppress the out of band ASE from the SOAs. The combined signal was then sent into an EAM with a 3 dB

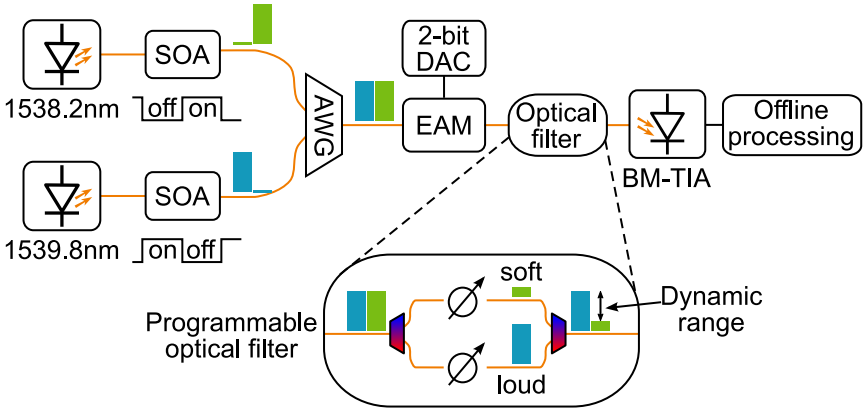


Figure 3.28: Experimental setup for BM-TIA characterisation.

measured bandwidth of 13.1 GHz. The modulator was driven by a two bit DAC generating a 25 Gb/s PAM4 burst signal, with a 20.5 ns guard-band period, synchronised with the gain switching of the SOAs where every burst was modulated during the on period of its transmitter. A programmable optical filter was then used to arbitrarily control the power of the two bursts, as independent attenuation values could be set across the wavelength spectrum. By setting a different attenuation for the two frequency channels, DR was generated in the system, that is the optical power difference between bursts. The use of a programmable optical filter was chosen for experimental convenience because it allows for a wider and more precise DR than using a single gating SOA at the transmitter [87] and also is a more realistic implementation as the signal is not optically amplified after modulation. In addition, it is simpler and does not require multiple DACs and modulators, as in a full burst-mode setup with independent ONUs [72,88]. In the remainder of this work, the optical bursts are conventionally named soft-burst and loud-burst to identify the one with lower and higher optical power, respectively. The output signal from the filter was sent to the BM-TIA whose electrical output was captured with a 50 GS/s DSO, with a 12.5 GHz 3 dB bandwidth. Off-line processing was then used on the waveform to synchronise the incoming signal and perform BER counting.

3.3.3 Receiver settling time

The receiver had a programmable capacitance on-chip whose value decided the baseline restoration loop bandwidth and, hence, the circuit time constant. The equivalent capacitance value was set by combining elements from a bank of different size capacitors in the desired way. The feedback loop time constant determines the settling time of the receiver, which is the time needed to align the DC level of two incoming bursts with optical power difference, or DR. On the other hand, it also affects the baseline wander, that is the DC component shift during a run of CID. The baseline wander has to be avoided as it causes BER increase due to the fixed receiver slicer threshold that would differ from the optimum decision threshold.

The settling time between bursts was measured for DR values of 0 dB, 6 dB and 12 dB (Figure 3.29). The settling times reported correspond to the time needed for an excursion from 5 % to 95 % of the final value. Increases in settling time with the DR was observed especially for the soft-bursts and, for some intermediate settings, longer settling times were measured, caused by oscillation of the signal. As expected, settings with

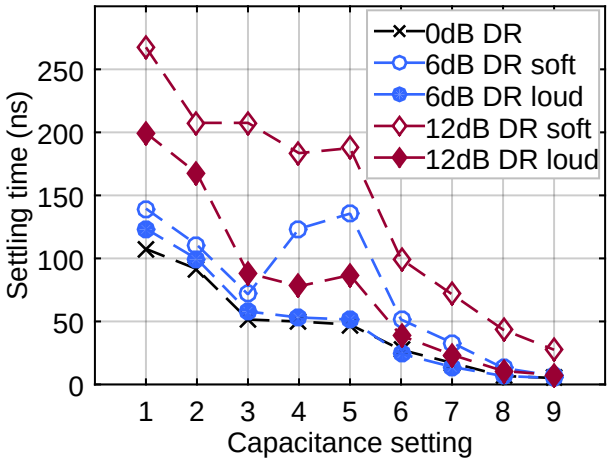


Figure 3.29: Settling time of BM-TIA for different restoration-loop bandwidths.

the lower circuit capacitance performed faster in term of settling time and appear more optimum for the desired burst-mode application. However, in order to quantify the performance, the BER sensitivity was measured for the various capacitance settings to capture the negative effect of base-

line wander. Sensitivities were measured for a 25 Gb/s PAM4 signal with different data patterns to capture the impact of the CID runs on the BER degradation. Data content was a PRBS of either order 7 or 15, mapped to the 4 symbols of the PAM4 constellation. Lower order PRBS have a shorter seed and shift register delay line, which causes shorter unique sequences in the final pattern and, hence, lower density disparity. While the PRBS 7 case showed less than 1 dB penalty even in the worst case, the PRBS 15 pattern had a penalty in excess of 7 dB, highlighting the negative effect of a restoration loop with a very high bandwidth and short settling time. Figure 3.31 shows the error distribution along the PRBS patterns for the two orders of PRBS used, 7 and 15. The performance of the shortest PRBS 7 was not significantly affected by the capacitance setting and, in both cases examined, the error contributions were generated by stressful symbols sequences evenly distributed along the pattern. For the PRBS 15, on the other hand, the analysis showed marked concentration of the errors in specific regions of the pattern when a low capacitance was selected. The error concentrations corresponded to pattern sections where the PAM4 symbols distribution was uneven, for example with a majority of 0 and 1 over 2 and 3. This caused baseline wandering and consequent envelope distortion of the waveform, as visible in the inset, which also resulted in BER increase. PRBS 15 was considered as a reference as the use of 64B/66B line coding, adopted for example in the 802.3av IEEE 10G-EPON standard, ensures statistical limits to the lengths of CID. Also, the off-line testing experimental setup could not support analysis with PRBS of higher order. An intermediate BM-Rx setting providing a convergence time within 100 ns, while ensuring less than 1 dB penalty for a PRBS 15 pattern was chosen as the operation regime for the measurements to follow (setting no. 6 in the reported graphs). It is also to be noted that the sensitivity penalty rises sharply for smaller capacitance values (setting no. 7 or higher), hence the chosen value offers more tolerance. This is compatible with future PON standards which are targeting burst overhead times of maximum 200 ns including BM-Rx settling, clock data recovery (CDR) and eventual equaliser training.

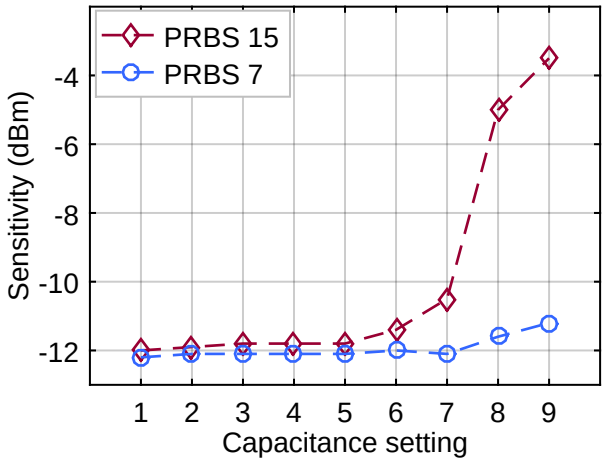


Figure 3.30: BER penalty induced by baseline wander.

3.3.4 Receiver dynamic range

The BM-Rx operation across a range of optical input powers is determined by two different noise mechanisms affecting the signal. The reception of the so-called soft-burst, with the lowest optical power, is impaired by the thermal noise coming either from the photodiode or the TIA, which lowers its SNR. On the other hand, the more energetic loud-burst is subject to distortions coming from the electrical amplifier being pushed into saturation. For the 25 Gb/s PAM4 transmission used in the experiment the BER was, at first, measured during a continuous signal reception, without using the burst-mode functionality of the receiver, to identify these boundaries. The sensitivity of the receiver for a 10^{-3} BER was measured to be -12 dBm and the overload power $+1.3$ dBm, resulting in a supported dynamic range of 13.3 dB. Similar measurements were then carried out in burst-mode to confirm that the BM-TIA was not adding any source of degradation to the received signal when dealing with optical bursts. The bursts from the two ONUs were separated by a 20.5 ns guardband period, where both transmitters were off and the initial 160 ns of every burst was used as a preamlbe for the BM-TIA baseline recovery. During the measurements of the soft-burst BER, the optical power of the loud-burst entering the receiver was kept fixed at its expected 10^{-3} BER sensitivity, and vice versa when acquiring the loud-burst BER trace. In this way, the receiver was stressed under the highest DR it could support while guaranteeing satisfactory pre FEC

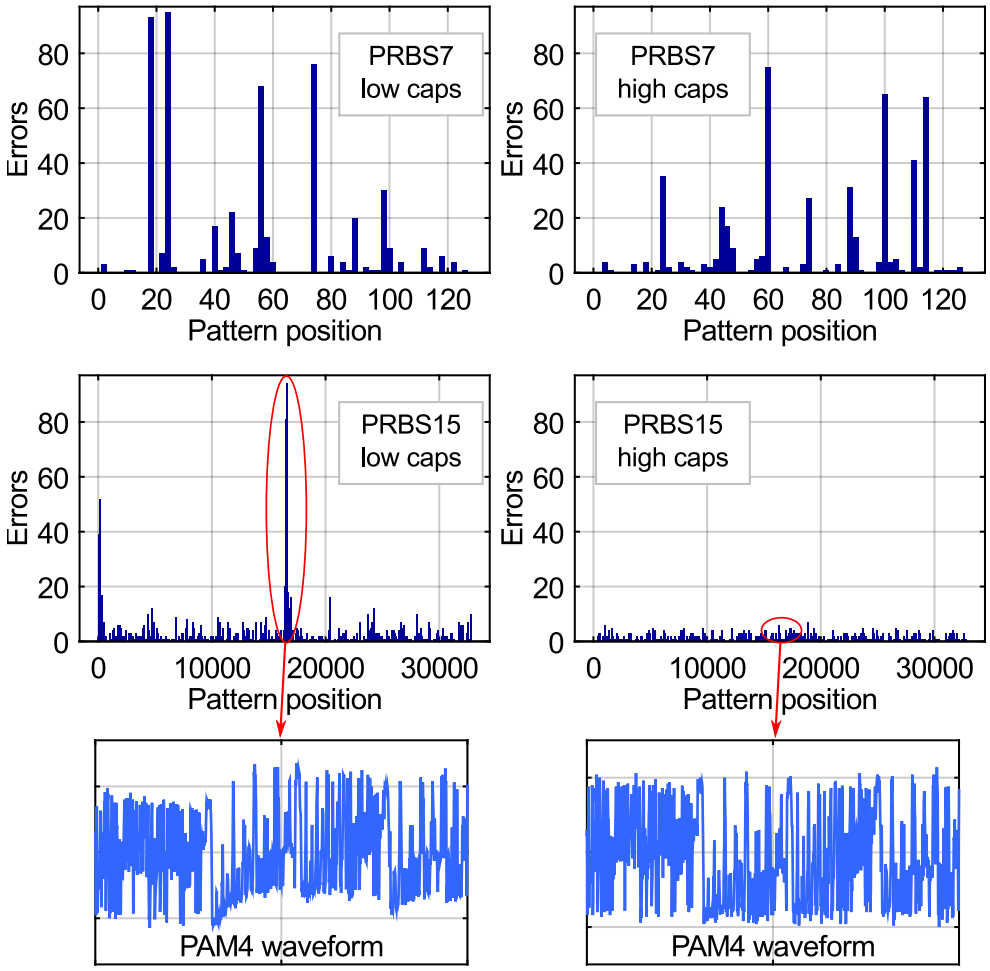


Figure 3.31: Error distributions along the PRBS patterns for different capacitance settings. Insets show the electrical waveform with visible baseline wandering in one case.

performance. The observed BER behaviour as a function of the received optical power did not show any significant differences between continuous mode operation and burst-mode, both for the soft and loud burst, confirming the suitability of the receiver to be employed in burst-mode application.

Further analysis featuring this BM-TIA, conducted to increase its sensitivity, in order to support a higher power budget, and enable transmission over up to 40 km of SMF, where linear electronic equalisation is employed, are treated in Section 4.1 of this work. In Chapter 5, on the other hand, an alternative approach where power equalisation is performed in the optical domain is presented in Section 5.2.

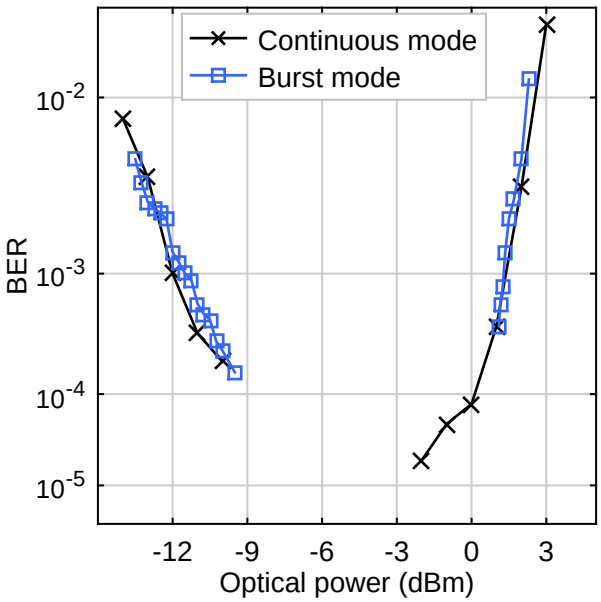


Figure 3.32: BER curves in continuous mode and burst-mode.

3.4 PAM4 hierarchical modulation

In the previous paragraphs of this Chapter, the use of more advanced modulation formats has been discussed and demonstrated as a way to increase the bit-rate of the current generation of optoelectronic devices, thanks to their higher spectral efficiency. A drawback of such modulation formats is the higher optical power required at the receiver that reduces the allowable power budget and drives the need for optical amplification in the access domain. This paragraph introduces an alternative approach to extend the maximum allowed power budget in the downstream direction, while maintaining the higher spectral efficiency of multilevel modulation. A peculiar characteristic of PONs is the difference in transmission path losses between the OLT at the head-end of the network and the various ONUs of the subscribers. This means that, in the downstream, for a given launched power from the OLT, different users will have different received powers. Hierarchical modulation can take advantage of the spread in differential reach and loss budget present in PON optical distribution networks to efficiently redistribute the optical power margin of the system between different ONUs and improve the overall power budget [89, 90]. In this Section, a hierarchical modulation scheme is implemented in a

PON downstream channel with the use of PAM4 modulation, which is achieved by combining an interleaved detection scheme [91] with unequal spacing of the PAM4 signal levels. Taking advantage of the asymmetry in the PON physical structure, this allows a redistribution of the power margin between ONUs that experience different path losses in order to increase the supported losses of the ONUs most impaired by attenuation, provided sufficient power margin is available in the ONUs nearer to the OLT [55]. The following Subsection explains in detail the proposed PAM4 interleaved detection scheme and hierarchical modulation and it is followed by the experimental validation and transmission results, where differential power budget is demonstrated, allowing for extended maximum path loss.

3.4.1 Hierarchical modulation with interleaved ONUs detection scheme

Hierarchical modulation, or layered modulation, is a multiplexing strategy used to transmit multiple data streams into a single symbol stream. It is generally realised with multi-dimensional constellations and can be used in broadcast type transmissions to provide users with different quality of service depending on their reception quality [90, 92, 93]. In point-to-multipoint TDMA networks, like PONs, hierarchical modulation can be used to adjust the downstream constellation to the different SNR or received power experienced by the various ONUs. It has been proposed in previous works with optical OFDM [89], PSK [94] or QAM [95] where two modulated data layers were simultaneously received by two ONUs and adjusting the constellation to the receiver SNR resulted in improved power budget or capacity. Here, hierarchical modulation is proposed using PAM4, which is a simple one-dimensional modulation format. Interleaved detection of its two NRZ components is used to multiplex the data stream into two layers and non-uniform spacing of the PAM4 levels to determine the degree of hierarchical modulation in the network. The system described in the following Sections allows the realisation of a PON with ONUs divided into two groups, depending on their distance from the OLT, with a different dedicated logical transmission channel (Figure 3.33). The advantage of the scheme is that it allows for redistribution

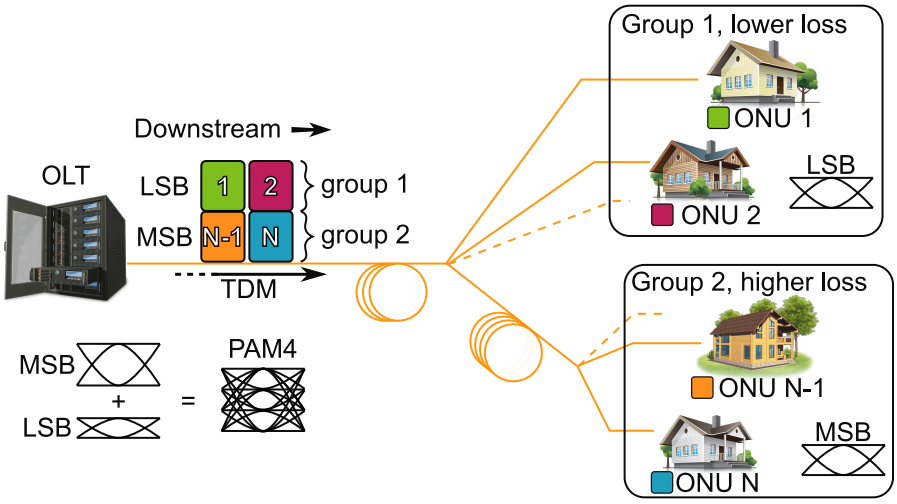


Figure 3.33: PON system with PAM4 hierarchical modulation.

of the PON differential loss budget, transferring available power margin from less impaired ONUs to the ones which suffer from a higher path loss. This can provide service to ONUs that otherwise would be out of reach due to the more severe impairments of the channel.

PAM4 Interleaved Detection

The traffic in PONs is generally managed by a TDMA protocol in which every user is exclusively allocated a periodic time slot during which data transmission is performed. In the downstream direction the OLT transmits a continuous sequence of packets, which are destined for the various ONUs, as specified in the packet header. The ONU receiver physically operates in continuous mode, as its CDR is synchronised during the whole transmission time, but the protocol layer only decodes payload data from the packets which are addressed to the specific subscriber. In such a situation, where multiple detectors are receiving the same signal, PAM4 reception can be implemented with an interleaved detection scheme where the MSB and LSB data streams are assigned to two different groups of ONUs [45, 55]. As a result, instead of a single ONU decoding two bits per symbol during an exclusively dedicated time-slot, two ONUs simultaneously decode one bit each from different NRZ streams encoded in the same PAM4 time division multiplexing (TDM) packet. If Gray coding is used to generate the PAM4 sequence, a single-threshold receiver is

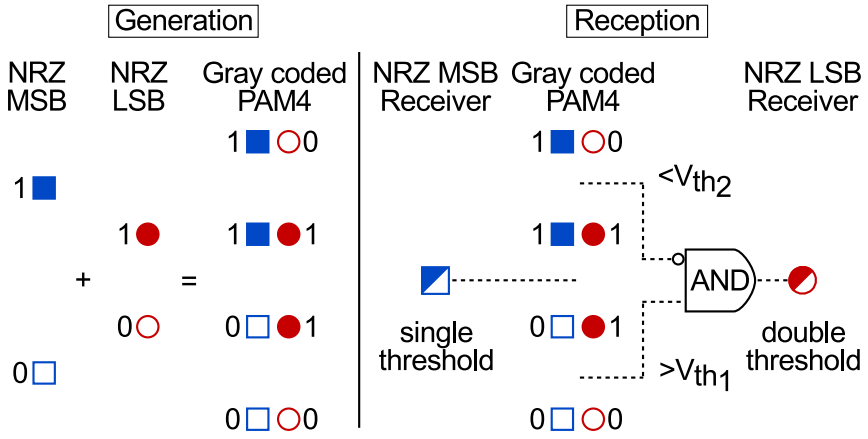


Figure 3.34: Gray coded PAM4 generation and interleaved detection of the tributary NRZ streams.

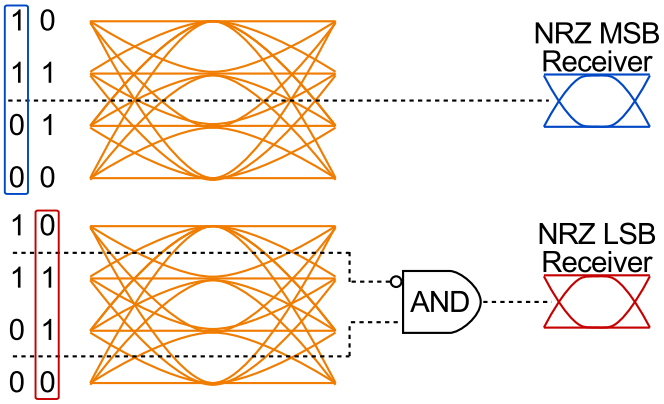


Figure 3.35: MSB and LSB receivers for PAM4 interleaved detection.

sufficient for the MSB ONU type and a dual-threshold receiver, coupled with an AND logic gate for the LSB ONU type (Figure 3.34, 3.35), both of which are simpler than a full PAM4 receiver with three thresholds. In practice, a single LSB ONU design can be deployed and electrically reconfigured to act as an MSB ONU where required, by connecting one of the threshold comparators to a logical one. In such an implementation the peak-rate of each ONU is halved, but the aggregate capacity of the PON system is unchanged, because two receivers are working simultaneously [55].

Non-uniform PAM4 level spacing

Combining the above scheme with unequal spacing of the PAM4 signal levels, a higher portion of the signal power can be allocated in the MSB stream, consequently reducing the relative power in the LSB. This translates to generating a signal with a symmetric eye diagram but with enhanced opening of the central eye and reduced opening of the outer eyes (Figure 3.36). The ER of the inner eye and the outer eyes determines, respectively, the sensitivity of the MSB and LSB receivers. Hence this strategy improves the single-threshold MSB receiver sensitivity, whereas the sensitivity is reduced for the corresponding double-threshold LSB receiver. In this implementation, the excess power budget from the ONUs with lower loss paths can be transferred to the ONUs closer to the sensitivity limit, effectively increasing the maximum power budget supported. Since the eye diagram is kept symmetric, the degree of unequal level spacing in the signal is quantified using the level mismatch separation ratio R_{lm} metric, as defined for PAM4 in IEEE P802.3bj clause 94.t. The minimum opening of the three eyes, S_{min}, is calculated as

$$S_{min} = min\left(V_3 - V_2, V_2 - V_1, V_1 - V_0\right) \tag{3.9}$$

where V_0 to V_3 are the average values of the PAM4 signal levels at the sampling point (Figure 3.36) and R_{lm} is calculated with the following expression:

$$R_{lm} = \frac{3S_{min}}{(V_3 - V_0)}. \tag{3.10}$$

Because of the eye diagram symmetry the outer eye's opening is the same for both of them as the inner eye opening is increased, hence the above metric corresponds to a unique condition of the transmitted signal. For a PAM4 eye diagram with equally spaced levels R_{lm} is 1 and increasing power allocated in the MSB stream corresponds to R_{lm} decreasing from 1 towards 0 (Figure 3.36). As the opening of the inner eye increases, the difference in required optical power between the two detectors becomes greater, with the MSB receiver achieving higher sensitivity than a full PAM4 receiver and the LSB showing decreased performance. To better understand the expected performance of the system, the symbol error probability for the two receivers in an AWGN scenario was calculated as

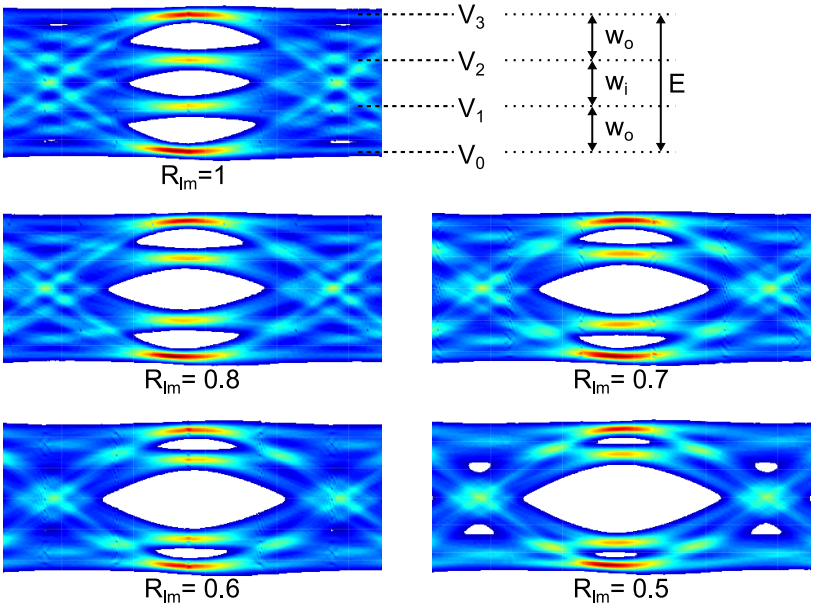


Figure 3.36: Eye diagrams with increasing asymmetry levels.

a function of R_{lm}. Defining w_i as the opening of the inner eye, w_o as the outer eye's opening and E as the opening of the full PAM4 eye, the following relations hold:

$$w_i + 2w_o = E \ , \tag{3.11}$$

$$w_o = \frac{E}{3} R_{lm} \ , \tag{3.12}$$

$$w_i = E\left(1 - \frac{2}{3} R_{lm}\right) \ . \tag{3.13}$$

If σ represents the added AWGN standard deviation for the rail, the error probability of single-threshold and double-threshold receivers can be expressed, respectively, as:

$$P_{MSB} = \frac{1}{4} erfc\left(\frac{w_i}{\sqrt{2}\sigma}\right) \ , \tag{3.14}$$

$$P_{LSB} = \frac{1}{2} erfc\left(\frac{w_o}{\sqrt{2}\sigma}\right) \tag{3.15}$$

which, as a function of R_{lm}, are equivalent to:

$$P_{MSB} = \frac{1}{4} erfc\left(E\left(1 - \frac{2}{3} R_{lm}\right) \frac{1}{\sqrt{2}\sigma}\right) \ , \tag{3.16}$$

$$P_{LSB} = \frac{1}{2} erfc\left(\frac{ER_{lm}}{3\sqrt{2}\sigma}\right). \tag{3.17}$$

Defining the SNR as

$$SNR = \frac{E^2}{\sigma^2} \tag{3.18}$$

the following expressions describe the BER as a function of SNR for the MSB and LSB receivers, respectively:

$$P_{MSB} = \frac{1}{4} erfc\left(\frac{\sqrt{SNR}}{\sqrt{2}}\left(1 - \frac{2}{3}R_{lm}\right)\right) , \tag{3.19}$$

$$P_{LSB} = \frac{1}{2} erfc\left(\frac{\sqrt{SNR}}{\sqrt{2}}\frac{R_{lm}}{3}\right). \tag{3.20}$$

Because the above expressions have a different factor multiplying R_{lm} as the argument inside the $erfc$ function, their behaviour is not exactly symmetrical, with the LSB performance degrading more rapidly in terms of SNR than the gain obtained by the MSB for the same R_{lm} settings. Figure 3.37 reports the theoretical BER for the two receivers as a function of the electrical signal SNR, also compared to a conventional PAM4 receiver and to an NRZ receiver of the same Baud-rate. As R_{lm} decreases, the MSB performance approaches that of a binary NRZ signal while a higher SNR is required for the LSB receiver which is affected by the smaller opening of the outer eyes. The difference between a full PAM4 receiver and the case where $R_{lm} = 1$ is due to the Gray coding adopted in the PAM4, which minimises the BER for a given SER. In order to better capture the trend when varying R_{lm}, the sensitivities from the theoretical curves for a BER of 10^{-3} are plotted in Figure 3.38, where the difference between the two offers a direct indication of the system differential power budget, acting as a guideline for the design of a system once its physical layer properties are known. The different slopes for the two receiver sensitivities are expected from the above BER expressions, due to how the R_{lm} term appears in the $erfc$ function.

3.4.2 Experimental demonstration of power budget extension

The system described above was experimentally implemented and demonstrated in a PON scenario. The test setup (Figure 3.39) had

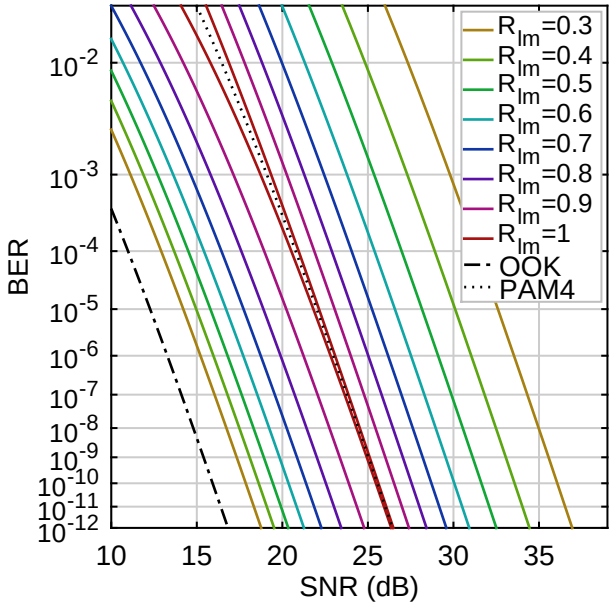


Figure 3.37: Theoretical BER curves for MSB and LSB receivers under different R_{lm}.

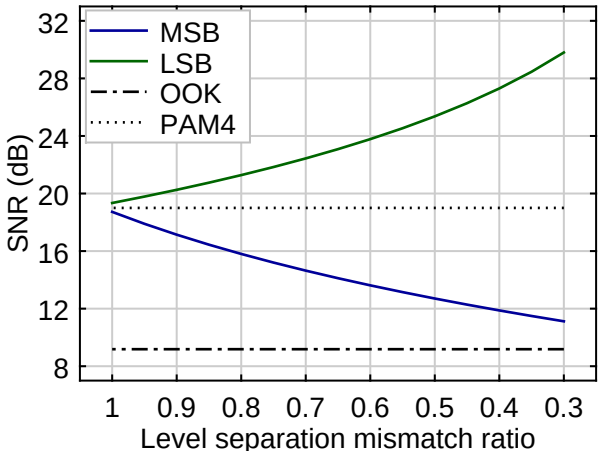


Figure 3.38: Sensitivities and differential power budget for MSB and LSB receivers under different R_{lm}.

an OLT capable of generating a PAM4 signal with the characteristic needed for hierarchical modulation and interleaved detection capabilities, an asymmetric network plant with users placed at different physical reaches, and two ONUs detecting, respectively, the MSB and LSB components of the downstream traffic.

Experimental setup

In the OLT of the experimental setup, a C-band laser centred at 1550 nm was externally modulated using an EAM with a 3 dB bandwidth of 13.1 GHz. The EAM was biased at -1.36 V to work in its linear region, to preserve the symbol spacing of the PAM4 constellation. The EAM input power from the laser was +9 dBm and the optical power of the output signal was +1.7 dBm. The modulator was driven by a 2-bit DAC whose output amplitude was kept constant to ensure that the ER, measured to be 5.8 dB, was unchanged for all the hierarchical modulation degrees investigated. The DAC was fed by two tributary NRZ streams, the MSB and LSB components of the resulting PAM4 signal. The DAC unit had a dedicated electrical amplifier controlling the output power of each of the NRZ components, so that their relative amplitudes could be set arbitrarily by tuning the bias voltages of their amplifiers. Adjusting these relative amplitudes, the module could generate a symmetric PAM4 signal with enhanced or reduced opening of the central eye (Figure 3.36). The DAC was operated at 12.5 GBd thus in order to obtain a 25 Gb/s bit-rate. The transmitted data content was a four-level pseudo-random sequence of order 15, obtained by combining one by one the bits of the two PRBS of order 15 used as tributaries, one of which was delayed by half a pattern length. An asymmetric network plant was employed with a common, 12 km span, SMF trunk line, a 50:50 colorless power splitter and VOAs used to emulate the additional power splitter insertion losses. A first ONU was connected directly after the power splitter, whereas a

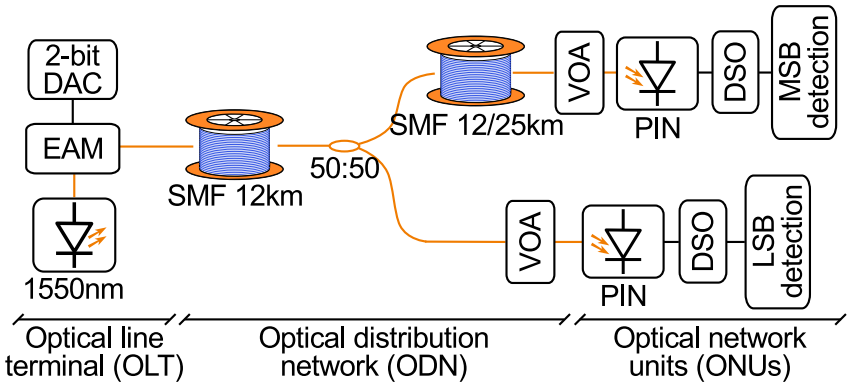


Figure 3.39: Experimental setup for hierarchically modulated PAM4 characterisation.

second ONU was connected after an additional span of either 12 km or 25 km of SMF, to emulate different degrees of differential reach. Both ONUs were equipped with commercial 10 G receivers, composed of a PIN photodiode and linear TIA, to detect the optical signal. The outputs of the PIN receivers were captured using a 12.5 GHz, 50 GS/s DSO and processed off-line for CDR implementation, pattern synchronisation and error counting. Separate error counting of the two NRZ tributary streams forming the PAM4 signal, MSB and LSB, was implemented off-line for this analysis, as described earlier (Figure 3.35).

Experimental results and discussion

The MSB and LSB detectors were characterised in optical B2B for different R_{lm} values, ranging from 0.8 to 0.5, and compared to the sensitivity of a 25 Gb/s PAM4 receiver (Figure 3.40). This PAM4 receiver was chosen for comparison, even though its peak data rate is higher, as it would provide a network capacity per wavelength equivalent to that of our interleaved approach. As the opening of the inner eye increases, meaning a lower R_{lm} is used, the difference in required optical power between the two detectors becomes greater, with the MSB receiver achieving higher sensitivity than a full PAM4 receiver and the LSB showing decreased performance. Symmetrical behaviour was obtained for MSB and LSB sensitivities at different degrees of hierarchical modulation, so that a lower R_{lm} setting corresponds to an increased differential reach that could accommodate higher differences in path losses in the network plant (Figure 3.40). As an example, the system operating with an R_{lm} of 0.5 had a 7.5 dB differential power budget between the two groups of users at a pre-FEC BER threshold of 10^{-3}. Separate detection of the MSB binary stream provided 3.5 dB improvement in sensitivity compared to PAM4, while the corresponding LSB receiver required optical power was increased by 4 dB, due to smaller opening of the upper and lower eyes. Intermediate values could be chosen to achieve a differential power budget that optimally adapts to the network physical plant conditions. The histogram in Figure 3.41 shows the differential power budget achieved for various transmitter settings and how they translate, in terms of power margin reduction, for the LSB detector and improved

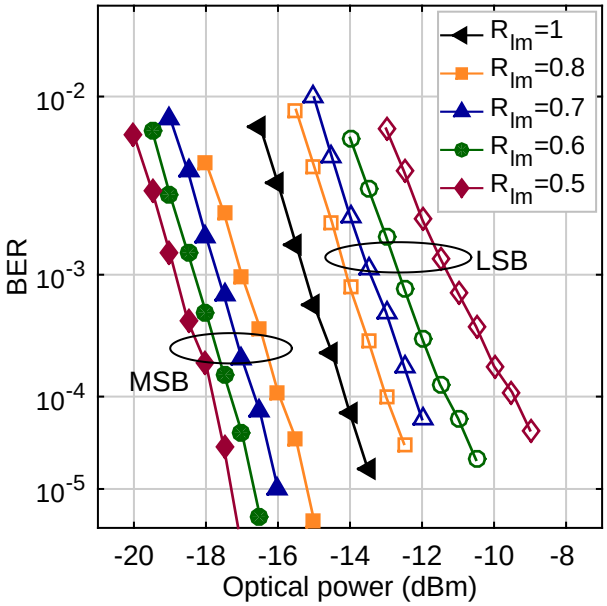


Figure 3.40: BER curves for optical back-to-back transmission.

power budget for the MSB receiver.

The sensitivity for a pre-FEC BER of 10^{-3} was then measured for both detectors adding transmission over various lengths of SMF, under different level separations conditions (Figure 3.42). The EAM bias was lowered from -1.36 V to -1.56 V, which was an optimised value for the

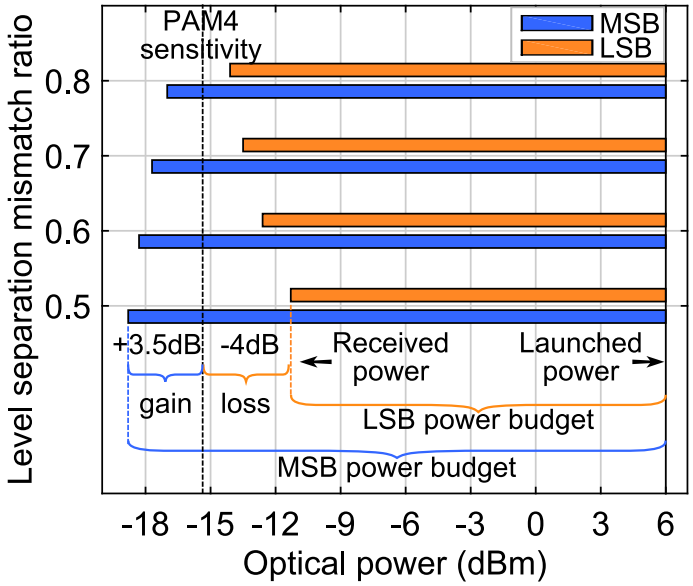


Figure 3.41: Power margin and differential power budget in asymmetric PON.

intermediate length of 25 km, to induce a certain amount of pre-distortion in the signal, which partially compensates for chromatic dispersion. The same bias value was used for all fibre lengths, as in a realistic scenario for a signal transmitted from the OLT to all the network ONUs. This bias setting explains why the B2B case did not have the highest sensitivity and the best performances were achieved for a positive overall value of chromatic dispersion. The extinction ratio was 6.2 dB for all the R_{lm} investigated in the experiment and the launched power from the EAM was +0.8 dBm. The MSB detector had similar performance between the optical B2B and with addition of fibre spans up to 25 km, meaning the chromatic dispersion had little effect, also thanks to the EAM bias setting explained previously. The same receiver showed increased sensitivity penalty when 40 km of fibre were used, in which case higher received optical powers were required and the maximum R_{lm} supported to achieve a 10^{-3} BER was 0.9. However, even in such conditions, the scheme clearly offered advantages over a PAM4 receiver, in terms of CD tolerance allowing for a 40 km transmission for half of the ONUs in the network, which would otherwise require dispersion compensation techniques [13]. Regarding the LSB detector performance, it could support 25 km of SMF or less but proved to be impractical for longer reach as the pre-FEC BER could not be achieved after a 40 km span without the use of chromatic dispersion compensation.

A full system implementation with different fibre spans was then re-

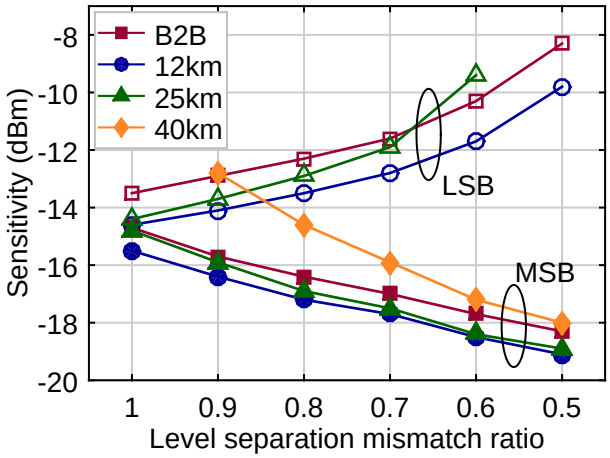


Figure 3.42: Sensitivity for different fibre spans and R_{lm}.

alised where the LSB detector was placed after 12 km of SMF and the MSB after an additional 12 km or 25 km for a total span of 24 km or 37 km, respectively. R_{lm} could be changed in the system to improve the MSB receiver sensitivity after the additional fibre attenuation and dispersion and achieve the desired differential power budget. BER performance for R_{lm} values from 0.6 to 0.8 are shown in Figure 3.43 for a 12 km differential distance, with MSB and LSB ONUs at distances of, respectively, 12 km and 24 km. Differential power budgets of 3.1 dB to 6.7 dB were measured between the 12 km and 24 km ONUs to accommodate for the extra fibre or splitter losses (Figure 3.43). Similarly, Figure 3.44 shows the measured BER curves for the 12 km and 37 km ONUs scenario where differential power budgets of 1.8 dB to 5.8 dB were obtained. This means that, provided the power margin in the LSB ONU is sufficient, the R_{lm} of the signal can be decreased to achieve better sensitivity for the MSB stream, if needed, to allow for longer reach. In this implementation, an R_{lm} value between 0.7 and 0.8 would provide the differential sensitivity needed to compensate for the 4.8 dB loss of the additional 25 km SMF and have the same power margin for both ONUs.

This scheme offers the possibility of optimising its performance to fit existing deployed network plants, by flexibly reconfiguring the degree of

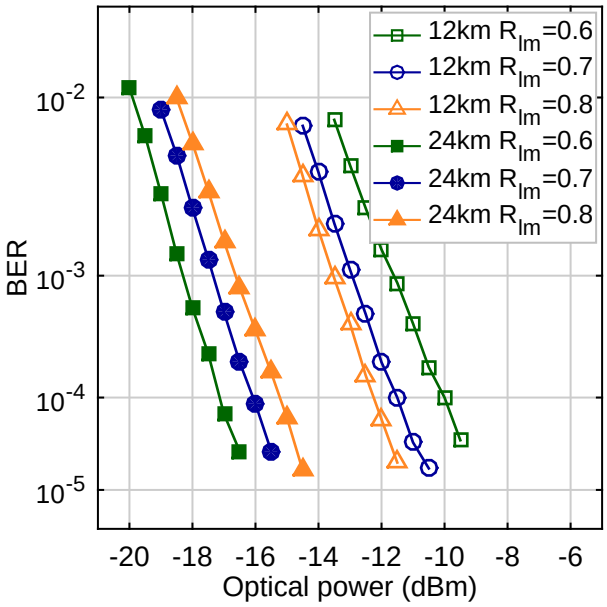


Figure 3.43: BER curves for 12 km and 24 km ONUs with various R_{lm}.

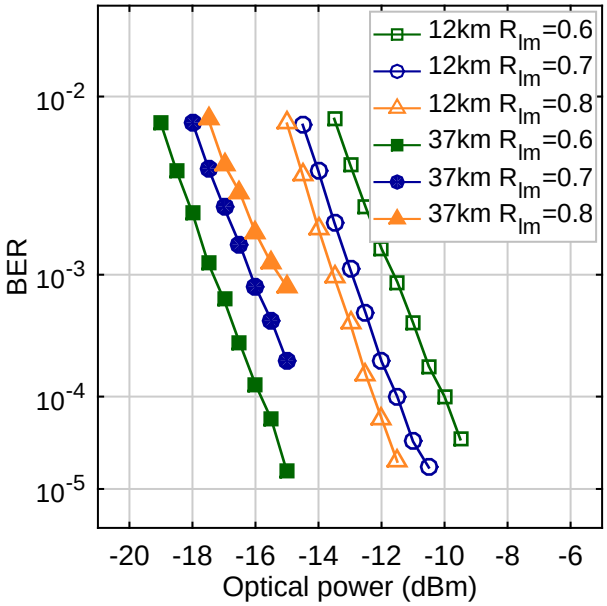


Figure 3.44: BER curves for 12 km and 37 km ONUs with various R_{lm}.

hierarchical modulation. Using a high resolution DAC at the OLT transmitter, the R_{lm} value could be changed on a burst by burst time-scale, therefore generating the optimum differential power budget between two ONUs, depending on their different optical path losses.

3.5 Summary

This Chapter discusses the advent of advanced modulation formats in PONs as a means to enable the bit-rate increase needed for the upcoming 100 G (4x25 Gb/s) systems in a cost-effective way. DMT, PAM4 and EDB modulations, in particular, are addressed and their potential is evaluated through experimental demonstrations.

In Section 3.1, a variation of OFDM, namely DMT modulation, is introduced. DMT can avail of high order modulation formats, such as QAM, to increase its spectral efficiency while keeping the attractive aspects of being suitable for IMDD systems like current PONs. While requiring substantial DSP for the implementation of all the functionalities, DMT relieves the requirements of the physical layer, in particular the bandwidth of the optoelectronic components. Its low spectral occupancy, along with the flexibility offered in shaping the spectral content,

allows previous generation devices to support the bit-rate of the successive PON standards leading to the demonstration of a 10.4 Gb/s, XG-PON compatible, bit-rate where a 1 GHz G-PON DML is used in the transmitter.

Section 3.2 looks into simpler multi-level modulation formats, in particular PAM4 and EDB. Their spectral efficiency is lower than DMT but they offer simpler implementation since, potentially, no DSP is required and the electrical front-end devices have less strict requirements. They are, hence, proving themselves a promising solution for the realisation of 25 Gb/s line-rates with the 10 G generation of optoelectronic devices. Their performance in term of bandwidth restrictions and chromatic dispersion tolerance are analysed and compared to NRZ and they emerge as attractive candidates as they do not require the newer and more expensive 25 G components and are less impaired by dispersion, thanks to their lower Baud-rate or the incorporated filtering.

Focusing then on the enabling devices, Section 3.3 introduces a novel linear BM-TIA developed in Tyndall National Institute, a key component necessary to support the mentioned advanced modulation formats in the upstream direction. The idea behind this BM-TIA architecture removes the common issue of transients introduced by AC interfaces and the need for DC coupling among chip parts in the integrated circuit, making the fabrication cheaper and open to the integration of components from different vendors. The BM-TIA prototype is tested with 25 Gb/s PAM4 traffic and shows burst-mode capabilities with a settling time between bursts of less than 100 ns and a supported dynamic range of up to 13.3 dB.

Finally, in Section 3.4, an innovative way of exploiting PAM4 characteristics is proposed to increase the power budget of PONs where a degree of asymmetry is present. A hierarchical modulation scheme for 25 Gb/s PAM4 downstream in PON systems is proposed using interleaved detection of the tributary binary streams and unequally spaced levels of the PAM4 signal. The network power budget is increased, benefiting from the improved MSB detector sensitivity which is increased by up to 3.5 dB. This receiver also has higher chromatic dispersion tolerance enabling data transmission over 40 km of fibre without the need for dispersion compensation techniques. An asymmetric network plant

with ONUs at 12 km and 37 km is demonstrated where the sensitivity of the latter has been improved to account for additional path losses and chromatic dispersion induced penalty.

Among the modulation formats discussed in this Chapter, DMT provides the best gain in terms of spectral efficiency, thanks to its ability to employ complex modulation formats. A 10 Gb/s system is realised with a 1 GHz device and similar conclusions hold for higher rates of 25 Gb/s, 40 Gb/s and 50 Gb/s which can be achieved with 10 G devices [50, 56–61, 85]. The DSP requirements limit its application in the cost-constrained field of PONs, with the results obtained for XG-PON holding for NG-PON 2 as well. Another limiting factor of DMT, when moving to higher Baud-rates, is that it relies on high-speed ADCs and DACs which are expensive and power hungry, both undesirable aspects for their employment in PON transceivers. This translates into the consideration that even though DMT will not be chosen for the 25 Gb/s line rate in PONs, it could be considered again for future standards where the target bit-rate will be increased further. Large scale development of DMT will also depend heavily on the advance and cost of the underlying CMOS technology necessary to support its DSP requirements. PAM4 and EDB, on the other hand, are more likely to be adopted in the short term where they can enhance the performance of the 10 G generation of devices but will require higher bandwidth components to scale up to future higher line rate. Hence the availability and affordability of such higher speed components will be key to determine whether they could provide an attractive solution.

4 Chromatic Dispersion Management in Passive Optical Networks

The most recent PON standards and the ones that are currently being drafted are aiming to reach SMF lengths of up to 40 km, as well as data-rates of 10 Gb/s and 25 Gb/s per wavelength. The desirable use of cost-effective transmitters such as DMLs or EMLs generates phase modulation in the optical signal which interacts with CD to induce distortions that translate into sensitivity penalties at the receiver, or loss of the signal altogether. The degrading effect of CD is enhanced by higher Baud-rates and by the use of multi-level modulation formats, such as the ones discussed in the previous Chapter. Hence, there is a need to investigate compensation strategies for the upcoming high data-rates in the access domain. There is still space for debate regarding the transmission window to adopt as the C-band, which is attractive for its low attenuation, has a high CD coefficient for long reach at high Baud-rates, while, on the other hand, the O-band offers low dispersion but higher attenuation. In the O-band FWM also needs to be considered as the systems operate near the zero dispersion wavelength. While the IEEE, in its upcoming 100G-EPON standard, is considering the use of O-band for the upstream and C-band for downstream, the ITU NG-PON 2 standard has specified both the upstream and downstream transmission windows to be in the C-band. The newest ITU XGS-PON standard, reuses the upstream O-band wavelength window, and downstream C-band window, of the previous G-PON and XG-PON systems. Understanding of CD induced limitations and effectiveness of compensation schemes is therefore vital for the design of next-generation optical access systems.

In high-rate and multi-span IMDD optical links, a common way to address the accumulated CD is to use DCF, which has an opposite and higher in magnitude dispersion coefficient than SMF, to optically com-

pensate for the dispersion introduced by the transmission fibre. Despite being an effective solution, DCF is bulky and expensive due to the several kilometres of fibre needed in the exchange nodes and it also introduces additional insertion losses. PONs can also have a high differential reach which means it is not possible to compensate for all the users simultaneously, due to the different amounts of accumulated CD. For such reasons it is not practical in PONs and, especially, at the subscriber ONU, where the cost and footprint per unit are critical. Another solution to optically compensate CD is represented by chirped fibre Bragg gratings which offer reduced footprint and insertion losses. However, they require additional components, such as a circulator, and their wavelength operational range is relatively narrow which again is not ideal for PONs. In addition, the installation and optimisation for both solutions requires physically different components based on every link reach and wavelength and has to be performed during the installation phase. EDC has recently become a topic of interest thanks to its small footprint, no insertion loss, wide range of adaptability for different compensation scenarios and potentially low production costs leveraging the state-of-the-art CMOS industry [96]. In particular, the ability to deal with different levels of impairments makes it a strong candidate for PON upstream where a burst-mode implementation of an EDC filter can compensate for different amounts of CD in the bursts. An EDC filter is not transparent to the modulation formats, whereas optical domain compensation is, hence it is also of interest to investigate its use with higher order modulation formats, for example PAM4.

In Section 4.1 a linear tapped delay-line filter with feed-forward equaliser (FFE) and decision-feedback equaliser (DFE) is introduced with a burst-by-burst adaptation feature tailored to PON upstream burst-mode application. The results of the investigation into its compensation capabilities are reported and it is then employed in a system demonstration, along with PAM4 and a linear BM-TIA, to demonstrate a burst-mode upstream 25 Gb/s single-lane bit-rate over an equivalent of 37.5 km SMF in the C-band. The application of EDC in the upstream direction is of particular interest as the cost of a single unit is shared among all network subscribers.

While the above solution is very attractive for the PON upstream,

it could be too expensive to equip every ONU receiver with a dedicated equaliser chip to compensate for CD in the downstream traffic. Ideally, the most complex components would be located in the OLT and their cost shared among all the subscribers, hence a pre-compensation scheme would be preferable for the downstream direction. The use of a chirp-free Mach-Zehnder modulator (MZM) could allow the target PON reach without the need for post-compensation at the receiver. However, the use of MZMs is generally undesirable due to their cost, size and added complexity of their control circuitry. When an EAM is used a simple strategy is to change the bias point of the modulator to change its chirp according to the target distance, even if this could offer sub-optimal performance when the differential distance between ONUs is large. The preferred transmitter would be a DML due to the cost related advantages, however the chirp generated by direct modulation heavily limits the reach when a dispersive fibre is used for transmission.

Section 4.2 discusses a chirp management technique for DMLs using narrow optical filtering with multi-level amplitude modulation. The proposed solution is particularly interesting for the PON downstream as it supports transmission of a 25 Gb/s PAM4 signal over up to 50 km SMF employing a simple slicer at the receiver as no DSP is required for post-compensation purposes.

4.1 Adaptive burst-mode linear equaliser for upstream traffic

EDC is a promising solution for CD impairment compensation in PONs thanks to the reduced footprint, no insertion loss or additional optical components needed and the attractive feature to be able to compensate for bursts with different levels of impairments, which is potentially required if the fibre plant is asymmetric [53, 54, 96]. EDC approaches the problem of CD induced ISI in the electrical domain rather than in the optical one. Various implementations of EDC for optical systems are possible. The simplest are continuous-time filters (CTFs) which present an adjustable frequency response that can be tuned to better compensate for the low-pass filtering effect of CD. While simple to implement and

cost-effective their application is limited to situations where CD is not large. FFE and DFE are another family of equalisers which use a tapped-delay line approach to compensate for ISI whose interference spreads over multiple symbol periods. The linear FFE quantifies how adjacent symbols affect the symbol under decision so that optimum tap coefficients can be determined to cancel the undesired contributions of the future and past symbols, namely pre-cursors and post-cursors. The DFE uses a feedback loop to determine the contribution of the post-cursors after their detection. FFE and DFE filters will be presented in more detail in Subsection 4.1.1 of this Chapter. Maximum likelihood sequence estimation (MLSE) equalisers are a more complex class of filters that implement a Viterbi decoding algorithm to estimate the channel frequency response and determine the symbol sequence with higher likelihood. They offer the best compensation performance but require a complex implementation due to the high amount of DSP involved, memory buffer which also increases latency and also higher power consumption when compared to the previous options.

A combination of FFE and DFE represents the preferred choice for PON systems offering the desired trade-off between complexity and performance [96]. They have significantly better dispersion compensation capabilities than CTF and do not require the large amount of DSP necessary for MLSE. Also, analog implementation of such filters is possible, thus avoiding the need for high-speed ADCs at the receiver front-end. This Section focuses on the adoption of FFE and DFE linear filters for EDC with higher modulation formats (PAM4) and in the burst-mode scenario typical of PON upstream traffic.

4.1.1 FFE and DFE filters

Tapped delay-line filters are designed to reduce the ISI by weighting the neighbouring symbols based on the estimated interference they have on the sample under reception, thereby removing their undesired contributions. Due to bandwidth limitations and/or CD, a symbol is spread outside of its period affecting the neighbouring ones and generating ISI. The symbol being detected at a given instant is named cursor and the preceding and following symbols are called post-cursors and pre-cursors,

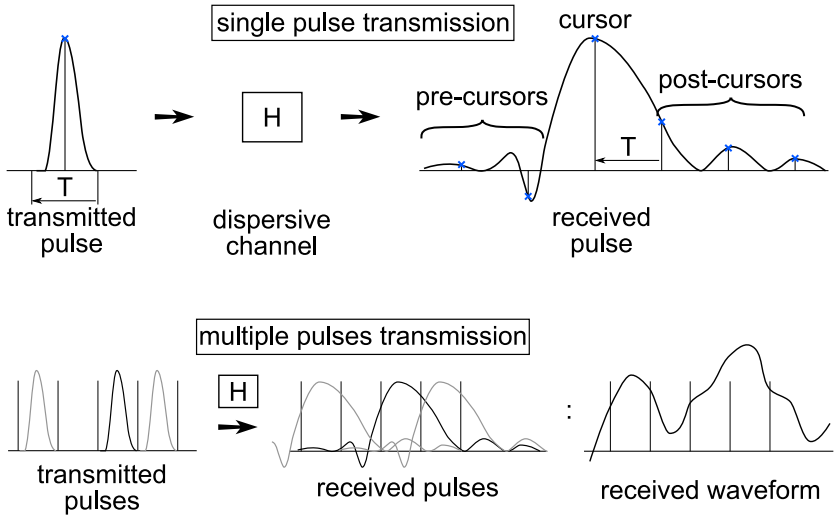


Figure 4.1: Pulse spreading through a dispersive channel and induced ISI between successive pulses.

respectively (Figure 4.1). The values of the post-cursors and pre-cursors outside their symbol period add to the cursor during detection and are responsible for ISI. The channel response determines the extent of the pulse spreading outside its symbol period and, hence, how much it affects its neighbouring symbols during detection. The idea behind FFE and DFE filters is that ISI can be compensated for using a delay line to preserve a copy of the neighbouring symbols while evaluating the cursor and selecting appropriate coefficients for the pre- and post-cursors, so that their interference can be subtracted.

General architecture

Figure 4.2 is a simplified scheme of a linear filter which incorporates a FFE part along with a DFE and the expanded block diagram of the same is in Figure 4.3. The FFE acts on a delay-line fed with the incoming sampled analog input, where tap coefficients are placed at intervals defined by delay blocks which can be a full symbol period or a fraction of it.

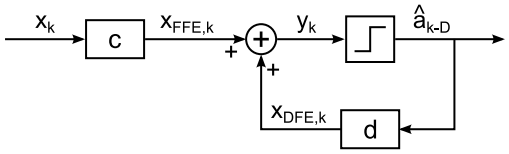


Figure 4.2: Block diagram of linear equaliser with FFE and DFE.

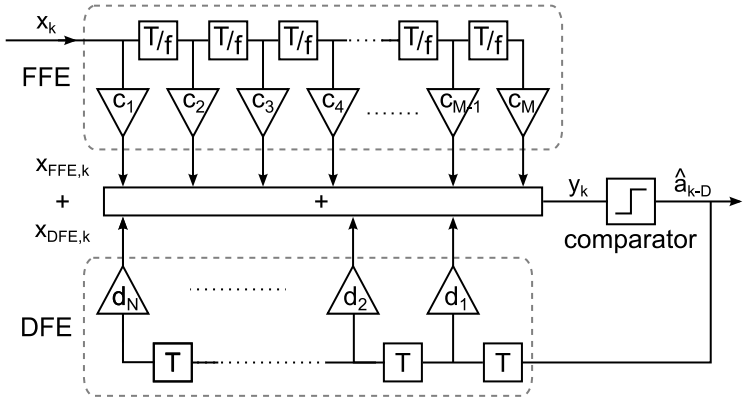


Figure 4.3: Schematic of linear equaliser with FFE and DFE where delay blocks and tap coefficients are visible.

The DFE, on the other hand, has a delay line with a full symbol period spacing only and its input is the output signal after a hard decision has been taken on the symbol values by a comparator block, or data slicer. The output x_{FFE} of the FFE filter, with a total of M taps, is calculated as

$$x_{FFE,k} = \sum_{i=1}^{M} c_i x_{k-i} \tag{4.1}$$

where c_i with $i = 1, 2, ..., M$ are the M coefficients of the FFE filter, while the output x_{DFE} of the DFE component having N taps is

$$x_{DFE,k} = \sum_{i=1}^{N} d_i \hat{a}_{k-i-D} \tag{4.2}$$

with d_i, $i = 1, 2, ..., N$ being its coefficients, D the filter delay and $\hat{a}$ the estimated output symbol obtained after the decision-threshold slicing of the output y, which is the sum of the two components above

$$y_k = x_{FFE,k} + x_{DFE,k}. \tag{4.3}$$

Due to the feedback loop, a DFE can only compensate for the post-cursor symbols, whose reception has already taken place, while a FFE can compensate for both pre- and post-cursors, depending on the position of the cursor symbol in the delay line. The filter delay D is determined by the reference tap chosen for the cursor symbol in the delay line of the FFE, which identifies the position of the output symbol being corrected,

and the amount of pre-cursors and post-cursors the filter is compensating for. While the FFE structure is independent of the system modulation format, the DFE requires a slicer commensurate with the constellation to ensure appropriate symbol decisions.

Burst adaptive design and convergence timing

The equaliser in this work was designed for burst-mode upstream traffic and had a training function running at the beginning of every burst to set the filter tap coefficients according to the level of impairment, which could vary from burst to burst. Similar equalisers have been studied for 10 Gb/s NRZ systems, where adaptive FFE and DFE filtering was implemented [72, 96]. While a similar architecture can be adopted for the FFE filter, additional complexity is necessary in the DFE comparator to correctly decode the received symbols. Also, the different SNR requirements and higher complexity of the constellation makes it necessary to reassess the filter performance and the convergence timing requirements. A detailed scheme of the equaliser is shown in Figure 4.4. Every optical burst was equipped with a common training sequence in their preamble and during the training process the filter output y_k was compared to the internally generated training signal a_k to compute the error $e_k = a_k - y_k$. A least mean square (LMS) algorithm was used to calculate the optimum coefficients of both FFE and DFE to minimise the error. The LMS al-

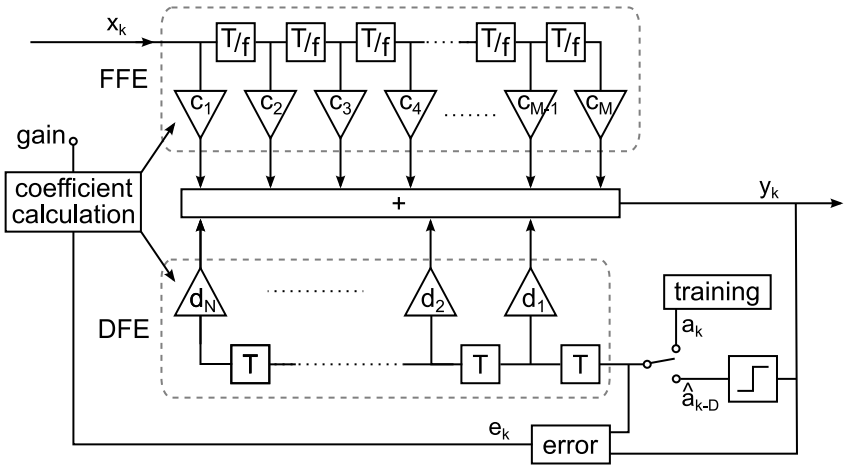


Figure 4.4: Block diagram of FFE and DFE equaliser with burst-by-burst adaptive training feature.

gorithm updates the vector of the filter coefficients, $\mathbf{w}$, which is formed by the FFE and DFE coefficients, $\mathbf{w}_k = [\ c_{1,k}\ c_{2,k}\ ...\ c_{M,k}\ d_{1,k}\ d_{N,k}\ ]$, following the Equation

$$\mathbf{w}_{k+1} = \mathbf{w}_k + \mu_{LMS}\mathbf{x}_k e_k \tag{4.4}$$

where the LMS gain, μ_{LMS}, has been introduced. The convergence speed of the LMS algorithm in setting the coefficients is determined μ_{LMS}, and the precision of the coefficient values depends on both μ_{LMS} and the duration of the training process. Careful choice of these parameters is needed to ensure limited transmission overhead while guaranteeing satisfactory ISI cancellation. After the training period, the coefficients could be tracked using the filter output $\hat{a}_k$ to compute the error instead of the training sequence. However, assuming the fibre channel to be time invariant within the duration of an optical burst, the adaptation could be carried out at the beginning of the reception and the coefficient then be used unvaried to filter the burst payload. The results offered by the two approaches are compared in the following to confirm whether the coefficient tracking during the burst payload is necessary.

4.1.2 Filter parameters optimisation

An appropriate experimental setup was realised in order to generate optical bursts of traffic and perform off-line analysis on them to test various EDC filter options. The adaptive equaliser was implemented in a numerical analysis environment where its parameters could be easily varied to provide an accurate characterisation of their effect on the performance for the desired application as a burst-mode capable upstream equaliser for PONs. With off-line processing it was also possible to use the same received waveforms to compare all the different variants in implementations and parameters settings of the equalisers, making the results less susceptible to experimental measurement variations.

In this type of filter, a variety of parameters can be tuned to obtain the optimal trade-off between performance and complexity which is key for application in PONs. The equaliser can have FFE components only or can also be supported by a DFE, both with a different number of taps. The delay line of the FFE portion can have different spacing between taps

with delay blocks of either a full symbol or a fraction, obtaining what are called symbol-spaced equalisers (SSEs) or fractionally-spaced equalisers (FSEs), respectively. The delay D introduced by the FFE is dictated by its reference tap which determines the balance between pre-cursors and post-cursors ISI compensation and can be adjusted depending on the channel response and the size of the DFE. For the desired burst-mode capable application, effective and fast training of the equaliser is required and the appropriate training sequence length and LMS gain coefficient have to be used. Also, the content of the training sequence can be varied and plays a role in the performance of the adaptive filter as it determines the coefficients' value.

All these aspects are experimentally investigated in the following in term of compensation performance and adaptation speed in order to provide useful guidelines for the design of EDC devices for the next generation of PONs with the use of multilevel modulation formats. Variations of the equaliser were implemented with or without DFE circuitry, looking at different FFE taps spacing and different number of taps for the FFE and DFE. The length of the training period and the modulation format of the training sequence were also varied for the FFE, being either NRZ or PAM4, to evaluate the different impact on the optimum coefficient setting.

Experimental setup

The adaptive linear filter described above was implemented off-line using a numerical computing environment. The experimental setup in Figure 4.5 was used to generate optical data bursts separated by a 20.5 ns guard time to evaluate the capabilities of the adaptive equaliser. A C-band DFB laser emitting at 1539.37 nm, or 194.75 THz, which is inside the NG-PON

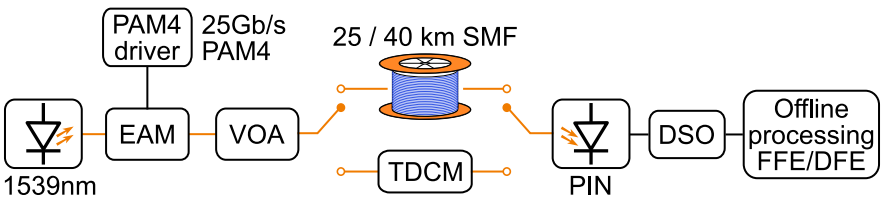


Figure 4.5: Experimental setup for EDC filter characterisation with 25 Gb/s PAM4.

2 allocated upstream band [18], was externally modulated by an EAM driven with a PAM4 signal. The small-signal modulation bandwidth of the EAM was 13.1 GHz and the PAM4 signal had a Baud-rate 12.5 GBd, resulting in a 25 Gb/s bit-rate. A VOA controlled the signal input power into a SMF of either 25 km or 40 km. Alternatively, a TDCM was used to have finer granularity in the CD analysis and confirm the results obtained with the fibre. A 10 G PIN receiver with linear TIA was used in front of a DSO that captured the traces for off-line analysis. Figure 4.6 shows how the logical portions of the optical bursts used in the experiment were organised. The initial part of the burst was a preamble which would be used by the BM-Rx for the alignment and gain equalisation of the incoming bursts. Subsequently, the PRBS used to train the filter coefficients was inserted, followed by the payload which was the predominant portion of the burst, carrying the data. The content of the training sequence was a PRBS of order 7, either modulated using NRZ or PAM4. The payload content was also a PRBS, in this case of order 15 and mapped into a PAM4 constellation. At the receiver the waveforms were synchronised off-line, the preamble was discarded and the received training sequence was then used as input to train the equaliser, using an ideal sequence internally generated as a reference for the error calculation. The payload was then filtered with the coefficients obtained after the training period and BER count was performed, taking into account the payload portion only.

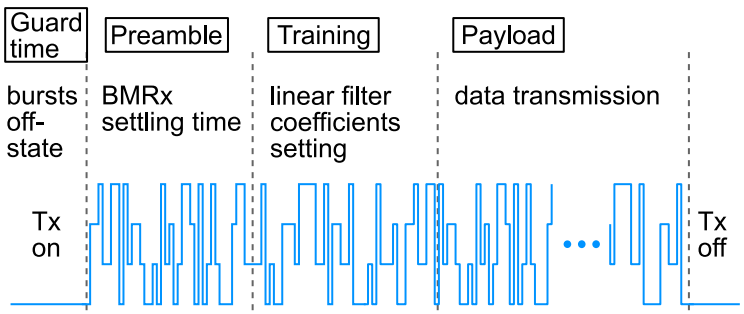


Figure 4.6: Logical structure of the optical bursts used in the experiment.

Taps spacing

The effect of different spacing of the FFE taps was investigated at first, looking at the BER sensitivity obtained with a SSE and various FSE whose input symbol-rate rate was $\frac{T}{f}$ with $f \in \{2, 3, 4\}$. For the measurements with just the FFE filters $7f$ and $13f$ coefficients were evaluated after 25 km and 40 km of fibre (Figure 4.7). For the BER evaluation the sampling point was optimised in each of the conditions investigated, in order to obtain the optimum performance. The 25 km measurements show that FSEs allowed for a better sensitivity over SSEs and no further improvement was obtained using a finer taps-spacing than 2 per period. Looking at the 40 km measurements obtained with a $7f$ taps FFE, an improvement can be seen between the 2 and 3 taps-per-symbol FSEs suggesting that when the equaliser was undersized and did not provide optimal ISI cancellation, as evident from the 2 dB difference with respect to the $13f$ taps FSE, finer spacing beyond 2 taps-per-symbol could provide superior performance.

In addition to the advantage in terms of ISI reduction, a fractionally spaced filter also offers better performance in term of tolerance to the phase delay of the incoming signal. Figure 4.8 shows the sensitivity penalty for different tap spacings when the input signal to the filter was delayed with respect to the optimum sampling point by fractions of unit intervals. SSEs and FSEs with $13f$ taps were used and measurements were taken after 25 km of fibre. While the ISI compensation capability

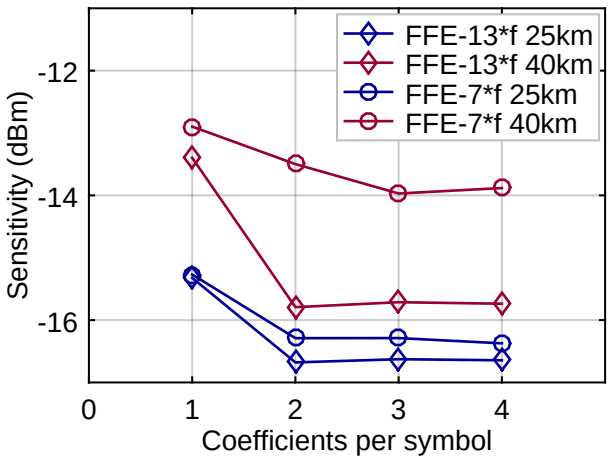


Figure 4.7: Sensitivity penalty for various FFE taps spacings.

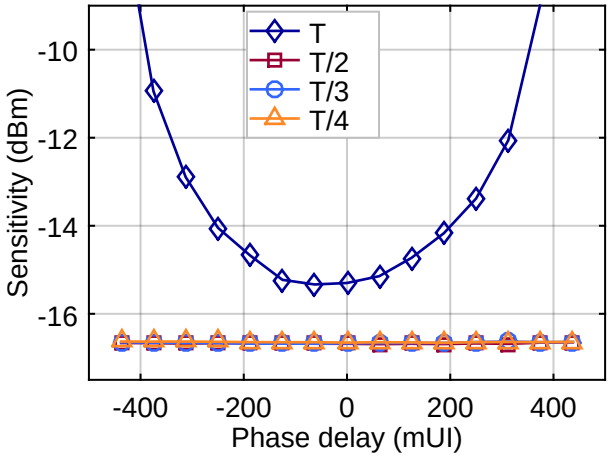


Figure 4.8: Sensitivity penalty for various FFE taps spacings as a function of input signal phase-delay.

was heavily affected in the case of a symbol-spaced FFE, the fractionally-spaced ones showed equal sensitivity across a range of phase delays spanning an entire symbol unit. This means that a fractionally-spaced FFE, provided its clock is locked to the transmitted symbol rate, does not need any phase adjustment to perform at its best and the filter itself can take care of phase recovery functionality [96]. This is particularly attractive in PON upstream where bursts can reach the OLT with different phase due to temperature and the devices' operational regime variations and no extra component is needed to perform the phase alignment.

Due to the above considerations, the 2 taps-per-symbol FSE was considered to be the best option and was used throughout the following analysis.

FFE reference coefficient

The delay of an FFE determines the capability of the filter to compensates for ISI induced by the pre-cursors or post-cursors indicating the position along the tapped delay line of the cursor, the received symbol which is being compensated for ISI. An FFE whose reference tap is 1 can only compensate for the post-cursors, introducing no latency in the reception, while when the reference tap is the N_{th}, the filter weights the contribution of the pre-cursor symbols only. Figure 4.9 show the sensitivity measured for a 26-taps FSE with 2 taps-per-symbol while its

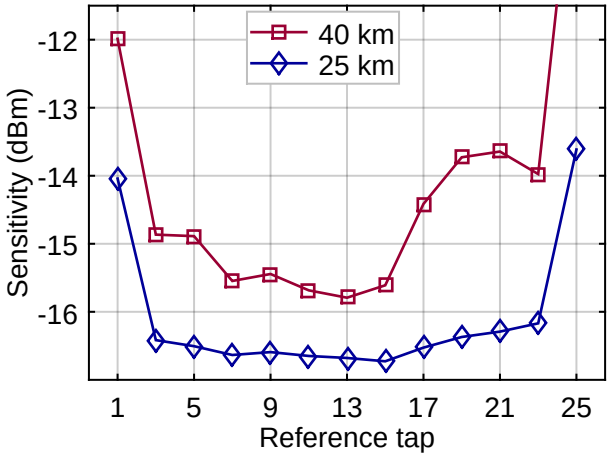


Figure 4.9: Sensitivity penalty for various FFE reference taps.

filter reference tap was shifted along the delay line for both 25 km and 40 km transmission lengths. While the behaviour is more evident in the 40 km case, due to the higher amount and extension of the ISI, both show a similar trend, namely that best performance is achieved when the reference-tap is centred in the delay-line, so that compensation is evenly spread among pre- and post-cursors. In the 25 km curve the tolerance was higher as the level of impairments was lower and the taps further from the cursor provided minimal contribution to the filter output. Based on these results, the position of the reference tap was kept in the middle of the tapped delay line when conducting the analysis to follow.

FFE coefficient number

The effect of the FFE size in the filter was then investigated for a $\frac{T}{2}$ FSE, whose reference tap was set as explained above, for 25 km and 40 km of SMF (Figure 4.10). Increasing the length of the FFE provided marked improvement up to a size that could compensate for the entire extent of the ISI trace of a symbol. As a matter of fact, beyond a certain size, further improvement was minimal or not present at all, and an excessive number of FFE taps could also reduce its effectiveness due to the amount of noise introduced. The optimum trade-off lengths were different for the two SMF lengths used due to the different amount of CD and, hence, the extent of the impulse response broadening in the two cases, but a similar trend was obtained. It is worth noting that, for

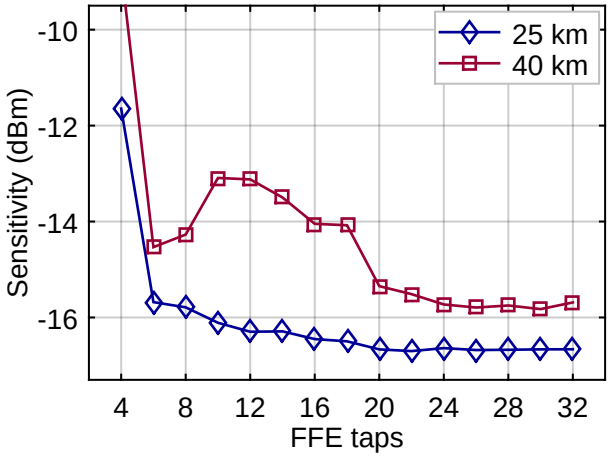


Figure 4.10: Sensitivity for various numbers of FFE coefficient in a $\frac{T}{2}$ FSE.

the 40 km measurements, intermediate lengths of 6 and 8 taps showed better sensitivity than some of the longer FFEs, probably due to a sub-optimum balance between ISI spread and noise in the farther pre- and post-cursors. However, best overall performance was still achieved with a longer delay-line. With respect to the 40 km case, a $\frac{T}{2}$ FFE size of 26 provided the best compensation capabilities without being oversized and was then kept as a reference size for the other parameter evaluations in the following.

DFE reference coefficient

The DFE portion of a linear equaliser compensates for the post-cursor symbols after a hard decision has been taken on their value with a set of comparators that assigns the received symbol to the most likely constellation value. Ideally, the FFE should provide a signal with very small pre-cursor ISI and the DFE compensate for the post-cursors with the advantage of not introducing noise propagation as its input symbols have undergone a hard decision before being fed to the DFE delay-line and weighted with the taps coefficients. To evaluate whether the optimum reference coefficient of the FFE would be different when a DFE filter was added, a similar analysis of the previous was conducted for the same $\frac{T}{2}$ 26-taps FSE. This FFE was used in conjunction with a DFE whose size was varied from 1 to 7 taps and the measured sensitivities are reported in Figure 4.11).

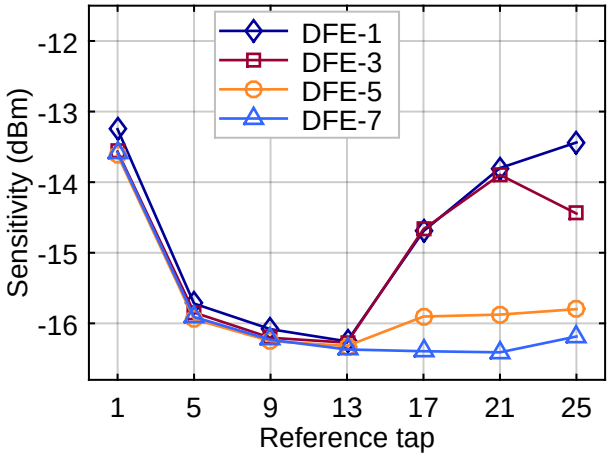


Figure 4.11: Sensitivity for various reference taps of the equaliser in a filter with various DFE sizes.

When the size of the DFE was not enough to compensate for the extent of ISI in the post-cursors, the optimum reference tap was again found to be in the middle of the delay line so that the FFE could cover a longer span of post-cursors. When the number of DFE taps was increased, less contribution in cancelling the post-cursors ISI was needed from the FFE and higher delays could be used. However, the sensitivity improvement was minimal suggesting that, in the scenario analysed, the frequency response of the channel did not have deep notches and the intrinsic noise propagation of the FFE did not have an important effect on the performance. As the choice of a reference tap in the middle of the FFE delay line provided optimum or near-optimum performance for every choice of DFE lengths it was the selected option for the next sets of measurements.

DFE coefficient number

The effect of the increasing number of DFE taps was then investigated for a combination of $\frac{T}{2}$ FSEs and again tested over 25 km and 40 km of fibre. The set of sensitivities are reported in Figures 4.12 and 4.13 for the two different fibre lengths as a function of number of taps for both parts of the equaliser. For both SMF lengths the observed trend was similar in that, when the number of FFE taps was sufficiently high, the addition of DFE taps did not provide significant further improvements. However, when the FFE size was not enough to cover for the full impulse response

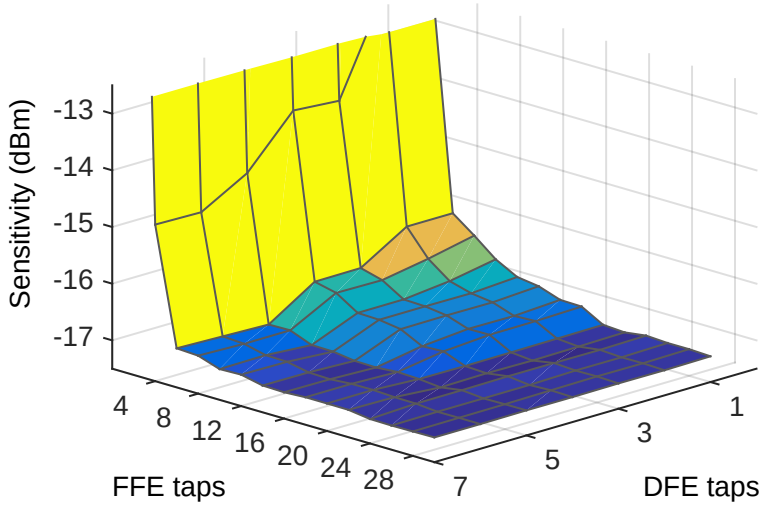


Figure 4.12: Sensitivities for various $\frac{T}{2}$ FFE and DFE numbers of tap combinations after 25 km SMF.

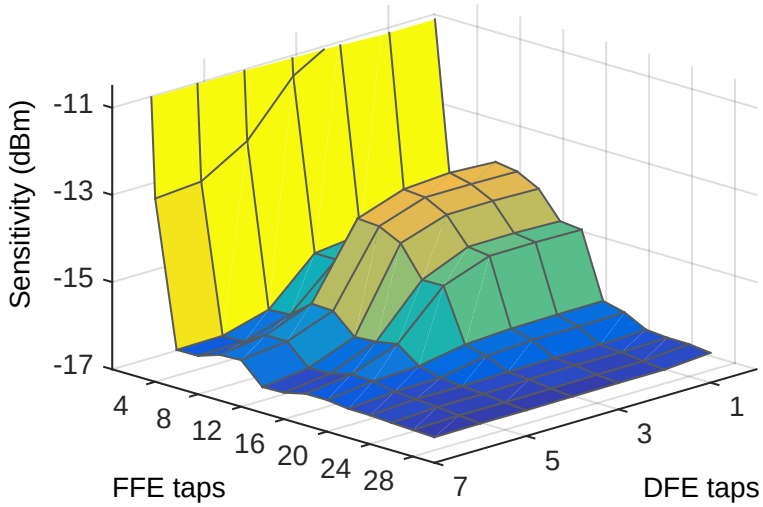


Figure 4.13: Sensitivities for various $\frac{T}{2}$ FFE and DFE numbers of tap combinations after 40 km SMF.

a DFE of increasing length compensated for the remaining post-cursors and offered improved sensitivity.

With reference to the previous $\frac{T}{2}$ FFE, Figure 4.14 shows its performance compared to when a 5-taps DFE was added. The DFE provided its greatest advantage when the FFE length was not appropriate for the channel response, while the sensitivity improvement offered was less than 1 dB if a proper size for the FFE was selected. The results can be used as guidelines for a practical implementation when deciding on the dimension of a linear equaliser and whether, in the specific design, a FFE alone is preferred for simplicity, or a DFE with smaller FFE size could be more convenient for the chip area and power consumption. For an analog or mixed implementation the size of the chip scales with the number of taps and an implementation with a lower number of combined FFE and DFE taps would likely occupy a smaller chip area, saving fabrication cost. The power consumption would also benefit from the lower number of taps used in the design. On the other, hand the circuit design is easier for an FFE-only chip thanks to the lack of the feedback circuitry. For an adaptive equaliser implementing the DFE, training also requires a slicer which could present complications in CMOS design, especially for a multi-level signal such as PAM4. For bit-rates beyond 10 G the design of analog filters with sizes bigger than 10 taps could prove very challenging. Hence, the preferred solution would be a DSP based implementation in which case most of the cost and power consumption would come from

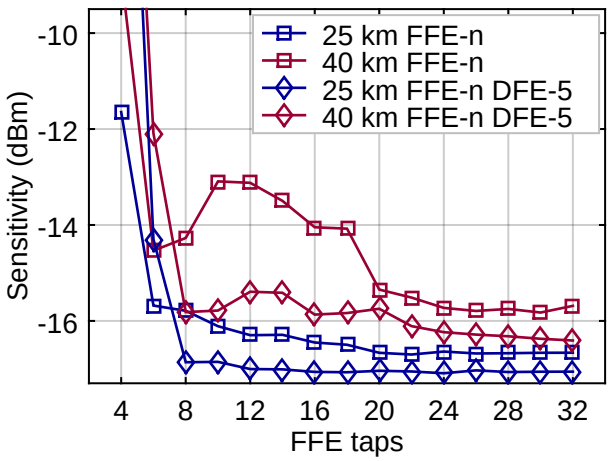


Figure 4.14: Sensitivities for various sizes $\frac{T}{2}$ FFEs combined with a 5-taps DFE.

the high-speed, high-resolution ADC.

LMS gain and training sequence length

In all the previously reported results the adaptation of the filter was achieved during a 4000 symbol long training sequence and a low gain coefficient for the LMS algorithm to ensure convergence of the equaliser as the focus was to evaluate the optimum capabilities in compensating for the ISI. However, due to the burst nature of the network, the adaptation speed is a key parameter and deserves a dedicated analysis. The choice of the LMS gain coefficient, μ_{LMS}, determines, on the one hand, the convergence speed of the algorithm and, on the other hand, the precision in the choice of the coefficients which can be affected by granularity noise if the adjustments at every iteration are too large. Before filtering, the received PAM4 signal is normalised between -3 and 3, and the constellation $\{-3, -1, 1, 3\}$ is used for the training signal. Figure 4.15 shows the sensitivities obtained for a combination of training sequence lengths and gain coefficients μ_{LMS} for the adaptation of a $\frac{T}{2}$ 26 taps FFE after a 40 km SMF. On one side of the graph, where the value of μ_{LMS} is higher, the sensitivity was impaired by the noise in the choice of the co-

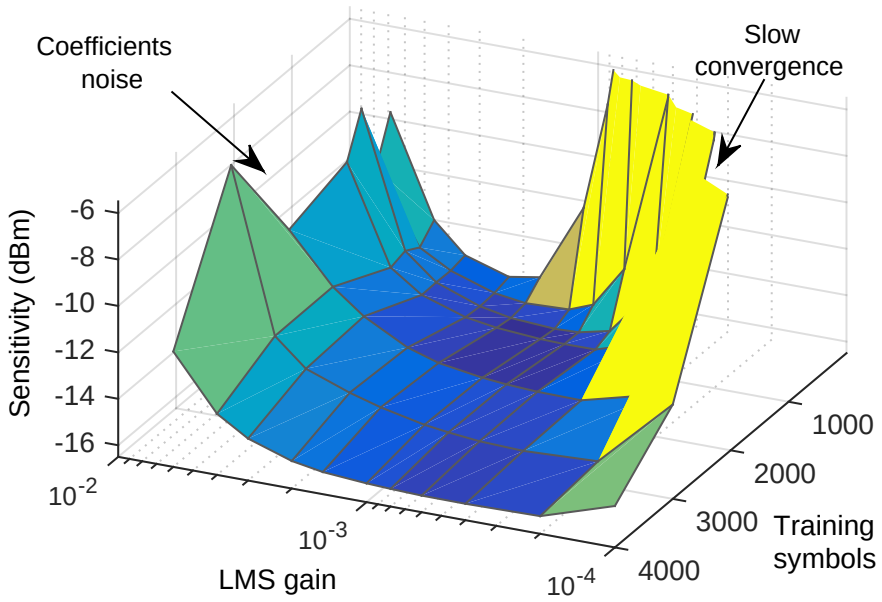


Figure 4.15: Sensitivity penalty for combination of LMS gains and training sequence lengths.

efficients as the steps of the LMS algorithm were too big to achieve a fine adjustment. This behaviour does not show dependence on the training length as, with a high μ_{LMS}, convergence is fast and the noise is intrinsic in the coefficient value. On the other hand, a low LMS gain required more time to converge to the optimum coefficient values and the penalty due to incomplete convergence was dependent on the training sequence length. A longer sequence allowed for a wider range of gain coefficients to be used relaxing the trade-off between convergence time and coefficient noise. However, it also introduced a higher burst overhead reducing the transmission efficiency. A satisfactory trade-off was found in using 1000 training symbols, for an equivalent of 80 ns, and $\mu_{LMS} = 0.001$. As the standardisation targets for the total overhead time are within the hundreds of nanoseconds [17,18] this represents a suitable approach without the need for faster but more complex convergence algorithms.

Training sequence constellation

An interesting aspect of FFE is that the coefficient training does not need a decision device and so does not need to be bonded to a specific data constellation, unlike a DFE. Hence, an FFE could be trained with a NRZ sequence when used in conjunction with a PAM4 transmission. This translates to a simpler implementation of the FFE, as the internally generated training sequence is binary and also means the same receiver could potentially be used at the network OLT to equalise transmissions from ONUs using different intensity modulation formats. To investigate the impact of the training sequence content, different bursts were tested at the receiver with either a binary or quaternary signal in the portion dedicated to the equaliser training (Figure 4.16). The data content was a PRBS of order 7 in both cases but in NRZ format for one experiment and mapped into a PAM4 signal for the other. For the NRZ training

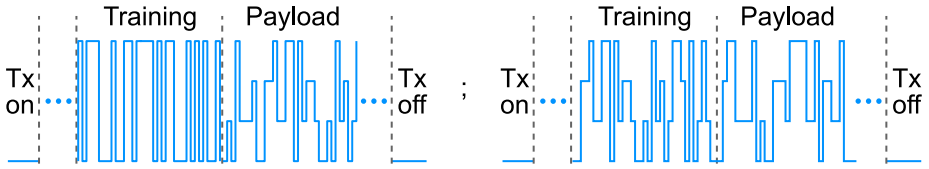


Figure 4.16: Structure of bursts for FFE training with either NRZ or PAM4 training sequence.

sequence, the amplitude was normalised to the PAM4 signal, meaning the equivalent of symbols "0" and "3" were transmitted. Figure 4.17 shows the mean squared error (MSE) of the payload after equalisation for different lengths of the training sequence and various LMS gains for the two approaches, using a 40 km SMF. A $\frac{T}{2}$ 26-taps FFE was used and the same received optical power was used for the two bursts, corresponding to the 10^{-3} BER sensitivity achieved using a PAM4 training sequence.

When training the equaliser with a PAM4 sequence the MSE converged to a stable value and the convergence time was dictated by the chosen LMS gain. When a binary sequence was used for training the convergence was faster for the same LMS gain, as only the outer points of the constellation were used and the measured errors had higher magnitude. Again, the MSE converged to the same value but ripples were visible during the training process with a periodicity of 127 symbols which is the length of the used PRBS 7, suggesting some critical portion of the sequence induced a coefficient setting different from the optimum one needed for the PAM4 payload. The extent of the ripples was dependent on the value of μ_{LMS} and could be reduced by using longer convergence time. The difference in the achieved MSE value is an indication of the different BER measured which was higher when binary filter training was used. Despite the worse BER, the approach is viable and choosing

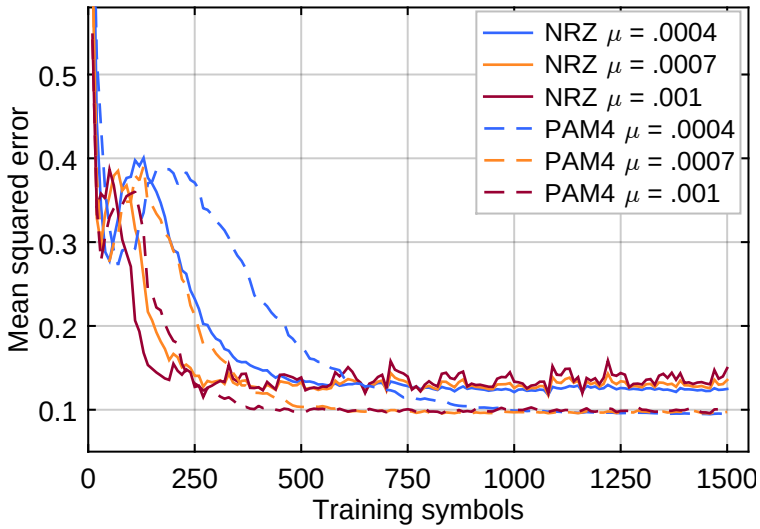


Figure 4.17: MSE measured for various training sequence lengths and LMS gains using binary or multi-level training.

the appropriate LMS gain still provides convergence in less than 1000 symbols and stability of the coefficients value. The performance loss, which is reported in more detail in the following, is compensated for by advantages in term of construction complexity, receiver inter-operability and the possibility of reusing chips designed for NRZ operation even in a PAM4 system, provided the proper training sequence is used.

Continuous coefficients adaptation

In the filters used in all the previous analysis, the taps coefficients were calculated during the training period and used unchanged for the entire payload filtering. An alternative is to keep track of the error, which is then calculated from the output of the filter instead of the training sequence, and to continuously adjust the coefficients accordingly during the filtering of the entire burst. This second approach is commonly used for continuous transmission where the channel conditions change over time while, in the PON upstream scenario considered here, bursts have a maximum duration of hundreds of microseconds. These two solutions are here compared to confirm whether the assumption of stable channel conditions during a burst is justifiable and does not lead to performance loss. Figure 4.18 shows BER curves, after a 40 km fibre, for different FFEs and DFEs whose adaptation was achieved with a 1000 symbol

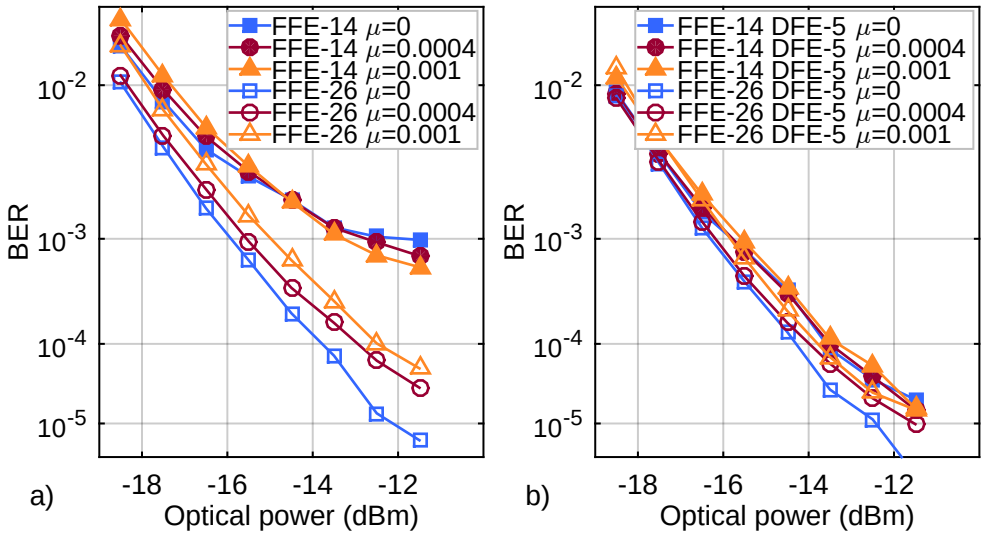


Figure 4.18: BER curves using various LMS gain coefficients during the payload adaptation for a) FFE only filters and b) FFE with DFE filters.

training sequence and $\mu = 0.001$ was used. An FSE filter with 2 taps per symbol was used where the FFE size was varied from 14 to 26 and the DFE size fixed to 5 taps, when used. Three approaches were investigated where the LMS gain after training was either unvaried ($\mu = 0.001$), changed to a lower value ($\mu = 0.0004$) or coefficient tracking was not performed at all ($\mu = 0$).

Adaptive tracking of the coefficients during the filtering of the payload did not actually offer any advantage compared to the approach of fixing them after training, even when the LMS gain was switched to a lower value to avoid abrupt changes. For larger filters the coefficients tracking actually resulted counter-intuitively in worse sensitivities. This validates the approach of using the taps coefficients without modification after training in an upstream transmission with sub-millisecond lengths of the optical bursts and also simplifies the filter architecture.

4.1.3 Impairment compensation

After the proposed overview of the optimisation process to adapt the architectural features of an EDC filter to provide the best performance for the target application, this Section reports on the capability of such equalisers to compensate for common impairments in PONs. Based on the results obtained previously, for all the following measurements a training sequence length of 1000 symbols was used in order to have a reduced burst overhead of 80 ns. A suitable LMS gain value of $\mu_{LMS} = 0.001$, or $\mu_{LMS} = 0.0005$ in the case of a binary training sequence, was used to ensure convergence within the training period and to reduce noise in the coefficients. The cursor position in the FFE delay line was selected as the middle tap.

Chromatic dispersion

With C-band SMF transmission, CD is one of the main limiting factors due to the symbols spreading during propagation, resulting in ISI at the receiver. A filter whose size was chosen according to the analysis described above was placed under test with a TDCM adding variable amounts of CD. The same measurements were also confirmed through 25 km and 40 km of real SMF. A 13-taps SSE and a 26-taps FSE, with

and without a 5-taps DFE, were compared to show their capability to compensate for CD induced ISI and the effect of taps spacing and feedback equalisation (Figure 4.19). In accordance with the trends observed in the previous analysis, an FSE offered improved sensitivity over an SSE with a consistent gain of 1 dB or more and improved performance especially for higher amounts of CD. The addition of a DFE in the equaliser offered an advantage but the sensitivity gain was minimal, since the FFE size was chosen in accordance with the previous results for 40 km and covered the entire symbol impulse response.

Similar measurements were carried out for the same SSE and FSE when their training sequence was a NRZ signal instead of a PAM4 signal and reported in Figure 4.20. Similar behaviours were observed for SSE and FSE with the latter offering consistently better compensation. The sensitivity trends show that little difference exists between a binary or quaternary coefficients training for small amounts of CD but the use of an NRZ training sequence exhibits reduced performance for longer spans of fibre. Nevertheless, it provides a valid alternative as the penalty difference after 40 km was 1.4 dB compared to the PAM4 but with the advantage of being a simpler and more versatile device.

All the filter varieties offered an important improvement over the uncompensated transmission that suffered high penalty for a 25 km SMF and could not reach FEC threshold over longer fibre lengths.

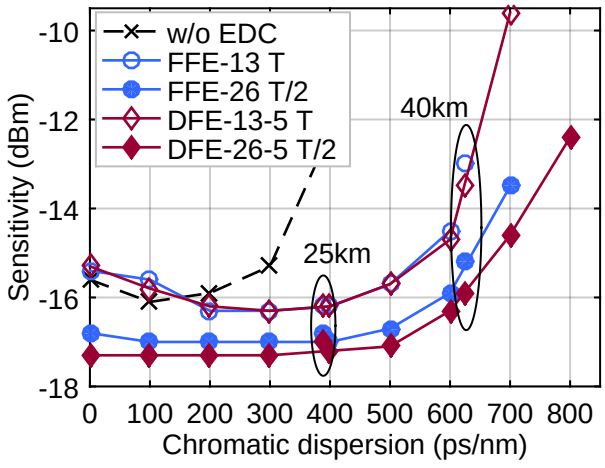


Figure 4.19: Sensitivity penalty for various EDC filters under increasing chromatic dispersion.

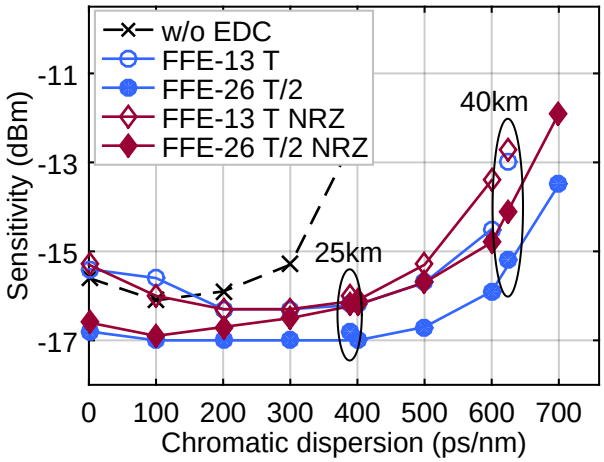


Figure 4.20: Sensitivity penalty for various training sequences of the FFE under increasing chromatic dispersion.

Bandwidth restriction

The bandwidth of the optoelectronic devices in the system is a key metric to enable higher symbol-rate transmissions. Restrictions are generally introduced by the components used at the transmitter and receiver such as DMLs, external modulators, TIAs and electrical amplifiers. The transmitter bandwidth was limited in the experimental setup using different electrical bandpass Bessel filters, with a 3 dB bandwidth of 5 GHz and 7.5 GHz, before the EAM, in order to emulate a bandwidth limited device. The results are reported in Figure 4.21 for measurements in optical B2B and after a 40 km SMF. Again, the analysis was carried out for SSE and FSE with and without DFE. Without the use of equalisation, the target BER could not be reached with a transmitter bandwidth of 7.5 GHz or lower, irrespective of the fibre length. In optical B2B, all 4 filters used could compensate for transmitter bandwidths as low as 5 GHz. After 40 km, on the other hand, only the FSE DFE was able to recover the signal at a 10^{-3} BER for the minimum bandwidth of 5 GHz, while the other filters only allowed for a transmitter restricted bandwidth of 7.5 GHz. Little difference was observed in B2B between DFE and FFE suggesting the prevalence of deterministic ISI coming from bandwidth restrictions and low amounts of noise amplification during the FFE filtering.

The receiver bandwidth was then limited using numerical analysis

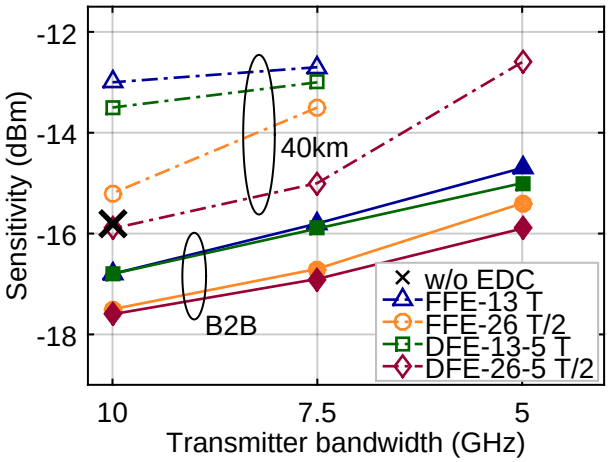


Figure 4.21: Sensitivity penalty for various transmitter bandwidth using different filters.

and filtering of the received waveform off-line with a 4th order Bessel filter before synchronisation, equalisation and error counting were performed (Figure 4.22). The same FSE filters as above with 2 taps per symbol were used, with 26 FFE taps and 5 additional taps when a DFE was used. In optical B2B without equalisation two effects are visible when changing the receiver bandwidth. A bandwidth restriction reduced the sensitivity due to the introduced ISI and below a certain threshold, 8.8 GHz was measured in this specific case, a 10^{-3} BER could not be obtained. On the other hand, an excessive receiver bandwidth affected the signal quality due to the increased electrical thermal noise coming from the higher frequency components. For the 12.5 GBd transmission

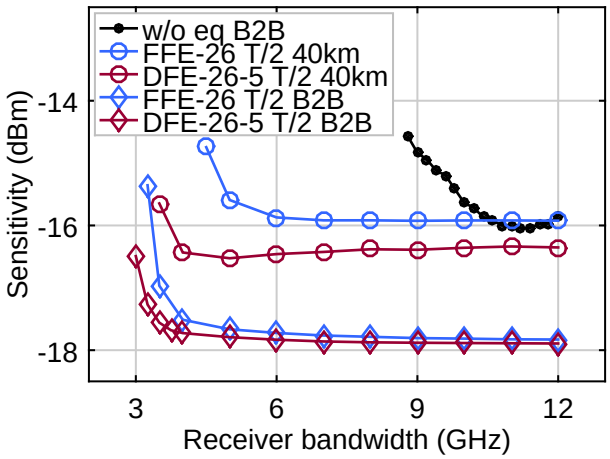


Figure 4.22: Sensitivity penalty for various receiver bandwidths.

used in the experiment, the optimum operating conditions were obtained for a 3 dB receiver bandwidth of 11.2 GHz. When equalisation was performed both FFE and DFE could very effectively eliminate the signal ISI in B2B with bandwidths as low as 4 GHz and the DFE proved to be more impactful in this scenario. Also in this case results were similar, meaning that the FFE was suffering minimally from noise amplification of the high frequencies which were suppressed by the filter. After transmission through a 40 km SMF similar behaviour was observed for both filters but with an additional penalty deriving from uncompensated CD which affected both the maximum sensitivity that could be reached and the receiver bandwidth beyond which the performance stabilised. After 40 km the difference between FFE and DFE was more marked, as in the transmitter case, highlighting the higher capability of dealing with CD and chirp interaction when a feedback loop is introduced. The equaliser also proved effective in eliminating the high frequency noise as a FSE can provide matched filtering and so the sensitivity did not degrade above 11.2 GHz.

Level mismatch ratio

When more advanced modulation formats, such as PAM4, are employed, linearity becomes a key requirement in the system to preserve the correct symbol spacing. For PAM4 the level of linearity distortion in this work was evaluated using the R_{lm} metric, as previously used in Section 3.4. The R_{lm} of the signal was intentionally lowered in the experimental setup, thereby distorting the transmitted signal and FFE and DFE filters were used at the receiver. The applied distortion was achieved by changing the gain of the electrical amplifiers controlling the MSB and LSB of the PAM4 signal and resulted in symmetric enhancement or reduction of the inner eye of the PAM4 eye diagram. This way of creating only symmetric distortion, which was dictated by limitations of the experimental setup, is a simplified analysis in that, non-symmetric distortion are not considered. During the synchronisation procedure at the receiver the decision thresholds were adjusted to optimise the BER of the received signal but the more pronounced eye closure was responsible for sensitivity degradation. Neither filter could provide effective compensation, due

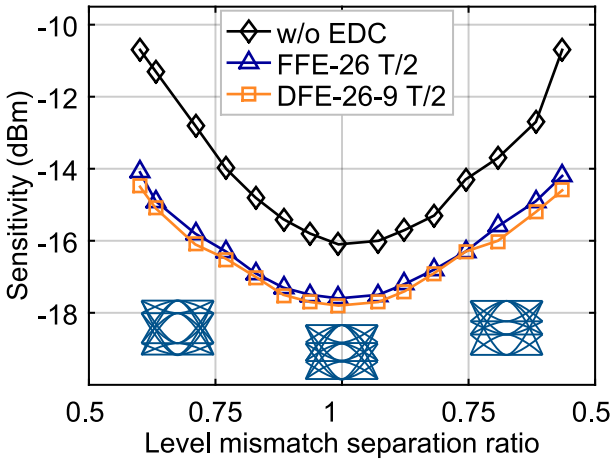


Figure 4.23: Sensitivity penalty for R_{lm} degradation of the PAM4 signal.

to the nature of the distortion which was not due to ISI or system frequency response. Both improved the tolerance to R_{lm} distortions thanks to the noise reduction through matched filtering but other techniques are required to provide an effective response to this type of impairment.

4.1.4 25G burst-mode upstream system demonstration

The adaptive linear equaliser described and characterised above was then employed in a system demonstration to enable a burst-mode 25 Gb/s PAM4 transmission over 40 km of SMF in C-band, where the signal is subjected to CD. The linear BM-TIA presented in Section 3.3 was used as an upstream receiver front-end to provide a linear AC-coupled copy of the optical signal as input to the tapped delay-line.

Experimental setup

The experimental setup implemented two ONUs with their DFB lasers tuned to different channels of the 50 GHz ITU grid, at wavelengths of 1538.19 nm and 1539.77 nm within the NG-PON 2 upstream band [18]. Each laser was followed by an SOA that was switched off during the burst-off state in order to carve bursts from the optical signals. The two signals were merged with an AWG and sent to a 13.1 GHz bandwidth EAM driven with a Gray coded PAM4 12.5 GBd burst signal. The choice of using an AWG was not dictated by the PON requirements but rather an experimental implementation convenience as it had lower

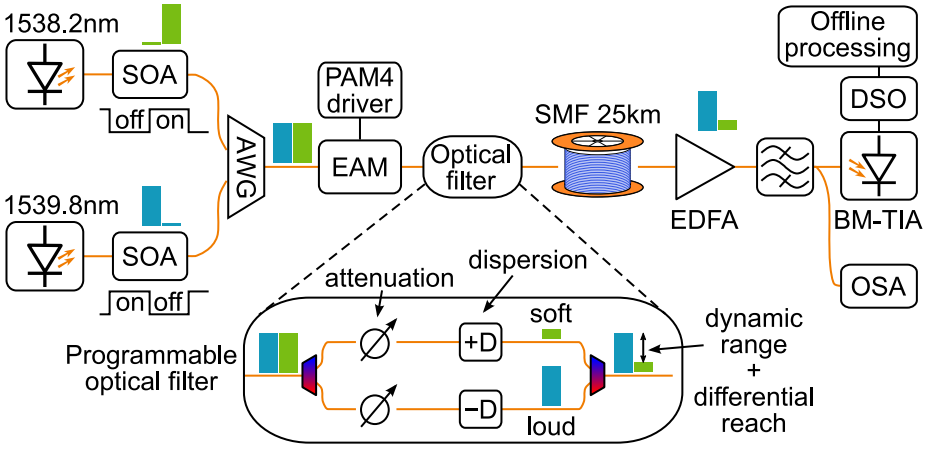


Figure 4.24: Experimental setup for 25 Gb/s PAM4 burst-mode upstream traffic.

insertion losses than a power coupler and also suppressed the SOA generated out-of-band ASE. The structure of the modulated bursts was the same as described in Figure 4.6, with the payload being a PAM4 mapped PRBS 15 and a 20.5 ns guardband period was set between bursts. A 25 km SMF was used as optical trunk line and an optical programmable filter was used to introduce variable attenuation and CD difference between the two channels creating a power DR between the bursts and emulating differential fibre reach. The filter could create DR in excess of 30 dB between soft-bursts and loud-bursts, and add CD in a range of ±200 ps/nm. It is important to remark that the transmission system is based on a TDMA protocol with the ONUs transmission windows time

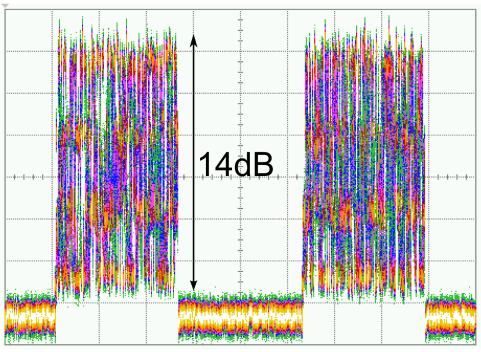


Figure 4.25: Optical burst-mode upstream traffic with a 14 dB DR between soft and loud burst.

synchronised and the use of different channels for the two transmitters was only an experimental expedient to enable the use of a programmable filter to emulate an asymmetric fibre plant. The two wavelengths were chosen to be close, with a spacing of 100 GHz only, in order to minimise any wavelength dependent effect from the optical components of the setup.

At the receiver, a linear BM-TIA integrated with a PIN photodiode was used in conjunction with an EDFA to enhance the sensitivity, acting as an optically pre-amplified receiver. The use of the optical amplifier was also necessary because the receiver tested was just a BM-TIA and not a full BM-Rx with post-amplifier stage. The EDFA employed had a fast transient control feature in order to suppress overshoots when used with burst-mode traffic. Its gain was set to 24 dB as it was found to be the optimum value to have an extended DR and good sensitivity, not saturating the BM-TIA or working below its thermal noise limit. More details about the BM-TIA design and technology can be found in Section 3.3 of this thesis. The BM-TIA settings for the baseline restoration loop were the same as used in Section 3.3 and proved to support DC-level convergence within 100 ns with less than 1 dB penalty on the sensitivity of a PRBS 15 payload. The EDFA was followed by a 4 nm wide optical bandpass filter to suppress the out of band ASE, while allowing both channels to be detected. A 10/90 optical splitter was used after the optical filter to send the smaller portion of the signal to an optical spectrum analyser (OSA) to facilitate power reading of the channels. Post-equalisation of the signal and error counting were done with off-line processing on the differential signal captured by a 50 GS/s, 12.5 GHz DSO. For this demonstration a fractionally spaced, 2-taps per symbol, adaptive FFE with 14 taps was used with a 500 symbol long training sequence.

Experimental results

The BM-TIA was characterised in optical B2B in Section 3.3 where burst-mode operation was confirmed not to add any penalty to the receiver performance and a DR of 13.3 dB was demonstrated. The same BM-TIA was here part of an optically pre-amplified OLT receiver and was

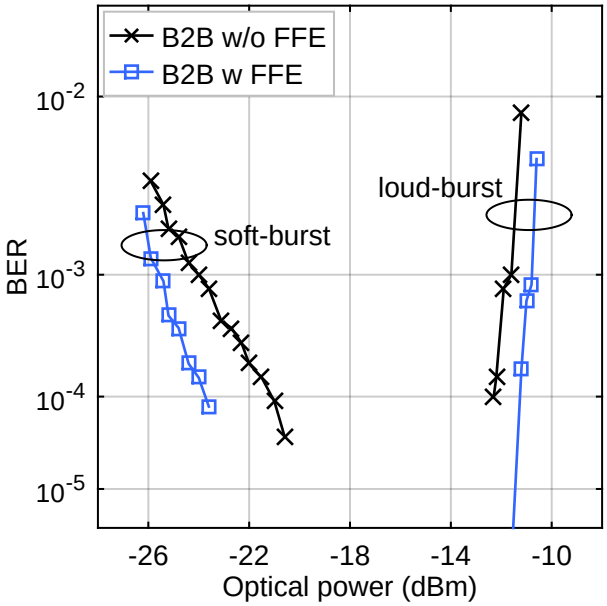


Figure 4.26: Optical burst-mode upstream traffic with a 14.7 dB DR between soft and loud burst.

characterised in B2B to measure the sensitivity achieved with an EDFA at the interface. Continuous mode and burst-mode operation were again compared and showed no performance degradation up to the maximum DR supported. The measurements in Figure 4.26 were obtained in burst-mode where, during the soft-burst measurements, the loud-burst power was fixed at the BER 10^{-3} overload threshold and the soft-packet power was progressively reduced, thereby increasing the DR. Similarly, for the loud-burst BER count, the soft-burst power was fixed at its 10^{-3} sensitivity. In B2B the soft-burst sensitivity observed at the input of the pre-amplified receiver was -24 dBm and the overload input power was -11.6 dBm, which translates to a supported DR of 12.4 dB. Using the adaptive FFE linear filter to compensate for ISI introduced by component non-idealities, the B2B sensitivity and overload powers were shifted to -25.5 dBm and -10.8 dBm, respectively, resulting in an extended 14.7 dB DR. The lowest soft-burst received power at the OLT interface of -25.5 dBm translates to a supported 34.5 dB power budget when considering a launched power of +9 dBm at the ONU [18].

The system was then tested with 25 km of SMF which made it necessary to compensate for CD with the EDC in order to obtain a BER below 10^{-3} for any input power. The loud-burst overload power was

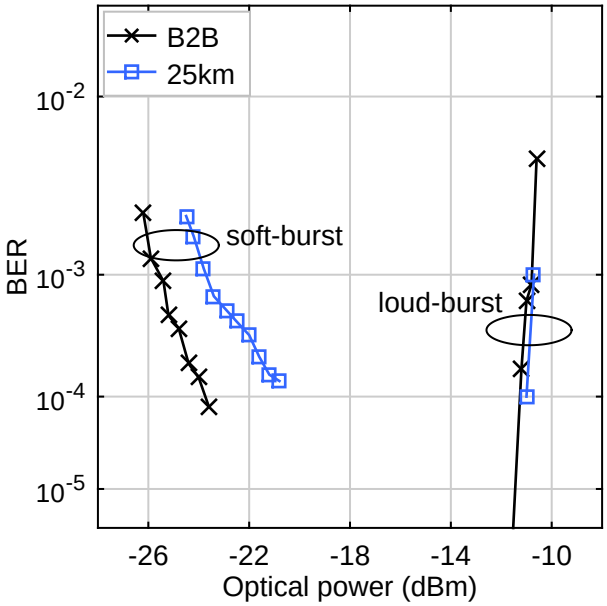


Figure 4.27: Optical burst-mode upstream traffic with a 13 dB DR between soft and loud burst after 25 km.

measured to be −10.7 dBm, similar to the B2B case, while the soft-burst sensitivity was −23.7 dBm, showing a 1.8 dB penalty caused by the residual CD induced ISI. The small change in the loud-burst overload power was expected as the eye closure due to CD distortion is a less impairing condition in the higher power regime of the loud-burst. It is also worth noting that the distortions caused by the TIA saturation could not be compensated by the FFE and were the dominant error cause, prevailing over CD distortion. The system was, therefore, demonstrated to support 13 dB DR after 25 km of fibre with the use of a 14-taps fractionally spaced FFE.

A demonstration of differential reach was also carried out to confirm the capabilities of the adaptive EDC to equalise independently every incoming burst, irrespective of the neighbouring ones. A different amount of CD between the loud and soft bursts was created with the optical programmable filter. After the 25 km long fibre of the optical trunk line, +195 ps/nm dispersion were added to the soft-burst, for an accumulated amount of CD equivalent to 37.5 km of fibre, and either +195 ps/nm or −195 ps/nm to the loud, emulating respectively 37.5 km and 12.5 km of SMF at the operating wavelength. The system was hence tested for a differential reach of 25 km, where the loud-burst would only have travelled

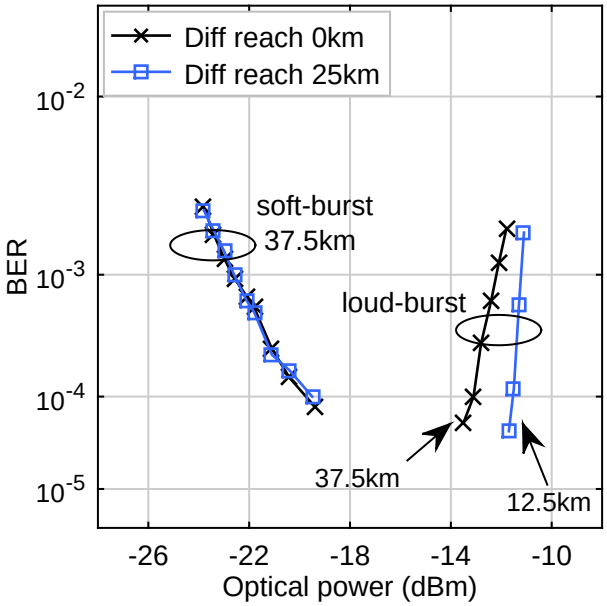


Figure 4.28: BER performance of soft and loud bursts under different differential fibre reach conditions.

through 12.5 km compared to the 37.5 km of the soft, and the results were compared to the reference case where both signals had a 37.5 km equivalent amount of CD with no differential fibre reach. Also, in this case, the fractionally spaced 14-taps FFE EDC was needed to achieve a BER value below the pre-FEC threshold at the receiver and all measurements were performed in burst-mode. The measured overload powers at BER 10^{-3} for loud-burst were -11.3 dBm and -12.3 dBm, respectively, for 12.5 km and 37.5 km (Figure 4.28). The 1 dB difference was due to the higher amount of accumulated CD in the loud-burst when subjected to an effective transmission distance of 37.5 km that caused eye-closure penalty, in addition to the TIA saturation distortion. The power of the loud-burst was then fixed at the receiver overload and the BER performance of the soft-bursts was acquired in burst-mode, changing the soft-burst attenuation to increase the DR. The measured sensitivity was -22.6 dBm for both sets of measurements, and so no penalty was introduced by the 25 km differential reach, demonstrating the burst-to-burst capabilities of the BM-TIA and adaptive EDC. The 2.9 dB penalty with respect to the B2B case was due to the residual CD, which could not be fully compensated by the equaliser and caused a closure of the eye diagram.

For all the measurements presented above, adaptation of the filter was observed within 500 training symbols corresponding to 40 ns, following a 160 ns long preamble. This translates to a 200 ns total overhead per burst which is compatible with the PON standards recommendations [17, 18, 97].

4.2 Chirp controlled directly modulated laser transmitters

This Section reports on the application of narrow optical filtering techniques at the transmitter side to enhance propagation performance of DMLs over SMF in the dispersive transmission window. Direct modulation of lasers, achieved by modulating their input current, is attractive when compared to the use of external modulation, in terms of production and operational costs and also in terms of higher output power, which is important for meeting the stringent power budgets of PONs. However, during direct modulation, chirp is inevitably generated and this broadens the modulated spectrum of the laser with, usually, detrimental effects on the transmitter performance, thereby heavily limiting the reach. The bias conditions of a DML determine the chirp magnitude of the output signal as well as its ER, both of which affect the receiver sensitivity in opposite ways. This means that, in a lightwave communication system, a DML can be operated at an optimal bias condition to optimise the performance by selecting the best trade-off between ER and chirp magnitude [98,99]. However, with the recent transition to the new generation of systems, where Baud-rates are increased and/or more advanced modulation formats are used, the mentioned trade-off would not represent a viable solution since the sensitivity penalty at the receiver would be too high or the transmission would not possible at all at the desired BER.

A class of NRZ transmitters called chirp managed lasers (CMLs) has been realised, by combining a DML with a multi-cavity filter acting as an optical spectral re-shaper. They have been shown to increase the dispersion tolerance of 10 G NRZ transmitters up to 200 km of SMF by managing the generated chirp [100]. In the work presented in this Section, a transmitter was designed with a DML followed by a narrow optical

filter whose purpose was to be able to operate the laser at a favourable chirp condition and improve the ER by selectively filtering the chirped component of the signal [52, 100]. In this way it is possible to overcome the direct modulation trade-off mentioned previously and obtain superior transmission performance. The transmitter was employed in a 25 Gb/s PAM4 system and proved to be effective for multi-level modulation formats. The proposed architecture is particularly suited and attractive for a PON downstream transmitter as it enables the use of simple receivers at the subscriber's ONU, while the cost of the additional components at the transmitter side is shared among all network users, making it more affordable. As a proof of concept, a reach of up to 50 km was demonstrated without the use of EDC or optical CD compensation at the receiver, which was a simple and cost-effective fixed-threshold slicer performing hard detection of the incoming symbols.

4.2.1 Chirp in directly modulated lasers

Direct intensity modulation of semiconductor lasers is an attractive way of generating an optically modulated signal as it does not require additional external modulators. It is achieved by modulation of the current flowing through the laser active region that results in a modulation of the carrier density which, in turn, modulates the gain. However, the carrier density also modulates the refractive index of the active region, causing modulation of the signal phase. The bias-current induced change in refractive index modulates the optical length of the cavity, causing the resonant mode to shift back and forth in frequency, depending on the modulating signal applied to the laser. In addition, for very low modulation frequencies, typically below 100 MHz, the chirp induced by temperature variations of the laser chip may be also observed but investigation of this effect is beyond the scope of this work.

Adiabatic and transient chirp

The chirp of a single-frequency laser may be described by the following equation [101]

$$\Delta\nu(t) \simeq -\frac{\alpha}{4\pi}\left(\frac{d}{dt}\ln P(t) + \kappa P(t)\right) \tag{4.5}$$

where $\Delta\nu(t)$ is the instantaneous frequency deviation, α is the linewidth enhancement factor of the active region material, κ is the adiabatic chirp coefficient, and $P(t)$ is the laser output power. Looking at the contributing terms on the right side of Equation 4.5 two mechanisms of phase modulation, or chirp, can be distinguished in a DML: transient chirp and adiabatic chirp. The first term in the expression, which is proportional to the derivative of the logarithm of the output power, is independent of the laser-structure and is called transient chirp, which leads to severe chirping during intensity state transitions. The second, which is a structure-dependent term directly proportional to the optical output power, is the adiabatic chirp and generates a wavelength shift between high-power and low-power constellation points in the optical waveform.

Transient chirp is manifest as an abrupt phase change during the transitions of the signal between symbols with different intensity, e.g. a modulated "0" and "1". When the injection current is suddenly increased, the carrier density rises before the light output can increase to re-establish the equilibrium in the cavity. The result is a temporary jump in carrier density which leads to a temporary reduction in the refraction index of the active region. As a consequence, the optical path length of the laser cavity is shortened and this causes a blue-shift of the signal, that is, a shift towards shorter wavelengths. Similarly, a decrease of injection current decreases the carrier density which briefly falls below its equilibrium value and the wavelength shifts to the red, lowering the signal frequency [102].

Adiabatic chirp, on the other hand, is the frequency gap between symbols with different intensity, due to the change in optical length of the semiconductor cavity during the symbol transmission period. Being the consequence of a steady-state condition, it is determined by the bias point and peak-to-peak excursion of the modulating signal and is frequency independent. The relative contribution of these chirp components can be controlled, to a certain extent, by changing the bias conditions of the DML.

For the generation of a 25 Gb/s NRZ signal a high bandwidth laser was needed, hence a high-speed DFB buried heterostructure multiple quantum well (MQW) DML from ExOptronics (EX-DY7005-C) with a 3 dB bandwidth of 18 GHz was used. Figure 4.29 shows the light cur-

rent (LI) curve of the device whose threshold current was found to be 8 mA. In order to capture its behaviour, a chirp characterisation was carried out for the high-speed DML. The laser was modulated varying both its bias point and the amplitude of the RF modulating signal and the chirp was measured for every combination of settings. Chirp traces of the DML were captured experimentally to evaluate the amount of phase induced modulation. The waveforms in Figure 4.30 are some of the measured phase traces obtained by applying a binary modulation to the laser under increasing bias conditions. The constant phase difference between symbols is the adiabatic chirp while the presence of sharp peaks between symbols of different intensity is the transient chirp contribution. Operation of the laser close to threshold generates both adiabatic and transient chirp, as clearly visible, for example, when the bias is set to 30 mA. Increase of the bias causes a suppression of the transient chirp and predominance of the adiabatic chirp. The chirp magnitude for the entire range of measurements is reported in Figure 4.31 as a function of the driving signal amplitude and for different bias points. The adiabatic chirp was extracted from the traces as in Figure 4.30, by averaging the values corresponding to different symbols and taking their difference. The transient chirp instead, was measured looking at the maximum excursion of the phase traces from the transient peak to the convergence value. The extent of the adiabatic chirp was also confirmed with an OSA, by looking at the lines of the optical spectrum. Lower bias of the device

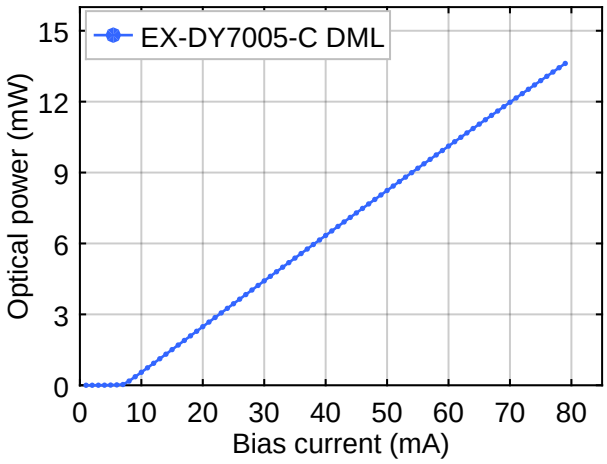


Figure 4.29: Experimentally measured LI curve of an ExOptronics EX-DY7005-C high-speed DFB laser.

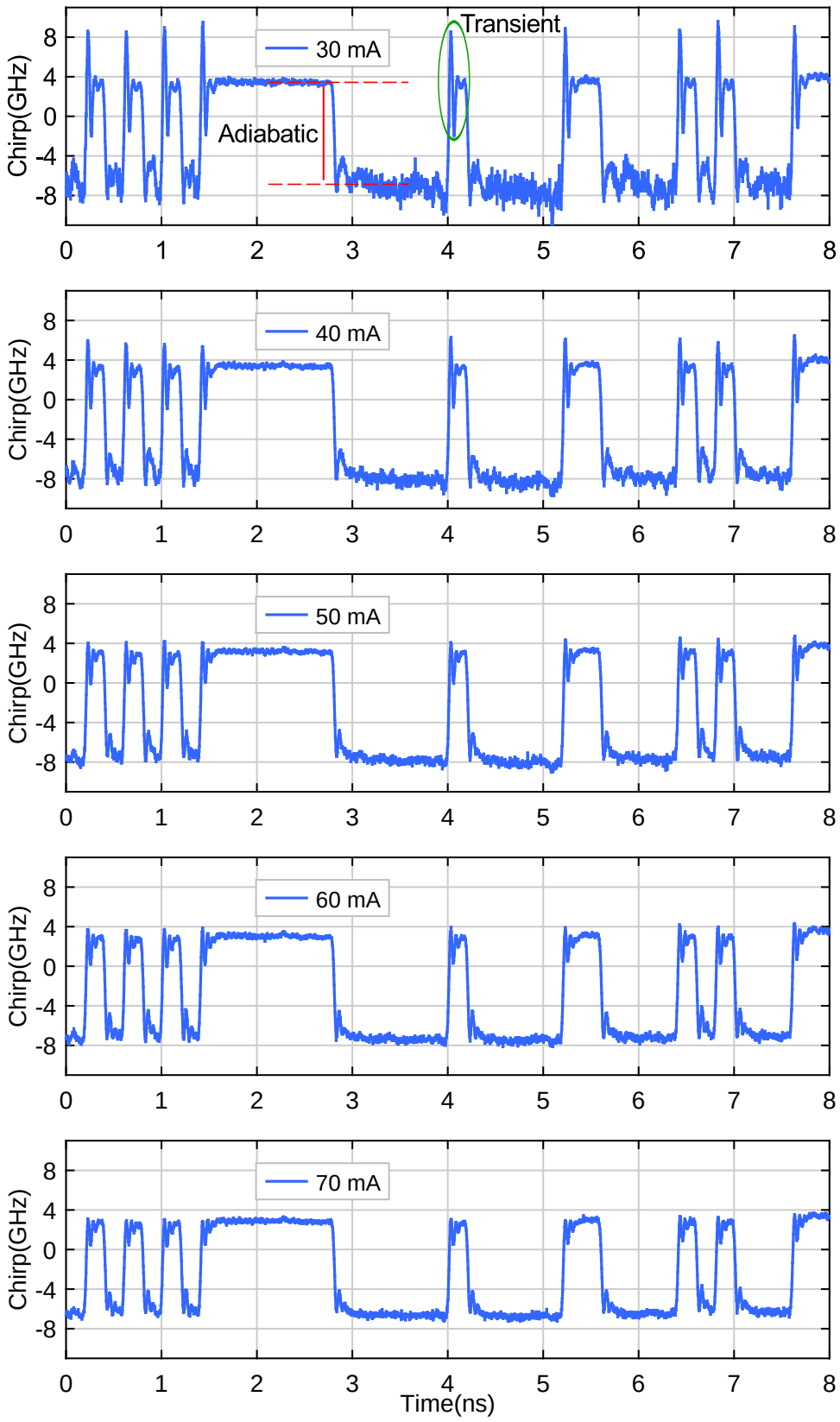


Figure 4.30: Experimentally measured chirp traces of an ExOptronics EX-DY7005-C DML under different bias conditions.

leads to a higher amount of generated chirp, while increasing the bias has the effect of lowering the chirp for the same modulation voltage. This change in chirp magnitude is less pronounced as the bias is progressively increased.

To offer a clearer picture of the chirp generation, Figure 4.32 separates the contributions coming from adiabatic and transient chirp. The two effects were measured separately from the chirp traces, as described previously. It is evident from the graphs that the two chirp mechanisms follow separate trends. Operation close to lasing threshold generates a high amount of transient chirp but, if the bias current is well above threshold, this is greatly reduced and almost completely masked

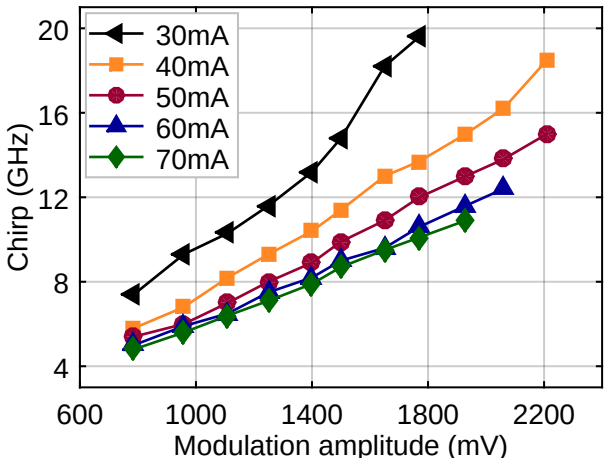


Figure 4.31: Measured chirp magnitude under varying DML bias conditions.

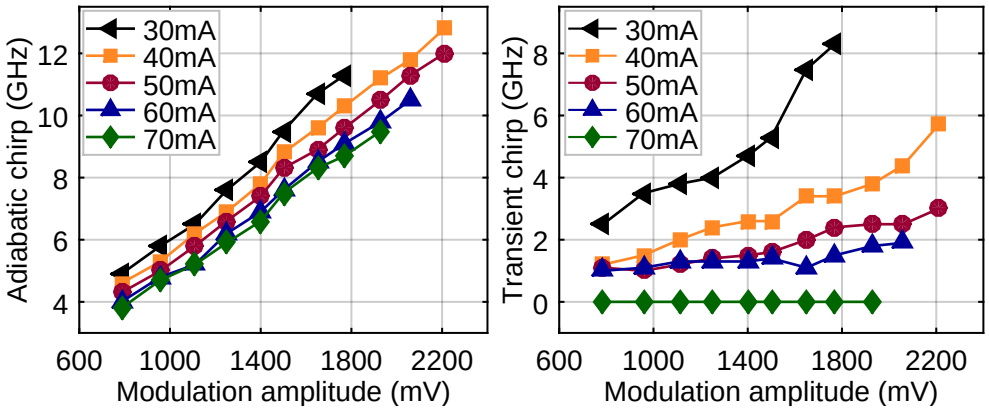


Figure 4.32: Measured adiabatic and transient chirp magnitudes for different bias conditions of the DML.

by the adiabatic chirp (Figures 4.30, 4.32). On the other hand, adiabatic chirp also changes with the bias but at a smaller rate and maintains a linear relation with the modulating signal amplitude. The two chirp mechanisms have different effects on the signal propagating through a dispersive medium and their role has to be taken into consideration in the design of the chirp managed transmitters proposed in this work.

Extinction ratio and chirp in DMLs

For intensity-modulation applications, frequency chirping broadens the modulated spectrum of the laser, hindering the transmitter effectiveness in optical fibre communications. When a signal is transmitted through a dispersive fibre, the transient chirp interacts with CD and distorts the signal, hence a DML regime that avoids transient chirp generation is preferred. However, the drawback of operating the laser well above threshold is the reduction in the signal ER due to the poor suppression of the modulated zeroes, which results in a receiver sensitivity penalty. Figure 4.33 summarises the operational regimes that can be identified for a DML. The common way of operating the DML close to threshold allows for high ER but is responsible for the generation of transient chirp that, as shown in the following, represents a serious limitation on the recovered signal quality after fibre propagation. The second regime, where the bias is well-above threshold, cannot offer a satisfactory ER for most applications but has the advantage of suppressing transient chirp, which is exploited in the following work.

The dependence of ER and chirp on bias current is shown in Figure 4.34. The lower ER (higher bias) results in poorer receiver sensitivity due to SNR degradation. On the other hand, small chirp (higher bias) improves the transmission distance by reducing the pulse broadening, so a trade-off exists between increased chirp at higher ER and reduced SNR at lower ER [98, 99]. The ER is limited at high bias by the achievable peak-to-peak amplitude of the modulating signal and values in excess of 3 dB could not be achieved. The penalty due to reduced ER of the signal can be expressed with a simple analytical expression. On the other hand, it is not trivial to extract a penalty trend from the combined effects of adiabatic and transient chirp and numerical modelling or experiments are

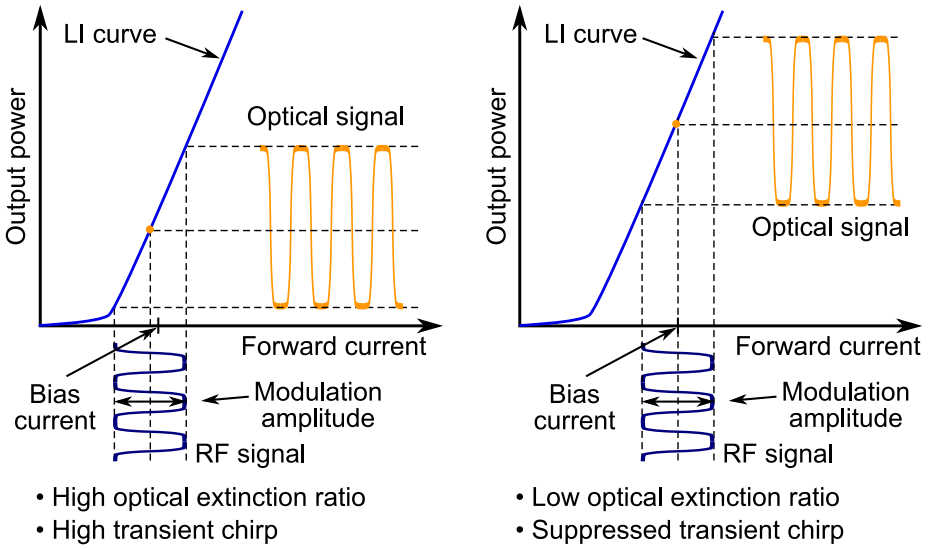


Figure 4.33: Operation regimes for a DML transmitter.

the best option. Hence, it is not generally simple to accurately describe analytically this optimum trade-off and, in this work, it is addressed through experimental results.

Figure 4.35 offers an insight into the chirp components and ER conditions in different operational regimes of the EX-DY7005-C DML. Different behaviours can be appreciated for adiabatic and transient chirp generated by amplitude modulation on their relation to ER. Increasing

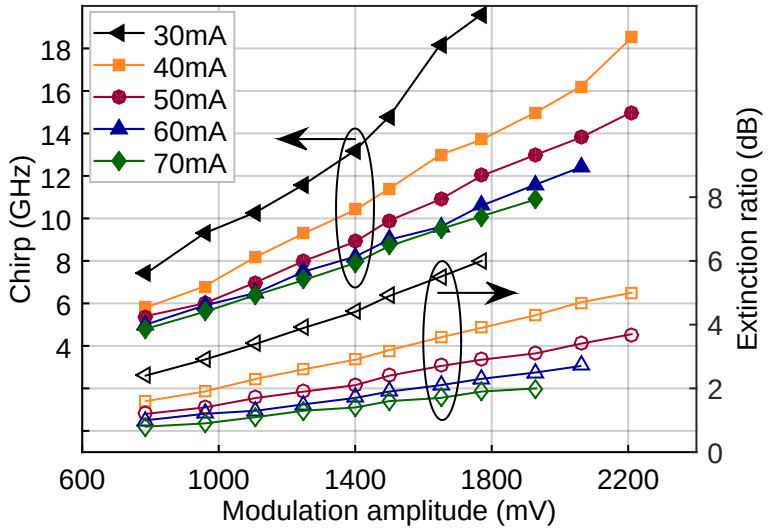


Figure 4.34: Measured total chirp magnitude and corresponding ER of the signal.

the laser bias the magnitude of the adiabatic chirp generated to obtain the same ER is higher and this is due to the necessity of using a higher voltage amplitude of the driving signal. On the other hand, the relation between ER and transient chirp does not show a marked dependence on the bias and suggests that, for the highest value of 70 mA, the transient chirp was masked by the adiabatic chirp, rather than being completely suppressed. The graph shows how high DML bias can be used to reduce transient chirp at the cost of having lower ER and higher adiabatic chirp, for the same ER of the signal.

In Section 3.2 it was discussed how multilevel modulation formats can be employed to enhance the bit-rate to 25 Gb/s while still using 10 G bandwidth limited devices. A 25 Gb/s transmission based on PAM4 was performed in this Section using a 10 GHz DML transmitter and will be reported in more detail in Subsection 4.2.3. In order to show the effect of chirp during transmission over a dispersive medium the receiver sensitivity of the 25 Gb/s PAM4 signal for a pre-FEC BER of 10^{-3} was measured in optical B2B and after having travelled through 12 km of SMF. From the curves in Figure 4.36 it is evident that the dashed lines, corresponding to the B2B measurements, are lying on top of each other, meaning that, the sensitivity in such cases is only dependent on the ER and did not vary with the DML bias and, hence, with the amount

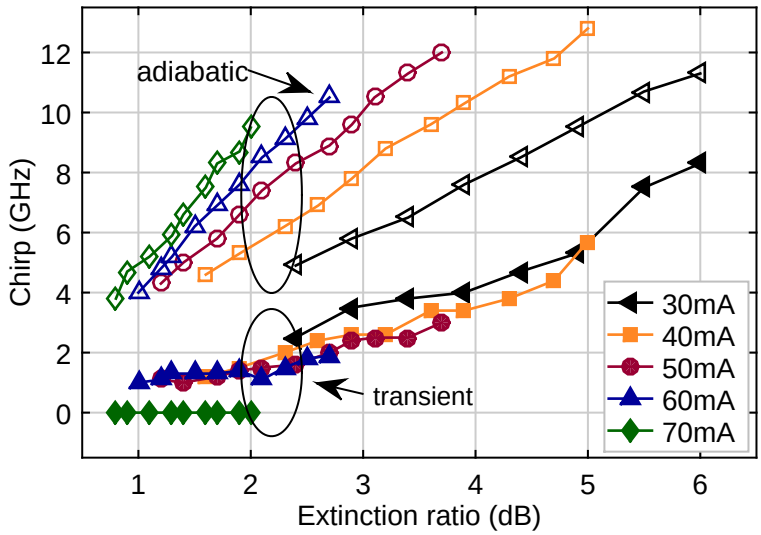


Figure 4.35: Magnitude of adiabatic and transient chirp as a function of the signal ER for different laser bias.

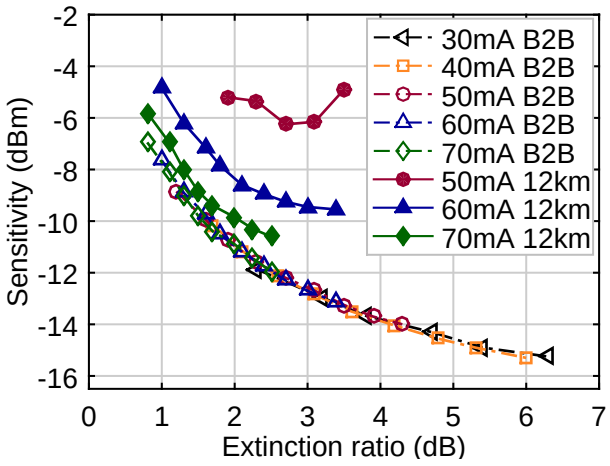


Figure 4.36: Sensitivities for a 10^{-3} BER in the PAM4 system, in optical B2B and with 12 km of SMF.

of chirp. Such behaviour is expected in a direct detection receiver as the phase noise does not affect the received signal. On the other hand, when the signal was transmitted through 12 km of SMF, the interaction of chirp and CD induced distortions led to sensitivity degradation. In particular, the trend that can be observed is that the transient chirp, generated by operation close to threshold, is interacting with CD heavily and affects the quality of the received signal. Higher bias must be used to avoid severe sensitivity penalties. The signals generated with bias values of 30 mA and 40 mA, which had a high magnitude of transient chirp (Figure 4.35), could not be detected at a BER below 10^{-3}. Only bias values of 50 mA or higher could lead to a pre-FEC BER at the receiver after the 12 km fibre, with performance improving as the bias was increased and the 70 mA setting showing results close to the B2B case.

The DMLs should thus be biased at high current to suppress the transient chirp and improve the tolerance to CD, thereby enabling higher reach over SMF. This approach, however, could not achieve high ER and this limited the sensitivity due to poor level-separation in the signal (Figure 4.36). The proposed solution to overcome such limitations, explained in the following Subsection, is to bias the DML at a high value well-above threshold (70 mA in this specific case) so that the detrimental effects of transient chirp and CD interaction are avoided and then increase the ER using a narrow optical filtering technique.

4.2.2 Narrow optical filtering technique

In the previous Section, the different operating conditions of a DML were analysed, resulting in the discussed trade-off between ER and amount of chirp generated. This Section describes the filtering technique used to improve the ER of a DML signal while avoiding transient chirp generation. The idea was to generate a signal with poor ER and suppressed transient chirp and successively employ an optical filter to improve the ER (Figure 4.37). For this purpose, a DML was operated in high bias conditions so that mostly adiabatic chirp was generated, with the transient component heavily suppressed. This means that, in an amplitude modulated scenario, the various logical signals have a different frequency shift from the carrier and, hence, uniquely correspond to different frequency lines. A schematic representation of the chirped spectrum for NRZ and PAM4 modulated signals is shown in Figure 4.38 where the frequency lines correspond to the amplitude modulated levels. Taking advantage of the symbol frequencies distribution, a narrow optical filter was used to selectively suppress the adiabatic components of the signal and improve their intensity level separation. Figure 4.39 shows the optical spectra obtained with the EX-DY7005-C DML for a binary and quaternary modulation with increasing ER. The modulation frequency used for these measurements was 1 GHz so that the adiabatic chirp contribution is dominant over the modulation spectrum in the frequency profile and, at the same time, thermal shift contributions to the chirp are negligible. The modulated symbols are clearly visible from the spectra, where two

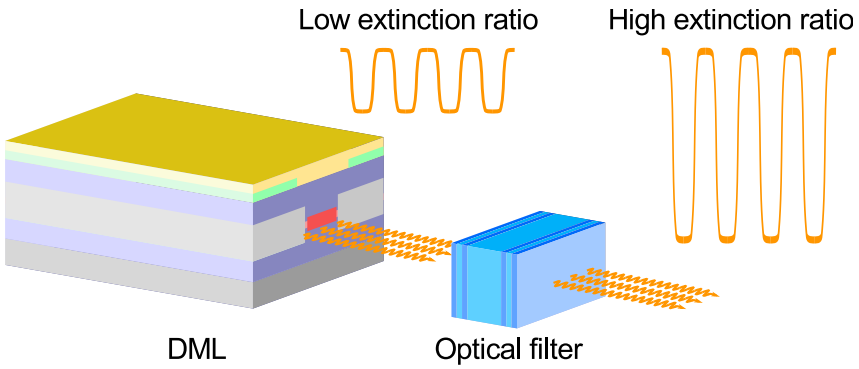


Figure 4.37: DML followed by a narrow optical filter to improve signal ER.

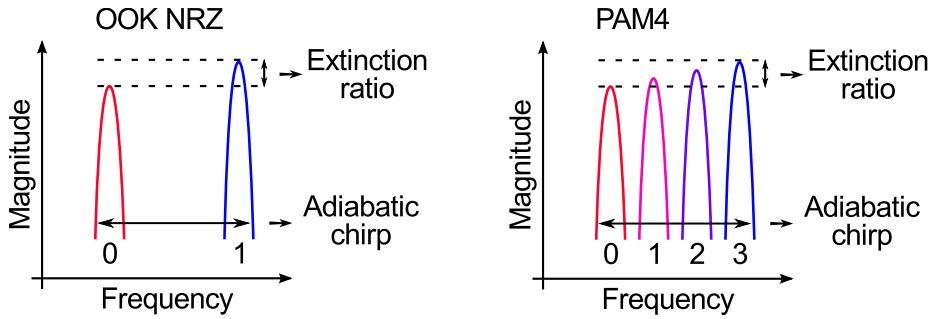


Figure 4.38: Adiabatic chirped spectral component for a 2 and 4 level amplitude modulated signal.

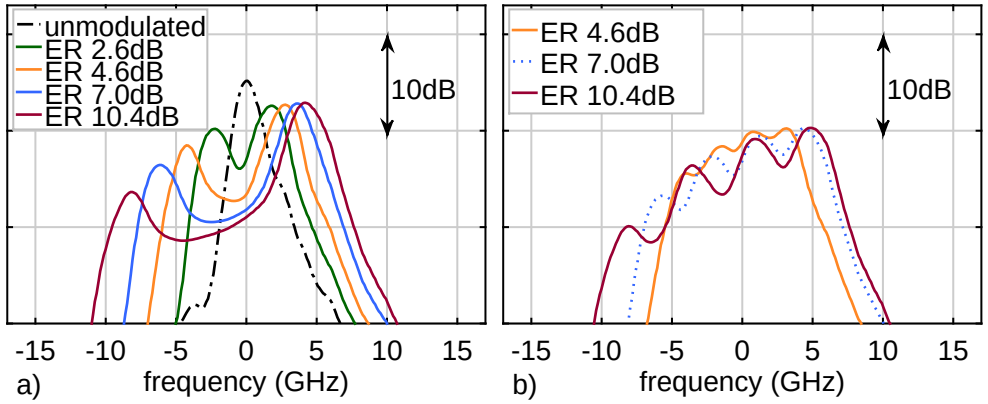


Figure 4.39: Measured optical spectra of EX-DY7005-C DML for a) 2 and b) 4 level amplitude modulated signal at 1 GHz.

peaks are visible for NRZ modulation and four peaks when PAM4 was used instead. At higher amplitudes of the modulating electrical signal the peak separation increases both in frequency and power, indicating increased chirp and ER, respectively.

Aligning the filter so that the linear region of its rising or falling edge is overlapped with the signal, the symbols of the multilevel constellation are attenuated while maintaining their original relative level spacing. The difference of the filter insertion-loss between the higher and lower symbol of the constellation is the amount by which the ER is increased. The slope of the filter edge and the chirp magnitude determine the ER gain obtained in the output signal. In the literature, the approach used with NRZ modulation [100] aligns the filter slope in such a way that the attenuation introduced enhances the original ER by adding additional

attenuation to the modulated "0". However, observing that the initial ER of the signal is generally low, an opposite solution with inverted filter slope can also be used. The two solutions represented in Figure 4.40 for PAM4 modulation are hence proposed and investigated in this work. The first, similar to the common approach used for NRZ, makes use of a filter to attenuate the red-shift of the signal. In this way, the lower energy symbols of the constellation are further suppressed and the ER increased. In the second approach, the filter has an opposite slope and is aligned in order to attenuate the blue-shifted higher energy symbols. A steeper filter edge is required to obtain the same ER of the previous scheme and the overall insertion loss is higher. However, this solution can have other advantages, as shown in the results Section. It is worth noting that, as a consequence of the blue-shift filtering, the logical higher symbol of the constellation corresponds to the lowest power hence the signal is logically inverted, as well as the relationship between adiabatic chirp and intensity level.

4.2.3 CML transmission performance

The transmitter described above was then implemented in its two variants to generate 25 Gb/s traffic, using both a 25 GBd NRZ OOK and a 12.5 GBd PAM4 modulation, and the scheme transmission performances were evaluated.

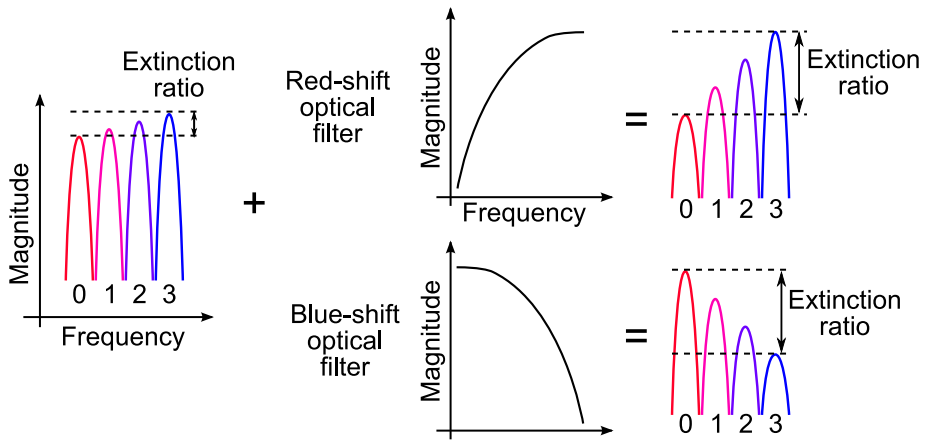


Figure 4.40: Two optical filters adopted for chirp management of a PAM4 signal.

Experimental setup

The experimental system in Figure 4.41 was assembled to characterise the CD tolerance of DML generated 25 Gb/s traffic with optical filtering for chirp management. Two different C-band transmitters were used for NRZ and PAM4 modulation due to the different bandwidth requirements. For NRZ, the ExOptronics EX-DY7005-C characterised above, which had an 18 GHz 3 dB bandwidth, was used in conjunction with a programmable optical filter. The DML had a temperature tuneable centre wavelength around 1532 nm and a Peltier cell for temperature control and centre frequency stabilisation. The programmable optical filter used after the DML had a 1 GHz resolution and could achieve a 1.6 dB/GHz slope. A rectangular shaped passband filter was used and the centre frequency was adjusted to align its edge in order to create either a blue-shift or red-shift filter. The PAM4 transmitter, on the other hand, was an integrated module (Finisar DM80-01) consisting of a 10 G DFB DML co-packaged with a multi-cavity etalon narrowband optical filter which generated a 50 GHz periodic passband response. Temperature tuning of both the DFB and the etalon filter allowed for appropriate optical reshaping, either blue-shift or red-shift filtering. The transmitter could operate on eight consecutive 50 GHz channels of the ITU grid around 1538 nm. In both cases, the filters were used in their linear region to preserve linearity of the signal and, in particular, equal symbol spacing for PAM4 levels.

The experimental setup had a 2-bit DAC for generation of either a 12.5 GBd PAM4 or 25 GBd NRZ OOK signal, modulated with a PRBS of order 15. External bias was applied to the lasers and the DAC signal was fed through a high-speed 50 Ω matched RF connector. Different lengths of SMF were used in the system, spanning from 12 km to 50 km,

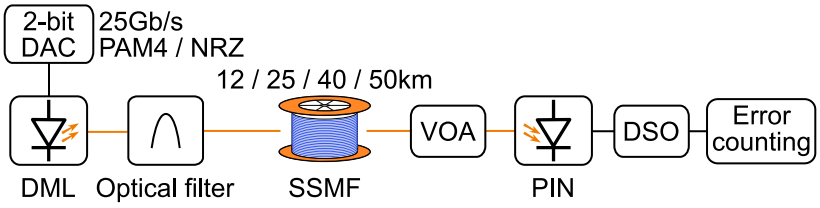


Figure 4.41: Experimental setup for characterisation of CML transmitters.

and a VOA was placed after the fibre to control the optical power entering the receiver. The PAM4 receiver was a 10 GHz PIN with integrated linear TIA followed by a 50 GS/s, 12.5 GHz 3 dB bandwidth DSO. The NRZ receiver used a 30 GHz PIN and a 80 GS/s, 36 GHz 3 dB bandwidth DSO. The captured waveforms were then analysed off-line for synchronisation and error counting, where a minimum of 1 million symbols were processed. It is worth noting that no pre- or post-equalisation was performed on the signal as the receiver was a simple slicer with 1 or 3 thresholds, depending on the modulation adopted.

NRZ experimental results

The sensitivity of the chirp managed 25 Gb/s NRZ transmitter was measured at a 10^{-3} BER for a range of ERs and SMF lengths (Figure 4.42). When the transmitter signal was reshaped with a red-shift filter, sensitivities of -14 dBm or better were measured up to 40 km, with less than 1 dB penalty for 12 km and 25 km. For the optimum ER value of 4.9 dB, transmission over 40 and 50 km showed, respectively, a 0.1 dB and 1.8 dB penalty compared with optical B2B. For the two longer distances, the best sensitivities were achieved for an ER which offered the optimum compromise between penalty due to low ER (poor symbol suppression) and chirp frequency spread and, hence, the distortion due to CD. When the blue-shift filter was used at the transmitter the maximum achievable ER was limited to 6.55 dB, due to the slope of the programmable optical filter. In B2B the sensitivities were similar to the red-shift filter case, with a < 0.5 dB penalty due to loss of linearity in the optical filtering. However, after 12 km or 25 km of SMF the signal had worse sensitivities compared to the previous filter and transmission through 40 km of SMF or more was not possible. The best NRZ performance was hence obtained using the conventional chirp suppression scheme as the blue-shift filter could not support SMF lengths of 40 km or 50 km. This was due to the loss of quality in the signal when using the external optical filter as an open NRZ eye diagram could not be achieved with the blue-shift filtering approach.

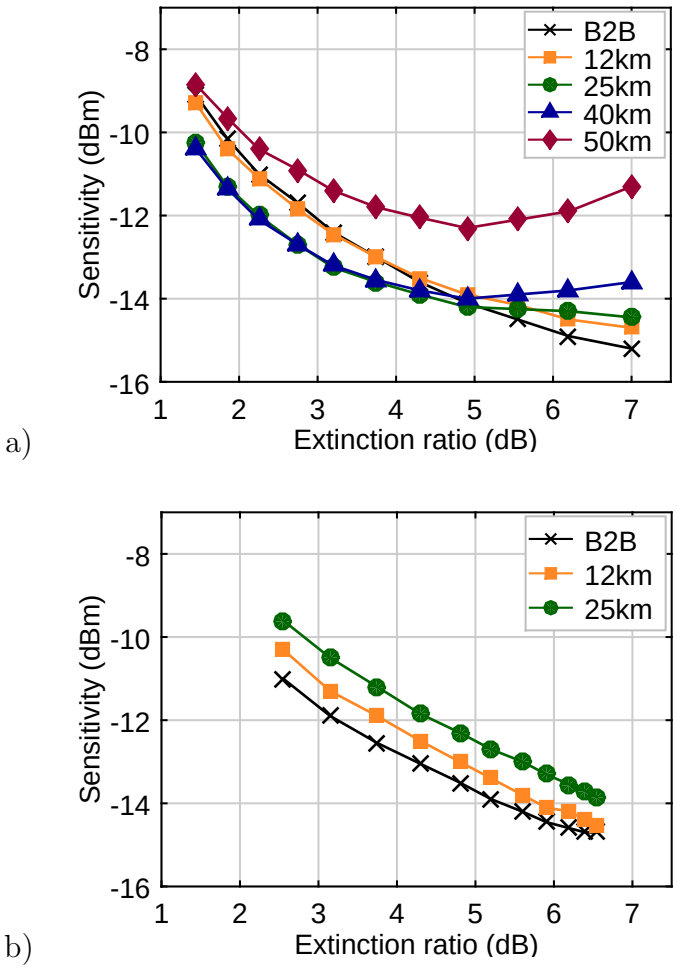


Figure 4.42: Sensitivities for a 10^{-3} BER in the NRZ system for a) red-shift filter and b) blue-shift filter.

PAM4 experimental results

The same sets of sensitivities were then measured for the 12.5 GBd PAM4 transmitter. Figure 4.43 shows that both filtering solutions were able to operate up to 50 km with different optimum operating points. The sensitivities of the red-shift filtered signal suffered progressive degradation with the fibre length increase, indicating a higher level of impairment as the accumulated CD increased. The blue-filtered signal, on the other hand, had poorer performance in B2B due to a slight linearity degradation, but it exhibited best overall performance for 12 km and 25 km and out-performed the conventional red-shift filtered signal for all the SMF spans investigated. After 50 km the sensitivity improvement over the red-shift filter was 1.75 dB. In Figure 4.44 the NRZ red-shift filter and the

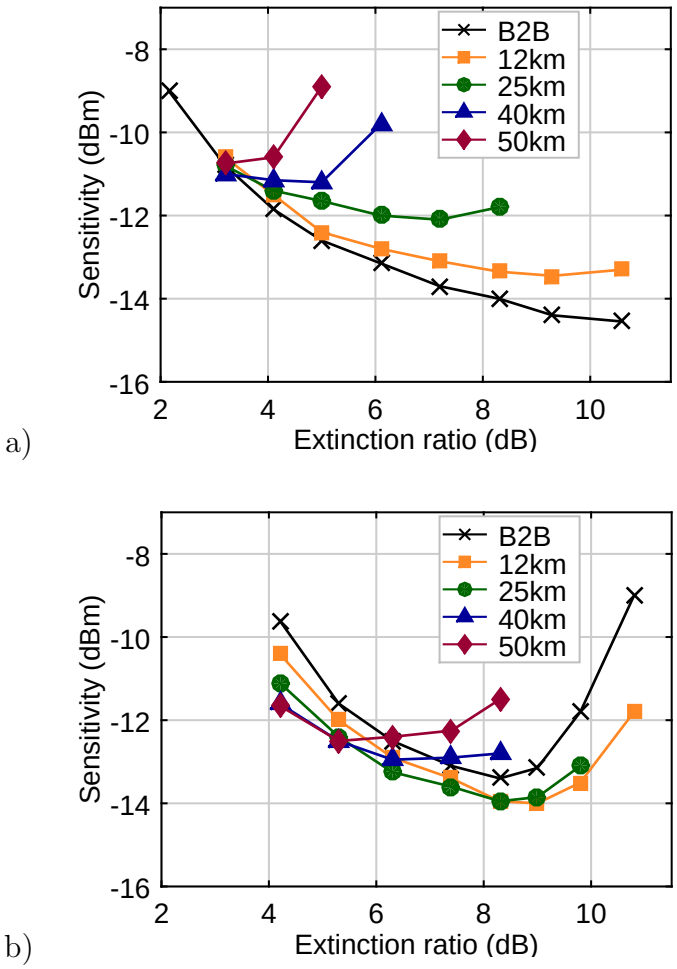
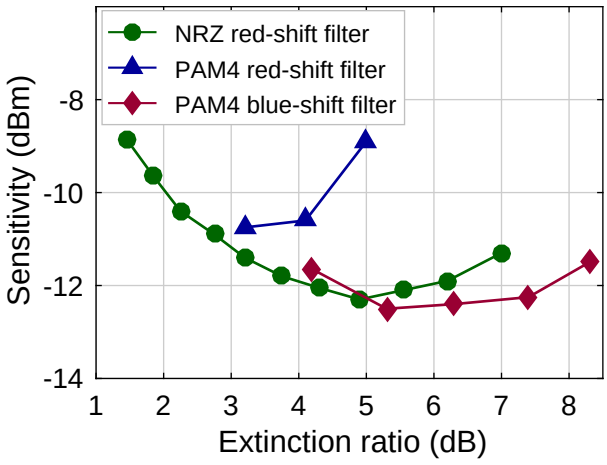


Figure 4.43: Sensitivities for a 10^{-3} BER in the PAM4 system for a) red-shift filter ans b) blue-shift filter.

two PAM4 filters are compared, for an SMF length of 50 km. The best overall sensitivity after 50 km for a 25 Gb/s line-rate was achieved using PAM4 with the chirp blue-shift filtering, which provided a -12.4 dBm sensitivity. A similar value of -12.3 dBm was achieved using NRZ and the conventional red-shift filter, but this was only possible using more expensive 25 G components, while the PAM4 system employed exclusively 10 G devices.

In order to explain the better transmission quality of the blue-shift filtered PAM4 signal, and the trend seen for its optimum sensitivity at an intermediate length of fibre, a deeper analysis was done to better understand the mechanism of CD induced distortion. In the transmitter the operation regime of the DML only generated adiabatic chirp which



a)

Figure 4.44: Sensitivities for a 10^{-3} BER after 50 km comparing three filters.

caused a frequency displacement of the symbols. The accumulated CD therefore caused the symbols of the constellation to have a different group delay at the receiver, as they experienced a different group velocity delay during fibre propagation. This generated an asymmetry in the eye diagram which is called skewing. An example of a skewed eye diagram, compared to an ideal one, was obtained through numerical simulation and is shown in Figure 4.45. A heavily skewed eye diagram reduces the sensitivity at the receiver for a multilevel signal as the optimum sampling points for the secondary eyes in the eye diagram are not aligned. In order to quantify the amount of skewing, the standard deviation of the four symbols, in case of a PAM4 constellation, was calculated for different time sampling points across a symbol period (Figure 4.45). The standard deviation value represents the spread of the signal rail and its minimum corresponds to the optimal sampling point to minimise the BER. In an ideal undistorted eye diagram, the minima of the four symbols are aligned at the same sampling instant and this is the optimum sampling delay for the decision thresholds which provides the best achievable BER. In a signal subject to skewing the opening of the three PAM4 eyes are not aligned in time and the standard deviation minima are spread along the sampling delay axis. This results in higher penalty when noise is added to the signal as the reduction in eye opening occurs asymmetrically and, depending on the sampling point, some of the secondary eyes dominate the BER contribution.

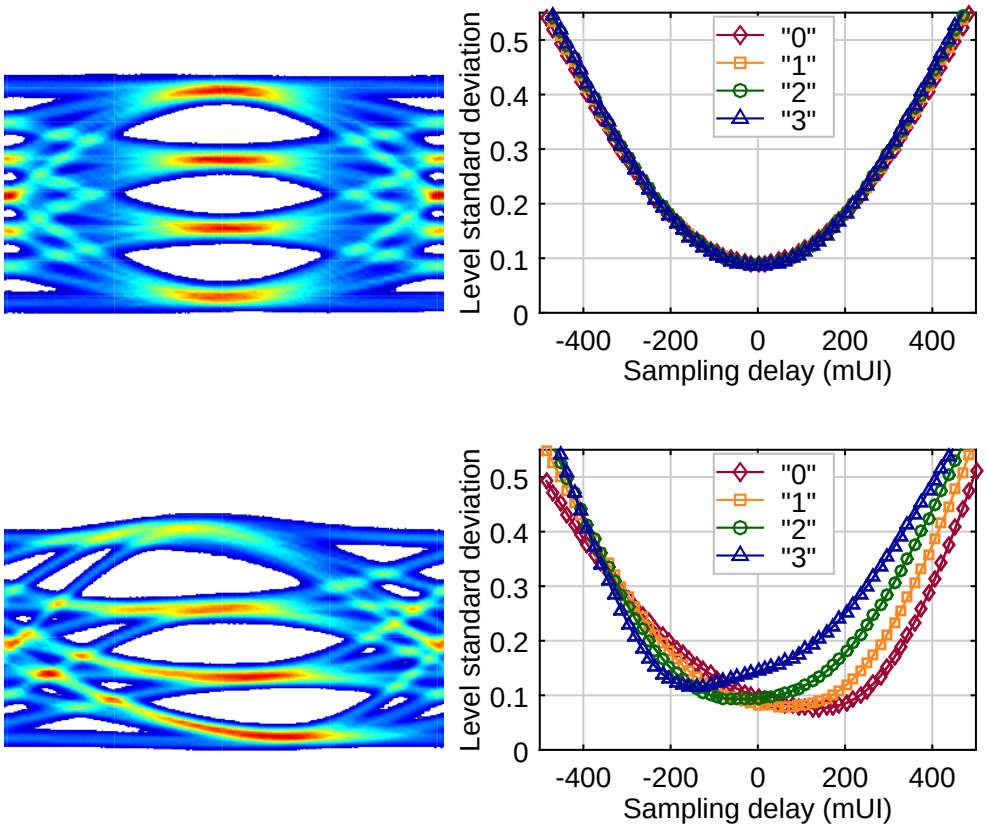


Figure 4.45: Ideal and skewed PAM4 eye diagrams and corresponding standard deviation of the signal rails.

Looking at the transmitter developed here, direct modulation of the device induced an initial skewing due to the laser dynamic, similar to the one in Figure 4.45, which was further emphasised after fibre transmission in the red-shift filter case when SMF was used and anomalous CD took place in the C-band. On the other hand, using blue-shift filtering to invert the relation between frequency chirped components and logical signal levels, the direct modulation distortion acted as a pre-compensation for the CD induced skewing. The eye diagrams in Figure 4.46 show how, after 50 km, the misalignment between optimum sampling points in the signal rails was improved for a transmitter performing blue-shift optical narrowband filtering. Considering the time difference between the two farthest standard deviation minima as a quantitative indication of the eye distortion, it is evident how the blue-shift filtered signal provided an advantage in terms of CD tolerance, resulting in a less impaired signal at the receiver. While for both filters the initial skew was -3.8 ps, due to

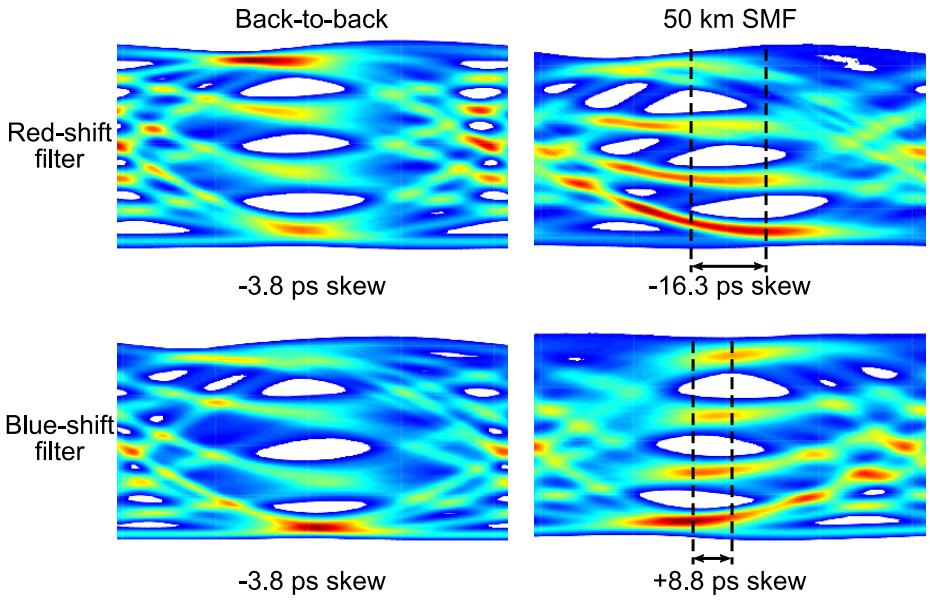


Figure 4.46: 25 Gb/s PAM4 eye diagrams in B2B and after 50 km for the two filtering techniques.

the laser modulation, after 50 km the blue-shift filter exhibited a +8.8 ps difference between the rails minima compared to the −16.3 ps of the red-filter, which explains the higher penalty observed in sensitivity. Also, the fact that for the blue-filtered signal the skew was initially negative and became positive after fibre propagation is the reason for the better performance of the 12 km and 25 km SMF, as the PAM4 eye diagram after fibre propagation was more symmetric than the one generated at the transmitter. The NRZ signal does not suffer from the CD induced skew because it only has a single decision threshold at the receiver and, hence, the blue-shift filter did not provide an advantage.

Extended reach results

For PON applications, where the link power-budget is a key parameter, further improvement in sensitivity could be achieved using FFE filters and/or APD receivers in combination with the chirp managed transmitter. Also, long reach PON or data centre interconnect (DCI) links could benefit from EDC to increase the maximum CD tolerance and, hence, supported fibre length. Figure 4.47 shows 25 Gb/s PAM4 BER curves after 50 km of SMF for the two filtering schemes and the improvement offered by the use of a fractionally spaced FFE equaliser with 16 taps

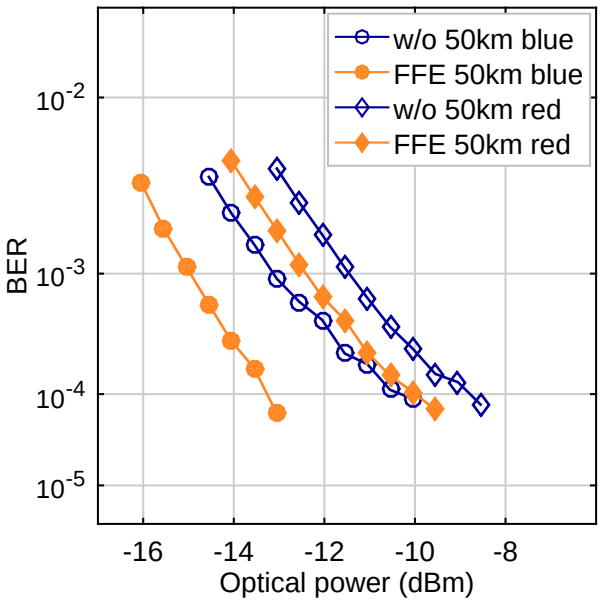


Figure 4.47: BER curves after a 50 km SMF for 25 Gb/s PAM4 with FFE employed at the receiver.

and 2 taps per symbol. A 1 dB improvement was offered by the FFE for the red-shift filtered signal and a 1.9 dB enhancement was achieved for the blue-shift filter with a measured sensitivity of −15 dBm.

Transmission of the blue-shift filtered 25 Gb/s PAM4 was also performed by equipping the receiver with a 10 G APD with linear TIA and the FFE described above for longer spans of fibre. Figure 4.48 reports some of the results obtained for SMF lengths of up to 90 km. After 50 km the measured sensitivity was −15.8 dBm for the APD receiver and improved to −21.2 dBm when combined with the FFE filter, compared to sensitivities of −13 dBm and −15 dBm, respectively, when a PIN was used. The APD provides an option to improve the power budget without resorting to optical amplification. When longer SMF spans were used an FFE was necessary to recover the signal and sensitivities of −19 dBm and −13.2 dBm were obtained after 75 km using an APD and a PIN receiver, respectively. For the longest reach tested of 90 km, only the APD could provide a BER below threshold due to the high fibre attenuation and a sensitivity of −16.8 dBm was measured. This suggests that the chirp managed DML technology combined with multi-level amplitude modulation is viable also for long reach PON and DCI application.

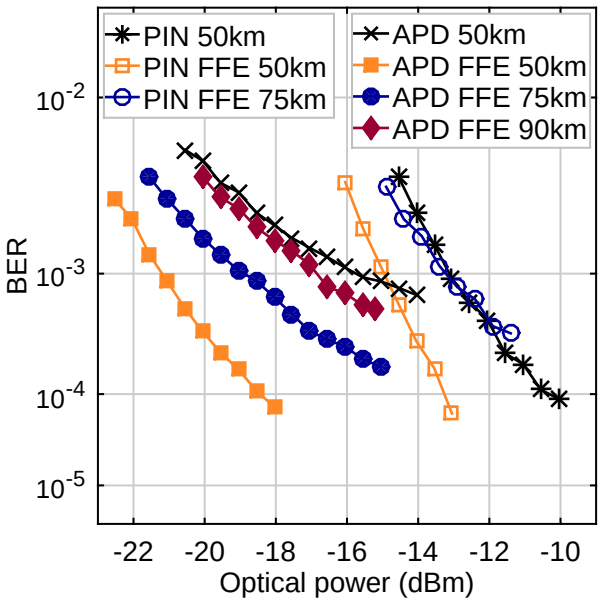


Figure 4.48: BER curves for 25 Gb/s PAM4 transmitter with blue-shift filter, for PIN and APD receivers.

4.3 Summary

In this Chapter, two different techniques to improve CD tolerance in PONs are reported, aimed at both upstream and downstream. Section 4.1 discusses the potential of DSP enabled EDC as a solution for extended reach and bit-rate enhancement of PON upstream channels where CD is a performance limiting factor. Analysis of the requirements and performance of linear FFE and DFE filters are carried out for an adaptive burst-by-burst implementation that could find application in PON upstream channels with minimal overhead requirements. A 25 Gb/s PAM4 burst-mode traffic is demonstrated, employing 10 G devices only, using a total preamble time of 200 ns including BM-TIA settling time and EDC training. Using an optically pre-amplified receiver and a 14-taps fractionally spaced FFE a sensitivity of -25 dBm is achieved and DRs of 14.7 dB and 13 dB are supported in B2B and after a 25 km SMF, respectively. The system is also demonstrated to operate under a 25 km differential reach with the adaptive filter successfully compensating for the different amounts of CD in the bursts confirming adaptation times within 200 ns and, hence, to be a suitable technology for PON upstream channels.

Section 4.2 deals with the issue of CD offering a solution tailored for the downstream which is located at the transmitter and implemented in the optical domain, instead of the electrical receiver design discussed previously. Narrow optical filtering is used to selectively suppress the adiabatically chirped components of a signal obtained through direct modulation to enhance its ER and allow the DML to operate in a regime where transient chirp is suppressed. Analysis of 25 Gb/s DML based chirp controlled transmitters, PAM4 and NRZ, is reported and their potential application as PON transmitters is demonstrated as they allow for a system configuration with a simple data-slicer at the receiver while supporting up to 50 km SMF transmission in the dispersive C-band. A novel optical filter suppressing the blue-shift component of the chirped signal is proposed and demonstrated to offer the best overall performance when used in combination with PAM4 modulation. The transmitter filter engineers the eye diagram skewing caused by direct modulation of the laser in order to provide a pre-compensation that mitigates the effect of CD induced skewing during fibre propagation. This allows for longer reach and the potential of the scheme for transmission through lengths of SMF of up to 90 km is demonstrated, opening to the possibility of its adoption in DCI or long-reach PONs.

5 Optical Amplification Strategies for Burst-Mode Systems

Chapter 3 discussed how the drive for higher speed links in access networks is driving the adoption of higher order modulation formats in PONs. These have several advantages among which are the higher spectral efficiency and increased tolerance to chromatic dispersion compared to an equivalent bit-rate NRZ modulation format. However, one of the drawbacks is the reduced sensitivity which means the minimum optical power required at the photoreceiver is higher. Classically, PONs are non amplified systems, in order to keep their design simple and cost-effective. However, optical amplification becomes necessary when the same power budget specifications of legacy PON systems are adopted in higher bit-rates systems [78]. In the downstream direction sufficient optical amplification can be achieved using a booster amplifier at the transmitter side so that the ONU receivers do not need pre-amplification. For the upstream, however, this design will not be cost-effective due to the high number of devices needed to equip every ONU with a high power booster amplifier. Hence, the strategy proposed is to use an optical amplifier in front of the OLT receiver so that a single component is shared among all users. In this application, the amplifier must be able to work effectively with high DR burst-mode upstream traffic. This Chapter reports on two different solutions investigated for amplification of PON upstream traffic which, as mentioned, is the most challenging of the two signal directions due to its burst nature. Section 5.1 presents the results obtained with O-band Raman based amplifiers for different standards-compatible upstream transmissions, G-PON and XG-PON in particular. Section 5.2 investigates the use of SOAs with an electrically controlled variable gain on a burst-by-burst basis to achieve optical DR compensation of the upstream traffic along with pre-amplification.

5.1 Raman amplifiers for PON upstream traffic

Raman amplification in lightwave systems is obtained through SRS along an optical fibre and the same fibre used for data transmission can be used as an active medium for amplification. Raman amplification has been successfully used in many diverse optical systems, particularly in long haul because of the advantage offered by its distributed nature which results in a lower NF than discrete amplifiers. However, recently Raman amplifiers have also found application in shorter optical links and access networks. The mechanism of Raman amplification for optical fibre systems is introduced in 5.1.1 and then, in the following Subsections, various applications of Raman based amplifier modules are proposed for PON upstream systems in the O-band.

5.1.1 Raman based optical amplification

The Raman effect is an inelastic scattering mechanism which takes place when a photon of an electro-magnetic field incident on a molecule is scattered at a different frequency. The incident photon interacts with the medium and its frequency is shifted to red or blue, where the extent of this shift is determined by the material. When part of the energy of the photon is transferred to the interacting medium and adds to its internal energy a red-shift is observed, called Stokes Raman scattering. On the other hand, when internal energy of the medium is transferred to the photon, a blue shift is observed and this process is called anti-Stokes Raman scattering. The energy gap between the incident and the scattered particle is equal to the energy difference between vibrational modes of the interacting molecule and is predominantly negative in spontaneous scattering, which means emission of Stokes photon generally dominates [103–105]. In a quantum mechanical description, the photon is inelastically scattered by a quasi-particle, representing an excited state of the molecule's modes of vibration, called a phonon. Photon energy can be lost, with a corresponding shift to lower frequencies and heating of the molecular lattice (Stokes process), or gained, with a consequent shift of the light to higher frequencies and lattice cooling (anti-Stokes process). The frequency shift is equal to the oscillation frequency of the created or

annihilated phonon, and the resulting spectrum is determined by the material properties. Raman scattering is a spontaneous process that occurs for a fraction of approximately 10^{-7} of the incident photons and takes place in every medium. During the dominant Stokes emission a pump photon at frequency ν_p excites a molecule up to a virtual energy level. The molecule quickly decays to a lower level emitting a signal photon in the process at frequency ν_s (Figure 5.1). The difference in energy between the pump and Stokes signal photons is dissipated by the molecular vibrations of the interacting material. These vibrational levels determine the frequency shift and shape of the Raman gain curve. In silica glass the dominant Raman lines are due to the bending motion of the Si-O-Si bond and, due to the amorphous nature of silica, the Raman gain curve is broad in optical fibres [104, 106, 107]. The peak of the Stokes shift in Germanium-doped SMF is observed at a distance of approximately 13.2 THz from the incident signal [103–105].

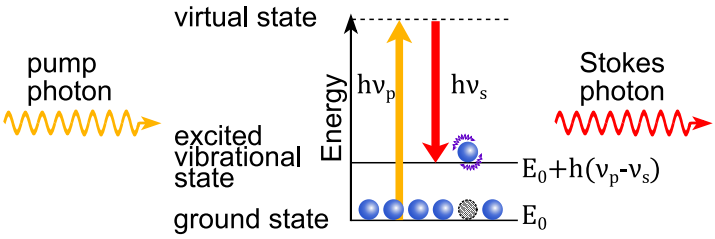


Figure 5.1: Generation of a Stokes photon through spontaneous Raman scattering.

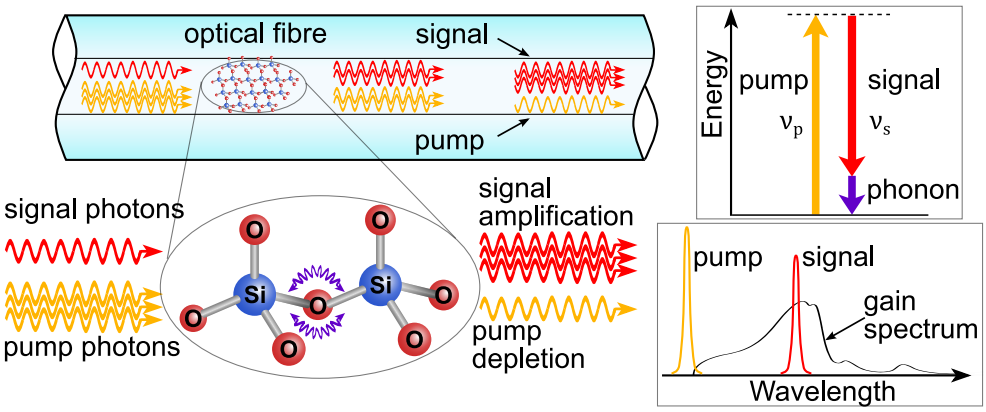


Figure 5.2: Signal optical amplification via stimulated Raman scattering in a silica optical fibre.

Raman scattering can also be stimulated if an intense pump is injected into the medium along with the signal, where the pump frequency is separated from that of the signal by the Stokes shift. When a signal with frequency ν_s is incident on the material, simultaneously with a light beam at ν_p, stimulated Raman scattering takes place and a quantum $h\nu_s$ is added to the probe signal at ν_s that becomes consequently amplified, while the pump beam loses a quantum $h\nu_p$ [108]. SRS was observed in optical fibres in 1972 [106] and is at the basis of the gain mechanism of Raman amplifiers, converting pump energy into signal energy.

Since Raman scattering is intrinsic to silica-based fibres, optical amplification is simply achieved by propagating a pump beam together with the signal beam in the same optical fibre, making it an optically pumped optical amplifier. The optimal frequency spacing between the pump and signal corresponds to the peak of the Stokes shift at a frequency of 13.2 THz lower than the pump signal. In its simplest configuration, a Raman amplifier has a WDM filter or a circulator to inject the pump beam into the same fibre used for signal transmission (Figure 5.3), either in a co-propagating or counter-propagating direction, because Raman gain does not depend on the relative direction of propagation of pump and signal beams [104]. SRS can occur in any fibre and, since the amplification happens in the transmission fibre itself over a long distance, the amplification has a distributed nature. The Raman gain spectral shape depends primarily on the frequency separation between pump and signal, not their absolute frequencies, hence Raman amplification can occur at any signal wavelength by proper choice of the pump wavelength. In the Raman gain process, the pump photon is excited to a short-lived virtual state and the response time of silica is evaluated to be less than 100 fs [105, 107]. This means that, for amplification applications in opti-

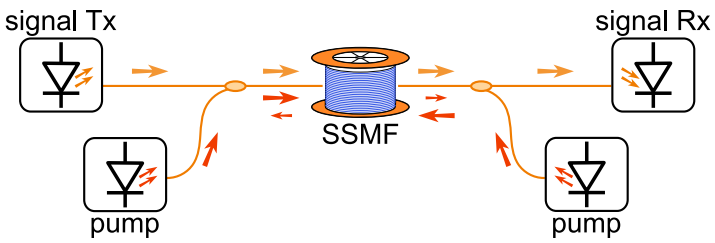


Figure 5.3: Schematic of a Raman optical amplifier.

cal systems, the gain appears instantaneous.

Raman amplification offers several advantages over discrete amplifiers such as SOAs and EDFAs. Due to its distributed nature the resultant NF is lower than for discrete amplifiers as the signal OSNR is maintained at higher values and this has led to extensive research into Raman amplification for long-haul high-capacity optical links [109–112]. The possibilities to flexibly allocate the amplifier wavelength window of operation means it can be employed in spectral regions where other amplification technologies are not available, being limited either by the fibre used as the active medium in doped fibre amplifiers, or by the semiconductor material in the SOA case. Also, the flexibility of Raman amplification allows control of the spectral shape of the gain and the NF by combining multiple pump wavelengths to make a polychromatic pump spectrum. Using similar multi-pump approaches, an improved gain flatness and extended bandwidth can be achieved over a wavelength range as wide as 200 nm [113], which is a much greater span than SOAs or EDFAs could achieve. The main disadvantage of Raman amplification is its inherently low efficiency, due to the low occurrence probability of SRS, which makes it necessary to use very high-power pump lasers. Such pump lasers can be expensive and, in the case of semiconductor devices, require intense cooling. In addition, the high-power beam propagating in the fibre adds practical difficulties ranging from the connectors care to the safety concerns for the installation workers.

Raman amplification could be very advantageous in PON upstream channels where a single centralised amplifier module could be shared and serve all the network customers. Amplification can be provided by placing the pump lasers in the OLT without the need for introducing active elements in the network plant, offering an architectural advantage over other reach extender solutions which require the presence of an active remote cabinet. Also, Raman scattering has advantageous properties such as high saturation power and a very fast gain process which makes it appealing for burst-mode traffic. Due to its relative immunity to gain saturation in the PON signals power regime, Raman amplification does not suffer from gain transients when the probe signal is bursty [88, 114, 115]. However, application in access networks has been limited by the lack of Raman pumps suitable for practical application

in PONs that could work in the wavelength transmission windows of interest. For wavelengths around 1.3 μm, Raman gain was traditionally obtained by resorting to expensive and bulky fibre lasers with the obvious disadvantages in terms of cost and physical footprint of integrating similar lasers into an OLT card. In recent years, however, high-power semiconductor lasers, which are cheaper and less bulky than their fibre based alternative, became available in the wavelength region suitable for O-band amplification. Subsequently, Raman amplification has been demonstrated as a way to extend the reach and power budget of PONs proving to be a valid alternative to other optical amplifiers [116–123].

5.1.2 G-PON reach extender

Raman amplification is used here to provide optical amplification in the G-PON upstream band. The regular G-PON upstream wavelength window is a 100 nm wide region from 1260 nm to 1360 nm [16] and, to cover the entire window, a multi-pump approach would be necessary. Instead, here single wavelength pumps were used which could still provide amplification for a reduced upstream window 20 nm wide. The pump lasers used had a centre wavelength of 1240 nm which was designed to provide the peak of the Raman on-off gain at a wavelength of 1310 nm, the centre of the G-PON upstream band [16]. The pump lasers employed were developed as part of the European FP7 project Quaternian [84] by the project partner Innolume [124]. One of the Quaternian project objectives was to develop high power semiconductor lasers to operate in the 1.1 μm to 1.3 μm wavelength range exploiting new materials. Quantum-dot materials grown on Gallium Arsenide substrates were chosen because they offer an advance in the control of the carrier density of states and this has led to significant device technology advances in the critical wavelength range of 1.1 microns to 1.3 microns. Thanks to the QD technology it was possible to access emission wavelengths not achievable with standard materials and, hence, to enable Raman amplification in new windows of the wavelength spectrum using semiconductor based pumps. Optical amplification based on Raman stimulated scattering was employed here to meet the higher power requirements of spectrally dense DMT, effectively exploiting a shared resource to enable the use of lower performance, po-

tentially lower cost, non-shared transmitters for the upstream.

Raman module characterisation

Two types of pump lasers were used, both emitting at 1240 nm but with different spectral shapes. One type was equipped with a FBG in the pigtail fibre to narrow the wavelength spectrum to a 1 nm width while the other was not and had a broad emission across 7 nm. The width of the emission spectrum prevented SBS of the pump signal at the power regime used and, hence, loss of the amplifier efficiency [125]. In both cases, a pump module was assembled with two similar lasers and a polarisation beam combiner (PBC) to combine the power of the two diodes with reduced insertion loss, to maximise the available power for Raman scattering. The gain profile for the two modules was measured for a counter-propagating configuration with the setup in Figure 5.4 across a range of wavelengths. The probe signal from the tuneable diode laser (TDL) was varied across the range of wavelengths of interest in steps of 2 nm to extract the gain profile of the Raman pumps. The on-off gain was measured with an OSA to evaluate the difference in probe signal power with the pumps on and off. The results for the two gain modules are shown in Figure 5.5 for different pump powers. Both amplifiers had their gain peak for a probe signal of 1312 nm but the profile of the laser without FBG was smoother due to the large spectral occupancy of the pump signal which was in excess of 7 nm [126,127]. The module without FBG had a maximum output pump power of 27.46 dBm for which the maximum gain was 13.2 dB for a probe signal from 1312 nm to 1314 nm. A wavelength window of 13 nm was obtained with a gain flatness of 1 dB, from 1306 nm to 1319 nm, and a 24 nm region with a gain flatness of 3 dB, from 1299 nm to 1323 nm. For the module equipped with FBG in the

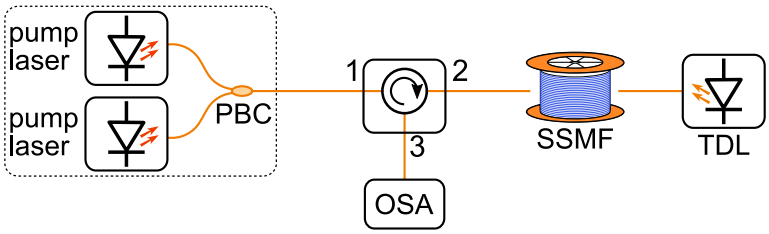


Figure 5.4: Experimental setup for on-off Raman gain measurements.

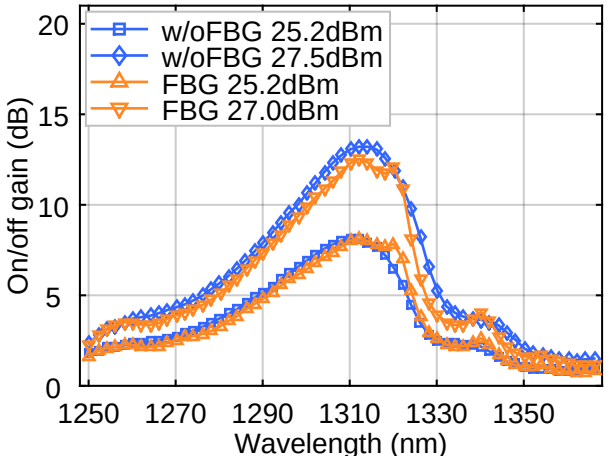


Figure 5.5: Raman on-off gain spectrum for 1240 nm pump lasers.

pigtail, the maximum pump power was 27.04 dBm, which corresponded to a 12.5 dB gain at 1312 nm. The region with a 1 dB gain flatness was 14 nm wide, from 1307 nm to 1321 nm, and the 3 dB region was 25 nm wide from 1299 nm to 1324 nm. Because the on-off gain scales proportionally with the pump power across the wavelength spectrum a lower peak gain would result in a wider gain-flattened region. The single pump approach could not cover the entire wavelength upstream window of G-PON systems for which a multi-pump approach would be necessary [128]. However, it provided gain with a maximum variation of 3 dB over a 20 nm window and so it could be sufficient for a narrower transmission window as in the XG-PON case [17].

Experimental setup

The amplifier module characterised above was employed to amplify a DMT transmission system based on the implementation reported in Section 3.1. A variety of amplification strategies were investigated for the upstream signal with the use of Raman pumps along with O-band SOAs. Mono-directional backward Raman amplification, bi-directional Raman amplification, a booster SOA and a booster SOA with additional backward Raman amplification were implemented and assessed. When the pump and the probe signals are counter-propagating, in the backward Raman configuration, the gain saturation threshold is increased and also relative intensity noise (RIN) transfer from the pump to the signal is mit-

igated. Most importantly, this allows the pump lasers to be conveniently placed at the OLT in PON systems and, hence, preserve the passive nature of the network. If the presence of a remote active node is allowed, then both discrete and distributed amplifiers could be used in order to improve the OSNR of the amplified signal. An SOA could provide advantages in terms of power consumption while a Raman forward amplifier typically exhibits a lower NF, higher saturation power and can work with a wider DR in the upstream, whilst not introducing patterning when the input power is high. Both can be used alone or assisted by the backward Raman amplifier module to increase the overall gain. The setup in Figure 5.6 was used to compare the different amplification strategies on a variable rate DMT signal. A DML transmitter operating at 1306 nm with a 3 dB bandwidth of 1 GHz was modulated with a DMT signal generated by an AWG. The DMT signal had a Baud-rate of 5 GBd and used QAM constellations of different orders, from 2 to 64, for an aggregated bit-rate ranging from 2.1 Gb/s to 10.4 Gb/s. A power loading scheme based on the SNR estimation of the channel and subsequent power compensation over the sub-carriers was adopted, as discussed in Section 3.1. The transmitter emission wavelength of 1306 nm was chosen to be within the G-PON upstream band (1260 nm – 1360 nm) [16], obtained with engineering of new QD materials investigated in the FP7 Quaternian project. The ODN loss was emulated using a VOA to adjust the launch power into the 40 km SMF of the OTL which introduced a fixed 14.5 dB loss.

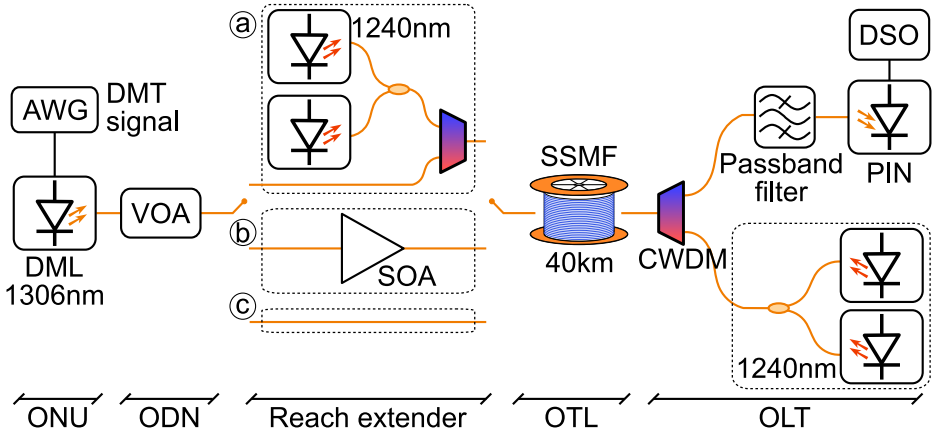


Figure 5.6: Experimental setup for the characterisation of various reach extender configurations in a DMT upstream system.

Two types of reach extender were placed after the VOA at the input into the OTL fibre, consisting of an optical pump for distributed forward Raman amplification, as in configuration (a) of Figure 5.6, or an SOA acting as a booster amplifier, configuration (b). At the OLT, a second pump module was used for distributed backward Raman amplification over the 40 km long OTL fibre. Each of the Raman modules consisted of two polarisation multiplexed, high power QD lasers emitting at 1240 nm. The forward and backward modules generated fibre launch powers of +25.2 dBm and +27.4 dBm, respectively, after their CWDM filters. On the other port of the OLT CWDM a 20 nm optical passband filter was placed before a 10 GHz PIN photodiode equipped with a linear TIA. The bandwidth of 20 nm was chosen to emulate a system where a wide upstream wavelength window could be received, from 1300 nm to 1320 nm. The photoreceiver output was captured with a 100 GS/s DSO and processed off-line for synchronisation, DMT decoding and error counting.

Experimental results and discussion

The system total loss budget was measured for the various amplification systems including the fixed 14.5 dB attenuation of the OTL 40 km fibre and assuming a minimum ONU transmitter power of +2 dBm [16]. The link budget was calculated measuring the input power into the OTL fibre, or into the reach extender, which resulted in a BER of 10^{-3} at the receiver. The available power budget was evaluated for the different amplification strategies employed and for different QAM constellations of the DMT signal and is shown in Figure 5.7.

The B2B is reported for comparison and is calculated from the DMT sensitivities adding the +2 dBm of minimum ONU launched power. No fibre transmission was used in the B2B case because its available power budget was not enough to support the attenuation of a 40 km SMF for bit-rates of 6 Gb/s or higher. The first amplification strategy considered to increase the supported ODN loss was the use of backward, or counter-propagating, Raman amplification at the OLT side, as in configuration (c) of Figure 5.6. The advantage of this scheme is that it offers amplification without introduction of any active elements in the outside

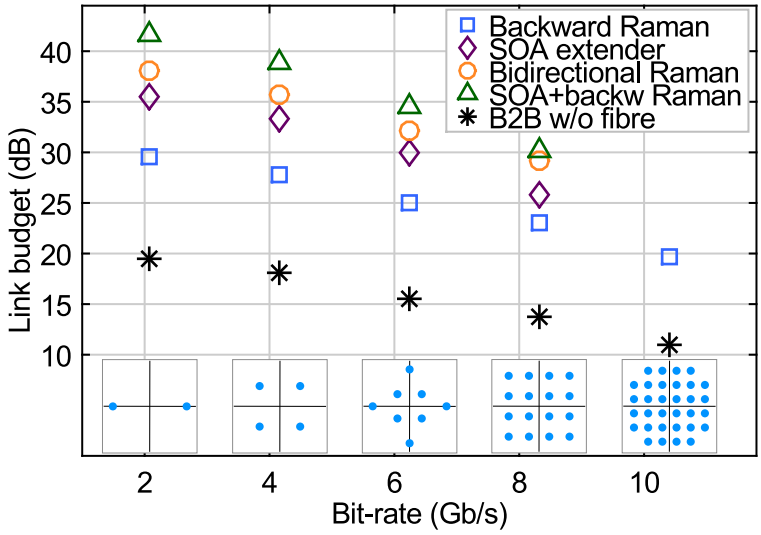


Figure 5.7: Measured sensitivities of DMT signals with different bit-rates for various reach extender configurations.

network plant because the Raman pumps are located in the Central Office. With a pump power of +27.4 dBm, or 549.5 mW, the upstream signal experienced a gain of 12.6 dB in comparison with the unamplified system.

The OSNR for all the working points was sufficiently high to support the QAM constellations used. The improvement in the link budget was 10.1 dB for the quadrature phase-shift keying (QPSK) 2.1 Gb/s DMT signal and decreased for higher order QAMs down to 8.7 dB for the 10.4 Gb/s transmission. The penalty observed with respect to the 12.6 dB Raman gain is attributed to the insertion losses of the passive components at the receiver and to the 20 nm wide optical bandpass filter in front of the PIN that did not suppress effectively out-of-band ASE noise and caused ASE-ASE beat noise at the photodetector. Increasing the modulation order improved the bit-rate at the cost of lower sensitivities and, hence, reduced ODN losses. The total link budgets achieved with backward Raman amplification ranged from 29.6 dB to 19.7 dB for the 2.1 Gb/s and 10.4 Gb/s signals, respectively. While the 29.6 dB power budget is enough to meet G-PON standard specifications [16], the higher 10.4 Gb/s signal could only allow for a reduced split ratio or short fibre span. In order to further improve the performance at higher bit-rates APD detectors could be used to enhance the sensitivity or higher

gain amplification systems can be employed.

As an alternative to backward Raman amplification the use of an SOA placed in an active reach extender at the passive splitter location was evaluated. The SOA exhibited superior performance in terms of achievable loss budget due to its higher gain of 16 dB and lower insertion loss of the passive elements at the receiver, as the CWDM was not necessary. However, higher order constellations exhibited a penalty with respect to Raman amplification due to the higher NF of the amplifier. Moreover, particular care should be observed when using an SOA to avoid operation in its gain saturation regime which would lead to significant BER penalty, especially when DMT is used which requires linearity. In contrast, the Raman amplifier worked in the linear regime for a wider range of input powers thereby preventing waveform distortion. The SOA booster allowed for link budgets of 35.6 dB and 25.8 dB for 2.1 Gb/s and 8.3 Gb/s, respectively, but could not support the 10.4 Gb/s transmission due to the higher NF.

More advanced higher gain configurations combining multiple optical amplifiers were also investigated to increase the overall supported ODN loss. These included bidirectional Raman amplification, configuration (a) in Figure 5.6, and the hybrid SOA booster with backward Raman amplification of configuration (b), which provided overall gains of 20 dB and 26.6 dB, respectively. The bidirectional Raman amplifier could support a maximum bit-rate of 8.3 Gb/s for which it provided a power budget of 29.2 dB. The main cause of performance degradation that prevented the use of higher order QAM constellations was the RIN transfer from the forward, co-propagating, pump lasers. The sensitivity penalty due to RIN transfer for increasing bit-rates was less pronounced than in the booster SOA case and so the noise added by the SOA had higher impact on the DMT waveform. This was also due to the fact that the RIN noise was frequency selective and the power loading feature of DMT mitigated its effect. The best power budget performance was achieved employing both an SOA reach extender and a Raman backward amplifier, supporting budget losses between 41.6 dB and 30.2 dB with bit-rates of 2.1 Gb/s and 8.3 Gb/s, respectively. In this scenario, the main factor limiting the use of higher order constellations was again the waveform degradation introduced by SOA amplification which prevented the use of QAM con-

stellations of order higher than 16.

Distributed backward Raman amplification among all the solutions presented preserves the passive nature of the outer plant of the network because no active reach extender is needed outside the Central Office. It also showed the best performance in term of signal SNR thanks to the lowest NF and was the only scheme that could support a 10.4 Gb/s bit-rate. On the other hand, the power budget of the network was the most constrained because the gain of the amplifier was the lowest among the various approaches. The limited performances were also due to the very restricted bandwidth of the DML transmitter, which forced the use of a very spectrally dense modulation format with the consequently high SNR requirements. With a higher-bandwidth transmitter higher Baud-rates could be used and with power loading to compensate for the high frequencies, attenuation could be mitigated. This would allow the use of lower order constellations and a more efficient power distribution, leading to an improved overall sensitivity at the receiver.

5.1.3 XG-PON reach extender

Raman optical amplification was also used in an XG-PON system to provide extended reach for its upstream traffic. A backward configuration was adopted adding suitable pump lasers in the OLT Central Office. The pump and the probe signals were configured to be counter-propagating which prevents gain saturation and also effectively mitigates RIN transfer from the pump to the signal. Most importantly, backward pumping allows the pump to be conveniently placed at the OLT in PON systems and preserve the passive nature of the network. The designated XG-PON upstream band is a 20 nm wide window allocated between 1260 nm and 1280 nm [17]. The Raman pumps' emission wavelength was engineered to be at 1210 nm in order to provide SRS in the XG-PON upstream window. The pump modules were developed by the Quaternian project partner Innolume [124] and based on the QD technology exploited for the 1240 nm high power lasers used in the previous G-PON Raman reach extender. High power semiconductor lasers emitting at the wavelength of 1210 nm were a novel element that could enable Raman amplification in the XG-PON upstream window, centred around 1270 nm, introducing Raman

amplification into a spectral region that was otherwise not accessible with other materials [129]. To ensure proper operation, however, the system needed thorough analysis as the pump lasers were above the single-mode frequency cut-off for SMFs and, hence, it was necessary to investigate the scheme efficiency. The upstream traffic used in the XG-PON system was a 2.5 Gb/s NRZ signal generated by uncooled DML transmitters.

Raman module characterisation

The pump lasers were high power modules emitting in excess of 500 mW of power and equipped with a FBG in the fibre pigtail to narrow their emission profile down to a 1 nm width. The relatively wide spectral line was designed to prevent SBS of the pump signal and the consequent efficiency loss that would accrue. Two of these devices were combined with a PBC to maximise the output power of the module and reduce polarisation dependent effects. A characterisation of the gain spectrum offered by the 1210 nm Raman pumps was carried out for different pump powers, similar to the previous one for the G-PON reach extender. The setup in Figure 5.4 was used to measure the backward Raman gain over a 50 km long SMF. The gain spectrum is visible in Figure 5.8 for different pump launched powers, up to a maximum of 28.8 dBm, for a range of wavelength from 1250 nm to 1320 nm. For the maximum pump power of +28.8 dBm the gain peak was obtained at 1278 nm and equal to 16.6 dB. The amplifier could provide amplification with a 1 dB gain flatness in a

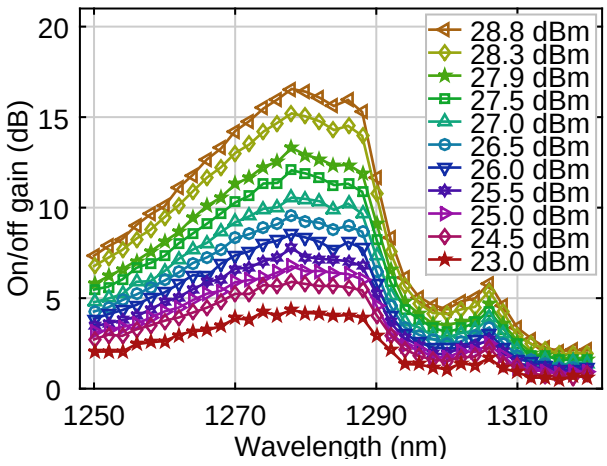


Figure 5.8: Raman on-off gain spectrum for 1210 nm pump lasers.

12 nm wide window, from 1275 nm to 1287 nm. Also, despite offering a simple single-pump approach, the module provided amplification with a 3 dB gain variation in a 20 nm wavelength window, from 1269 nm to 1289 nm. It could be observed that the pumps used were not optimal for the XG-PON upstream band as the gain dropped to 14.2 dB at 1270 nm and 10 dB at 1260 nm. However, it is possible to design the pump wavelength to be at 1200 nm which would centre the Raman gain peak in the middle of the upstream band and provide amplification in the entire region between 1260 nm and 1280 nm with a gain ripple within 3 dB.

Despite the fact that the pump wavelength of 1210 nm was well below the single mode cut-off wavelength for SMF of 1260 nm, the measured peak gain value of 16.6 dB is comparable with gain achieved in prior work [122] for similar pump powers at longer wavelength, and in line with the results of the previous Subsection 5.1.2, which suggests an efficient mode coupling. Also, simulation results showed that a negligible part of the pump power was coupled in secondary modes and that it still provided Raman amplification due to the high physical overlap of the modes in the fibre core [128].

Experimental setup

The experimental setup in Figure 5.9 was used to characterize the impact of the Raman amplifier on XG-PON 2.5 Gb/s NRZ upstream traffic. The data signal from the ONU was generated by an uncooled DFB DML

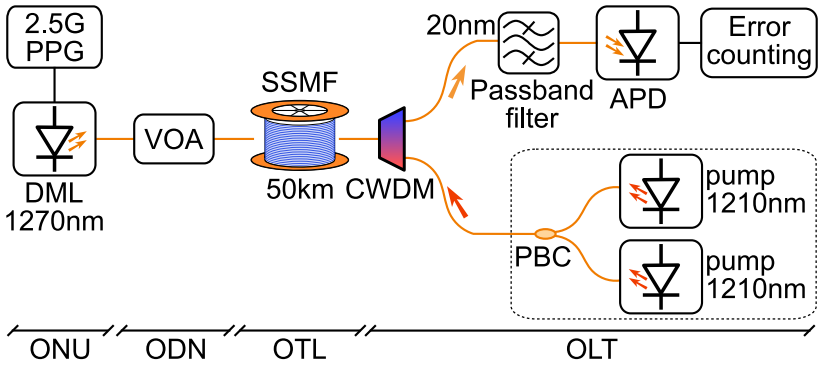


Figure 5.9: Experimental setup for Raman amplifier characterisation in an XG-PON system.

emitting at 1270 nm. The laser was packaged in a planar transmitter optical sub-assembly and directly modulated with a 2.5 Gb/s NRZ pattern formed of a PRBS of order 7 using a commercial electrical driver. The ODN, which in a real scenario would include splitters and distribution fibre, was emulated here with a VOA to adjust the launch power into the 50 km long trunk fibre. The Raman pumps were configured in a single module, as described above, and a CWDM filter was used to inject the pump signal into the OTL fibre and counter-propagate with respect to the data signal. A 20 nm wide optical bandpass filter centred at 1270 nm was placed in front of the OLT upstream receiver in order to suppress the out-of-band ASE while still allowing the entire XG-PON upstream band to reach the receiver. The upstream signal was detected with a commercially available transceiver equipped with an APD and limiting TIA and an error detector (ED) was used to measure the BER in real-time. The XG-PON downstream, located in the L-band window between 1575 nm and 1580 nm, well beyond the Raman gain bandwidth, was not implemented since it was expected to have negligible impact on upstream Raman amplification.

Experimental results and discussion

The impact of the reach extender module was evaluated in terms of power budget extension offered to the upstream system, which experimentally translated to the maximum attenuation supported in the ODN before launching the signal into the OTL fibre. The OTL had a total loss of 22.6 dB, which was fixed for all the measurements due to the combination of the 50 km SMF attenuation and the CWDM and band-pass filter insertion losses. The attenuation from the VOA was varied in the experiment to emulate the passive splitter and distribution fibre losses. Hence the total loss budget considered was the sum of ODN and OTL loss, with the latter fixed to a value of 22.6 dB. In the power budget analysis, the worst-case of an XG-PON transmitter with a launch power of +2 dBm was considered [17]. Under this condition, for example, an input power of −19.5 dBm into the OTL fibre would correspond to an ODN loss of 21.5 dB, that could account for a 1:64 split loss [130].

The APD receiver sensitivity measured after 50 km of fibre without

the Raman pump module active was −36 dBm for a BER of 10^{-4}, which is the XG-PON BER reference level for the 2.5 Gb/s NRZ upstream [17]. For an OSNR limited transmission, the minimum required OSNR for the same 10^{-4} BER was measured to be 8.2 dB. In order to determine the maximum loss budget that could be supported, BER curves were measured as a function of OTL fibre input power for the fixed 50 km loss of 22.6 dB. Measurements were repeated for different pump powers and are shown in Figure 5.10. For increasing Raman pump power the optical power needed at the OTL interface decreased, which means the available system power budget increased. This was due to the higher optical gain experienced by the probe signal and means that, even at its maximum gain, the amplifier was not operating in a saturation regime and not introducing distortions in the signal. Hence, the amplifier module could be operated at its maximum pump power of 28.8 dBm (759 mW) which provided a gain of 14.2 dB for the 1270 nm upstream signal. In this regime, an OTL input power of −22.1 dBm was achieved for a pre-FEC BER of 10^{-4} for XG-PON [17], which corresponded to a maximum ODN loss budget of 24.1 dB. This translates into a total system loss budget of 46.7 dB when considering an ONU launch power of +2 dBm and the OTL loss of 22.6 dBm. The 46.7 dB total power budget allows for a fully

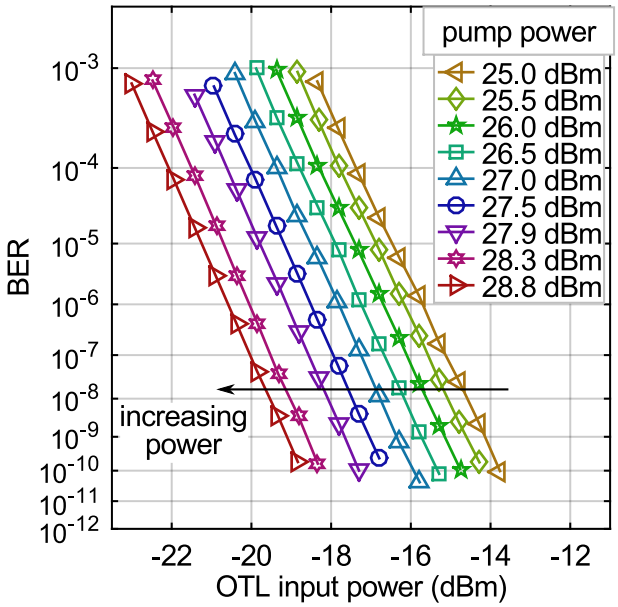


Figure 5.10: BER curves as a function of the OTL input power for different Raman pump powers.

passive network configuration with a 50 km SMF trunk fibre and a split ratio of up to 1:64. At this operating point the received optical power at the APD receiver for a BER of 10^{-4} was -31 dBm which was 5 dB above the measured sensitivity in B2B. The OSNR in this condition, measured with an OSA at 0.1 nm noise resolution, was 15.9 dB, which was 7.7 dB better than the OSNR required for a 10^{-4} BER.

In order to investigate the cause of this penalty the ODN loss was varied to assess its impact on the Raman amplified link. For different values of OTL input power the OSNR, Raman gain and BER curves were measured. Figure 5.11 reports the measured OSNR and Raman gain when varying the OTL interface input power. The corresponding ODN loss is also shown on the upper axis of the graph and was calculated considering a +2 dBm ONU transmitter. The gain had a stable value of 14.2 dB for the entire range of input powers, confirming that the amplifier did not reach the saturation regime, even for the higher input powers of the probe signal into the OTL fibre. The OSNR increased proportionally to the input power, which is expected since the ASE noise from the amplifier is constant when the pump power is not changed. For all the ODN losses investigated, the OSNR was above the minimum required for a 10^{-4} BER for the 2.5 Gb/s NRZ transmission. This indicates that the amplification scheme is robust to variations in ODN losses since no satu-

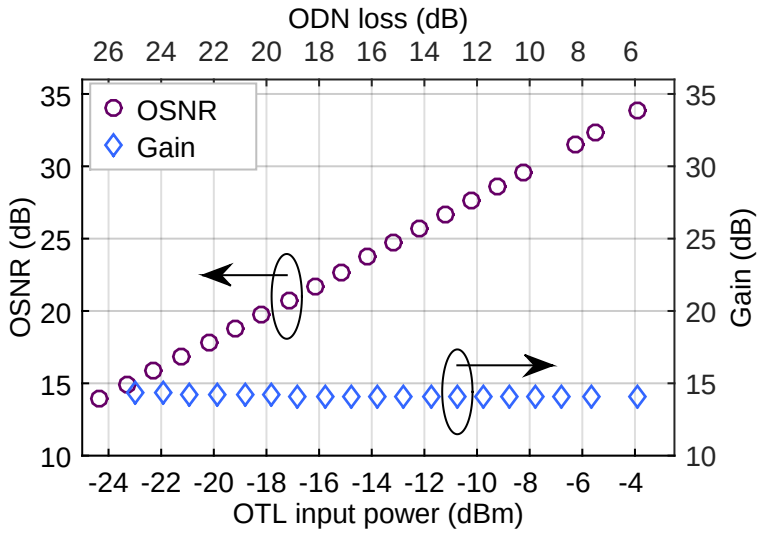


Figure 5.11: Raman on-off gain and signal OSNR for different attenuation of the ODN.

ration was observed for high OTL input power and, hence, it can handle a high DR in the upstream signal without degrading its performance.

Figure 5.12 shows the BER curves measured as a function of the APD received optical power for various input powers at the OTL interface. The sensitivity at a BER of 10^{-4} as a function of the latter is reported in Figure 5.13. For high input powers into the 50 km OTL the sensitivity was measured to be −36 dBm, as for the case with no Raman

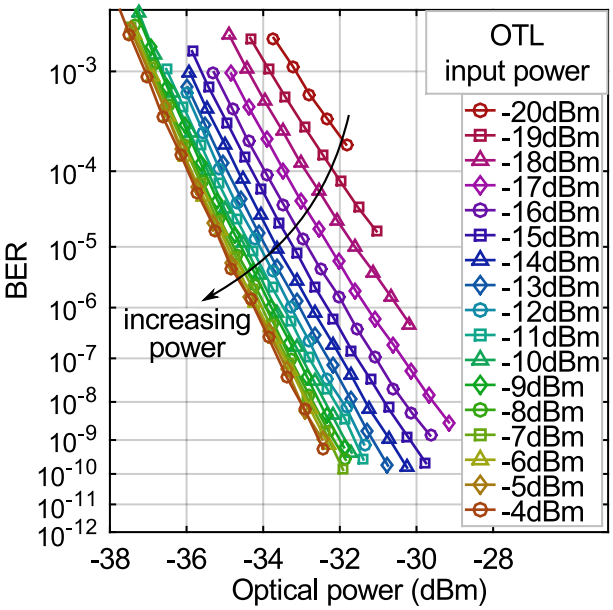


Figure 5.12: BER curves for different input powers into the OTL fibre.

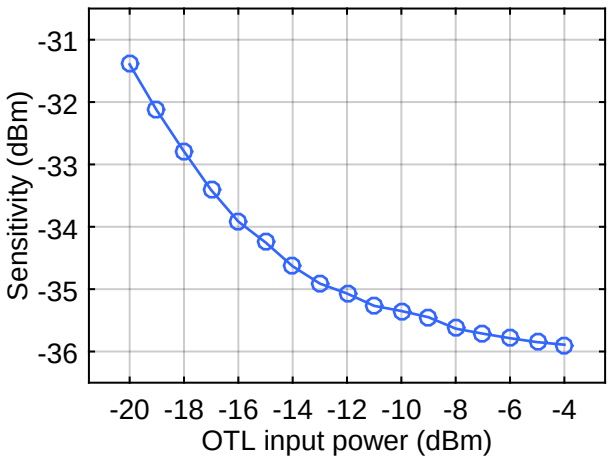


Figure 5.13: Sensitivity at the OLT receiver measured at a BER of 10^{-4} for different input powers into the OTL fibre.

amplification, while a penalty arose when the input power was lowered. The OSNR was, however, above the minimum value required (Figure 5.11) and so the dominant contribution to the performance degradation was attributed to the significant ASE-ASE beat noise. This was caused by the 20 nm width of the bandpass filter employed in front of the APD receiver that allowed out-of-band ASE noise into the photodiode. This broad bandpass region was responsible for the ASE-ASE beating but was necessary at the OLT to allow signal reception for the entire XG-PON upstream wavelength range. Narrow filtering could be used to enhance the system performance by avoiding the ASE-ASE beat noise but that would require a different network design, with more stringent emission wavelength of the upstream devices [128].

Despite this source of penalty, the first quantum dot based Raman amplified XG-PON upstream was demonstrated using 1210 nm pump lasers which allowed optical amplification in the 1270 nm upstream window. The Raman on-off gain of 14.2 dB enabled a total loss budget of 46.7 dB allowing for a total fibre length of 50 km and a split ratio of 1:64 in a fully passive network configuration. Along with the demonstrated Raman gain peak of 16.6 dB in the XG-PON upstream band these were successful outputs of the FP7 Quaternian project and highlighted the potential of Raman pumps for reach extension in PONs [84].

The above measurements were performed in continuous mode but burst-mode operation of the system was also demonstrated by building a setup where two DMLs were driven by burst-mode drivers and combined in a TDMA upstream signal. Under a DR of up to 14 dB, the Raman amplifier was demonstrated not to cause degradation in performance, matching the results obtained for a continuous transmission [88, 131]. Figure 5.14 shows that the sensitivity penalty measured for decreasing input powers into the OTL fibre does not depend on whether the transmission is performed in continuous or burst-mode. This is due to the very fast response times of the Raman scattering which prevents transients in the signal envelope. Also, the high saturation threshold of the amplifier is responsible for the linear gain of the amplifier across a high DR [88,115]. Raman amplifiers exhibit gain transients when they are in a saturated regime but, in the application demonstrated here, the amplifier showed a constant gain across the entire range of power, indicating that

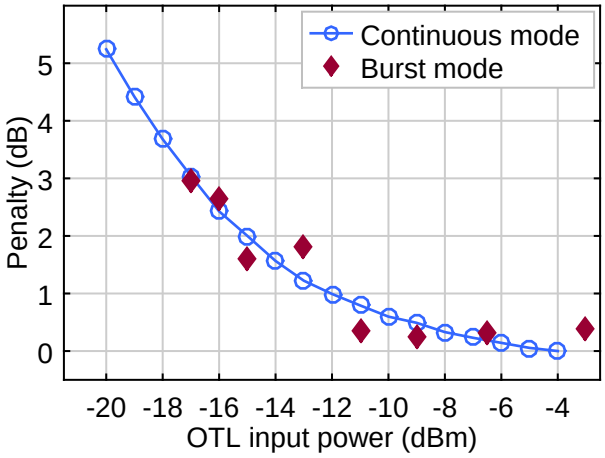


Figure 5.14: Penalty at the OLT receiver for different input powers into the OTL fibre for a continuous mode and burst-mode transmission.

pump depletion was negligible, even for the higher input power from the ODN and the amplifier did not saturate [132–135]. The burst-mode compatibility of this Raman amplifier shows its advantage over techniques based on SOAs with a fast feedback control loop for the bias [136, 137]. The Raman amplifier offers greater implementation simplicity because no dedicated high-speed electronic control boards are required to control the pump lasers and their bias current would only need adjustment in case it is desired to reconfigure the system to modify the Raman gain. However, a critical point to determine whether Raman amplification could be implemented in commercial systems is the cost of the pump modules, that limits its attractiveness. Also, special measures need to be put in place in order to operate the very high-power amplifier cards.

5.1.4 100G-PON reach extender

The upcoming 100 G PON systems that will be enabled by wavelength multiplexing 25 Gb/s single lane data-rate channels is likely to adopt optical amplification to support the required power budget due to the lower sensitivities of higher bit-rate signals [78]. A solution that does not require introduction of active reach extenders in the network plant is represented by optically pre-amplified receivers. As seen in Subsections 5.1.2 and 5.1.3 Raman amplification can operate in burst-mode with a simple amplifier module architecture without high-speed control circuitry [88].

Also, Raman amplifiers work in their linear regime over a wide range of input powers and so can be employed with multi-level modulation formats. The IEEE P802.3 standard proposes to place the upstream wavelength window in the O-band to reduce the effect of chromatic dispersion, albeit the wavelength plan is still under investigation [78]. In this scenario, the pump lasers suitable for the G-PON or XG-PON upstream could be employed and the Raman broad gain spectrum would advantageously provide gain for multiple channels.

In this Subsection, a Raman module using the high power QD pump lasers at 1240 nm is proposed to provide optical amplification to a 1310 nm 25 Gb/s signal using either PAM4 or EDB modulation [51]. A counter-propagating configuration is adopted with the advantage of having all the active devices located in the OLT and hence preserve the passive nature of the network.

Experimental setup

The experimental setup in Figure 5.15 was used to characterise the performance of Raman amplification for 25 Gb/s upstream transmission. The ONU was emulated using a commercial 10 G DFB DML operating at 1311 nm with an average output power of +8 dBm. The device had a 3 dB small-signal modulation bandwidth of 16 GHz. The electrical drive signal for the DML was created using two 12.5 Gb/s NRZ pattern generators and a 2-bit DAC with multiplexer which could be configured to generate either a 12.5 GBd (25 Gb/s) PAM4 or a 25 Gb/s NRZ electrical

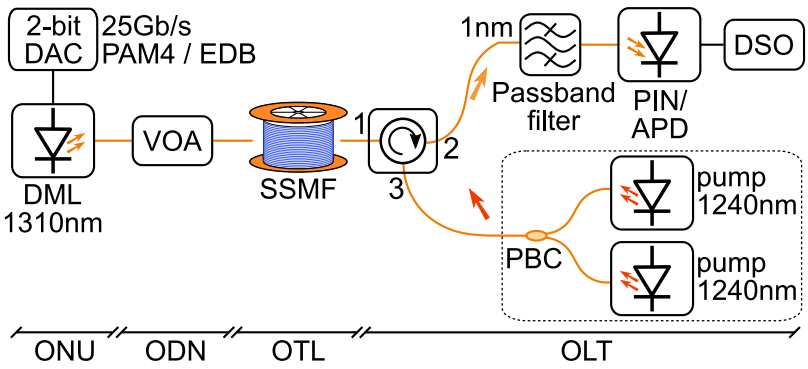


Figure 5.15: Experimental setup for Raman amplifier characterisation in a PON system.

signal. The pattern used in both cases was a PRBS sequence of order 15. For the 12.5 GBd PAM4 signal, Gray-coding of the constellation symbols was used to minimise the BER at the receiver. The ODN was emulated by a VOA placed between the ONU and the OTL fibre. The ODN loss was calculated as the difference in power between the DML output of +8 dBm and the launched power into the fibre at the ONU and OTL interface. Trunk fibre lengths of 6 km, 10 km, 20 km, 30 km and 40 km were used in the experiment to investigate the capabilities of Raman amplification for different PON reach and split ratios. At the OLT side an optical circulator with a 0.8 dB insertion loss was used at the fibre interface to inject the Raman pump signal into the transmission fibre and redirect the upstream signal to the receiver. The Raman module was formed by combining the output of two 1240 nm high power lasers, the same used in Subsection 5.1.2, with a PBC to maximise the output power. The lasers were equipped with a FBG in their fibre pigtail to narrow the spectrum to a 1 nm width around the central wavelength of 1240 nm. A 1 nm wide optical bandpass filter was placed in front of the OLT receiver to suppress the out of band ASE noise generated by the amplifier. Two different 10 G class receivers were employed, being either a 7 GHz APD or a 10 GHz PIN photodiode, both equipped with a co-packaged linear TIA. The detected signal was sampled by a 12.5 GHz, 50 GS/s DSO and analysed off-line using a numerical computing environment to provide BER values and FFE filtering, where employed. For the EDB system the optical signal generated by the DML was a bandwidth-limited 25 Gb/s NRZ waveform because of the 16 GHz bandwidth of the transmitter. The use of 10 G receivers performed additional low-pass filtering so that the signal could be detected as a 3-level EDB encoded signal. The system therefore resembled the NRZ-EDB discussed in Section 3.2. For the PAM4 implementation, post-equalisation was also considered at the receiver using a T/2 spaced 10-tap FFE equaliser to compensate for the bandwidth limitation imposed by the 10 G devices, especially for the 7 GHz APD. All measurements were performed here in continuous mode but, as discussed above, burst-mode operation of the system is expected to have negligible impact on the Raman gain and signal BER, even with a high degree of DR [88].

Experimental results and discussion

The Raman pumps used at the OLT had a lasing wavelength of 1240 nm providing a peak-gain close to the DML output wavelength of 1311 nm. The same pumps were used in Subsection 5.1.2 and their gain profile was shown in Figure 5.5. The maximum launch power of the pump signal into the OTL after the optical circulator was +27.6 dBm with both pump lasers biased at 1700 mA. With this power the distributed Raman on-off gain and probe signal OSNR were measured for various fibre lengths (Figure 5.16). The measurements were repeated, varying the input power of the probe signal into the OTL across a wide rage of values to emulate different losses of the ODN. The on-off gain was constant across the range of ODN losses showing a decrease in magnitude for input powers higher than −2 dBm. Similar behaviour was observed for all the fibre lengths analysed and indicates that the amplifier was partially saturated in this high input power regime. Due to the counter-propagating configuration the saturation effect was more evident in shorter fibre. However, the gain drop was less than 1 dB for a maximum input power of +4.6 dBm, meaning that the degree of saturation was low. Also, in a PON system, typically the input power from a ONU into the OTL fibre is below −5 dBm and so the amplifier would not operate in saturation in the intended application. The OSNR increased proportionally to the input

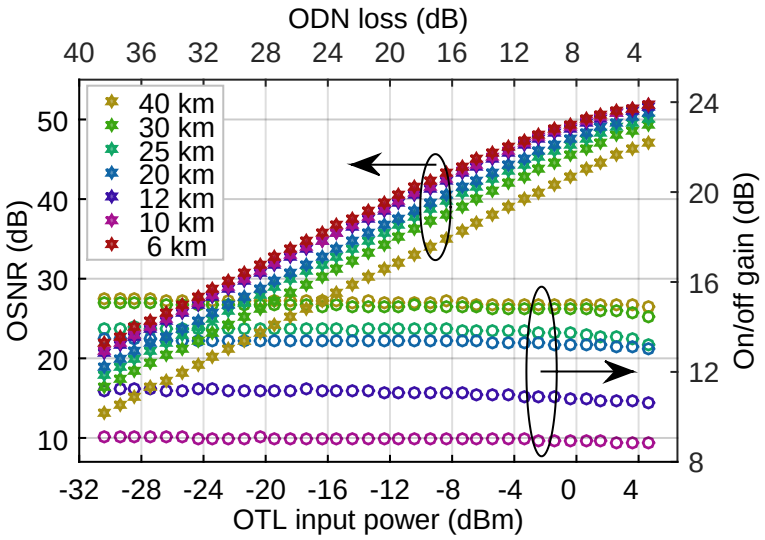


Figure 5.16: Measured OSNR and Raman on-off gain for different fibre lengths.

power, as expected, because of the constant power of the ASE noise generated by the amplifier. Also, the OSNR showed a decrease in the curve slope for high OTL input powers, which was due partially to saturation but also to the limited OSNR of the ONU signal for OSNR values in excess of 50 dB.

The on-off gain obtained for different fibre lengths are shown in Figure 5.17 for an OTL input power of −6 dBm. An on-off gain of 13.3 dB was measured for the 20 km long trunk fibre, which rose to a maximum gain of 15.0 dB with an extended OTL of 40 km. While the gain was significantly lower for a 10 km fibre, measuring 9 dB, using 20 km of SMF for the OTL the gain was within 1.7 dB of its maximum value, obtained along the 40 km span. Most of the gain occurs within the first portion of fibre because the pump signal is weakened by absorption and depletion during propagation and a small portion is left available after the initial 20 km. This shows how the distributed nature of Raman amplification makes it attractive for use over optical access length scales. To offer an interpretation more oriented to the system implementation, the net gain offered by the amplifier was also calculated. This was done by subtracting the measured fibre loss experienced by the probe signal during transmission and is shown in Figure 5.18. The fibre loss coefficient measured at the signal wavelength of 1311 nm was 0.35 dB/km. The optimum length, in terms of maximum net-gain achieved, was 12 km for which the net-gain was 6.9 dB. This means a higher ODN loss is

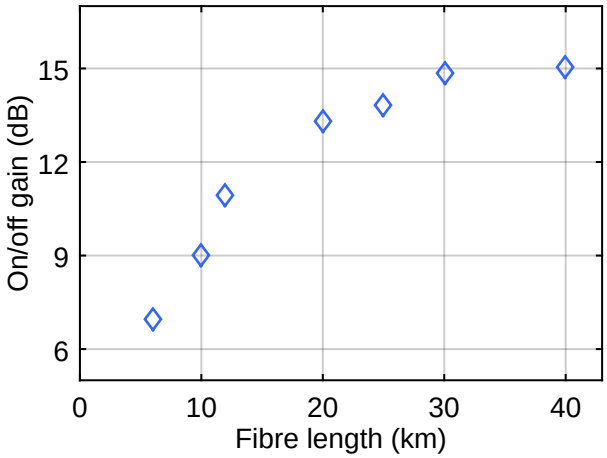


Figure 5.17: Raman on-off gain for various lengths of the OTL fibre.

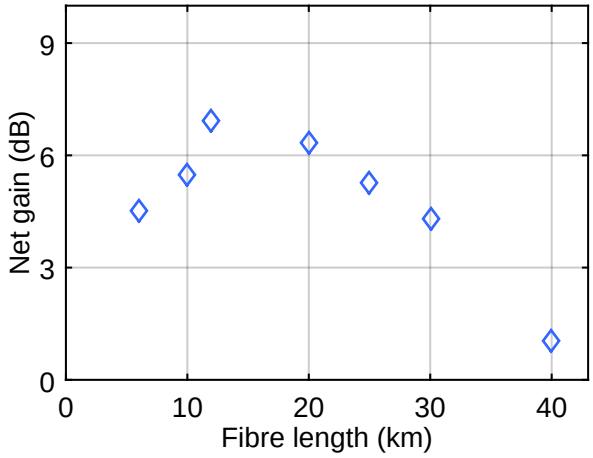


Figure 5.18: Net signal gain along the OTL fibre for various SMF lengths.

supported for such a length but at the cost of a reduced OTL length. This trend will be reflected in the network system performance shown in the remainder of this Subsection.

After the gain characterisation, BER curves were measured for both the PAM4 and EDB ONU transmitter in optical B2B and after 40 km of fibre. Using the 40 km fibre, the Raman amplifier was switched on to evaluate eventual sources of penalty. Figure 5.19 shows the BER of

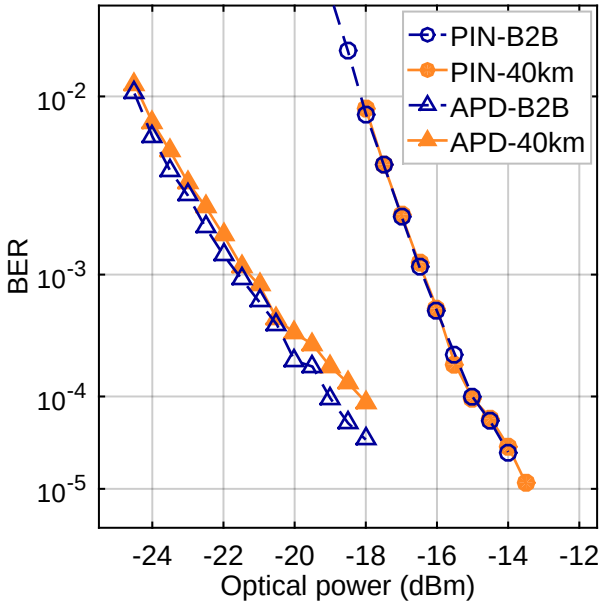


Figure 5.19: BER curves for the 25 Gb/s EDB system for various receivers.

the 25 Gb/s EDB system as a function of the received power in optical B2B and after transmission through a 40 km SMF. Raman amplification was used for the 40 km scenario and measurements were acquired for both the PIN and APD receiver. No difference was observed for the PIN receiver curves while a negligible penalty was measured using the APD. The received power sensitivities at a pre-FEC threshold BER of 10^{-3} was -16.4 dBm using the PIN and improved to -21.5 dBm with the APD. The results confirmed that the limited amount of CD accumulated in the fibre and the Raman amplifier are not affecting the signal quality.

Similar measurements were repeated for the PAM4 system and are shown in Figure 5.20. In this case, the PIN receiver was also combined with a 10-taps FSE T/2 FFE filter to improve its sensitivity compared to a simple comparator. The APD was also used with the same 10-taps FSE to compensate for its reduced bandwidth of 7 GHz. Similar to the EDB case, no difference was observed between B2B and 40 km with distributed Raman gain for a PIN receiver while a difference of less than 0.5 dB was measured with the APD module. Receiver sensitivities of -15 dBm and -16.5 dBm were measured for the PIN without and with the FSE filter, respectively. The minimum received power decreased to -22.4 dBm with the APD in B2B and -21.9 dBm after 40 km of SMF. The sensitivity of

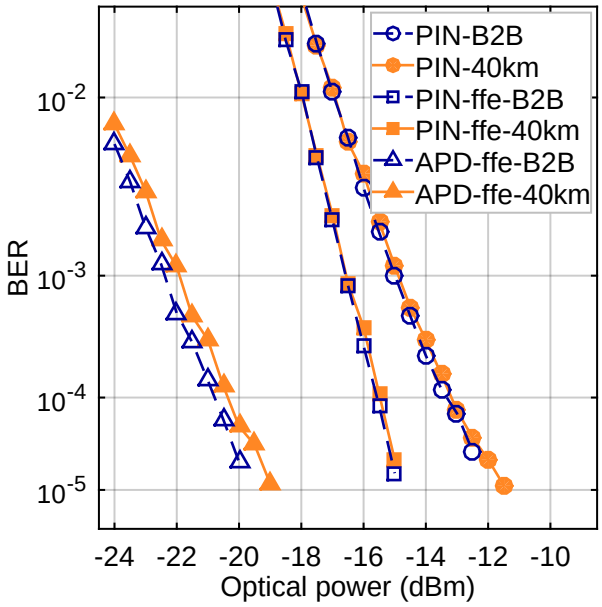


Figure 5.20: BER curves for the 25 Gb/s PAM4 system for various receivers.

the PAM4 was 1.4 dB worse than the EDB for the same PIN receiver but could be improved to similar values with the T/2 FFE. A similar 1.5 dB difference was observed in Section 3.2 between NRZ-EDB and PAM4 and is here confirmed after a 40 km Raman amplified link. Despite the higher bandwidth of the transmitter used in the experiment in Section 3.2 their NRZ-EDB performances were similar.

The system BER was then evaluated as a function of the input optical power into the OTL fibre for a fixed trunk loss. This included the SMF attenuation of 0.35 dB/km at 1311 nm and an additional insertion loss of 3 dB due to the circulator and band-pass filter used at the OLT. The OTL losses had values for example of 17 dB and 10 dB for the 40 km and 20 km fibre case, respectively. Different optical power into the OTL corresponded to a different ODN loss budget which was extrapolated considering the +8 dBm launch power of the ONU DML. These values were obtained by changing the attenuation of the VOA placed after the DML that determined the input power at the OTL interface. The BER curves obtained for different OTL lengths are shown in Figure 5.21 for both the PIN and APD receiver. Because the receiver sensitivity was not affected by the fibre length the trend reflected the net gain offered by the distributed amplifier for different SMF lengths (Figure 5.18). To offer a clearer picture, Figure 5.22 shows the maximum ODN loss sup-

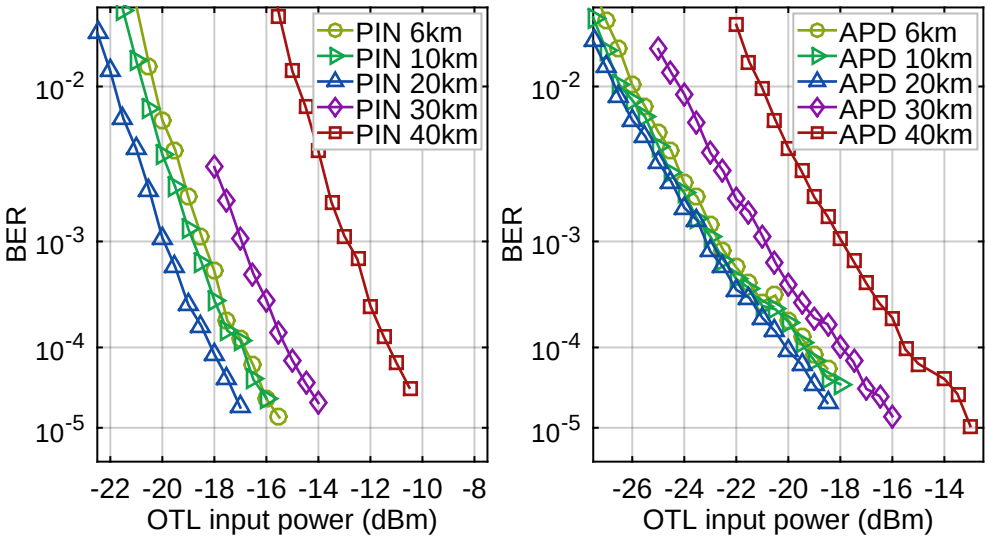


Figure 5.21: BER curves for the 25 Gb/s EDB system for various fibre lengths and two receivers type.

ported by the two receivers as a function of the OTL length, which recalls the pattern seen in Figure 5.18. The ODN loss budget, which does not include the loss of the trunk fibre, followed the same trend as the net gain shown earlier. The advantage offered by Raman gain was dominant for shorter fibre lengths and the increase of on-off gain allowed for higher ODN loss for increasing SMF lengths up to 20 km. Beyond this reach, the fibre attenuation played a more important role and the ODN power budget supported decreased because of the higher OTL loss. The maximum ODN power budget supported among the SMF spans tested was obtained for 20 km and was equal to 27.9 dB and 31.2 dB, respectively, for a PIN and APD receiver. For an extended reach of 40 km the achieved ODN losses dropped to 20.9 dB and 26.0 dB, respectively, due to the reduction in net gain, as observed in Figure 5.18. The ODN supported losses measured using the APD receiver could accommodate a total split ratio of 1:512 for the 20 km trunk fibre, which reduced to a 1:128 ratio for the 40 km extended reach, according to the splitter insertion-loss values specified in [130]. In the 40 km reach-extended case, accounting for a fixed OTL loss of 17 dB, the PIN receiver could support a 37.9 dB link budget, which became 43 dB with adoption of an APD for an EDB 25 Gb/s transmission. For the shorter 20 km trunk line, with a 10 dB OTL loss, the achieved link budgets were 37.9 dB and 41.2 dB, respectively, for a PIN and APD receiver.

Similar measurements were also conducted for the PAM4 system for

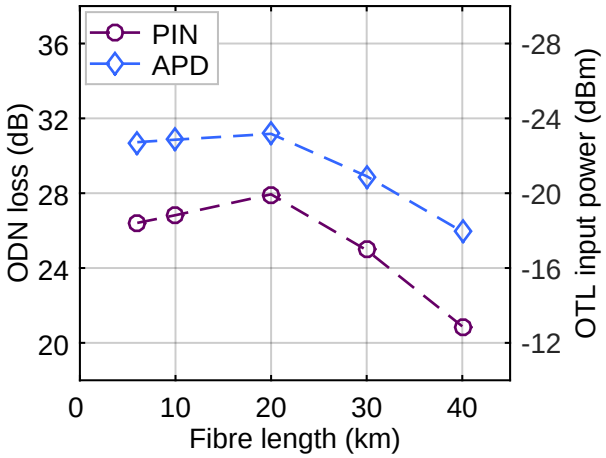


Figure 5.22: Supported ODN loss at a BER sensitivity of 10^{-3} for the 25 Gb/s EDB system.

the three receiver configurations showed earlier, a PIN without and with FFE and an APD supported by FFE. The three sets of BER curves measured by varying the input power into the trunk fibre are reported in Figure 5.23 for fibre lengths of 6 km, 10 km, 20 km, 30 km and 40 km. Also, the ODN supported loss for the combination of OTL lengths and OLT receivers is shown in Figure 5.24 for a BER of 10^{-3} in the upstream signal. Similar to the EDB system, the trend of the ODN power budget reflects the net gain experienced for different fibre lengths. The PIN receiver offered the best performance at a length of 20 km with a

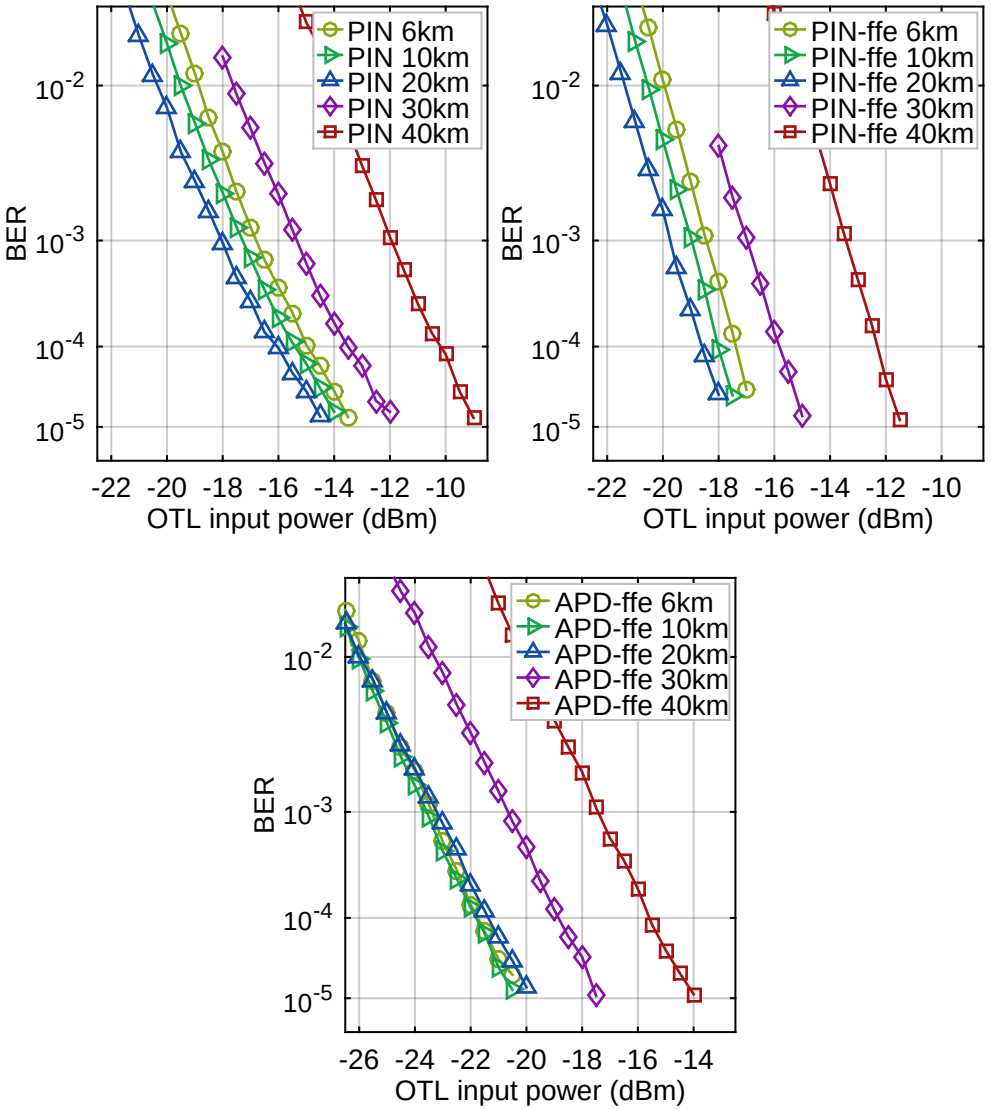


Figure 5.23: BER curves for the 25 Gb/s PAM4 system for various fibre lengths and three receivers type.

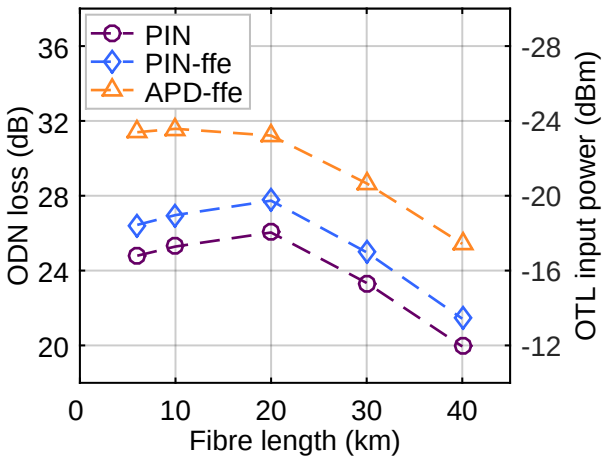


Figure 5.24: Supported ODN loss at a BER sensitivity of 10^{-3} for the 25 Gb/s PAM4 system.

supported ODN attenuation of 26 dB and 27.7 dB without and with FFE respectively. This decreased to 20 dB and 21.4 dB for a 40 km trunk line. The APD receiver was more affected by OSNR drop and accumulated CD for longer fibres and offered the highest ODN power budget of 31.6 dB for a 10 km SMF length. For the same APD, the supported ODN losses for a 10^{-3} BER were 31.2 dB and 25.4 dB with an OTL of 20 km and 40 km, respectively. The ODN power budget values obtained for the 25 Gb/s PAM4 signal with an APD receiver supported by FFE were close to the one seen for an EDB system and, similarly, could accommodate a split ratio of 1:512 and 1:128 with a 20 km and 40 km trunk line, respectively. Also, for the PAM4 system, the total power budget can be extrapolated taking into account the fixed attenuation of the OTL fibre and passive devices and the DML output power of +8 dBm. For the 40 km reach-extended case, the PIN receiver supported a 37 dB or 38.4 dB total link loss without or with FFE post-compensation, respectively, and, with the APD receiver, the total loss budget increased to 42.4 dB.

For the entire range of BER measurements, in the worst case, the OSNR was as high as 26 dB, indicating that the dominant noise source was the thermal noise from the receivers. Also, the narrow optical filtering in front of the photodiodes at the OLT receiver ensured that ASE-ASE beat-noise was not a dominant source of impairment. This was confirmed by the good agreement of the BER curves in optical B2B and the ones after the 40 km amplified link (Figures 5.19, 5.20). All the com-

ponents used in the transceiver implementation were devices designed for 10 Gb/s transmission systems, highlighting the benefit of using spectrally efficient multi-level modulation formats for the target 25 Gb/s single line bit-rate.

With the maximum achievable pump power of +27.6 dBm, the 25 Gb/s EDB system with an APD receiver could support a 20 km OTL with a 31.2 dB ODN loss, enough to accommodate for a split ratio of 1:512. For the extended fibre reach of 40 km, the ODN loss decreased to 26 dB, which is sufficient for the insertion loss of a 1:128 optical splitter. If PAM4 is used instead, the supported ODN losses were 31.2 dB and 25.4 dB for 20 km and 40 km, respectively, sufficient to support the same split ratios seen for EDB. Highest split ratios are possible with a fibre length of 20 km but Raman amplification is also very effective in enabling extended reach links without having to drastically reduce the number of ONUs. Comparing the various 25 Gb/s modulation formats, EDB offers the best performance both in terms of sensitivity, which is the highest, and simplicity, in which it does not require post-equalisation at the receiver, contrary to PAM4.

5.2 Burst-mode gain controlled SOAs

The previous Section discussed the potential of Raman-based optical amplifiers for burst-mode compatible amplification of PON upstream traffic and presented experimental demonstrations applicable to various PON standards. Raman amplifiers are attractive because they do not require complex control circuitry to work in a burst-mode scenario and can operate in wavelength windows inaccessible to other amplification technologies. Raman amplifiers do, however, require high-power lasers and offer an inherently low-efficiency amplification process. In this Section, SOAs are investigated as an alternative for adoption in burst-mode networks. SOAs require lower driving currents, have lower temperature management requirements than Raman pump lasers and could be integrated monolithically with other optoelectronic devices. The SOAs are proposed in a pre-amplified receiver architecture which provides both a sensitivity improvement and optical power equalisation of bursts. Variable gain operation of the SOA on a burst-by-burst time scale is used to obtain a

constant output power stream in front of the electrical receiver, thereby removing the need for an electronic BM-Rx. Such implementation offers improvement in term of maximum DR supported and also proves advantageous when higher order modulation formats, which require a linear channel, are used.

5.2.1 Semiconductor optical amplifiers

Semiconductor optical amplifiers (SOAs) are optical amplifiers realised with a semiconductor material as the active medium providing gain. SOAs are based on the same principles as laser diodes in which they exploit the stimulated emission effect of specific materials to produce photons from an electrically pumped semiconductor material [138]. The simplest implementation of an SOA is based on a semiconductor pn junction which creates a two energy level system with a ground state level, called the valence band, and an excited state level, named the conduction band. If a light beam with photons at a suitable energy is incident on the material it can cause an electron-hole pair recombination in which an electron moves from the conduction band to the valence band and loses energy in the form of a photon. This photon, generated by stimulated emission, has identical frequency, phase and direction as the incident photon. In order to achieve optical amplification, a population inversion condition has to be created, where the concentration of electrons in the conduction band exceeds that in the valence band, thereby increasing the probability of an incident photon causing stimulated emission. This can be achieved by providing external electrical pumping to the pn junction in order to supply the conduction band with electrons. The simple

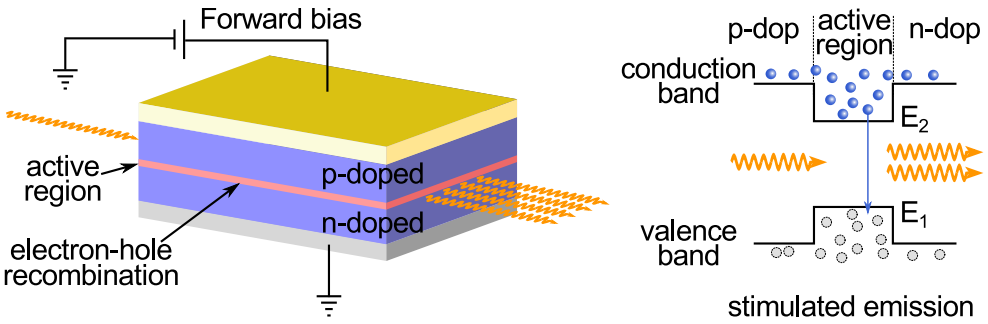


Figure 5.25: Schematic representation of semiconductor optical amplifier.

scheme of a SOA in Figure 5.25 shows the basic blocks. The pn junction of the bulk semiconductor material defines the active region where optical gain is taking place when a light beam is propagating through it and causing stimulated emission. The semiconductor material is engineered to create a waveguide structure across the active region to confine the beam and increase the efficiency. The amplification takes place on the travelling wave and so reflections are undesired and particular care is needed in fabricating anti-reflective coating of the facets. The external forward bias provides electrical pumping of the material to ensure the population inversion of the carriers across the pn junction and to provide electrons in the conduction band.

SOAs historically had lower performance than fibre-doped amplifiers exhibiting lower gain, higher NF, lower saturated output power and suffering from polarisation dependent gain and higher coupling losses at the fibre and semiconductor device interface. However, with the renewed interest, many of these aspects have been addressed and modern SOAs have significantly improved performance which, added to their small physical footprint, potential for monolithic integration with other optoelectronic components [139] and lower fabrication costs has rekindled interest in SOAs for applications in access networks [140]. Another advantage of SOAs is their fast carrier dynamics which makes them suitable for burst-mode traffic, unlike EDFAs which need electronic transient suppression circuitry.

SOAs have been demonstrated as a way to extend the power budget in PONs for both downstream and upstream traffic [141–143]. While they can be used as a booster for the downstream, the most interesting application for the upstream direction is to employ the SOAs as part of a pre-amplified receiver. In this way, a single amplifier is shared among multiple ONUs and no active components are needed in the ODN, preserving its passive nature. The fast carrier dynamics makes them suitable for burst-mode traffic, however the limited input saturation power of the device can limit its operational DR due to saturation of the loud-bursts [144]. Employing an SOA based pre-amplifier with fixed bias current provides sensitivity improvement but is limited in its DR capability [140, 143]. As an alternative, the SOA can be operated by varying its bias current, and hence gain, on a burst-by-burst time-scale to work in an optimal

condition for every power of an incoming burst. If the bias current is carefully chosen so that the output power of the SOA is kept constant across bursts, the amplifier can also perform optical power equalisation of the upstream signal eliminating the DR at its output [87, 145]. In this way, a burst-mode receiver can be realised combining a variable gain SOA with a PIN photodiode and a simple AC coupled TIA removing the need for an electronic BM-Rx. This is particularly advantageous when multi-level modulation formats are used because high-bandwidth linear BM-Rx are still not commercially available, while linear PIN receivers with bandwidth in excess of 40 GHz can be readily obtained.

In some implementations in the previous literature, SOAs have been used with fixed gain to reduce the signal DR inducing amplifier saturation [146–148], however a similar implementation is not suitable for multi-level modulation formats where linearity must be preserved during transmission. Other works have implemented SOA power equalisation with complex structures employing multiple amplification stages [136,137,147–150] or additional components. In this work, we propose the use of a single SOA to realise a simple and more cost-effective receiver for PONs that could potentially be monolithically integrated. The receiver implemented here was tested with 25 Gb/s EDB and PAM4 upstream signals to evaluate its performance in a linear burst-mode system.

Gain and OSNR characterisation

A C-band SOA was employed for the experimental realisation of the pre-amplified burst-mode receiver with optical power equalisation. Because the SOA was used in front of a PIN photodiode, high gain and low NF of the device were preferred over high saturation output power in order to enhance the receiver sensitivity. The device chosen for pre-amplification purposes was an SOA-S from CIP operating around 1.55 μm offering a wide optical bandwidth, low NF and low drive current with its maximum gain at a 100 mA bias current. The SOA was initially characterised in terms of optical gain and OSNR of the output signal under different conditions of bias current and optical input power into the amplifier. The experimental setup in Figure 5.26 was used for the characterisation of the SOA parameters. The simple setup controlled the optical input

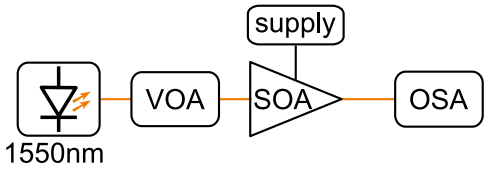


Figure 5.26: Experimental setup for optical B2B continuous mode SOA characterisation.

power of a 1550.1nm signal entering the SOA and the amplifier bias current. An OSA measured the optical power and OSNR of the SOA output for every operational regime and, consequentially, the gain was calculated from these values.

Figure 5.27 shows the output power of the probe signal from the SOA for given input power and bias conditions. A linear increase of the output power with the SOA input power can be observed for lower bias currents or when the device input power is below −10 dBm. On the other hand, for higher SOA input powers, the slope of the curves changes noticeably, indicating that the amplifier is in a saturation regime. Figure 5.28 shows the gain of the device extrapolated from the previous measurements for different operating conditions. It is evident that gain saturation is determined by both the SOA bias current and the optical power of its input. For the maximum bias of 120 mA, a gain drop of 3 dB was measured with an input power of −10 dBm. On the other hand, with

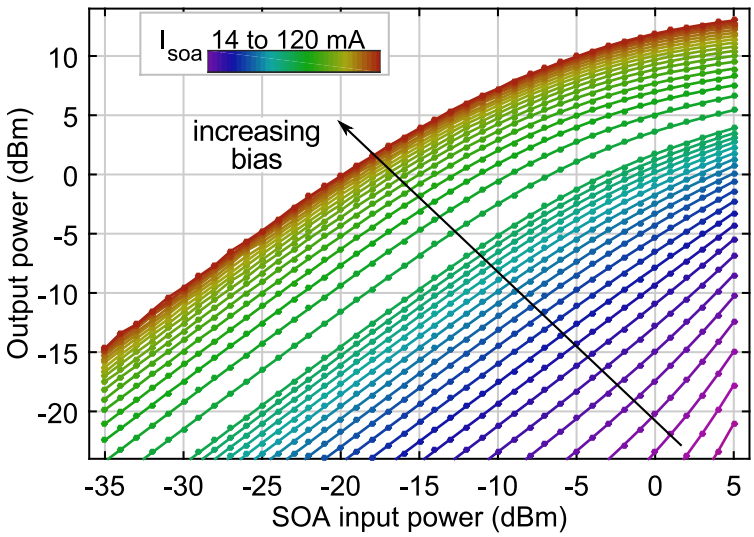


Figure 5.27: Output power of the SOA for varying input powers and bias currents.

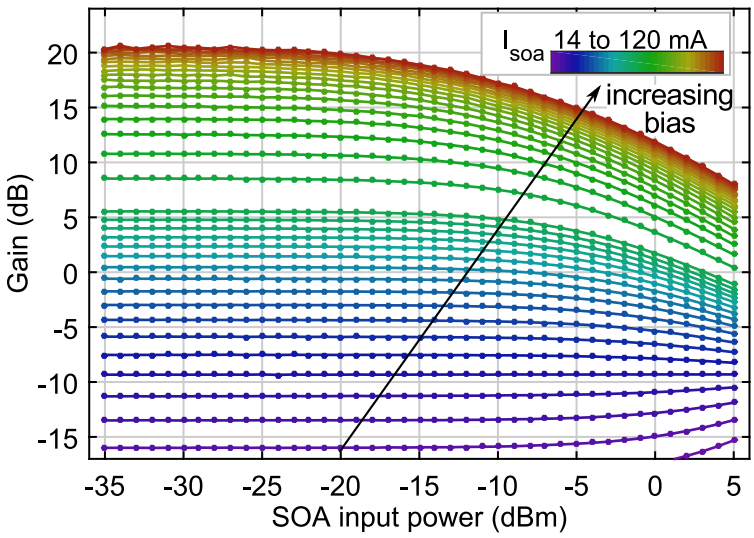


Figure 5.28: Gain of SOA as a function of its input power for different bias currents.

a bias current lower than 20 mA, the gain could be kept constant for input powers up to +5 dBm. For the lowest bias values the gain introduced by the SOA was negative and so the signal was attenuated at the output.

To evaluate the gain compression when varying the input power the saturation input power was also calculated. This metric corresponds to the input power value that causes a drop in the gain with respect to its maximum value, for a fixed bias current. It is reported in Figure 5.29

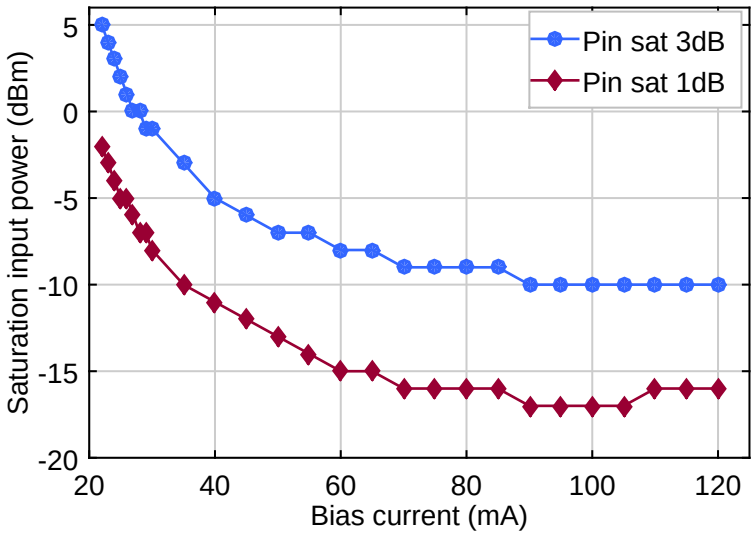


Figure 5.29: Saturation input power of SOA as a function of its bias current.

for a gain compression of 1 dB and 3 dB. To have minimum distortion of the signal, the bias should be chosen so that the optical power of the incoming burst is below the input saturation power. Looking at the graph it is evident how it is advantageous to change the SOA bias on a burst-by-burst scale to enlarge its optimum operation with a wide DR of the input upstream transmission. For bias currents below 22 mA, the gain did not show saturation across the entire range of input powers from −35 dBm to +5 dBm.

The OSNR of the output signal was also measured, with an OSA at a resolution of 0.1 nm (Figure 5.30). The OSNR increases proportionally to the input power for bias of 20 mA or higher, which indicates the amount of ASE generated by the amplifier was constant. For lower bias, when the population inversion condition is not ensured, the spontaneous emission contribution is higher and, when the gain is negative, the ASE is influenced by the signal input power, also affecting the OSNR trend. For the intended application in burst-mode, without a dedicated electronic burst-mode receiver, the SOA should provide identical output power for every incoming burst by adjusting its bias accordingly on a nanosecond scale. Figure 5.31 shows the conditions under which the output power is constant using an appropriate bias value for a certain signal input power. The output power is shown from −19 dBm to +12 dBm in steps

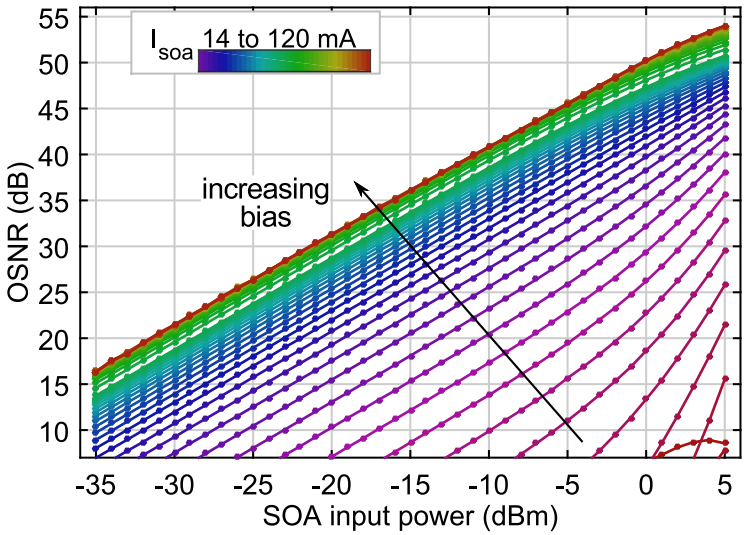


Figure 5.30: OSNR of SOA as a function of its input power for different bias currents.

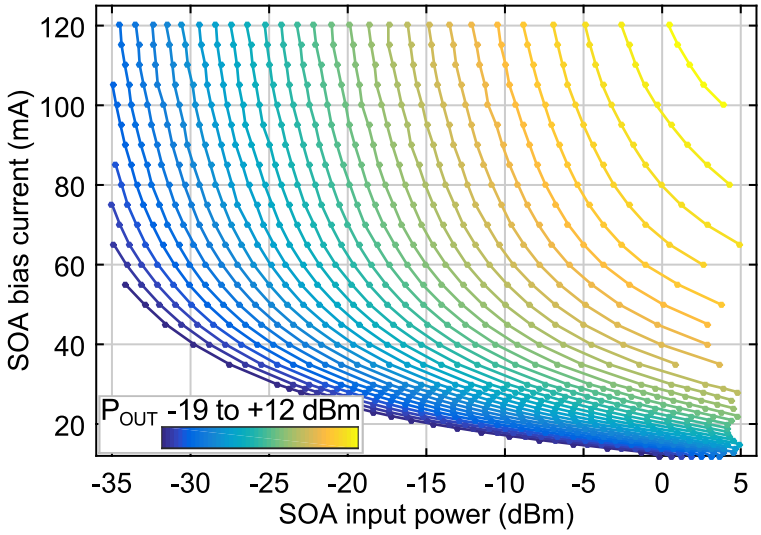


Figure 5.31: Operational conditions of the SOA to obtain a constant desired output power for a given input power.

of 1 dB. If the device is operated along one of these lines of constant output power it could be employed in front of a photoreceiver with AC coupled electrical interface to provide both optical pre-amplification and bursts power equalisation. Operating the SOA below its saturation input power for every optical burst and using a commercially available PIN with linear TIA a linear burst-mode receiver can be implemented without gain switching of the electrical RF amplifier.

5.2.2 SOA and multilevel modulation formats

The effect of OSNR degradation and SOA saturation on the signal quality was evaluated for 25 Gb/s multilevel modulation formats, PAM4 and EDB, by measuring their sensitivity at the PIN receiver under different operating conditions. For EDB modulation, the transmitter was used both in a bandwidth limited configuration and in a full bandwidth one to implement either an EDB transmitter or an NRZ transmitter with EDB detection, as explained in Section 3.2. Both were investigated to asses whether sending a two or a three level optical signal into the SOA could cause significant difference in the impairments suffered.

The setup in Figure 5.32 was used for the measurements. A DFB laser was tuned to 1550.1 nm and its signal was modulated by an EAM with a 3 dB bandwidth of 21 GHz. The modulator was driven by a

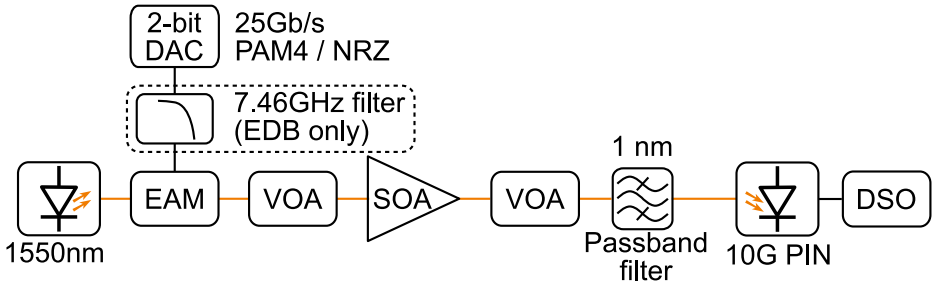


Figure 5.32: Experimental setup for optical B2B continuous mode SOA characterisation.

DAC generating a 25 Gb/s signal either NRZ or PAM4. To emulate a bandwidth limited EDB transmitter, a 7.46 GHz electrical Bessel low-pass filter was used in front of the EAM. The power of this modulated signal entering the SOA was controlled with a VOA and the SOA bias was changed from 14 mA to a maximum of 120 mA. A second VOA was placed after the amplifier to control the signal reaching the photodiode and a 1 nm optical bandpass filter was used to suppress the out-of-band ASE noise. The receiver was a 10 GHz PIN photodiode co-packaged with a linear TIA and its output was captured by a 50 GS/s DSO for off-line waveform synchronisation and error counting.

Figures 5.33 and 5.34 show the sensitivity measured at a BER of 10^{-3} for a combination of SOA input powers and bias currents for the

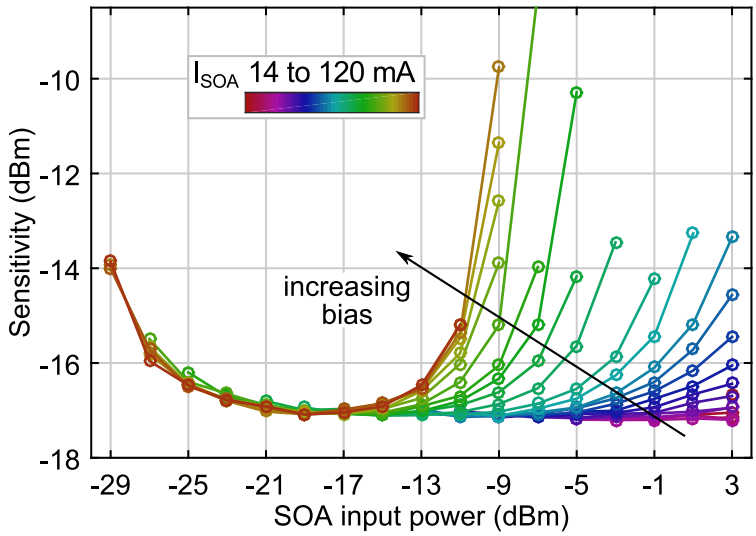


Figure 5.33: Sensitivities for the SOA output under various operating conditions for an NRZ system with EDB detection.

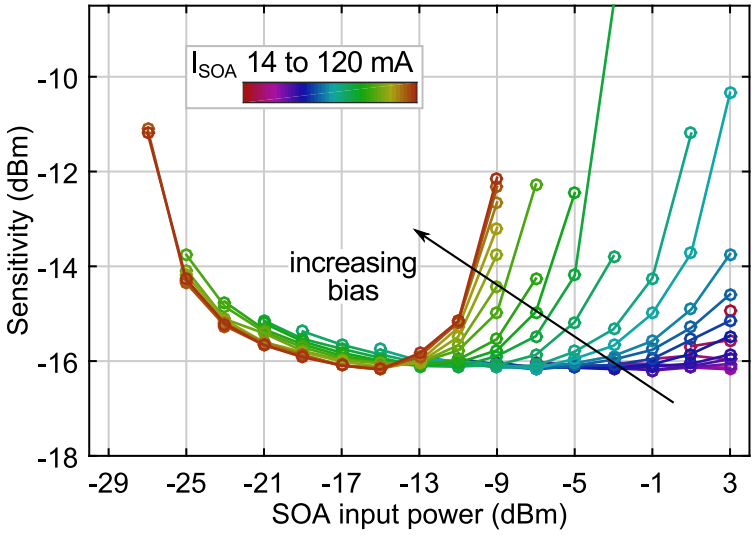


Figure 5.34: Sensitivities for the SOA output under various operating conditions for an EDB system.

two EDB systems, the NRZ with EDB detection and the EDB transmitter respectively. Two effects are visible from the graphs, the OSNR degradation when the SOA input power is lowered and gain saturation when the SOA input powers are above a certain value. For lower input powers high gain settings of the SOA ensured the best OSNR conditions and hence the best sensitivities, while low bias currents needed to be used for high optical powers entering the SOA. The NRZ system with EDB detection showed a best case sensitivity of -17.2 dBm, better than the -16.2 dBm of the EDB transmitter, confirming the results of Section 3.2. The NRZ transmitter also had better performance in the OSNR limited condition because of the lower SNR requirements. The NRZ transmitter with EDB detection had a < 0.5 dB penalty region between -23 dBm and $+3$ dBm of SOA input power which was, instead, reduced to the range -21 dBm to $+3$ dBm for the EDB system. The latter also showed higher dependence of the sensitivity on the bias current in the OSNR limited regime.

The same set of measurements were performed for a PAM4 transmission system and are shown in Figure 5.35. Similar trends are visible at both ends of the SOA input power ranges measured but PAM4 showed a narrower optimum operation region due to the lower tolerance to both OSNR degradation and gain saturation distortion. The best sensitivity

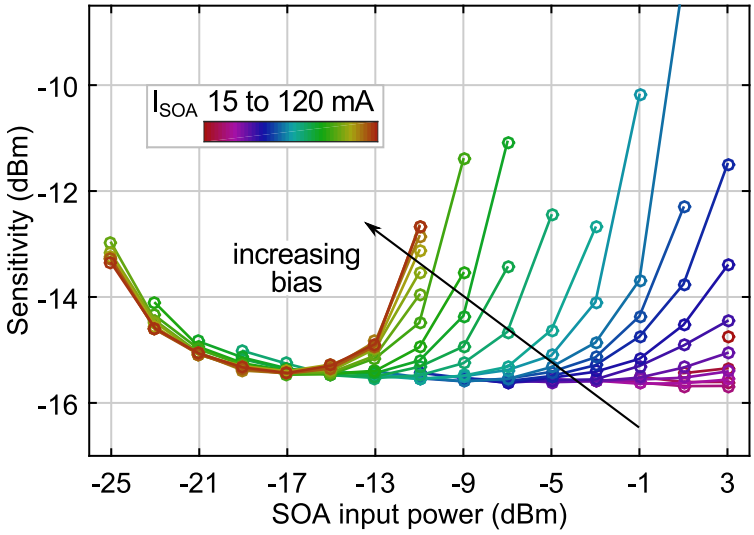


Figure 5.35: Sensitivities for the SOA output under various operating conditions for an PAM4 system.

measured for the PAM4 signal was −15.7 dBm, 0.5 dB worse than EDB as would be expected from previous characterisations. The range of input powers from −19 dBm to +3 dBm showed sensitivities within a variation of less than 0.5 dB, provided the appropriate bias was chosen, and signal reception was possible down to −25 dBm, although with an additional penalty due to the OSNR degradation. For all three modulation formats input powers higher than −13 dBm introduced an increasing sensitivity penalty at high bias currents due to operation above the saturation input power threshold. As seen in Figure 5.29, an input power of −13 dBm would cause a gain compression within 1 dB and 3 dB when the SOA is biased with a high current. The penalty due to lowering of the OSNR, on the other hand, was more pronounced in EDB and PAM4, which have multiple amplitude levels in the optically modulated signal.

From these measurements it can be inferred that if an SOA is used as a pre-amplifier with an incoming burst signal and operated at a fixed bias, a penalty, or complete signal loss, will occur for a high DR in the upstream. This is because both the OSNR and the saturation input power depend on the bias current used. Figure 5.36 shows, for every SOA bias used, the range of input powers for which the sensitivity lies within a 1 dB or 3 dB of its best value. Using NRZ-EDB or EDB the widest DRs that can be supported to limit the sensitivity penalty to 1 dB

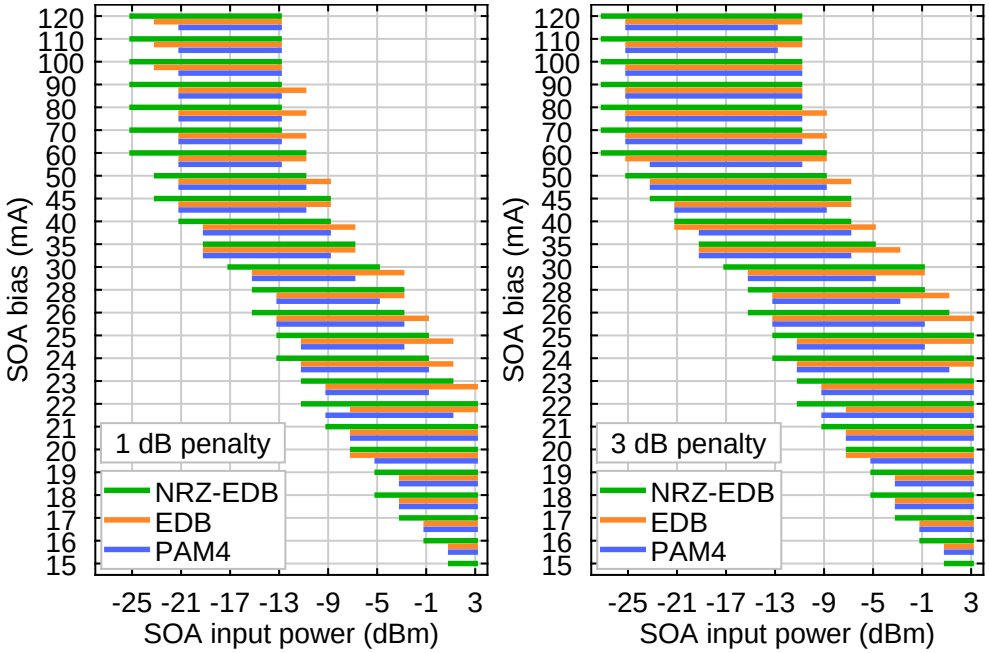


Figure 5.36: SOA input power ranges within a 1 dB or 3 dB sensitivity penalty for a fixed gain SOA pre-amplified receiver.

are 14 dB and 12 dB, respectively, which increase to 18 dB and 16 dB, respectively, if considering a 3 dB penalty. For PAM4 the operating range is even narrower, equal to 10 dB or 14 dB for a sensitivity loss of 1 dB and 3 dB, respectively. Also, careful ODN design must be ensured to avoid overload and potentially permanent damage to the photodiode from the high power output of the amplifier. The use of a fixed gain SOA can provide benefits in terms of improved sensitivity at the OLT but still requires an electrical BM-Rx to detect the upstream bursty traffic. In particular, for the multi-level modulation formats used, a 10 GHz linear burst-mode receiver is required, which is not available yet as a commercial product.

In order to provide optical power equalisation with a single pre-amplifier SOA, its output power must be kept constant for any input condition. Changing the bias current on a burst-by-burst time-scale removes the need for an electrical BM-Rx and an AC coupled photodiode with TIA can be used instead. An optimum condition for the SOA output power can be found to balance the OSNR and gain saturation penalties and obtain the widest operational range. Figures 5.37, 5.38, 5.39 show a colormap of the sensitivities obtained previously as a function of optical

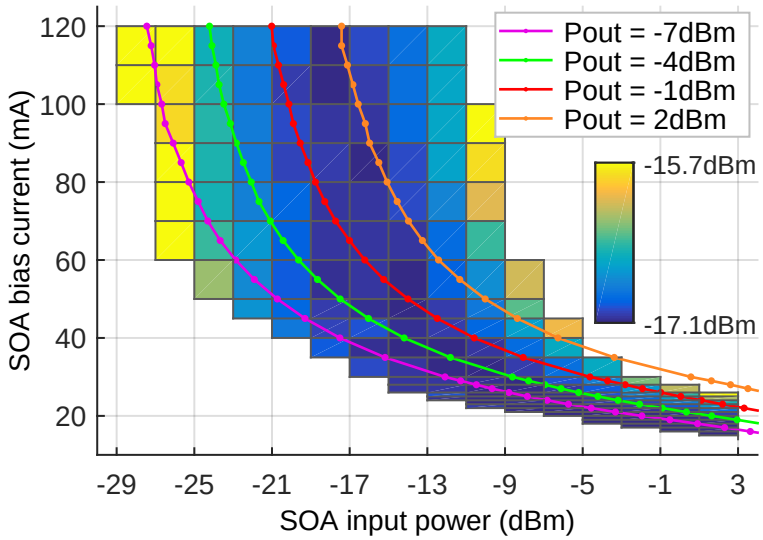


Figure 5.37: Sensitivity map of the SOA pre-amplifier for the NRZ system with EDB detection.

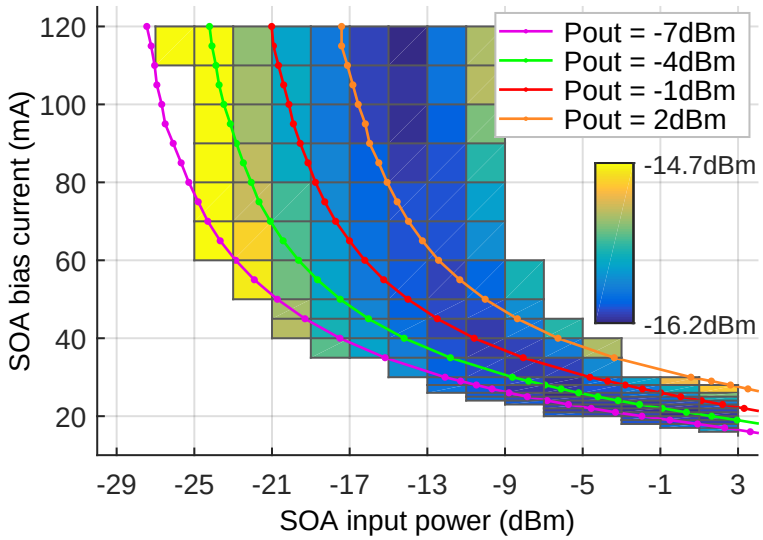


Figure 5.38: Sensitivity map of the SOA pre-amplifier for the EDB system.

input power and SOA bias current. Also overlaid on the graphs are lines from Figure 5.31 that indicate the conditions to obtain a constant SOA output power and perform optical DR equalisation. The desired operating condition of the device must be along one of the constant output power lines and ensure that the minimum required optical power for a BER of 10^{-3} is lower than the SOA output power. When an optimum

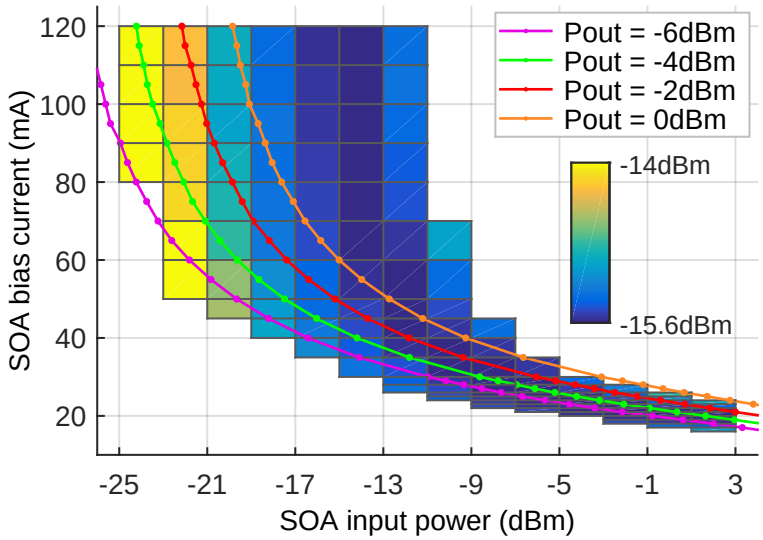


Figure 5.39: Sensitivity map of the SOA pre-amplifier for the PAM4 system.

SOA output power is selected, the signal reaching the photodiode is far from sensitivity and, hence, not impaired by thermal noise. At the same time, it has to be ensured that saturation is avoided in the entire range of SOA input powers.

In order to optimally choose the operating regime the sensitivities obtained for a constant output power condition are plotted in Figures 5.40, 5.41 and 5.42 for the three modulation formats. An output power higher

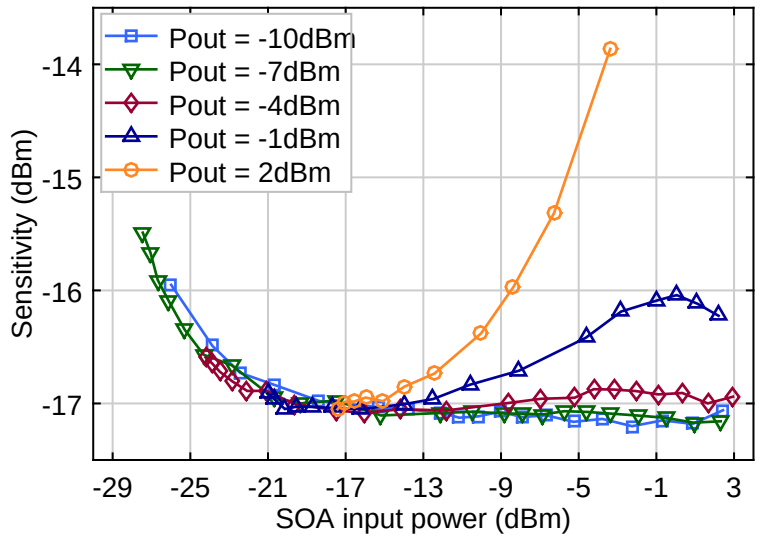


Figure 5.40: Sensitivity of the SOA output along a constant output power operating condition for the NRZ system with EDB detection.

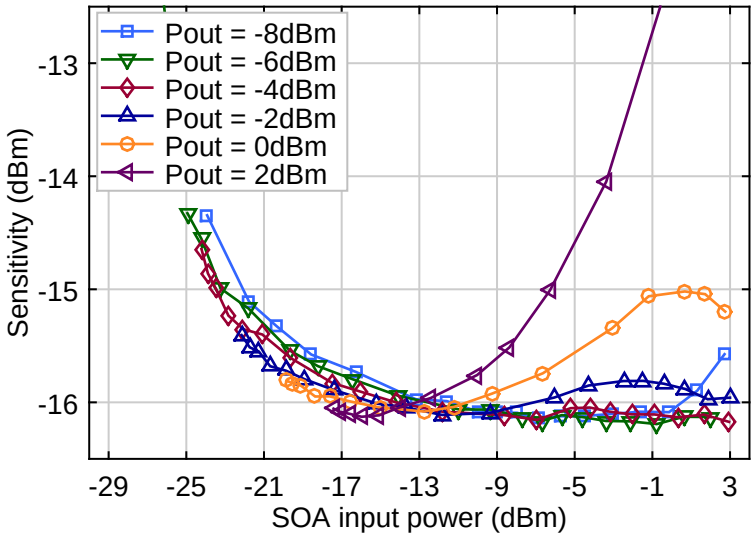


Figure 5.41: Sensitivity of the SOA output along a constant output power operating condition for the EDB system.

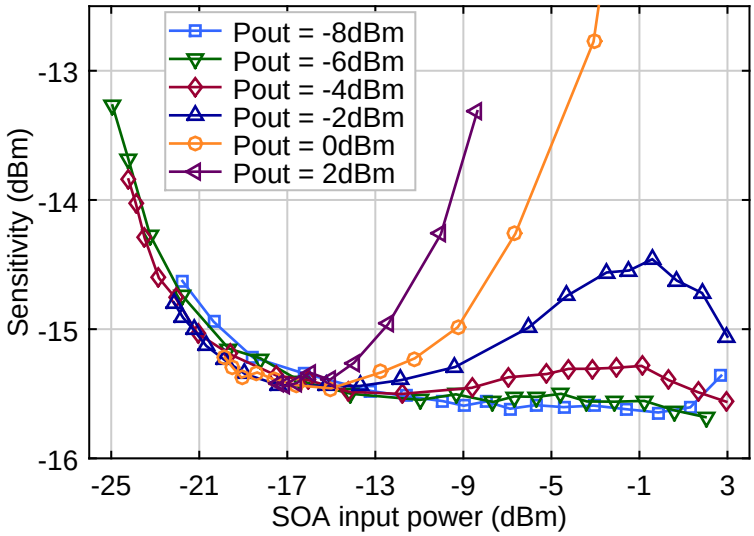


Figure 5.42: Sensitivity of the SOA output along a constant output power operating condition for the PAM4 system.

than 0 dBm causes the performance to be limited by gain saturation on one side and cannot be achieved for low input powers due to the limited SOA gain. Output powers below −10 dBm instead suffer from poor NF at high input powers, when a low bias current leads to a negative gain and, hence, limits the OSNR in the low input power regime. For the NRZ-EDB transmitter an output power of −7 dBm could support SOA

input powers ranging from −27 dBm to +2 dBm without suffering from signal saturation at high input powers. The OSNR penalty leads to a worst case sensitivity of −15.5 dBm for an SOA input power of −27 dBm, which, considering the SOA output power of −7 dBm, is sufficient to ensure that the photodiode is working well above sensitivity. For the EDB system an optimum compromise was identified for an SOA output power of −6 dBm and, similarly for the PAM4 system, such a value provided the widest range of accepted input powers with a reduced sensitivity penalty. In the three cases the selected output powers ensured that the power entering the PIN receiver was above the sensitivity so that it could operate in a regime not limited by thermal noise, to ensure a BER lower than 10^{-3} for the entire DR of interest. The lower and higher input optical powers used indicate that more than 25 dB DR can be supported in the incoming burst-mode signal. When selecting the appropriate SOA working condition it is also worth remembering that for the intended application, as PON upstream pre-amplifier, optical powers reaching the OLT are limited by the ONU launched power and minimum path loss. In the most recent NG-PON 2 standard the maximum OLT overload power is −5 dBm for the N1 class networks [18]. It is therefore preferable to allow for reduced performance at SOA input powers > −5 dBm, that are unlikely to be seen in a real scenario, and improve the performance for received powers around −20 dBm or less.

5.2.3 Gain controlled pre-amplified receiver demonstration

The previous characterisation provided an insight into the capabilities and optimisation of a pre-amplified SOA based receiver with variable gain to provide optical power equalisation on a burst-by-burst basis. This Subsection presents the experimental demonstration of optical power equalisation of a 25 Gb/s burst-mode traffic by means of a switched gain SOA. From the previous analysis the highest performing modulation format was NRZ with duobinary detection which supported the widest DR. This was hence used at first to conduct a comparison of different optical filter bandwidths to be employed between the SOA and PIN for ASE filtering. The full burst-mode upstream system was then tested under increasing DR for the three modulation formats in optical B2B and with

SMF lengths of 25 km and 40 km.

Experimental setup

The experimental setup in Figure 5.43 was built to confirm the results obtained in the continuous mode characterisation of an emulated TDM burst-mode upstream system. The two DFB lasers in the setup were tuned to two C-band ITU-T channels at a 100 GHz spacing with frequencies of 193.4 THz and 193.5 THz, corresponding to 1550.116 nm and 1549.315 nm respectively. A gain-controlled SOA driven by an arbitrary function generator (AFG) was used after each laser to carve the signal suppressing its output during the off-state between optical bursts. Two ONUs were implemented and the TDMA protocol was emulated by synchronising the two SOAs's "on" and "off" states to alternate. A guardband period of 20.5 ns was introduced between successive bursts during which no data transmission took place to allow for the switching on and off of the transmitters. The optical bursts were 5.24 μm long and consisted of payload and a 10.2 ns long end-of-burst sequence which provides time for disabling the transmitter. The BER was selectively measured only in the payload of the bursts which consisted of a PRBS 15 sequence for the loud burst and an inverted PRBS 15 for the

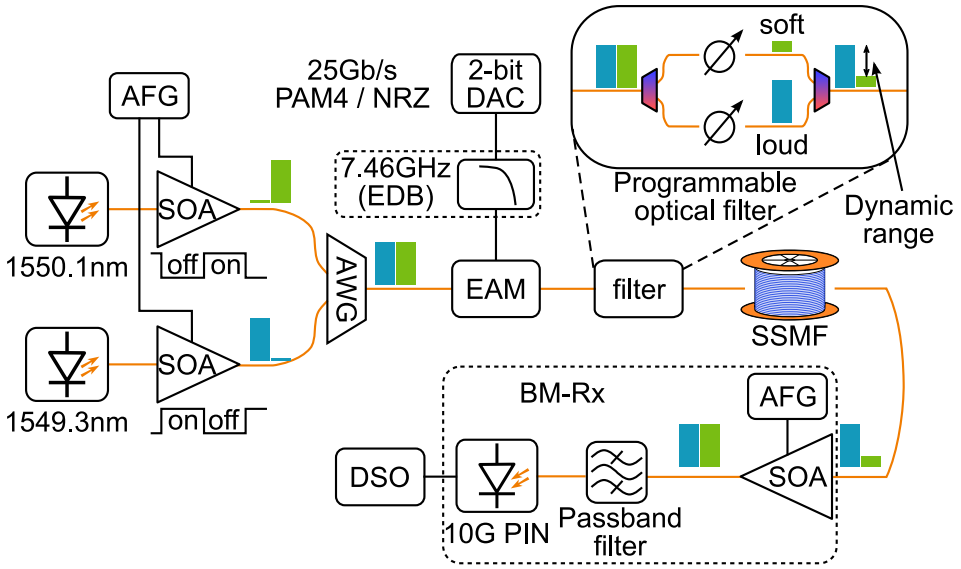


Figure 5.43: Experimental setup for for burst-mode traffic analysis with SOA based pre-amplified receiver performing optical equalisation.

soft. No preamble was used in front of the payload at the beginning of the bursts and, hence, no transmission overhead was introduced. An AWG was used to merge the two optical signals, as it had lower insertion losses than a power coupler and also could suppress the out of band ASE from the SOAs, and the stream was then sent into an EAM. The modulator was driven by a two bit DAC generating a 25 Gb/s NRZ or PAM4 burst signal synchronised with the gain switching of the SOAs, where every burst was modulated during the on period of its transmitter. A 7.46 GHz Bessel low-pass filter was used after the DAC to emulate the bandwidth of an EDB transmitter. The EAM bias was changed following the guidelines obtained in Section 3.2 to provide optimised performance for the amount of CD introduced by the fibre. A programmable optical filter was then used to arbitrarily control the power of the two bursts setting independent attenuation values across the wavelength spectrum and generating the system DR, that is, the optical power difference between bursts. The optical bursts with lower and higher optical power were conventionally named soft-burst and loud-burst, respectively. The filter output signal was launched into a fibre of length 25 km or 40 km and then fed into an SOA driven with variable bias current and, hence, gain to act as a pre-amplifier with power equalisation capability. The SOA output was sent to a 10 G PIN photodiode equipped with a linear TIA and its electrical output was captured with a 50 GS/s DSO with a 12.5 GHz 3 dB bandwidth. Off-line processing was then used on the waveform to synchronise the incoming signal and perform BER counting of the bursts separately.

Experimental results

The BER was measured independently for the loud and soft burst payloads at first without the SOA pre-amplifier at the receiver, to confirm the transmitter quality and whether the SOA carving was introducing any source of impairment. No DR was introduced in this case because the simple AC coupled PIN receiver could not detect burst traffic. The BER curves in Figure 5.44 show that soft and loud bursts had very similar performance and their sensitivity was measured to be -16.7 dBm, close to the expected value from Section 3.2. No preamble was introduced at

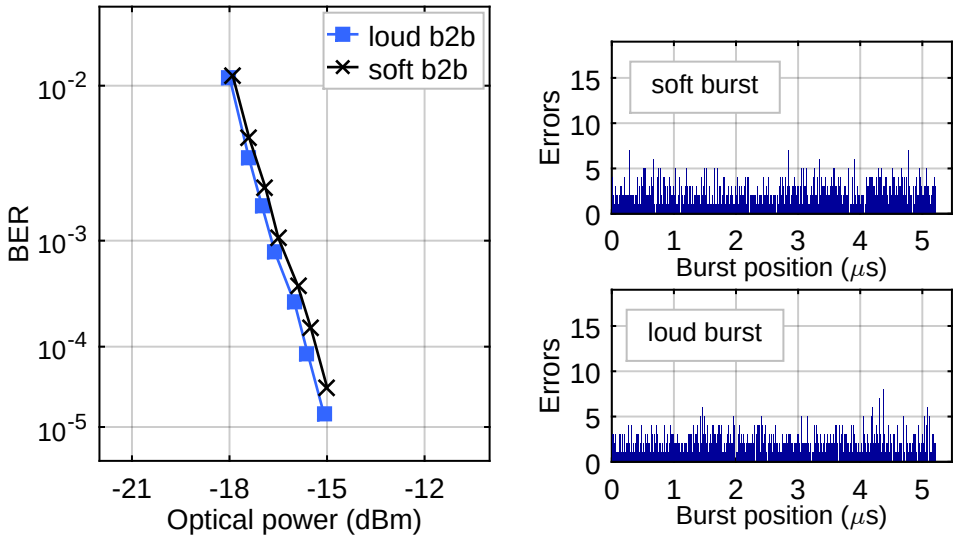


Figure 5.44: BER curves for soft and loud bursts in optical back-to-back.

the start of the optical bursts which means the payload, and hence the BER measurements, started from the first bit after the guardband period. This was only possible because the measurements were done using off-line processing and the SOA gains were set programmatically knowing the DR of the incoming signal. In a practical implementation the preamble time will depend on the speed of the electronic control feedback-loop used to set the gain of the SOA. Figure 5.44, along with the BER curves, also shows the errors distribution in the payload of both soft and loud bursts which appeared evenly distributed along the burst duration. This means that the SOAs carving did not introduce any error correlation.

The system sensitivity was then measured for the OLT pre-amplified receiver adding the gain-switched SOA. The SOA input power was measured for both soft and loud bursts with 0 dB DR and, also in this case, their performance was similar and the error distribution analysis revealed no error concentration along the burst to be attributed to the SOA gain switching. Figure 5.45 shows the NRZ-EDB BER lines in B2B and for 25 km and 40 km of SMF. Two different optical bandpass filters between the SOA and PIN were compared, with widths of 4 nm and 13 nm. Less than 1 dB penalty was observed between the two filters meaning the ASE-ASE beat noise contribution was limited and integrated devices can be designed with ASE filters wide enough to accommodate the entire upstream band. The B2B sensitivities were -28 dBm and -27.5 dBm for

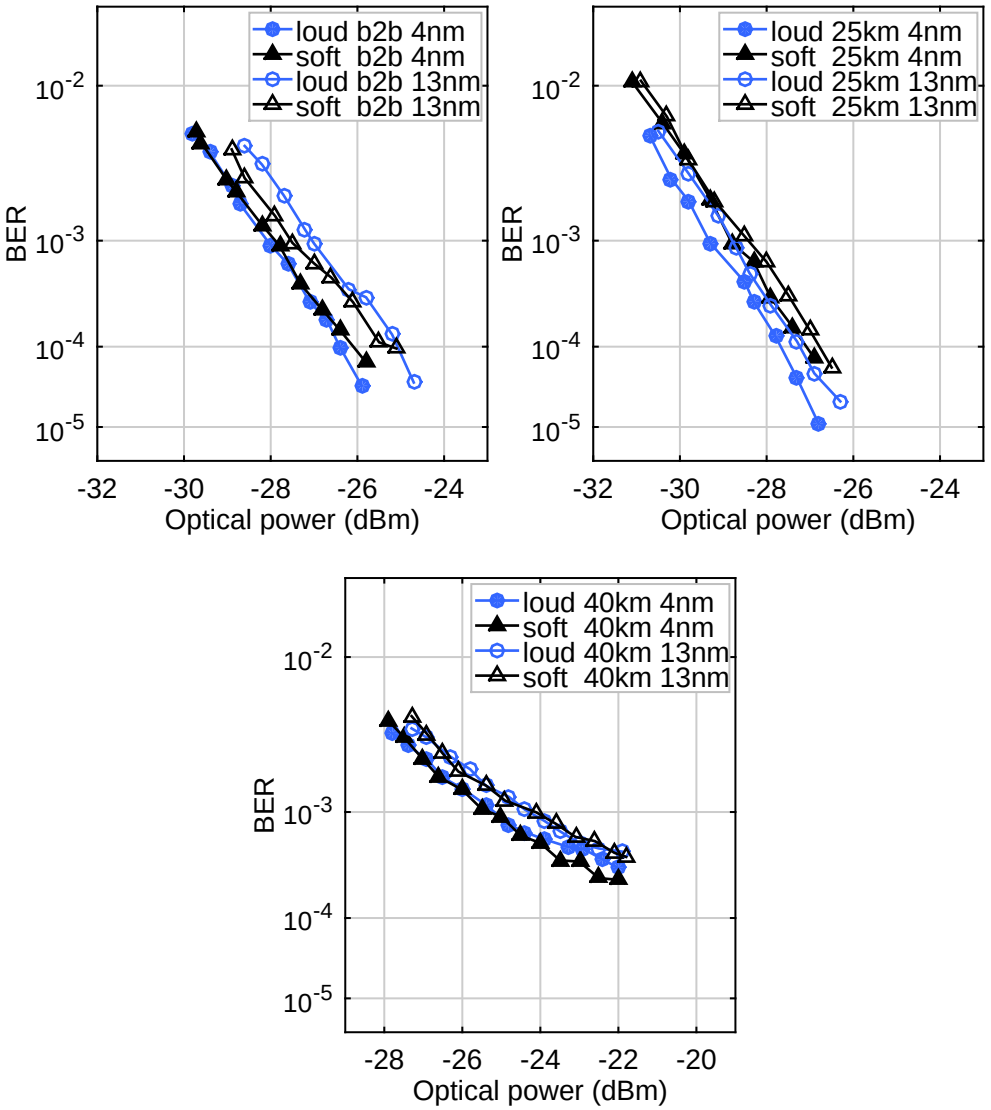


Figure 5.45: BER curves of soft and loud bursts for different fibre lengths and optical filter bandwidth.

the soft burst with the 4 nm and 13 nm optical filter, respectively, an improvement over the unamplified PIN receiver of more than 10 dB.

The system DR was then gradually increased keeping the soft burst power into the SOA fixed at its sensitivity and increasing the power of the loud burst, by changing the attenuation profile of the programmable optical filter. The bias of the SOA was kept fixed for the soft burst and adjusted accordingly during the loud burst period to have a constant output power. A bias of -1.68 V was used for the EAM in this case, to avail of the linear region of its transfer function. In B2B the BER

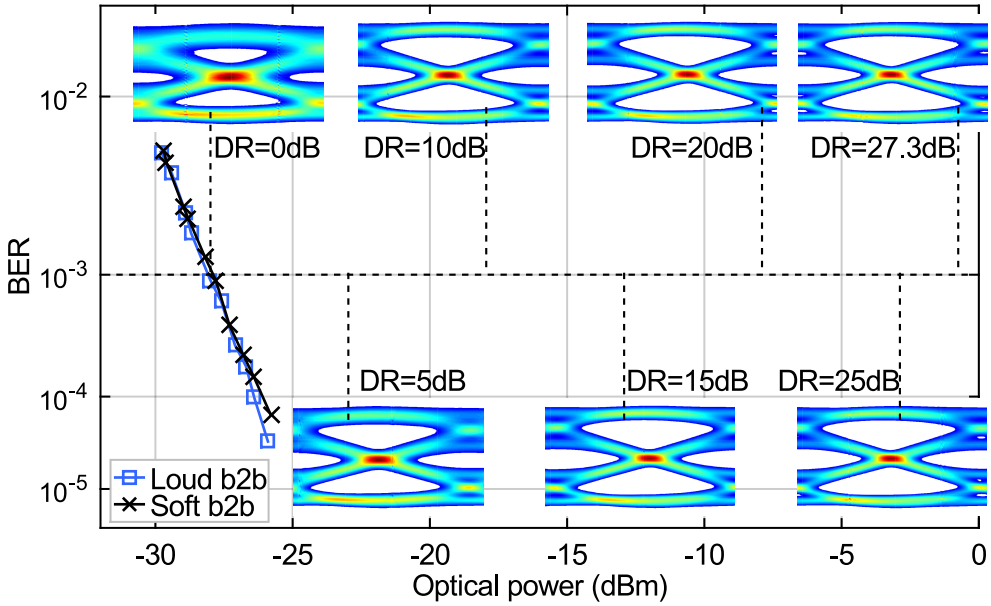
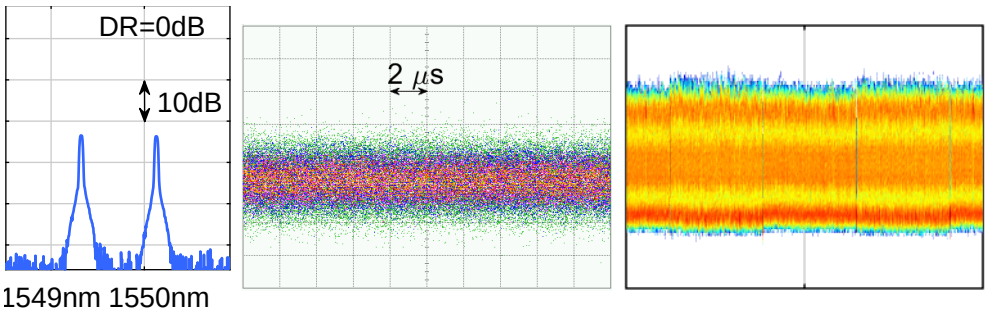
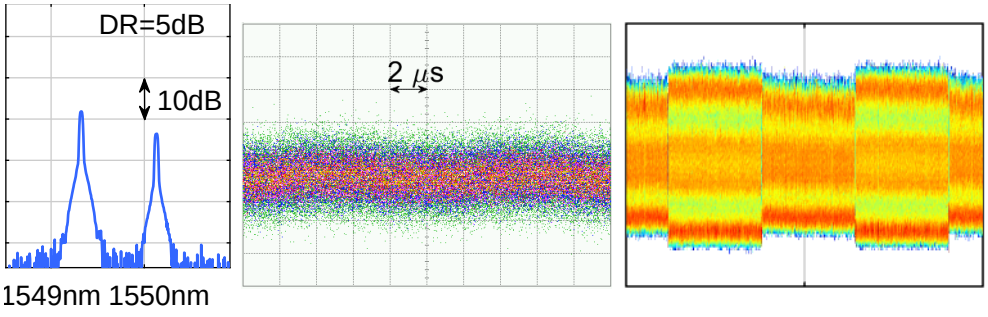


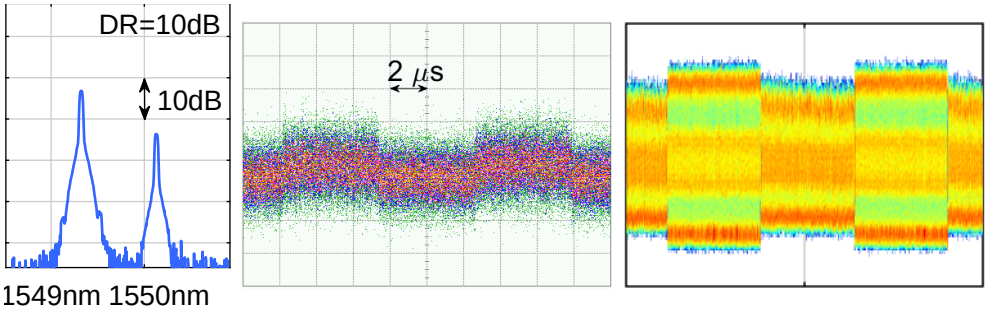
Figure 5.46: BER curves of soft and loud bursts and eye diagrams of the loud burst under different DR conditions for NRZ-EDB in optical B2B.

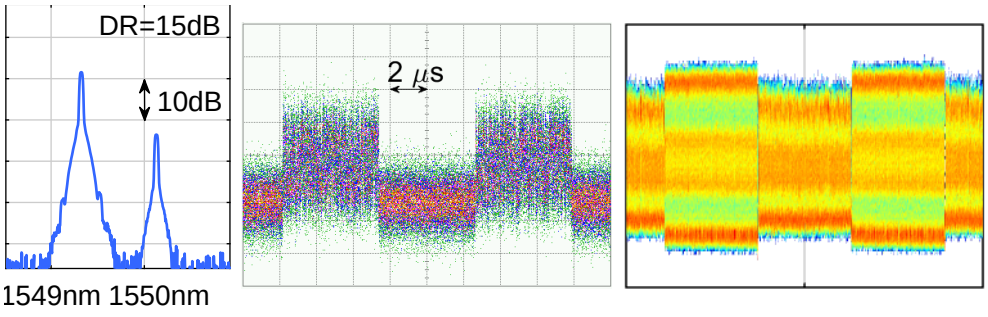
of the loud burst measured for DRs ranging from 5 dB to 27.3 dB was lower than 10^{-6} and, even at the highest input power into the SOA of -0.7 dBm, the degradation effect due to gain saturation was negligible. The eye diagrams of the loud burst are reported in Figure 5.46 and show no sign of linearity degradation. Also in this case, no preamble was used between guardband and payload in the bursts structure and the error distribution did not show concentration of errors at the beginning of the bursts. This means the SOA fast dynamic does not introduce overhead in the transmission to perform optical power equalisation and the adjustment time depends on the electronic circuit implementation for the gain setting.

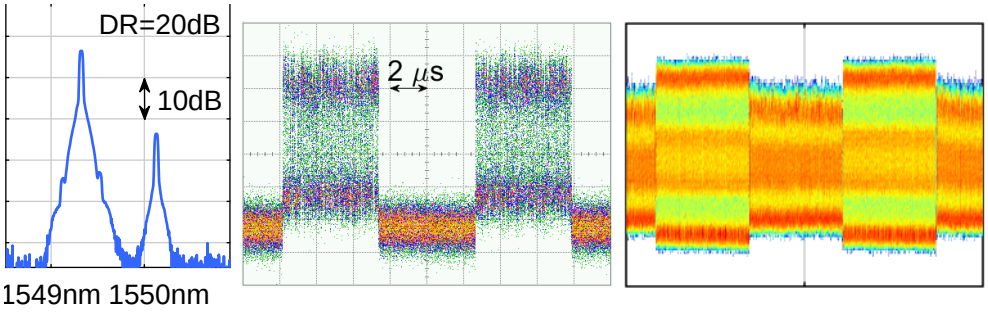
Figure 5.47 shows the wavelength profile measured with an OSA, the optical signal entering the receiver SOA and the electrical signal at the output of the 10 G photodiode for the various DRs used above. From the Figures, it can be appreciated how the average signal power at the receiver output is constant and no electrical transients are being introduced by the photodidoe AC interface. As the DR range is increased, the loud bursts have a higher peak to peak amplitude because of the better OSNR of the signal and, hence, better suppression of modulated zeros. Also, it can be noticed that the optical signal was a binary NRZ


DR=0dB
10dB
2 μs
1549nm 1550nm


DR=5dB
10dB
2 μs
1549nm 1550nm


DR=10dB
10dB
2 μs
1549nm 1550nm


DR=15dB
10dB
2 μs
1549nm 1550nm


DR=20dB
10dB
2 μs
1549nm 1550nm

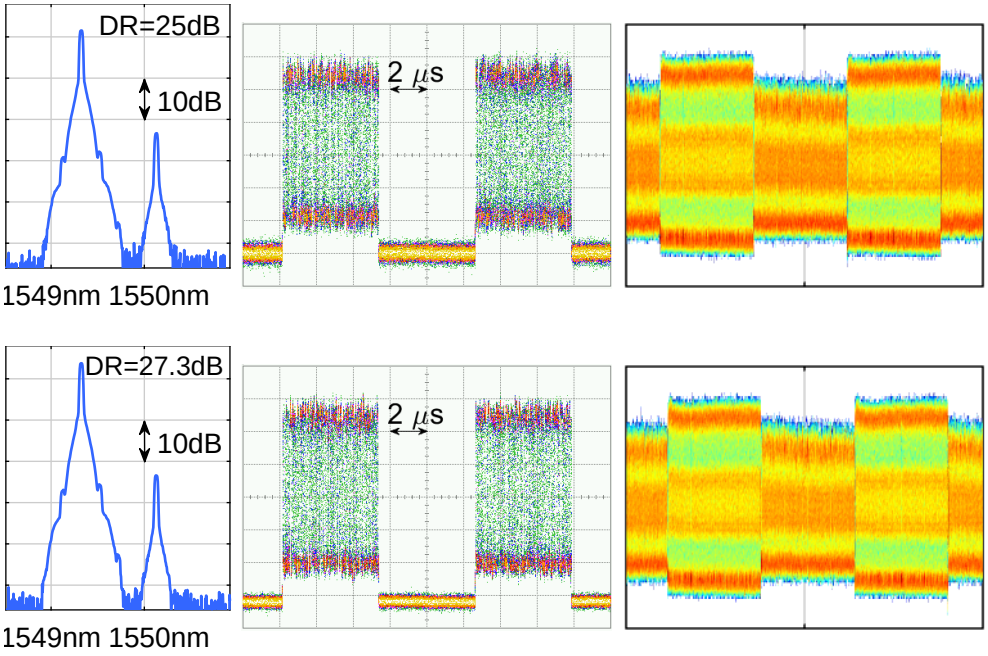


Figure 5.47: Optical spectrum, optical waveform before SOA equalisation and electrical waveform after power equalisation for increasing DR measured with the NRZ-EDB system.

while the electrical signal after detection with the 10 G receiver became a three level EDB. The maximum DR investigated was 27.3 dB because of the experimental system limitations for the input power of the loud burst which was limited to a maximum of −0.7 dBm. The analysis of Section 5.2.2 suggests that a higher DR could be supported. However, typically the maximum DR in a PON is 20 dB when considering a maximum differential optical path loss of 15 dB and the variation in the ONUs launched power [18]. Also, among the NG-PON 2 ODN classes, the maximum overload power at the OLT is −5 dBm and so the analysis covers the implementation cases of an upstream PON channel [18].

The use of an SOA burst equaliser is demonstrated not only to remove the necessity of an electrical BM-Rx but also to greatly improve the receiver sensitivity, providing a solution to the power budget requirements when higher modulation formats are adopted. The pre-amplified system sensitivity of −27.5 dBm measured with the 13 nm filter was 10.8 dB better than the one of the PIN based photoreceiver and allowed for a link budget of 32.5 dB, assuming a minimum ONU launched power of +5 dBm with an EML [78, 140]. Also, the DR demonstrated is higher

than that which is currently achievable with 25 G BM-Rxs [54, 75, 76].

Similar measurements were then repeated with the addition of 25 km and 40 km of SMF after the programmable optical filter. The EAM bias was lowered to −2 V and −2.24 V, respectively, to avail of the higher dispersion tolerance despite compromised signal linearity. Figures 5.48 and 5.49 show the BER lines when reaching the OSNR limited regime of the soft burst and the eye diagrams of the loud bursts for increasing DR. Sensitivities of −28.5 dBm and −24.1 dBm were measured, respectively, for the 25 km and 40 km case. In this case, the loud-burst maximum powers that could be obtained were −7.2 dBm and −10.9 dBm for a DR of 21.7 dB and 14.6 dB, respectively, using the 25 km and 40 km SMFs. The BER of the loud burst for a DR of 5 dB or higher was lower than 10^{-6} when 25 km of SMF were used, while it showed a floor at a BER of 10^{-4} for the 40 km case due to the accumulated CD.

The eye diagrams in Figure 5.49 show the eye closure caused by CD which was responsible for the BER flooring. Also, the slope of the BER curve was different because of the influence of uncompensated dispersion. Nevertheless, the system could operate over an extended reach of 40 km using duobinary detection without any CD compensation scheme. The

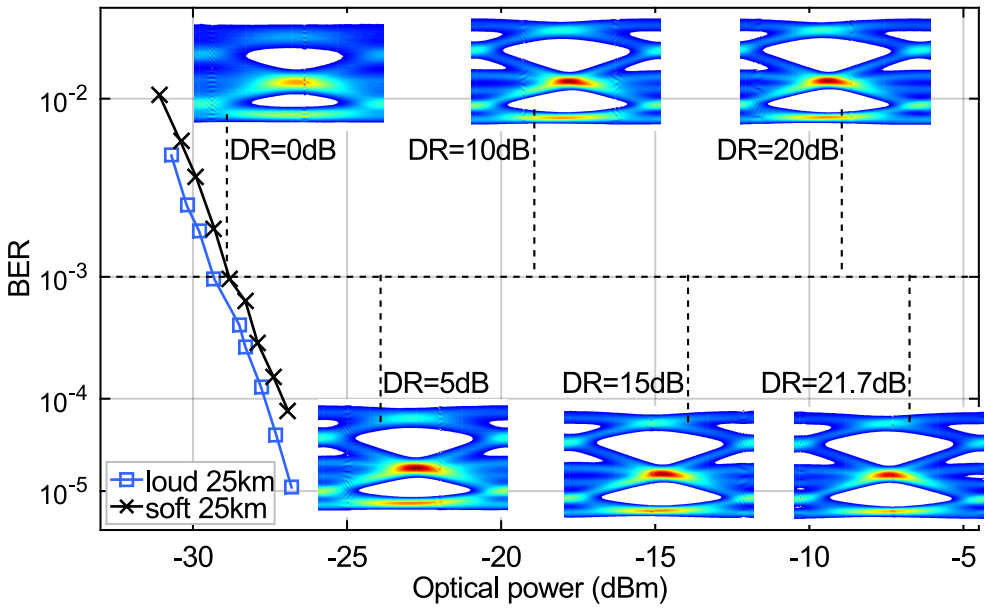


Figure 5.48: BER curves of soft and loud bursts and eye diagrams of the loud burst under different DR conditions for NRZ-EDB with 25 km of SMF.

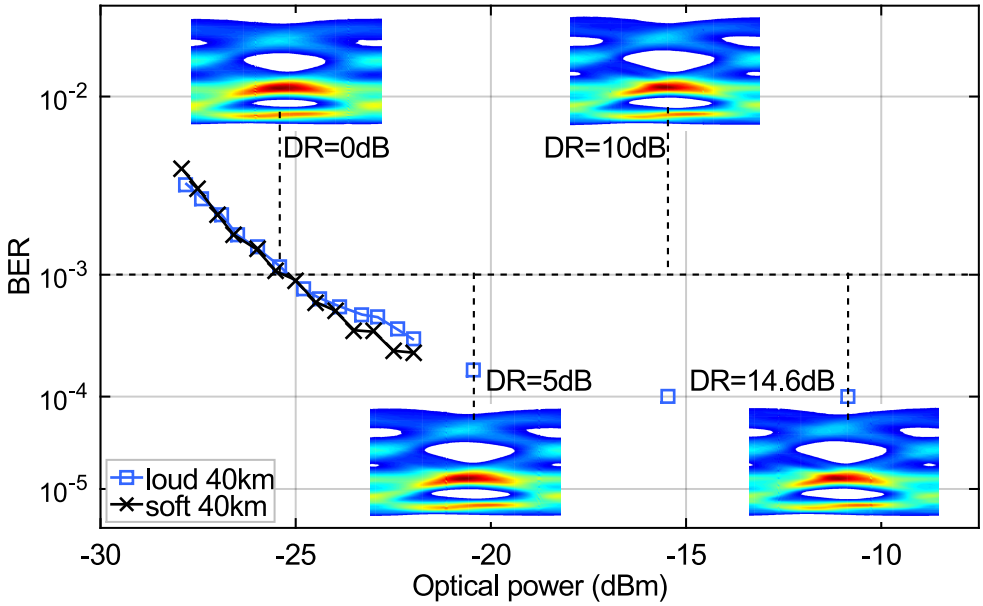


Figure 5.49: BER curves of soft and loud bursts and eye diagrams of the loud burst under different DR conditions for NRZ-EDB with 40 km of SMF.

receiver sensitivities allow for a power budget of 33.5 dB and 29.1 dB for the 25 km and 40 km system, respectively, assuming +5 dBm of launched power at the ONU [78]. Also, in this configuration, there was no error concentration at the beginning of the bursts, suggesting that the SOA did not cause signal envelope transients and, hence, no transmission overhead was required.

The burst-mode system was also demonstrated using EDB and PAM4 in B2B and with reaches of 25 km and 40 km. The 13 nm wide optical filter was used to account for the more relaxed design specification which offers more flexibility during the network design at the price of reduced sensitivity. Figures 5.50, 5.51 and 5.52 show for EDB modulation the soft burst BER at the OSNR limit and the loud burst eye diagrams for the three reaches. Sensitivities of −25.9 dBm, −24.9 dBm and −22.9 dBm were measured in the three cases, sufficient for power budgets above 29.5 dB in B2B or after 25 km. An extended reach of 40 km with EDB modulation would require CD compensation to support a higher link budget. The system was again tested in burst-mode up to the highest DR achievable with the experimental setup and did not show performance penalties arising from burst-mode operation or gain saturation in the

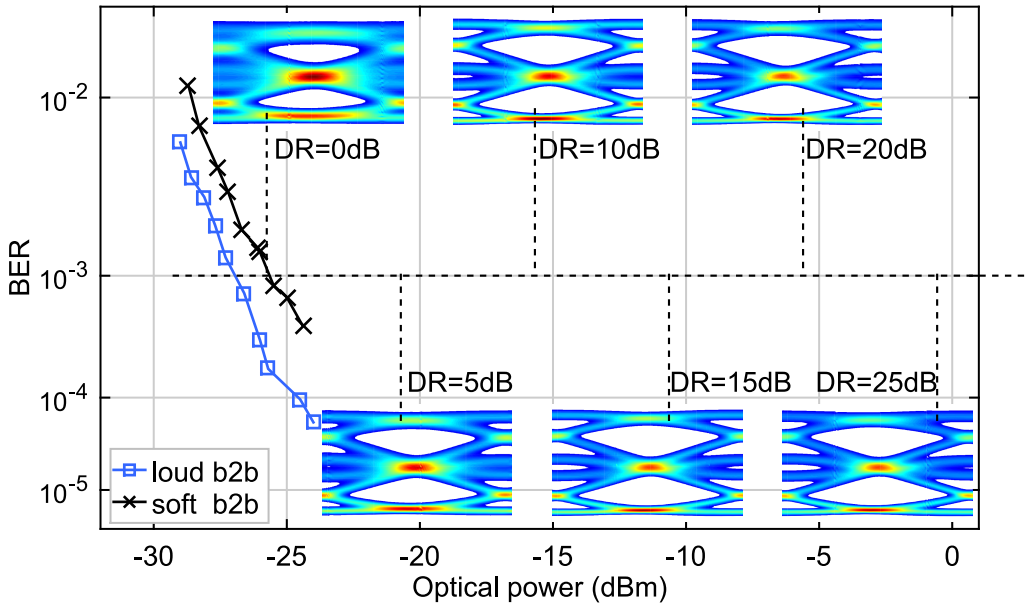


Figure 5.50: BER curves of soft and loud bursts and eye diagrams of the loud burst under different DR conditions for EDB in optical B2B.

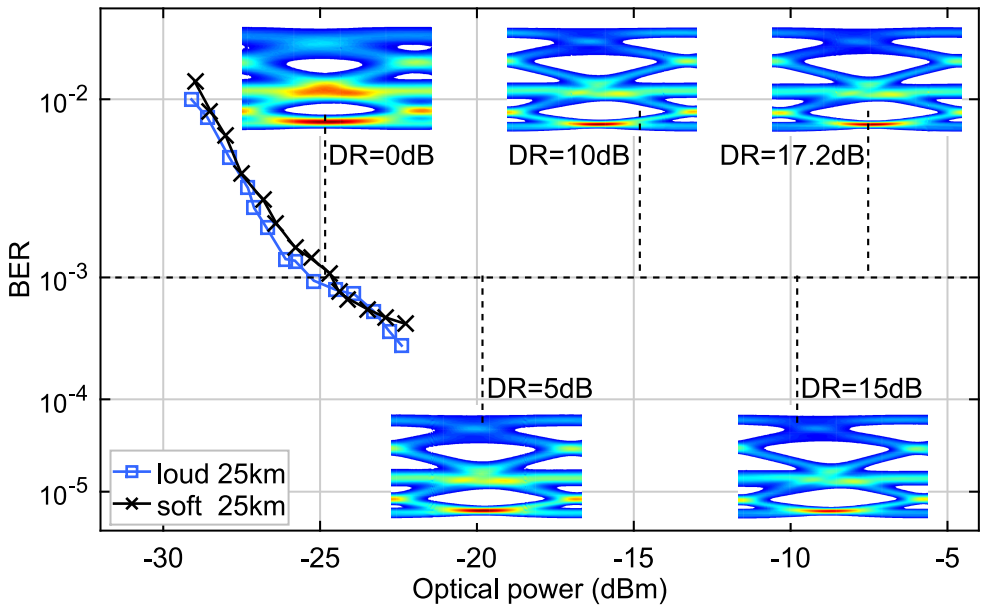


Figure 5.51: BER curves of soft and loud bursts and eye diagrams of the loud burst under different DR conditions for EDB with 25 km of SMF.

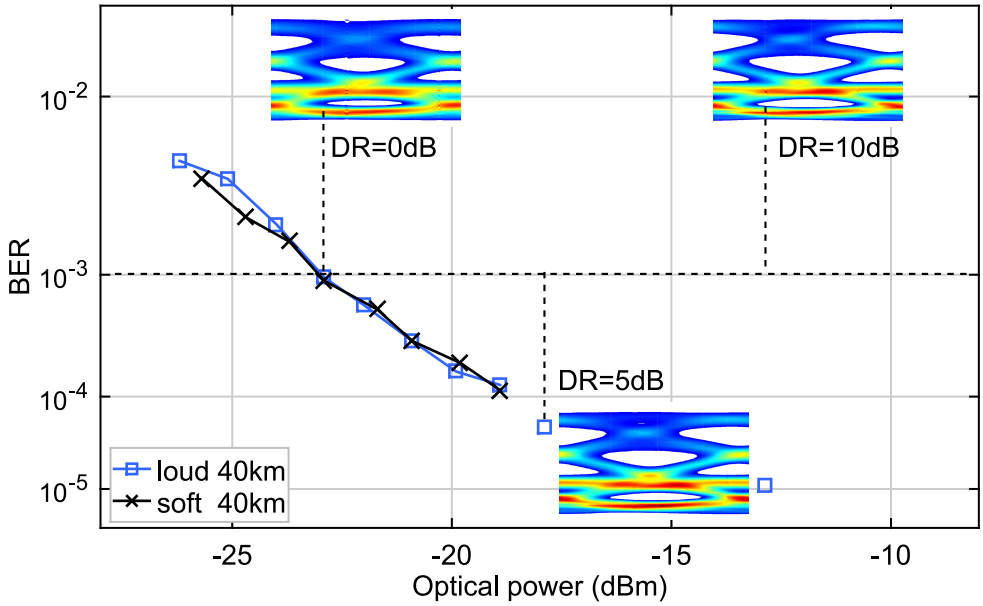


Figure 5.52: BER curves of soft and loud bursts and eye diagrams of the loud burst under different DR conditions for EDB with 40 km of SMF.

loud-burst.

Finally, the same measurements performed with PAM4 are shown in Figures 5.53, 5.54 and 5.55. The minimum received optical powers for a BER of 10^{-3} were -24.6 dBm, -24 dBm and -21.5 dBm for increasing fibre reach. For all the DRs investigated the linearity of the loud-burst was not affected by the SOA, while the eye diagrams clearly show the effect of accumulated CD on the uncompensated signal.

The optically pre-amplified BM-Rx was demonstrated in this Section to operate with linear multi-level modulation formats without employing specifically designed burst-mode electrical components. A 25 Gb/s bit-rate was achieved using EDB or PAM4 in a system realised with 10 G components only. A DR of the incoming upstream signal of up to 27.3 dB was demonstrated with no penalty in the loud-bursts. The best performing NRZ-EDB modulation supported a power budget of 32.5 dB 33.5 dB and 29.1 dB in optical B2B and for fibre lengths of 25 km and 40 km. The system was also demonstrated to support transmission at a pre-FEC BER of 10^{-3} after 40 km of fibre with no chromatic dispersion compensation techniques at the receiver. The fast carrier dynamics of the amplifier, combined with the wide range of saturation input powers that are supported by a variable gain architecture, makes SOAs a promising

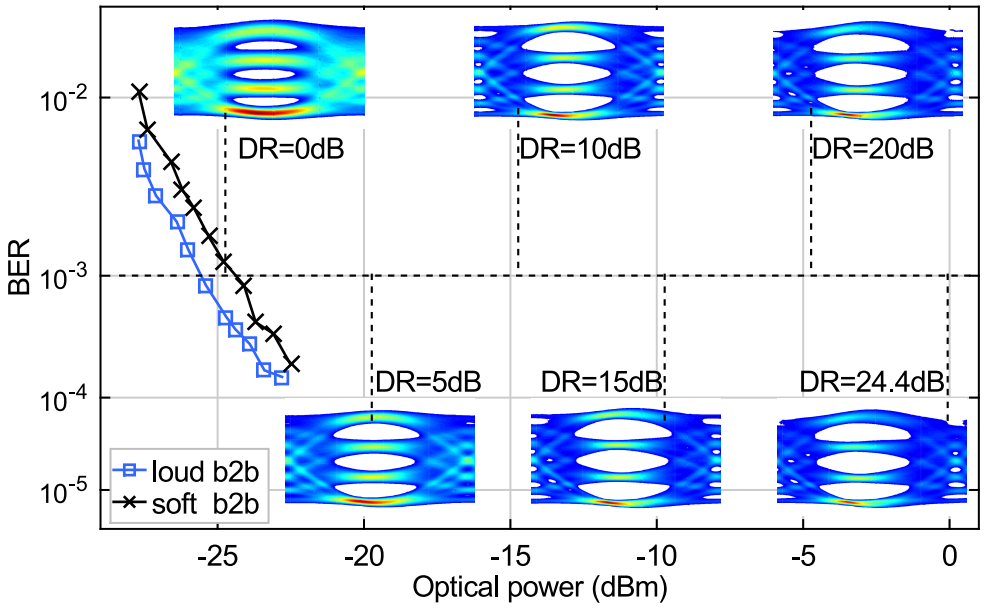


Figure 5.53: BER curves of soft and loud bursts and eye diagrams of the loud burst under different DR conditions for PAM4 in optical B2B.

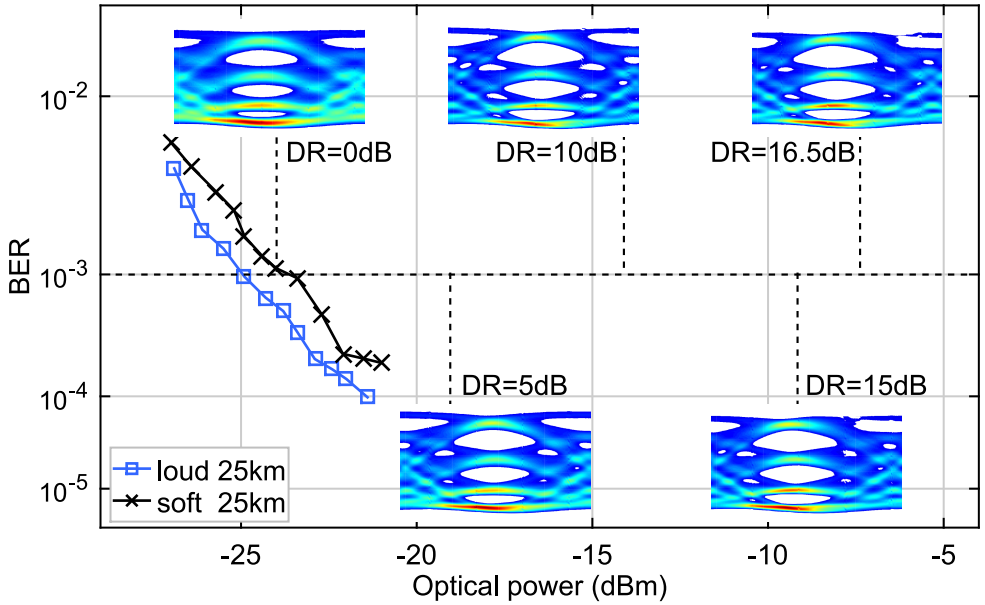


Figure 5.54: BER curves of soft and loud bursts and eye diagrams of the loud burst under different DR conditions for PAM4 with 25 km of SMF.

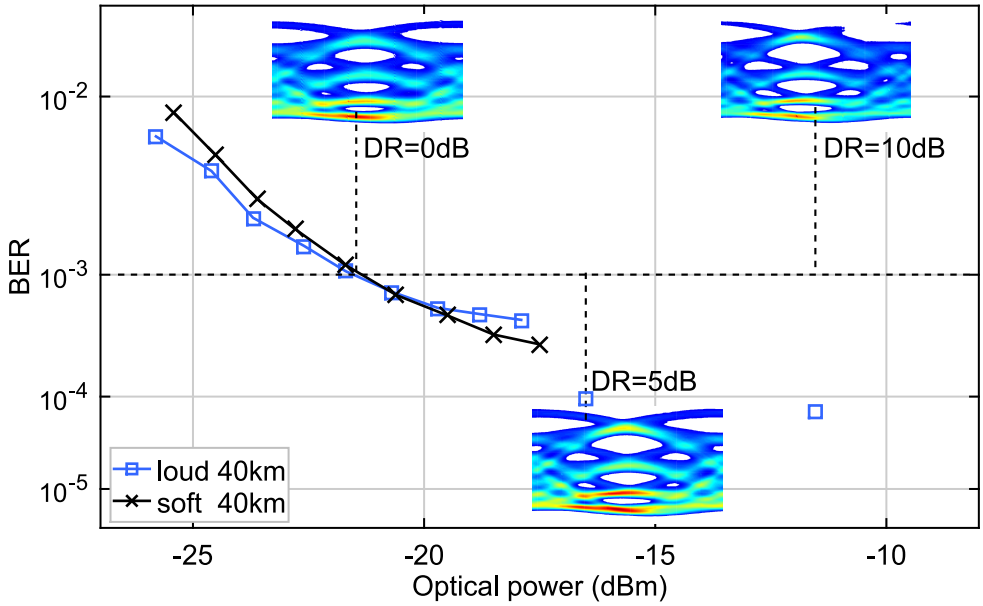


Figure 5.55: BER curves of soft and loud bursts and eye diagrams of the loud burst under different DR conditions for PAM4 with 40 km of SMF.

candidate for the realisation of high-speed, high-dynamic range, linear BM-Rxs without complex variable-gain electrical amplifiers.

5.3 Summary

Optical amplification strategies compatible with the upstream burst-mode traffic of PONs were analysed and discussed in this Chapter in order to provide a solution to meet the power budget requirements of more spectrally efficient modulation formats.

Section 5.1 presented Raman based amplifiers operating in the O-band for reach extension of the upstream transmission in different scenarios. A DMT based PON system was integrated with distributed Raman amplification for reach extension. The upstream link employing G-PON O-band quantum dot DML transmitters adopted flexible data-rate DMT and transmission over a 40 km long optical trunk fibre was performed employing various reach extender solutions based on Raman optical amplification or/and SOA. The link showed high design flexibility with a trade-off between data-rate and power budget and a maximum 41.6 dB loss budget for the lowest speed 2.1 Gb/s DMT was demonstrated.

The first quantum dot based Raman amplified XG-PON upstream

was then demonstrated using 1210 nm pump lasers which allowed optical amplification in the 1270 nm window which is not reachable by other amplifier technologies. A pump power of 759 mW yielded a Raman on-off gain of 14.2 dB which accommodated a total loss budget of 46.7 dB allowing a fully passive network configuration with a total fibre length of more than 50 km and a split ratio of up to 1:64.

Raman amplification in the 1310 nm O-band window was then presented for a 25 Gb/s upstream transmission using 1240 nm pumps. The reach of 25 Gb/s EDB and PAM4 transmissions systems, with 10 G class transmitter and receivers, was extended using backward propagating Raman amplification. A total loss budget in excess of 42 dB was demonstrated for both modulation formats allowing transmission over 40 km and accommodating 1:128 splits. For a 20 km OTL a 41 dB loss budget was achieved which allowed for a 1:512 split ratio.

Section 5.2 reported an analysis of the use of SOAs to realise a pre-amplified OLT receiver for burst-mode traffic with optical power equalisation functionality. Driving the SOA with a variable bias current extended its dynamic range of operation and removed the need for an electronic BM-Rx. A characterisation of the SOA device showed its potential to be used with a linear 25 Gb/s traffic and equalise a DR in excess of 27 dB. The different multi-level modulation formats used were PAM4, EDB and NRZ with duobinary detection, with the latter showing the best overall performance. The SOA showed potential to be used in its linear region over a wide DR and support the linearity requirements of multi-level amplitude modulation formats.

A full system demonstration was realised implementing a burst-mode upstream traffic with arbitrary DR and an SOA based bursts equaliser and pre-amplified receiver. NRZ-EDB was demonstrated to work with up to 27.3 dB of DR in optical B2B providing improved sensitivity and without the need for an electronic BM-Rx. A commercial 10 GHz PIN photodiode with linear AC coupled TIA was used after the SOA burst equaliser. The system was demonstrated for the three modulation formats over an extended reach of 40 km of SMF without using CD compensation techniques. NRZ-EDB allowed for a power budget of 33.5 dBm and 29.1 dB when 25 km and 40 km of SMF were used, respectively.

6 Conclusions

Access networks are currently under increasing pressure in order to respond effectively to the constantly increasing demand in bandwidth which is occurring globally. Nowadays access networks still largely rely on copper based communication but DSL technologies will not be able to support the traffic growth foreseen in the near future. These networks will have to go through an extensive upgrade of the physical layer and move towards optical fibre, which can offer a much higher bandwidth and will provide a solution for the next generation of access systems.

6.1 Contributions overview

Access networks are currently shifting towards the adoption of optical fibre based networks, mostly based on the cost efficient PON architecture. The structure of a PON is based on a tree topology point to multi-point architecture where a single Central Office provides connection between a metro node and the end customers. Fibre networks based on PON technology are gradually replacing copper cables in access networks thanks to the superior performance and comparable costs.

In the past decades the evolution of PON systems was mostly driven by technological advances in the supporting optoelectronic devices which enabled enhanced bit-rates over a similar network topology. Recently, because of the challenges of developing affordable optics for operation beyond 10 Gb/s, WDM systems have been, or are in the process of being, standardised. The 100 Gb/s PON system currently under study will be enabled by wavelength multiplexing 4 channels providing a 25 Gb/s bit-rate each. The challenges in the realisation of higher bit-rate PONs are coming from the bandwidth limitation of the optoelectronic devices and more advanced modulation formats can be adopted as a solution

because they can more efficiently exploit the available bandwidth. The network reach is limited by CD impairments, which are more severe at higher Baud-rates, and power budget restrictions coming from the higher required optical power at the receiver and insertion losses of wavelength selective components. Propagation of a signal through an optical fibre causes both attenuation, which has to be accounted for in the power budget, and CD, which limits the maximum reach of a communication system, because of the resultant ISI.

Advanced modulation formats in PONs can be the enabling technology behind the bit-rate increase needed for the upcoming 100 G (4x25 Gb/s) systems in a cost-effective way. DMT, PAM4 and EDB modulations, in particular, have been implemented in this study and their potential is evaluated through experimental demonstrations.

DMT can avail of high order modulation formats, such as QAM, to increase its high spectral efficiency while keeping the attractiveness of being compatible with IMDD systems like current PONs. While requiring intense DSP for the implementation of all the functionalities, DMT relieves the requirements of the physical layer, in particular with regards to the bandwidth of the optoelectronic components. Its low spectral occupancy along with the flexibility offered in shaping the spectral content allows previous generation devices to support enhanced bit-rates leading to the demonstration of a 10.4 Gb/s, XG-PON compatible, bit-rate where a 1 GHz G-PON DML is used in the transmitter.

Simpler multi-level modulation formats, in particular PAM4 and EDB, can also be employed. Their spectral efficiency is lower than DMT but they offer simpler implementation since potentially no DSP is required and the electrical front-end devices have less strict linearity requirements. They are hence proving themselves a promising solution for the realisation of 25 Gb/s line-rates with the 10 G generation of optoelectronic devices. Their performance in terms of bandwidth restrictions and chromatic dispersion tolerance are higher than NRZ at the same bit-rate and, hence, they are attractive candidates as they do not require the newer and more expensive 25 G components and are less impaired by dispersion, thanks to their lower Baud-rate or the incorporated filtering.

Among the modulation formats investigated DMT provides the best gain in terms of spectral efficiency thanks to its capability to employ

complex modulation formats. However it has higher DSP requirements and requires high-speed ADCs and DACs which are expensive and power hungry. Even though DMT will not be chosen for the 25 Gb/s line rate in PONs, it could be considered again for future standards where the target bit-rate will be increased further. Large scale development of DMT will also depend heavily on the advance and cost of the underlying CMOS technology necessary to support its DSP requirements. PAM4 and EDB, on the other hand, are more likely to be adopted in the short term where they can enhance the performance of the 10 G generation of devices but will require higher bandwidth components to scale up to higher line rates. Hence, the availability and affordability of such higher speed components will be key to determine whether they could provide an attractive solution in future higher capacity PONs.

A novel linear BM-TIA, a key component necessary to support the mentioned advanced modulation formats in the upstream direction, was developed in Tyndall National Institute and analysed in this thesis. The idea behind this BM-TIA architecture removes the common issue of transients introduced by AC interfaces and the need for DC coupling among chip parts in the integrated circuit, making the fabrication cheaper and open to the integration of components from different vendors. The BM-TIA prototype is tested with 25 Gb/s PAM4 traffic and shows burst-mode capabilities with a settling time between bursts of less than 100 ns and a supported dynamic range of up to 13.3 dB.

An innovative way of exploiting PAM4 characteristics is also proposed as a solution to increase the power budget of PONs. A hierarchical modulation scheme for 25 Gb/s PAM4 downstream in PON systems is designed using interleaved detection of the tributary binary streams and unequally spaced levels of the PAM4 signal. The network power budget benefits from the improved MSB detector sensitivity, which is increased by up to 3.5 dB if a degree of asymmetry is present in the path losses. This receiver also has higher CD tolerance enabling data transmission over 40 km of fibre without the need for dispersion compensation techniques. An asymmetric network plant with ONUs at 12 km and 37 km is demonstrated, where the sensitivity of the latter has been improved to account for additional path losses and chromatic dispersion induced penalty.

In order to improve the tolerance to CD, which becomes a more seri-

ous impairment when the bit-rate is increased, two different techniques are reported, aimed at upstream and downstream. A DSP enabled burst-mode EDC is investigated as a solution for extended reach and bit-rate enhancement of PON upstream channels where CD is a performance limiting factor. Analyses of the requirements and performance of linear FFE and DFE filters are carried out for an adaptive burst-by-burst implementation that could find application in PON upstream channels with minimal impact on overhead requirements. Support for 25 Gb/s PAM4 burst-mode traffic is demonstrated, employing 10 G devices only, using a total preamble time of 200 ns, including BM-TIA settling time and EDC training. The system is also demonstrated to operate under a 25 km differential reach with the adaptive filter successfully compensating for the different amounts of CD in the bursts confirming adaptation times within 200 ns and, hence, that it is a suitable technology for PON upstream systems.

The issue of CD was also addressed in the optical domain, instead of the electrical domain, by designing a solution tailored for the downstream based on a CML transmitter. Narrow optical filtering is used to selectively suppress the adiabatically chirped components of a signal obtained through direct modulation to enhance its ER and allow the DML to operate in a regime where transient chirp is suppressed. Analysis of 25 Gb/s DML based chirp controlled transmitters, PAM4 and NRZ, is reported and their potential application as PON transmitters is demonstrated as they allow for a system configuration with a simple data-slicer at the receiver, while supporting up to 50 km SMF transmission in the dispersive C-band. A novel optical filter suppressing the blue-shift component of the chirped signal is proposed and demonstrated to offer the best overall performance when used in combination with PAM4 modulation. The transmitter filter engineers the eye diagram skewing caused by direct modulation of the laser in order to provide a pre-compensation that mitigates the effect of CD induced skewing during fibre propagation. This allows for longer reach and the potential of the scheme for transmission through lengths of SMF of up to 90 km is demonstrated, opening the possibility of its adoption in DCI or long-reach PONs.

Optical amplification strategies compatible with the upstream burst-mode traffic of PONs were analysed and discussed in Chapter 5 in order

to provide a solution to meet the power budget requirements of more spectrally efficient modulation formats.

Raman based amplifiers operating in the O-band were investigated for reach extension of the upstream transmission in PON scenarios. A DMT based PON system was integrated with distributed Raman amplification for reach extension. The upstream link employing G-PON O-band quantum dot DML transmitters adopted flexible data-rate DMT and transmission over a 40 km long optical trunk fibre was performed employing various reach extender solutions based on Raman optical amplification or/and SOA. The first quantum dot based Raman amplified XG-PON upstream was then demonstrated using 1210 nm pump lasers which allowed optical amplification in the 1270 nm window which is not reachable by other amplifier technologies. A pump power of 759 mW yielded a Raman on-off gain of 14.2 dB, which accommodated a total loss budget of 46.7 dB, allowing a fully passive network configuration with a total fibre length of more than 50 km and a split ratio of up to 1:64. Raman amplification in the 1310 nm O-band window was also presented for a 25 Gb/s upstream transmission using 1240 nm pumps. The reach of 25 Gb/s EDB and PAM4 transmissions systems, with 10 G class transmitter and receivers, was extended using backward propagating Raman amplification. A total loss budget in excess of 42 dB was demonstrated for both modulation formats allowing transmission over 40 km and accommodating 1:128 splits. For a 20 km OTL, a 41 dB loss budget was achieved, which allowed for a 1:512 split ratio.

An alternative solution was studied considering the use of SOAs to realise a pre-amplified OLT receiver for burst-mode traffic with optical power equalisation functionality. Driving the SOA with a variable bias current extended its dynamic range of operation and removed the need for an electronic BM-Rx. A characterisation of the SOA device showed its potential to be used with 25 Gb/s traffic and equalise a DR in excess of 27 dB. The different multi-level modulation formats used were PAM4, EDB and NRZ with duobinary detection, with the latter showing the best overall performance. The SOA showed potential to be used in its linear region over a wide DR and support the linearity requirements of multi-level amplitude modulation formats. A full burst-mode system was demonstrated to work with up to 27.3 dB of DR in optical B2B providing

improved sensitivity and without the need for an electronic BM-Rx. A commercial 10 GHz PIN photodiode with linear AC coupled TIA was used after the SOA burst equaliser. The system was demonstrated for the three modulation formats over an extended reach of 40 km of SMF without using CD compensation techniques. NRZ-EDB allowed for a power budget of 33.5 dB and 29.1 dB when 25 km and 40 km of SMF were used, respectively.

6.2 Future work

The 100 G PON standard is not in force yet and already the need for a 400 G system is being discussed and, eventually, 1 Tb/s networks will likely become the norm in less than a decade from now. During the coming years, the increase of single wavelength bit-rate beyond 25 Gb/s, to 40 or 50 Gb/s, will be the next challenge to be addressed in the short term. The increase of the Baud-rate in access systems is likely to plateau in the near future and, hence, both multi-level amplitude modulation and DMT could be successful in providing an appropriate solution making more efficient use of the available modulation bandwidth to increase the bit-rate. This will most likely happen with the support of DSP techniques for increasing complexity beyond linear filtering. Machine learning and neural networks could represent a more efficient alternative to FFE and DFE filters both for pre- and post-compensation purposes, provided they become available at an affordable price for access networks.

The development of multi-wavelength capable devices will also be a key point in the successful diffusion of WDM PONs. Increase in the number of wavelengths of WDM systems is a possible solution that could be more cost-effective than adopting single channel bit-rates beyond 40 Gb/s or 50 Gb/s, due to the complexity and cost of the electronics and opto-electronic devices required. The number of wavelengths and the choice of deploying either colourless or coloured devices will be determined by the research and development advances and, eventually, the fabrication cost of the necessary WDM components.

Optical amplification will also play an increasingly important role in next-generation systems where WDM operation and the increase of single-channel bit-rate will make it challenging to meet the power budget

requirements. SOAs are interesting because they enable monolithic integration with other optoelectronic devices, potentially reducing cost and physical footprint, and could represent a short term solution to increase the network power budget. However, SOA performance is limited in multi-wavelength systems due to channel crosstalk effects and gain saturation. In the longer term evolution, Raman amplification could provide a solution for WDM networks with numbers of channels in excess of four or eight, thanks to the very high saturation power that prevents gain compression and transient effects in the power regimes typical of PONs. It is also to be remembered that Raman amplifiers can be designed with an arbitrary optical gain profile and bandwidth in excess of 100 nm to accommodate multi-wavelength environments.

Looking at a later stage of PON evolution, as IMDD will reach its practical capacity limits, coherent transmission will likely find an increasing role for application in access networks, enabled by lower cost and simplified architectures of coherent DSP. A promising solution for the entry point of coherent technology in PONs is the use of a single coherent receiver at the OLT for the upstream traffic which will be more efficient in compensating for transmission impairments caused by the use of lower cost ONU transmitters and will see the cost of a single module shared among the users. The availability of technologies derived from core/metro networks at a more affordable price will be essential in determining when coherent solutions will take their place in access systems. The eventual adoption of coherent technologies in data-centre optical links could accelerate the development of simplified coherent transmission systems suitable for low-cost large-volume applications and their adoption in access networks.

List of Publications

Published journals and conferences

1. **M. Dalla Santa**, C. Antony, G. Talli, and P. D. Townsend , Variable Gain SOA Pre-Amplifier for Optical Equalization of a 25Gb/s Burst-Mode PON Upstream with 10G Optics," to be presented at Optical Fiber Communication Conference (OFC), San Diego, California, 2019, W4J.2.

2. **M. Dalla Santa**, C. Antony, M. Power, A. Jain, P. Ossieur, G. Talli, and P. D. Townsend , 25Gb/s PAM4 Burst-Mode System for Upstream Transmission in Passive Optical Networks," in Proc. Optical Fiber Communication Conference (OFC), Los Angeles, California, 2017, M3H.7.

3. **M. Dalla Santa**, C. Antony, G. Talli, and P. D. Townsend, "Chirp Control in Directly Modulated 25G PAM4 Transmitters for Optical Access Networks", in Proc. Conference on Lasers and Electro-Optics (CLEO), San Jose, California, 2017, SF1L.3

4. **M. Dalla Santa**, C. Antony, G. Talli and P. D. Townsend, "Power Budget Improvement in Passive Optical Networks Using PAM4 Hierarchical Modulation," in IEEE Photonics Technology Letters, vol. 29, no. 20, pp. 1747-1750, Oct. 15, 2017.

5. C. Antony, **M. Dalla Santa**, G. Talli, and P. D. Townsend, "Raman Amplification for O-band 25Gbps PAM-4 and Duobinary Using 10G Optics," in Proc. European Conference on Optical Communication (ECOC), Gothenburg, Sweden, 2017.

6. **M. Dalla Santa**, C. Antony, G. Talli, and P. D. Townsend, "25Gb/s PAM4 Adaptive Receiver Equalisation Requirements for

Burst-Mode Transmission Systems," in Proc. European Conference on Optical Communication (ECOC), Dsseldorf, Germany, 2016, Tu.3.F.2.

7. **M. Dalla Santa**, C. Antony, G. Talli, I. Krestnikov, and P. D. Townsend, "Burst-mode analysis of XGPON Raman reach extender employing quantum-dot lasers," Electronics Letters, v. 52, no. 13, pp. 1157-1158, 2016.

8. C. Antony, **M. Dalla Santa**, G. Talli, and P. D. Townsend, "Design and Performance Analysis of Raman Amplified XG-PON System," Journal of Lightwave Technology, vol. 34, no. 11, pp. 2692-2701, 2016.

9. C. Antony, G. Talli, **M. Dalla Santa**, B. Murray, S. Hegarty, E. Kehayas, I. Krestnikov, and P. D. Townsend, "XG-PON Raman reach extender based on quantum dot lasers," in Proc. European Conference on Optical Communication (ECOC), Cannes, France, 2014, Tu.3.2.4.

Unpublished conferences contributions

10. **M. Dalla Santa**, C. Antony, G. Talli and P. D. Townsend, "PAM4 Interleaved Detection System for Extended Power Budget in Passive Optical Networks" Photonics Ireland, Cork, 2018.

11. **M. Dalla Santa**, C. Antony, M. Power, A. Jain, P. Ossieur, G. Talli, and P.D. Townsend, "Burst-mode 25 Gb/s Solutions for Passive Optical Networks Upstream Channels" Photonics Ireland, Galway, 2017.

12. C. Antony, **M. Dalla Santa**, G. Talli, and P. Townsend, "Raman Amplification for Future 100G Optical Access Networks" Photonics Ireland, Galway, 2017.

13. **M. Dalla Santa**, C. Antony, G. Talli, S. Hegarty, I. Krestnikov, D. Byrne, and P. D. Townsend, "Optical OFDM for bit-rate Exten-

sion of GPON Directly Modulated Quantum Dot Transmitters“, Photonics Ireland, Cork, 2015.

14. C. Antony, **M. Dalla Santa**, G. Talli, and P. D. Townsend, “Design of Quantum Dot Based Raman Amplified Passive Optical Networks,“ Photonics Ireland, Cork, 2015.

Publicity and awards

15. “Quantum Networks,“ Electronics Letters, vol. 52, no. 13, pp. 1087-1087, 2016.

16. BOC Gases Bursary Award 2017.

List of Acronyms

Acronyms

100G-EPON 100G Ethernet passive optical network
ADC analog to digital converter
AFG arbitrary function generator
APD avalanche photodiode
ASE amplified spontaneous emission
AWG arbitrary waveform generator
AWGN additive-white-Gaussian-noise
AWG arrayed waveguide grating
B2B back-to-back
BER bit error rate
BM-Rx burst-mode receiver
BM-TIA burst-mode transimpedace amplifier
CAGR compound annual growth rate
CD chromatic dispersion
CDR clock data recovery
CID consecutive identical digits
CML chirp managed laser
CMOS complementary metal-oxide-semiconductor
CP cyclic prefix
CTF continuous-time filter
CWDM coarse wavelength division multiplexing
DAC digital to analog converter
DCF dispersion compensating fibre
DCI data centre interconnect
DFB distributed feedback
DFE decision-feedback equaliser

DFT discrete Fourier transform
DML directly modulated laser
DMT discrete multitone
DR dynamic range
DSL digital subscriber line
DSO digital storage oscilloscope
DSP digital signal processing
EAM electro-absorption modulator
ED error detector
EDB electrical duo-binary
EDC electronic dispersion compensation
EDFA erbium doped fibre amplifier
EML externally modulated transmitter
EPON Ethernet passive optical network
ER extinction ratio
FBG fibre Bragg grating
FEC forward error correction
FFE feed-forward equaliser
FFT fast Fourier transform
FPGA field-programmable gate array
FSE fractionally-spaced equaliser
FTTB fibre to the building
FTTC fibre to the cabinet
FTTH fibre to the home
FTTN fibre to the node
FTTx fibre to the x
FWM four-wave mixing
G-PON Gigabit-capable passive optical network
HS-PON high-speed passive optical network
IDFT inverse discrete Fourier transform
IEEE Institute of Electrical and Electronics Engineers
IFFT inverse fast Fourier transform
IMDD intensity-modulation/direct-detection
ISI inter-symbol interference
ITU International Telecommunication Union
LI light current

LMS least mean square
LSB least significant bit
MLSE maximum likelihood sequence estimation
MQW multiple quantum well
MSB most significant bit
MSE mean squared error
MZM Mach-Zehnder modulator
NEP noise equivalent power
NF noise figure
NG-PON 2 next-generation passive optical network 2
NRZ non-return to zero
NRZ-EDB non-return to zero with duobinary detection
ODN optical distribution network
OECD Organisation for Economic Co-operation and Development
OFDM orthogonal frequency division multiplexing
OLT optical line terminal
ONU optical network unit
OOK on-off keying
OSA optical spectrum analyser
OSNR optical signal to noise ratio
OTL optical trunk line
PA post-amplifier
PAM4 4-level pulse-amplitude modulation
PBC polarisation beam combiner
PIN positive-intrinsic-negative
PMD polarisation mode dispersion
PON passive optical network
PRBS pseudo random binary sequence
P/S parallel-to-serial
PSK phase-shift keying
QAM quadrature amplitude modulation
QD quantum dot
QPSK quadrature phase-shift keying
RF radio frequency
RIN relative intensity noise
SBS stimulated Brillouin scattering

SER symbol error rate
SMF single mode fibre
SNR signal to noise ratio
SOA semiconductor optical amplifier
S/P serial-to-parallel
SPM self-phase modulation
SRS stimulated Raman scattering
SSE symbol-spaced equaliser
TDCM tuneable dispersion compensation module
TDL tuneable diode laser
TDM time division multiplexing
TDMA time division multiple access
TIA transimpedance amplifier
TWDM time and wavelength division multiplexing
VOA variable optical attenuator
WDM wavelength division multiplexing
xDSL digital subscriber line
XG-PON 10-Gigabit-capable passive optical network
XPM cross-phase modulation

List of Figures

1.1 Structure of the Internet physical network layers. Adapted from [2]. 2
1.2 Percentage of fibre based fixed-broadband in OECD countries, December 2017. 4
1.3 Fibre based fixed-broadband growth from December 2016 to December 2017 in OECD countries. 4
1.4 Access medium distribution between 2013 and 2017 in Sweden [5]. 5
1.5 Major impairments in PON systems addressed in this thesis. 6
1.6 Overview of contributions presented in the thesis with relevant Sections in brackets. 9
1.7 Areas of investigation in PONs addressed in this thesis. . 9

2.1 Optical access networks architectures. 14
2.2 Passive optical network structure. 15
2.3 Evolution of PON standards capacities in 20 years. . . . 17
2.4 Gaussian distribution of binary symbols and decision regions. 20
2.5 Generation of an eye diagram through superposition of delayed copies of a waveform. 22
2.6 Binary eye diagram with constellation symbol distributions at the sampling point. 22
2.7 Effect of various optical link impairments on a binary eye diagram. 23
2.8 BER of a thermal noise limited 10 Gb/s NRZ OOK transmission. 29
2.9 SMF attenuation profile for different generations of fibre and transmission windows used for optical communication [30]. 32

2.10 Inter-symbol interference caused by pulse spreading over dispersive fibre. 34

3.1 DMT generation scheme and frequency distribution of the resultant signal. 54
3.2 DMT sub-carriers SNR profile without and with power loading adjustment at the transmitter. 55
3.3 DMT transmitter block diagram. 57
3.4 DMT receiver block diagram. 58
3.5 Experimental setup for DMT performance characterisation. 60
3.6 Measured bandwidth of DML transmitter under increasing bias. 60
3.7 System frequency response and power loading profile for data-carrying sub-carriers, with a 5 GBd DMT modulation. 61
3.8 BER measured for data sub-carriers with and without power re-distribution. 63
3.9 Experimental sensitivities in optical B2B for DMT signals at various Baud-rates and NRZ-OOK. 63
3.10 Eye diagrams measured in optical B2B and detection schemes for the three modulation formats: a) OOK NRZ, b) EDB and c) PAM4. 67
3.11 Block diagram of a duobinary transmitter with pre-coder and duobinary encoder. 68
3.12 Experimental setup for BER measurement of different modulation formats in a 10 G network. 71
3.13 Error rate probability of different modulation formats using 10 G class optoelectronic components. 72
3.14 Experimental setup for receiver bandwidth requirements measurements. 73
3.15 Spectra of the three modulation formats at 25 Gb/s at the output of the 2-bit DAC. 74
3.16 Sensitivities of the four modulation formats as a function of the 3 dB bandwidth of the receiver. 75
3.17 Sensitivities of the three modulation formats as a function of the 3 dB bandwidth of the receiver for a 10 G system. 76
3.18 Experimental setup for chromatic dispersion measurements. 77

3.19 Sensitivity of a 25 Gb/s NRZ signal for various EAM bias. 78
3.20 Sensitivity of a 25 Gb/s EDB signal for various EAM bias. 78
3.21 Sensitivity of a 25 Gb/s NRZ signal with EDB detection for various EAM bias. 79
3.22 Sensitivity of a 25 Gb/s PAM4 signal for various EAM bias. 80
3.23 Sensitivity of NRZ, EDB, NRZ-EDB and PAM4 modulation under increasing chromatic dispersion. 81
3.24 Comparison of coupling schemes for BM-TIA and BM PA: a) AC-coupled interface, b) DC-coupled interface, c) AC-coupled interface with novel TIA design. 84
3.25 Block diagram of developed BM-TIA. 86
3.26 Measured bandwidth of BM-TIA. 87
3.27 Packaged BM-TIA on optical probe station. 87
3.28 Experimental setup for BM-TIA characterisation. 88
3.29 Settling time of BM-TIA for different restoration-loop bandwidths. 89
3.30 BER penalty induced by baseline wander. 91
3.31 Error distributions along the PRBS patterns for different capacitance settings. Insets show the electrical waveform with visible baseline wandering in one case. 92
3.32 BER curves in continuous mode and burst-mode. 93
3.33 PON system with PAM4 hierarchical modulation. 95
3.34 Gray coded PAM4 generation and interleaved detection of the tributary NRZ streams. 96
3.35 MSB and LSB receivers for PAM4 interleaved detection. 96
3.36 Eye diagrams with increasing asymmetry levels. 98
3.37 Theoretical BER curves for MSB and LSB receivers under different R_{lm}. 100
3.38 Sensitivities and differential power budget for MSB and LSB receivers under different R_{lm}. 100
3.39 Experimental setup for hierarchically modulated PAM4 characterisation. 101
3.40 BER curves for optical back-to-back transmission. 103
3.41 Power margin and differential power budget in asymmetric PON. 103
3.42 Sensitivity for different fibre spans and R_{lm}. 104

3.43 BER curves for 12 km and 24 km ONUs with various R_{lm}. 105
3.44 BER curves for 12 km and 37 km ONUs with various R_{lm}. 106

4.1 Pulse spreading through a dispersive channel and induced ISI between successive pulses. 113
4.2 Block diagram of linear equaliser with FFE and DFE. . . 113
4.3 Schematic of linear equaliser with FFE and DFE where delay blocks and tap coefficients are visible. 114
4.4 Block diagram of FFE and DFE equaliser with burst-by-burst adaptive training feature. 115
4.5 Experimental setup for EDC filter characterisation with 25 Gb/s PAM4. 117
4.6 Logical structure of the optical bursts used in the experiment. 118
4.7 Sensitivity penalty for various FFE taps spacings. . . . 119
4.8 Sensitivity penalty for various FFE taps spacings as a function of input signal phase-delay. 120
4.9 Sensitivity penalty for various FFE reference taps. . . . 121
4.10 Sensitivity for various numbers of FFE coefficient in a $\frac{T}{2}$ FSE. 122
4.11 Sensitivity for various reference taps of the equaliser in a filter with various DFE sizes. 123
4.12 Sensitivities for various $\frac{T}{2}$ FFE and DFE numbers of tap combinations after 25 km SMF. 124
4.13 Sensitivities for various $\frac{T}{2}$ FFE and DFE numbers of tap combinations after 40 km SMF. 124
4.14 Sensitivities for various sizes $\frac{T}{2}$ FFEs combined with a 5-taps DFE. 125
4.15 Sensitivity penalty for combination of LMS gains and training sequence lengths. 126
4.16 Structure of bursts for FFE training with either NRZ or PAM4 training sequence. 127
4.17 MSE measured for various training sequence lengths and LMS gains using binary or multi-level training. 128

4.18 BER curves using various LMS gain coefficients during the payload adaptation for a) FFE only filters and b) FFE with DFE filters. 129
4.19 Sensitivity penalty for various EDC filters under increasing chromatic dispersion. 131
4.20 Sensitivity penalty for various training sequences of the FFE under increasing chromatic dispersion. 132
4.21 Sensitivity penalty for various transmitter bandwidth using different filters. 133
4.22 Sensitivity penalty for various receiver bandwidths. . . . 133
4.23 Sensitivity penalty for R_{lm} degradation of the PAM4 signal. 135
4.24 Experimental setup for 25 Gb/s PAM4 burst-mode upstream traffic. 136
4.25 Optical burst-mode upstream traffic with a 14 dB DR between soft and loud burst. 136
4.26 Optical burst-mode upstream traffic with a 14.7 dB DR between soft and loud burst. 138
4.27 Optical burst-mode upstream traffic with a 13 dB DR between soft and loud burst after 25 km. 139
4.28 BER performance of soft and loud bursts under different differential fibre reach conditions. 140
4.29 Experimentally measured LI curve of an ExOptronics EX-DY7005-C high-speed DFB laser. 144
4.30 Experimentally measured chirp traces of an ExOptronics EX-DY7005-C DML under different bias conditions. . . . 145
4.31 Measured chirp magnitude under varying DML bias conditions. 146
4.32 Measured adiabatic and transient chirp magnitudes for different bias conditions of the DML. 146
4.33 Operation regimes for a DML transmitter. 148
4.34 Measured total chirp magnitude and corresponding ER of the signal. 148
4.35 Magnitude of adiabatic and transient chirp as a function of the signal ER for different laser bias. 149

4.36 Sensitivities for a 10^{-3} BER in the PAM4 system, in optical B2B and with 12 km of SMF. 150
4.37 DML followed by a narrow optical filter to improve signal ER. 151
4.38 Adiabatic chirped spectral component for a 2 and 4 level amplitude modulated signal. 152
4.39 Measured optical spectra of EX-DY7005-C DML for a) 2 and b) 4 level amplitude modulated signal at 1 GHz. . . 152
4.40 Two optical filters adopted for chirp management of a PAM4 signal. 153
4.41 Experimental setup for characterisation of CML transmitters. 154
4.42 Sensitivities for a 10^{-3} BER in the NRZ system for a) red-shift filter and b) blue-shift filter. 156
4.43 Sensitivities for a 10^{-3} BER in the PAM4 system for a) red-shift filter ans b) blue-shift filter. 157
4.44 Sensitivities for a 10^{-3} BER after 50 km comparing three filters. 158
4.45 Ideal and skewed PAM4 eye diagrams and corresponding standard deviation of the signal rails. 159
4.46 25 Gb/s PAM4 eye diagrams in B2B and after 50 km for the two filtering techniques. 160
4.47 BER curves after a 50 km SMF for 25 Gb/s PAM4 with FFE employed at the receiver. 161
4.48 BER curves for 25 Gb/s PAM4 transmitter with blue-shift filter, for PIN and APD receivers. 162

5.1 Generation of a Stokes photon through spontaneous Raman scattering. 167
5.2 Signal optical amplification via stimulated Raman scattering in a silica optical fibre. 167
5.3 Schematic of a Raman optical amplifier. 168
5.4 Experimental setup for on-off Raman gain measurements. 171
5.5 Raman on-off gain spectrum for 1240 nm pump lasers. . 172
5.6 Experimental setup for the characterisation of various reach extender configurations in a DMT upstream system. 173

5.7 Measured sensitivities of DMT signals with different bit-rates for various reach extender configurations. 175
5.8 Raman on-off gain spectrum for 1210 nm pump lasers. . 178
5.9 Experimental setup for Raman amplifier characterisation in an XG-PON system. 179
5.10 BER curves as a function of the OTL input power for different Raman pump powers. 181
5.11 Raman on-off gain and signal OSNR for different attenuation of the ODN. 182
5.12 BER curves for different input powers into the OTL fibre. 183
5.13 Sensitivity at the OLT receiver measured at a BER of 10^{-4} for different input powers into the OTL fibre. 183
5.14 Penalty at the OLT receiver for different input powers into the OTL fibre for a continuous mode and burst-mode transmission. 185
5.15 Experimental setup for Raman amplifier characterisation in a PON system. 186
5.16 Measured OSNR and Raman on-off gain for different fibre lengths. 188
5.17 Raman on-off gain for various lengths of the OTL fibre. . 189
5.18 Net signal gain along the OTL fibre for various SMF lengths. 190
5.19 BER curves for the 25 Gb/s EDB system for various receivers. 190
5.20 BER curves for the 25 Gb/s PAM4 system for various receivers. 191
5.21 BER curves for the 25 Gb/s EDB system for various fibre lengths and two receivers type. 192
5.22 Supported ODN loss at a BER sensitivity of 10^{-3} for the 25 Gb/s EDB system. 193
5.23 BER curves for the 25 Gb/s PAM4 system for various fibre lengths and three receivers type. 194
5.24 Supported ODN loss at a BER sensitivity of 10^{-3} for the 25 Gb/s PAM4 system. 195
5.25 Schematic representation of semiconductor optical amplifier. 197
5.26 Experimental setup for optical B2B continuous mode SOA characterisation. 200

5.27 Output power of the SOA for varying input powers and bias currents. 200
5.28 Gain of SOA as a function of its input power for different bias currents. 201
5.29 Saturation input power of SOA as a function of its bias current. 201
5.30 OSNR of SOA as a function of its input power for different bias currents. 202
5.31 Operational conditions of the SOA to obtain a constant desired output power for a given input power. 203
5.32 Experimental setup for optical B2B continuous mode SOA characterisation. 204
5.33 Sensitivities for the SOA output under various operating conditions for an NRZ system with EDB detection. . . . 204
5.34 Sensitivities for the SOA output under various operating conditions for an EDB system. 205
5.35 Sensitivities for the SOA output under various operating conditions for an PAM4 system. 206
5.36 SOA input power ranges within a 1 dB or 3 dB sensitivity penalty for a fixed gain SOA pre-amplified receiver. . . . 207
5.37 Sensitivity map of the SOA pre-amplifier for the NRZ system with EDB detection. 208
5.38 Sensitivity map of the SOA pre-amplifier for the EDB system. 208
5.39 Sensitivity map of the SOA pre-amplifier for the PAM4 system. 209
5.40 Sensitivity of the SOA output along a constant output power operating condition for the NRZ system with EDB detection. 209
5.41 Sensitivity of the SOA output along a constant output power operating condition for the EDB system. 210
5.42 Sensitivity of the SOA output along a constant output power operating condition for the PAM4 system. 210
5.43 Experimental setup for for burst-mode traffic analysis with SOA based pre-amplified receiver performing optical equalisation. 212

5.44 BER curves for soft and loud bursts in optical back-to-back. 214
5.45 BER curves of soft and loud bursts for different fibre lengths and optical filter bandwidth. 215
5.46 BER curves of soft and loud bursts and eye diagrams of the loud burst under different DR conditions for NRZ-EDB in optical B2B. 216
5.47 Optical spectrum, optical waveform before SOA equalisation and electrical waveform after power equalisation for increasing DR measured with the NRZ-EDB system. . . 218
5.48 BER curves of soft and loud bursts and eye diagrams of the loud burst under different DR conditions for NRZ-EDB with 25 km of SMF. 219
5.49 BER curves of soft and loud bursts and eye diagrams of the loud burst under different DR conditions for NRZ-EDB with 40 km of SMF. 220
5.50 BER curves of soft and loud bursts and eye diagrams of the loud burst under different DR conditions for EDB in optical B2B. 221
5.51 BER curves of soft and loud bursts and eye diagrams of the loud burst under different DR conditions for EDB with 25 km of SMF. 221
5.52 BER curves of soft and loud bursts and eye diagrams of the loud burst under different DR conditions for EDB with 40 km of SMF. 222
5.53 BER curves of soft and loud bursts and eye diagrams of the loud burst under different DR conditions for PAM4 in optical B2B. 223
5.54 BER curves of soft and loud bursts and eye diagrams of the loud burst under different DR conditions for PAM4 with 25 km of SMF. 223
5.55 BER curves of soft and loud bursts and eye diagrams of the loud burst under different DR conditions for PAM4 with 40 km of SMF. 224

Bibliography

[1] Cisco, "Cisco VNI Global IP Traffic Forecast, 20162021." Cisco, Tech. Rep., 2017.

[2] Huangxi, "Bandwidth Needs in Core and Aggregation nodes in the Optical Transport Network, http://www.ieee802.org/3/ad_hoc/bwa/public/nov11/huang_01_1111.pdf," Tech. Rep., 2011.

[3] https://www.itu.int/en/ITU-D/Statistics/Documents/facts/ICTFactsFigures2017.pdf, [Online; accessed October-2018].

[4] http://www.oecd.org/sti/broadband/broadband-statistics, [Online; accessed October-2018].

[5] http://www.ftthcouncil.eu/documents/FTTH_Council_report__FINAL_and_proofread-update-20180214.pdf, [Online; accessed October-2018].

[6] https://www.zionmarketresearch.com/report/gpon-equipment-market, [Online; accessed October-2018].

[7] X. Liu and F. Effenberger, "Emerging optical access network technologies for 5G wireless [invited]," *IEEE/OSA Journal of Optical Communications and Networking*, vol. 8, no. 12, pp. B70–B79, 2016.

[8] J. S. Wey and J. Zhang, "Passive Optical Networks for 5G Transport: Technology and Standards," *Journal of Lightwave Technology*, pp. 1–1, 2018.

[9] F. C. Europe, "Fibre for 5G: a story of convergence," FTTH Council Europe, Tech. Rep., 2018.

[10] http://techblog.comsoc.org/tag/gpon/, [Online; accessed October-2018].

[11] http://www.ieee802.org/3/ca/, [Online; accessed October-2018].

[12] *G.sup64: PON transmission technologies above 10 Gbit/s per wavelength;*, ITU-T Standard, 2018.

[13] F. Effenberger, "Future Broadband Access Networks [Point of View]," *Proceedings of the IEEE*, vol. 104, no. 11, pp. 2078–2081, 2016.

[14] D. Nesset, "PON roadmap [invited]," *IEEE/OSA Journal of Optical Communications and Networking*, vol. 9, no. 1, pp. A71–A76, 2017.

[15] K. Wang, C. Masmachuca, L. Wosinska, P. J. Urban, A. Gavler, K. Brunnstrom, and J. Chen, "Techno-economic analysis of active optical network migration toward next-generation optical access," *IEEE/OSA Journal of Optical Communications and Networking*, vol. 9, no. 4, pp. 327–341, 2017.

[16] *G.984.2: Gigabit-capable Passive Optical Networks (G-PON): Physical Media Dependent (PMD) layer specification*, ITU-T Standard, 2008.

[17] *G.987.2: 10-Gigabit-capable passive optical networks (XG-PON): Physical media dependent (PMD) layer specification*, ITU-T Standard, 2010.

[18] *G.989.2: 40-Gigabit-capable passive optical networks 2 (NG-PON2): Physical media dependent (PMD) layer specification*, ITU-T Standard, 2014.

[19] *G.9807.1: 10 Gigabit-capable passive optical networks (XG(S)-PON)*, ITU-T Standard, 2016.

[20] G. P. Agrawal, *"Fiber-Optic Communication Systems, third edition"*. Wiley, 2002.

[21] D. Marcuse, "Derivation of analytical expressions for the bit-error probability in lightwave systems with optical amplifiers," *Journal of Lightwave Technology*, vol. 8, no. 12, pp. 1816–1823, 1990.

[22] K. Szczerba, P. Westbergh, J. Karout, J. Gustavsson, x00C, Haglund, M. Karlsson, P. Andrekson, E. Agrell, and A. Larsson, "4-PAM for high-speed short-range optical communications," *IEEE/OSA Journal of Optical Communications and Networking*, vol. 4, no. 11, pp. 885–894, 2012.

[23] C. G. Benvenuto N., *"Algorithms for Communications Systems and Their Applications"*. Wiley, 2004.

[24] E. Sackinger, *"Broadband Circuits for Optical Fiber Communication"*. Wiley, 2005.

[25] N. Massa, *Fundamentals of Photonics*. SPIE, 2000, ch. Fiber Optic Telecommunication.

[26] R. J. Nuyts, L. D. Tzeng, O. Mizuhara, and P. Gallion, "Effect of transmitter speed and receiver bandwidth on the eye margin performance of a 10-Gb/s optical fiber transmission system," *IEEE Photonics Technology Letters*, vol. 9, no. 4, pp. 532–534, 1997.

[27] B. R. G. W. Dakin J. P., *"Handbook of Optoelectronics"*. Taylor & Francis Group, 2006.

[28] K. T. Ajoy Ghatak, *"An Introduction to Fiber Optics"*. Cambridge University Press, 1998.

[29] Z. M. Benvenuto N., *"Principles of Communication Networks and Systems"*. Wiley, 2011.

[30] Cisco, "Fiber Types in Gigabit Optical Communications," Cisco, Tech. Rep., 2008.

[31] J. A. Jay, "An Overview of Macrobending and Microbending of Optical Fibers," Corning, Tech. Rep., 2010.

[32] N. A. Olsson, "Lightwave systems with optical amplifiers," *Journal of Lightwave Technology*, vol. 7, no. 7, pp. 1071–1082, 1989.

[33] G. R. Walker, R. C. Steele, and N. G. Walker, "Optical amplifier noise figure in a coherent optical transmission system," *Journal of Lightwave Technology*, vol. 8, no. 9, pp. 1409–1413, 1990.

[34] D. T. v. Veen and V. E. Houtsma, "Proposals for Cost-Effectively Upgrading Passive Optical Networks to a 25G Line Rate," *Journal of Lightwave Technology*, vol. 35, no. 6, pp. 1180–1187, 2017.

[35] J. Chen, A. Tan, Z. Li, Y. Guo, Y. Yin, Q. Zhang, Y. Song, Y. Li, and M. Wang, "Adaptive Equalization Enabled 25Gb/s NRZ Modulation Based on 10-G Class Optics for Upstream Burst-Mode Transmission," in *Optical Fiber Communication Conference*, ser. OSA Technical Digest (online). Optical Society of America, 2018, Conference Proceedings, p. M1B.8.

[36] A. Stark and T. Detwiler, "Equalization strategies for 25G PON," in *2017 Optical Fiber Communications Conference and Exhibition (OFC)*, 2017, Conference Proceedings, pp. 1–3.

[37] J. Xia, Z. Li, Y. Li, T. Xu, J. Chen, Y. Song, and M. Wang, "Comparison of NRZ and duo-binary format in adaptive equalization assisted 10G-optics based 25G-EPON," *Optics Communications*, vol. 410, pp. 328–332, 2018.

[38] Z. Li, J. Xia, Y. Guo, Y. Yin, Y. Li, Y. Song, J. Chen, and M. Wang, "Investigation on the equalization techniques for 10G-class optics enabled 25G-EPON," *Optics Express*, vol. 25, no. 14, pp. 16 228–16 234, 2017.

[39] J. Man, S. Fu, H. Zhang, J. Gao, L. Zeng, and X. Liu, "Downstream Transmission of Pre-Distorted 25-Gb/s Faster-than-Nyquist PON with 10G-Class Optics Achieving over 31 dB Link Budget without Optical Amplification," in *Optical Fiber Communication Conference*, ser. OSA Technical Digest (online). Optical Society of America, 2016, Conference Proceedings, p. Th1I.5.

[40] M. Tao, L. Zhou, S. Yao, D. Zou, S. Li, H. Lin, and X. Liu, "28-Gb/s/, TDM-PON with narrow filter compensation and enhanced FEC supporting 31.5 dB link loss budget after 20-km downstream

transmission in the C-band," in *2016 Optical Fiber Communications Conference and Exhibition (OFC)*, 2016, Conference Proceedings, pp. 1–3.

[41] J. Zhou, C. Yu, G. Mohan, and H. Kim, "25-Gb/s OOK Transmission Using 1.5um 10G-Class VCSEL for Optical Access Network," *Journal of Lightwave Technology*, vol. 34, no. 16, pp. 3790–3795, 2016.

[42] J. Xia, Z. Li, Y. Li, T. Xu, J. Chen, Y. Song, and M. Wang, "Comparison of NRZ and duo-binary format in adaptive equalization assisted 10G-optics based 25G-EPON," *Optics Communications*, vol. 410, pp. 328–332, 2018.

[43] H. Ji, L. Yi, Z. Li, L. Xue, X. Li, Q. Yang, S. Wang, Y. Yang, S. Yu, and W. Hu, "Field Demonstration of a Real-Time 100-Gb/s PON Based on 10G-Class Optical Devices," *Journal of Lightwave Technology*, vol. 35, no. 10, pp. 1914–1921, 2017.

[44] L. Xue, L. Yi, H. Ji, P. Li, and W. Hu, "Symmetric 100-Gb/s TWDM-PON in O-Band Based on 10G-Class Optical Devices Enabled by Dispersion-Supported Equalization," *Journal of Lightwave Technology*, vol. 36, no. 2, pp. 580–586, 2018.

[45] V. Houtsma and D. van Veen, "A Study of Options for High-Speed TDM-PON Beyond 10G," *Journal of Lightwave Technology*, vol. 35, no. 4, 2017.

[46] Z. Li, L. Yi, H. Ji, and W. Hu, "100-Gb/s TWDM-PON based on 10G optical devices," *Optics Express*, vol. 24, no. 12, pp. 12 941–12 948, 2016.

[47] R. V. D. Linden, N. C. Tran, E. Tangdiongga, and A. M. J. Koonen, "Increasing flexibility and capacity in real PON deployments by using 2/4/8-PAM formats," *IEEE/OSA Journal of Optical Communications and Networking*, vol. 9, no. 1, pp. A1–A8, 2017.

[48] Z. Li, L. Yi, X. Wang, and W. Hu, "28 Gb/s duobinary signal transmission over 40 km based on 10 GHz DML and PIN for 100

Gb/s PON," *Optics Express*, vol. 23, no. 16, pp. 20 249–20 256, 2015.

[49] X. Li, S. Zhou, H. Ji, M. Luo, Q. Yang, L. Yi, R. Hu, C. Li, S. Fu, A. Alphones, W. D. Zhong, and C. Yu, "Transmission of 4x28-Gb/s PAM-4 over 160-km single mode fiber using 10G-class DML and photodiode," in *2016 Optical Fiber Communications Conference and Exhibition (OFC)*, 2016, Conference Proceedings, pp. 1–3.

[50] C. Ye, X. Hu, and K. Zhang, "Demonstration and Analysis on PAM-4/8, DB-PAM-2/4 and DMT Formatted TDM-PON with 25Gbps, 40Gbps, 50Gbps Capacity per Lane using Economical 10Gbps," in *ECOC 2016; 42nd European Conference on Optical Communication*, 2016, Conference Proceedings, pp. 1–3.

[51] C. Antony, M. Dalla Santa, G. Talli, and P. D. Townsend, "Raman Amplification for O-band 25Gbps PAM-4 and Duobinary Using 10G Optics," in *2017 European Conference on Optical Communication (ECOC)*, 2017, Conference Proceedings, pp. 1–3.

[52] M. Dalla Santa, C. Antony, G. Talli, and P. D. Townsend, "Chirp Control in Directly Modulated 25G PAM4 Transmitters for Optical Access Networks," in *Conference on Lasers and Electro-Optics*, ser. OSA Technical Digest (online). Optical Society of America, 2017, Conference Proceedings.

[53] M. Dalla Santa, C. Antony, G. Talli, and P. Townsend, "25Gb/s PAM4 Adaptive Receiver Equalisation Requirements for Burst-Mode Transmission Systems," in *ECOC 2016, 42nd European Conference on Optical Communication*, 2016, Conference Proceedings.

[54] M. Dalla Santa, C. Antony, M. Power, A. Jain, P. Ossieur, G. Talli, and P. D. Townsend, "25Gb/s PAM4 Burst-Mode System for Upstream Transmission in Passive Optical Networks," in *Optical Fiber Communication Conference*, ser. OSA Technical Digest (online). Optical Society of America, 2017, Conference Proceedings.

[55] M. Dalla Santa, C. Antony, G. Talli, and P. D. Townsend, "Power Budget Improvement in Passive Optical Networks Using PAM4

Hierarchical Modulation," *IEEE Photonics Technology Letters*, vol. 29, no. 20, 2017.

[56] A. Gatto, P. Parolari, C. Neumeyr, and P. Boffi, "Beyond 25 Gb/s Directly-Modulated Widely Tunable VCSEL for Next Generation Access Network," in *2018 Optical Fiber Communications Conference and Exposition (OFC)*, 2018, Conference Proceedings, pp. 1–3.

[57] C. Wagner, A. Dochhan, M. H. Eiselt, K. Grobe, M. Ortsiefer, C. Grus, C. Neumeyr, S. Paul, J. Cesar, F. Kppers, J. J. V. Olmos, and I. T. Monroy, "26-Gb/s DMT Transmission Using Full *C* -Band Tunable VCSEL for Converged PONs," *IEEE Photonics Technology Letters*, vol. 29, no. 17, pp. 1475–1478, 2017.

[58] M. Tao, L. Zhou, H. Zeng, S. Li, and X. Liu, "50-Gb/s/ TDM-PON based on 10G DML and 10G APD supporting PR10 link loss budget after 20-km downstream transmission in the O-band," in *2017 Optical Fiber Communications Conference and Exhibition (OFC)*, 2016, Conference Proceedings, pp. 1–3.

[59] M. Tao, H. Zeng, L. Zhou, S. Yao, S. Li, and X. Liu, "Experimental Demonstration of 25/30/40-Gb/s Flexible-PON Downstream Transmission by Using Pre-Compensated DMT with Adaptive Modulation/Bandwidth and," in *ECOC 2016; 42nd European Conference on Optical Communication*, 2016, Conference Proceedings, pp. 1–3.

[60] C. Qin, V. Houtsma, D. V. Veen, J. Lee, H. Chow, and P. Vetter, "40 Gbps PON with 23 dB power budget using 10 Gbps optics and DMT," in *2017 Optical Fiber Communications Conference and Exhibition (OFC)*, 2017, Conference Proceedings, pp. 1–3.

[61] T. Takahara, T. Tanaka, M. Nishihara, Y. Kai, L. Lei, T. Zhenning, and J. C. Rasmussen, "Discrete Multi-Tone for 100 Gb/s optical access networks," in *OFC 2014*, 2014, Conference Proceedings, pp. 1–3.

[62] N. Eiselt, D. Muench, A. Dochhan, H. Griesser, M. Eiselt, J. J. V. Olmos, I. T. Monroy, and J. P. Elbers, "Performance Comparison

of 112-Gb/s DMT, Nyquist PAM4, and Partial-Response PAM4 for Future 5G Ethernet-Based Fronthaul Architecture," *Journal of Lightwave Technology*, vol. 36, no. 10, pp. 1807–1814, 2018.

[63] R. Hirai and N. Kikuchi, "Experimental demonstration of 100G/lambda Nyquist-PAM4 transmission with digital pre-equalization of chromatic dispersion for extended-reach 400GbE," in *Optical Fiber Communications Conference and Exhibition (OFC), 2015*, 2015, Conference Proceedings, pp. 1–3.

[64] J. Wei, N. Eiselt, H. Griesser, K. Grobe, M. H. Eiselt, J. J. V. Olmos, I. T. Monroy, and J. P. Elbers, "Demonstration of the First Real-Time End-to-End 40-Gb/s PAM-4 for Next-Generation Access Applications Using 10-Gb/s Transmitter," *Journal of Lightwave Technology*, vol. 34, no. 7, pp. 1628–1635, 2016.

[65] S. Yin, D. van Veen, V. Houtsma, and P. Vetter, "Investigation of Symmetrical Optical Amplified 40 Gbps PAM-4/Duobinary TDM-PON using 10G Optics and DSP," in *Optical Fiber Communication Conference*, ser. OSA Technical Digest (online). Optical Society of America, 2016, Conference Proceedings, p. Tu3C.2.

[66] C. Chen, T. Xuefeng, and Z. Zhuhong, "Transmission of 56-Gb/s PAM-4 over 26-km single mode fiber using maximum likelihood sequence estimation," in *Optical Fiber Communications Conference and Exhibition (OFC), 2015*, 2015, Conference Proceedings, pp. 1–3.

[67] P. Li, L. Yi, L. Xue, and W. Hu, "56 Gbps IM/DD PON based on 10G-Class Optical Devices with 29 dB Loss Budget Enabled by Machine Learning," in *Optical Fiber Communication Conference*, ser. OSA Technical Digest (online). Optical Society of America, 2018, Conference Proceedings, p. M2B.2.

[68] L. Xue, L. Yi, P. Li, and W. Hu, "50-Gb/s TDM-PON Based on 10G-Class Devices by Optics-simplified DSP," in *Optical Fiber Communication Conference*, ser. OSA Technical Digest (online). Optical Society of America, 2018, Conference Proceedings, p. M2B.4.

[69] K. Zhang, Q. Zhuge, H. Xin, Z. Xing, M. Xiang, S. Fan, L. Yi, W. Hu, and D. V. Plant, "Demonstration of 50Gb/s/ Symmetric PAM4 TDM-PON with 10G-class Optics and DSP-free ONUs in the O-band," in *Optical Fiber Communication Conference*, ser. OSA Technical Digest (online). Optical Society of America, 2018, Conference Proceedings, p. M1B.5.

[70] J. Zhang, J. Yu, J. Shi, J. S. Wey, X. Huang, Y. Guo, Z. Ma, and M. Li, "64-Gb/s/A Downstream Transmission for PAM-4 TDM-PON with Centralized DSP and 10G Low-Complexity Receiver in C-Band," in *2017 European Conference on Optical Communication (ECOC)*, 2017, Conference Proceedings, pp. 1–3.

[71] P. Ossieur, N. A. Quadir, S. Porto, M. Rensing, C. Antony, W. Han, P. O'Brien, Y. Chang, and P. D. Townsend, "A 10G linear burst-mode receiver supporting electronic dispersion compensation for extended-reach optical links," in *Optical Communication (ECOC), 2011 37th European Conference and Exhibition on*, 2011, Conference Proceedings, pp. 1–3.

[72] S. Porto, C. Antony, A. Jain, D. Kelly, D. Carey, G. Talli, P. Ossieur, and P. D. Townsend, "Demonstration of 10 Gbit/s burst-mode transmission using a linear burst-mode receiver and burst-mode electronic equalization [invited]," *Optical Communications and Networking, IEEE/OSA Journal of*, vol. 7, no. 1, pp. A118–A125, 2015.

[73] X. Yin, B. Moeneclaey, X.-Z. Qiu, J. Verbrugghe, K. Verheyen, J. Bauwelinck, J. Vandewege, M. Achouche, and Y. Chang, "A 10Gb/s APD-based linear burst-mode receiver with 31dB dynamic range for reach-extended PON systems," *Optics Express*, vol. 20, no. 26, pp. B462–B469, 2012.

[74] X. Yin, J. Put, J. Verbrugghe, J. Gillis, X. Qiu, J. Bauwelinck, J. Vandewege, H. Krimmel, and M. Achouche, "A 10Gb/s burst-mode TIA with on-chip reset/lock CM signaling detection and limiting amplifier with a 75ns settling time," in *2012 IEEE International Solid-State Circuits Conference*, 2012, Conference Proceedings, pp. 416–418.

[75] K. Chen and A. Emami, "A 25Gb/s APD-based burst-mode optical receiver with 2.24ns reconfiguration time in 28nm CMOS," in *2018 IEEE Custom Integrated Circuits Conference (CICC)*, 2018, Conference Proceedings, pp. 1–4.

[76] Y. Xin, J. Verbist, T. D. Keulenaer, B. Moeneclaey, J. Verbrugghe, Q. Xing-Zhi, and J. Bauwelinck, "25Gb/s 3-level burst-mode receiver for high serial rate TDM-PONs," in *Optical Fiber Communications Conference and Exhibition (OFC), 2015*, 2015, Conference Proceedings, pp. 1–3.

[77] X. Yin, J. V. Kerrebrouck, J. Verbist, B. Moeneclaey, X. Qiu, J. Bauwelinck, D. Lanteri, F. Blache, M. Achouche, and P. Demeester, "An Asymmetric High Serial Rate TDM-PON With Single Carrier 25 Gb/s Upstream and 50 Gb/s Downstream," *Journal of Lightwave Technology*, vol. 34, no. 2, pp. 819–825, 2016.

[78] V. Houtsma, D. v. Veen, and E. Harstead, "Recent Progress on Standardization of Next-Generation 25, 50, and 100G EPON," *Journal of Lightwave Technology*, vol. 35, no. 6, pp. 1228–1234, 2017.

[79] J. Armstrong, "OFDM for Optical Communications," *Lightwave Technology, Journal of*, vol. 27, no. 3, pp. 189–204, 2009.

[80] N. Cvijetic, "OFDM for Next-Generation Optical Access Networks," *Lightwave Technology, Journal of*, vol. 30, no. 4, pp. 384–398, 2012.

[81] R. P. Giddings, X. Q. Jin, E. Hugues-Salas, E. Giacoumidis, J. L. Wei, and J. M. Tang, "Experimental demonstration of a record high 11.25Gb/s real-time optical OFDM transceiver supporting 25km SMF end-to-end transmission in simple IMDD systems," *Optics Express*, vol. 18, no. 6, pp. 5541–5555, 2010.

[82] Z. Lei, N. Chand, L. Xiang, P. Guikai, L. Huafeng, L. Zebin, W. Zhenping, Z. Xiaofeng, W. Sam, and F. Effenberger, "Demonstration of software-defined flexible-PON with adaptive data rates

between 13.8 Gb/s and 5.2 Gb/s supporting link loss budgets between 15 dB and 35 dB," in *Optical Communication (ECOC), 2014 European Conference on*, 2014, Conference Proceedings, pp. 1–3.

[83] S. Weinstein and P. Ebert, "Data Transmission by Frequency-Division Multiplexing Using the Discrete Fourier Transform," *Communication Technology, IEEE Transactions on*, vol. 19, no. 5, pp. 628–634, 1971.

[84] https://cordis.europa.eu/project/rcn/109002_en.html, [Online; accessed September-2018].

[85] Y. Weizhen, T. Tanaka, L. Bo, M. Nishihara, L. Lei, T. Takahara, T. Zhenning, J. C. Rasmussen, and T. Drenski, "100 Gb/s optical IM-DD transmission with 10G-class devices enabled by 65 GSamples/s CMOS DAC core," in *2013 Optical Fiber Communication Conference and Exposition and the National Fiber Optic Engineers Conference (OFC/NFOEC)*, 2013, Conference Proceedings, pp. 1–3.

[86] C. Kottke, C. Schmidt, R. Freund, and V. Jungnickel, "Bandwidth Extension Techniques for High-Speed Access Networks," in *2018 Optical Fiber Communications Conference and Exposition (OFC)*, 2018, Conference Proceedings, pp. 1–3.

[87] C. Antony, G. Talli, and P. D. Townsend, "SOA based upstream packet equalizer in 10Gb/s extended-reach PONs," in *Optical Fiber Communication - incudes post deadline papers, 2009. OFC 2009. Conference on*, 2009, Conference Proceedings, pp. 1–3.

[88] M. Dalla Santa, C. Antony, G. Talli, I. Krestnikov, and P. D. Townsend, "Burst-mode analysis of XGPON Raman reach extender employing quantum-dot lasers," *Electronics Letters*, vol. 52, no. 13, 2016.

[89] P. Cao, X. Hu, Z. Zhuang, L. Zhang, Q. Chang, Q. Yang, R. Hu, and Y. Su, "Power margin improvement for OFDMA-PON using hierarchical modulation," *Optics Express*, vol. 21, no. 7, 2013.

[90] J. Hong and P. A. Wilford, "A hierarchical modulation for upgrading digital broadcast systems," *IEEE Transactions on Broadcasting*, vol. 51, no. 2, 2005.

[91] V. Houtsma, D. v. Veen, and H. Chow, "Demonstration of Symmetrical 25 Gb/s TDM-PON With Multilevel Interleaving of Users," *Journal of Lightwave Technology*, vol. 34, no. 8, pp. 2005–2010, 2016.

[92] K. Ramchandran, A. Ortega, K. M. Uz, and M. Vetterli, "Multiresolution broadcast for digital HDTV using joint source/channel coding," *IEEE Journal on Selected Areas in Communications*, vol. 11, no. 1, pp. 6–23, 1993.

[93] U. Reimers, "DVB-T: the COFDM-based system for terrestrial television," *Electronics & Communication Engineering Journal*, vol. 9, no. 1, pp. 28–32, 1997.

[94] N. Shibata, N. Iiyama, J. i. Kani, S. Y. Kim, J. Terada, and N. Yoshimoto, "Star-QAM Constellation Design for Hierarchically Modulated PON Systems With 20-Gbps PSK and 10-Gbps OOK Signals," *Journal of Lightwave Technology*, vol. 32, no. 18, pp. 3184–3191, 2014.

[95] N. Iiyama, J. i. Kani, J. Terada, and N. Yoshimoto, "Feasibility Study on a Scheme for Coexistence of DSP-Based PON and 10-Gbps/ PON Using Hierarchical Star QAM Format," *Journal of Lightwave Technology*, vol. 31, no. 18, pp. 3085–3092, 2013.

[96] S. Porto, C. Antony, G. Talli, P. Ossieur, and P. D. Townsend, "Requirements for adaptive electronic dispersion compensation in burst-mode systems," in *Optical Fiber Communication Conference and Exposition and the National Fiber Optic Engineers Conference (OFC/NFOEC), 2013*, 2013, Conference Proceedings, pp. 1–3.

[97] IEEE, "10Gb/s Ethernet Passive Optical Networks," 2009.

[98] J. C. Cartledge and G. S. Burley, "The effect of laser chirping on lightwave system performance," *Lightwave Technology, Journal of*, vol. 7, no. 3, pp. 568–573, 1989.

[99] K. Geun-Young and L. Yong-Gi, "The influence of chirp and extinction ratio on directly modulated DFB lasers," in *Lasers and Electro-Optics, 2001. CLEO/Pacific Rim 2001. The 4th Pacific Rim Conference on*, vol. 2, 2001, Conference Proceedings, pp. II–II.

[100] D. Mahgerefteh, Y. Matsui, Z. Xueyan, and K. McCallion, "Chirp Managed Laser and Applications," *Selected Topics in Quantum Electronics, IEEE Journal of*, vol. 16, no. 5, pp. 1126–1139, 2010.

[101] T. L. Koch and R. A. Linke, "Effect of nonlinear gain reduction on semiconductor laser wavelength chirping," *Applied Physics Letters*, vol. 48, no. 10, pp. 613–615, 1986.

[102] R. A. Linke, "Modulation induced transient chirping in single frequency lasers," *Quantum Electronics, IEEE Journal of*, vol. 21, no. 6, pp. 593–597, 1985.

[103] C. Headley and G. P. Agrawal, *Raman Amplification in Fiber Optical Communication Systems*. Elsevier Academic Press, 2005.

[104] J. Bromage, "Raman amplification for fiber communications systems," *Lightwave Technology, Journal of*, vol. 22, no. 1, pp. 79–93, 2004.

[105] K. Rottwitt and J. H. Povlsen, "Analyzing the fundamental properties of Raman amplification in optical fibers," *Journal of Lightwave Technology*, vol. 23, no. 11, pp. 3597–3605, 2005.

[106] R. H. Stolen, E. P. Ippen, and A. R. Tynes, "Raman Oscillation in Glass Optical Waveguide," *Applied Physics Letters*, vol. 20, no. 2, pp. 62–64, 1972.

[107] R. H. Stolen, W. J. Tomlinson, H. A. Haus, and J. P. Gordon, "Raman response function of silica-core fibers," *Journal of the Optical Society of America B*, vol. 6, no. 6, pp. 1159–1166, 1989.

[108] N. Bloembergen, "The Stimulated Raman Effect," *American Journal of Physics*, vol. 35, no. 11, pp. 989–1023, 1967.

[109] M. Nissov, C. R. Davidson, K. Rottwitt, R. Menges, P. C. Corbett, D. Innis, and N. S. Bergano, "100 Gb/s (10/spl times/10 Gb/s)

WDM transmission over 7200 km using distributed Raman amplification," in *Integrated Optics and Optical Fibre Communications, 11th International Conference on, and 23rd European Conference on Optical Communications*, vol. 5, 2011, Conference Proceedings, pp. 9–12 vol.5.

[110] T. N. Nielsen, A. J. Stentz, K. Rottwitt, D. S. Vengsarkar, Z. J. Chen, P. B. Hansen, J. H. Park, K. S. Feder, S. Cabot, S. Stulz, D. W. Peckham, L. Hsu, C. K. Kan, A. F. Judy, S. Y. Park, L. E. Nelson, and L. Gruner-Nielsen, "3.28-Tb/s transmission over 3 x 100 km of nonzero-dispersion fiber using dual C- and L-band distributed Raman amplification," *IEEE Photonics Technology Letters*, vol. 12, no. 8, pp. 1079–1081, 2000.

[111] W. S. Pelouch, "Raman Amplification: An Enabling Technology for Long-Haul Coherent Transmission Systems," *Journal of Lightwave Technology*, vol. 34, no. 1, pp. 6–19, 2016.

[112] M. Tan, P. Rosa, M. A. Iqbal, L. Son Thai, I. D. Phillips, S. K. Turitsyn, and P. Harper, "Raman fibre laser based amplification in long-haul/unrepeatered coherent transmission systems," in *2017 19th International Conference on Transparent Optical Networks (ICTON)*, 2017, Conference Proceedings, pp. 1–4.

[113] T. Tanaka, K. Torii, M. Yuki, H. Nakamoto, T. Naito, and I. Yokota, "200-nm Bandwidth WDM Transmission around 1.55 um using Distributed Raman Amplifier," in *2002 28TH European Conference on Optical Communication*, vol. 5, 2002, Conference Proceedings, pp. 1–2.

[114] C. Reis, A. M. Rocha, B. Neto, N. Wada, and P. Andre, "Raman amplification in high 10 Gbit/s and 40 Gbit/s packet optical networks," in *Mediterranean Winter, 2008. ICTON-MW 2008. 2nd ICTON*, 2008, Conference Proceedings, pp. 1–4.

[115] R. Kjaer, I. T. Monroy, L. K. Oxenlowe, P. Jeppesen, and B. Palsdottir, "Impairments Due to Burst-Mode Transmission in a Raman-Based Long-Reach PON Link," *Photonics Technology Letters, IEEE*, vol. 19, no. 19, pp. 1490–1492, 2007.

[116] S. Namiki, S. Koji, N. Tsukiji, and S. Shikii, "Challenges of Raman Amplification," *Proceedings of the IEEE*, vol. 94, no. 5, 2006.

[117] P. P. Iannone and A. H. Gnauck, "Distributed Raman amplification in a 8 x 10-Gb/s, 40-km, 1:128 TWDM PON," *Optics Express*, vol. 24, no. 22, pp. 25 084–25 090, 2016.

[118] Z. Benyuan and D. Nesset, "GPON reach extension to 60 km with entirely passive fibre plant using Raman amplification," in *Optical Communication, 2009. ECOC '09. 35th European Conference on*, 2009, Conference Proceedings, pp. 1–2.

[119] B. Zhu, "Entirely passive coexisting 10G-PON and GPON compatible reach extender using Raman amplification," *Optics Express*, vol. 20, no. 3, pp. 2290–2296, 2012.

[120] Z. Benyuan, D. Au, K. Farooq, and L. Yaowen, "Coexistence of 10G-PON and GPON reach extension to 50-km with entirely passive fiber plant," in *Optical Communication (ECOC), 2011 37th European Conference and Exhibition on*, 2011, Conference Proceedings, pp. 1–3.

[121] D. Nesset, K. Farrow, P. Wright, and D. Menashe, "Raman amplifier module for GPON reach extension," in *OFC/NFOEC*, 2012, Conference Proceedings, pp. 1–3.

[122] D. Nesset and P. Wright, "Raman extended GPON using 1240 nm semiconductor quantum-dot lasers," in *Optical Fiber Communication (OFC), collocated National Fiber Optic Engineers Conference, 2010 Conference on (OFC/NFOEC)*, 2010, Conference Proceedings, pp. 1–3.

[123] D. Nesset, K. Farrow, and P. Wright, "Bidirectional, Raman extended GPON with 50 km reach and 1:64 split using wavelength stabilised pumps," in *Optical Communication (ECOC), 2011 37th European Conference and Exhibition on*, 2011, Conference Proceedings, pp. 1–3.

[124] www.innolume.com, [Online; accessed September-2018].

[125] A. R. Chraplyvy, "Limitations on lightwave communications imposed by optical-fiber nonlinearities," *Lightwave Technology, Journal of*, vol. 8, no. 10, pp. 1548–1557, 1990.

[126] D. Vakhshoori, M. Azimi, P. Chen, B. Han, M. Jiang, K. J. Knopp, C. C. Lu, Y. Shen, G. V. Rhodes, S. Vote, P. O. Wang, and X. Zhu, "Raman amplification using high-power incoherent semiconductor pump sources," in *OFC 2003 Optical Fiber Communications Conference, 2003.*, 2003, Conference Proceedings, pp. PD47–P1.

[127] T. J. Ellingham, L. M. Gleeson, and N. J. Doran, "Enhanced Raman Amplifier Performance Using Non-Linear Pump Broadening," in *2002 28TH European Conference on Optical Communication*, vol. 2, 2002, Conference Proceedings, pp. 1–2.

[128] C. Antony, M. Dalla Santa, G. Talli, and P. D. Townsend, "Design and Performance Analysis of Raman Amplified XG-PON System," *Journal of Lightwave Technology*, vol. 34, no. 11, 2016.

[129] C. Antony, G. Talli, M. Dalla Santa, B. Murray, S. Hegarty, E. Kehayas, I. Krestnikov, and P. D. Townsend, "XG-PON Raman reach extender based on quantum dot lasers," in *Optical Communication (ECOC), 2014 European Conference on*, 2014, Conference Proceedings.

[130] *G.671: Transmission characteristics of optical components and subsystems*, ITU-T Standard, 2012.

[131] M. Dalla Santa, "Raman Based Reach Extender for Application in XG-PON System," Master's thesis, University of Padua, 10 2014.

[132] C. Chien-Jen and W. S. Wong, "Transient effects in saturated Raman amplifiers," *Electronics Letters*, vol. 37, no. 6, pp. 371–373, 2001.

[133] S. Gray, "Transient gain dynamics in wide bandwidth discrete Raman amplifiers," in *Optical Fiber Communication Conference and Exhibit*, 2002, Conference Proceedings, pp. 512–513.

[134] M. Karasek and M. Menif, "Channel addition/removal response in Raman fiber amplifiers: modeling and experimentation," *Journal of Lightwave Technology*, vol. 20, no. 9, pp. 1680–1687, 2002.

[135] L. L. Wang, B. C. Hwang, and L. M. Yang, "Gain transients in copumped and counterpumped Raman amplifiers," *Photonics Technology Letters, IEEE*, vol. 15, no. 5, pp. 664–666, 2003.

[136] M. Fujiwara, T. Imai, K. Taguchi, K. Suzuki, H. Ishii, and N. Yoshimoto, "Field Trial of 100-km Reach Symmetric-Rate 10G-EPON System Using Automatic Level Controlled Burst-Mode SOAs," *Lightwave Technology, Journal of*, vol. 31, no. 4, pp. 634–640, 2013.

[137] M. Fujiwara and R. Koma, "Long-Reach and High-Splitting-Ratio WDM/TDM-PON Systems Using Burst-Mode Automatic Gain Controlled SOAs," *Journal of Lightwave Technology*, vol. 34, no. 3, pp. 901–909, 2016.

[138] D. R. Zimmerman and L. H. Spiekman, "Amplifiers for the masses: EDFA, EDWA, and SOA amplets for metro and access applications," *Journal of Lightwave Technology*, vol. 22, no. 1, pp. 63–70, 2004.

[139] R. Borkowski, W. Poehlmann, R. Brenot, R. Bonk, P. Angelini, C. Caillaud, M. Achouche, F. Blache, M. Goix, K. Mekhazni, B. Duval, J.-Y. Dupuy, J. F. Paret, and T. Pfeiffer, "Real-Time Burst-Mode Operation of an Integrated SOA-PIN/TIA Receiver for 25 Gbit/s/ and Faster T(W)DM-PON," in *Optical Fiber Communication Conference*, ser. OSA Technical Digest (online). Optical Society of America, 2017, Conference Proceedings, p. Tu3G.6.

[140] R. Bonk, "SOA for future PONs," in *Optical Fiber Communication Conference*, ser. OSA Technical Digest (online). Optical Society of America, 2018, Conference Proceedings, p. Tu2B.4.

[141] D. Nesset, D. Grossman, S. Appathurai, J. Fitzgerald, P. Wright, K. Farrow, and S. Yang, "Field experiment with a hardened GPON reach extender with dual-parenting protection," in *Optical Communication, 2008. ECOC 2008. 34th European Conference on*, 2008, Conference Proceedings, pp. 1–2.

[142] I. Yang, N. Suzuki, T. Suehiro, J. Nakagawa, and T. Mizuochi, "Full MAC system demonstration of extended 10G-EPON uplink with 512 ONU splits access span via burst-mode SOA and enhanced-FEC combined with burst-mode 3R," in *Optical Fiber Communication Conference and Exposition (OFC/NFOEC), 2012 and the National Fiber Optic Engineers Conference*, 2012, Conference Proceedings, pp. 1–3.

[143] J. Zhang, J. S. Wey, J. Yu, Z. Tu, B. Yang, W. Yang, Y. Guo, X. Huang, and Z. Ma, "Symmetrical 50-Gb/s/ PAM-4 TDM-PON in O-band with DSP and Semiconductor Optical Amplifier Supporting PR-30 Link Loss Budget," in *Optical Fiber Communication Conference*, ser. OSA Technical Digest (online). Optical Society of America, 2018, Conference Proceedings, p. M1B.4.

[144] R. Bonk, T. Vallaitis, J. Guetlein, C. Meuer, H. Schmeckebier, D. Bimberg, C. Koos, W. Freude, and J. Leuthold, "The Input Power Dynamic Range of a Semiconductor Optical Amplifier and Its Relevance for Access Network Applications," *IEEE Photonics Journal*, vol. 3, no. 6, pp. 1039–1053, 2011.

[145] J. Sugawa and H. Ikeda, "Development of OLT using semiconductor optical amplifiers as booster and preamplifier for loss-budget extension in 10.3-Gb/s PON system," in *OFC/NFOEC*, 2012, Conference Proceedings, pp. 1–3.

[146] H. Xiaobin, H. Weiping, and W. Jian, "Burst mode receiver based on SOA," in *Optical Fiber Communication and Optoelectronics Conference, 2007 Asia*, 2007, Conference Proceedings, pp. 324–326.

[147] S. V. Pato, R. Meleiro, D. Fonseca, P. Andre, P. Monteiro, and H. Silva, "All-Optical Burst-Mode Power Equalizer Based on Cascaded SOAs for 10-Gb/s EPONs," *IEEE Photonics Technology Letters*, vol. 20, no. 24, pp. 2078–2080, 2008.

[148] A. Emsia, Q. T. Le, M. Malekizandi, D. Briggmann, and F. Kuppers, "10 Gbit/s PON Upstream Burst-mode Equalization Based on SOAs," in *Asia Communications and Photonics Conference*

2014, ser. OSA Technical Digest (online). Optical Society of America, 2014, Conference Proceedings, p. ATh1H.2.

[149] M. Fujiwara, "Gain-controlled optical amplifier technologies for long-reach and high-splitting-ratio PON systems," in *Optical Fiber Communications Conference and Exhibition (OFC), 2014*, 2014, Conference Proceedings, pp. 1–3.

[150] L. Liu, C. Michie, A. E. Kelly, and I. Andonovic, "Packet equalisation in PONs using adjustable gain-clamped semiconductor optical amplifiers (AGC-SOA)," in *2011 13th International Conference on Transparent Optical Networks*, 2011, Conference Proceedings, pp. 1–4.